Sulfo-functionalization of lignin and its impact on the stabilization of colloidal systems

A Thesis Presented to

the Faculty of Graduate Studies of Lakehead University

by Nasim Ghavidel

DEDICATION

To my parents for their unconditional guidance and support

To my husband, Ali for his invaluable support and patience

ABSTRACT

Lignin macromolecules, derived from renewable biomass resources, have gained extensive interest during the past decade as a sustainable substitute for synthetic oil-based materials. The main goal of this dissertation was to formulate and investigate lignin-based materials (dispersants or adsorbents) that are renewable, biodegradable, and non-toxic from the molecular level to the macroscopic level. To obtain desired physicochemical properties, chemical modifications or self-assembly were conducted to alter solubility, size, functionality, and surface energy of products with hydrophobic, hydrophilic, or near neutral wettability. After following various techniques of functionalization, polymerization, and nanoprecipitation (acidification), the desired structure of polymers or particles were formed, which were extensively characterized by implementing various analytical techniques. The correlations between physicochemical properties of unmodified hydrolysis lignin samples and their chemical reactivities toward sulfo-alkylation reactions were evaluated. The fundamental understanding of interactions of lignin derivatives and particles was further evaluated in variable systems (solid films, oil-water systems, and solid suspensions) by evaluating surface and interfacial properties. The formulated (nano) materials were successfully used in different applications including, the adsorption of metal ions, stabilization of emulsions (Pickering/non-Pickering), and the dispersion of clay suspension. The results showed the suitability of the lignin-derived additives in wide-range applications.

The results on the material synthesis, physicochemical properties, and their fundamental correlation to their effectiveness in various colloidal systems, can be utilized as guidelines for the development of sustainable processes for the utilization of lignin-based products.

ACKNOWLEDGEMENTS

I would like to express my sincere gratitude to my supervisor Dr. Pedram Fatehi for all his hope, efforts and precious time he has put on my work. His guidance and immense support helped me in all the time of research and writing of this thesis. I would like to extend my sincere thanks to my committee members Dr. Baoqiang Liao, Dr. Aicheng Chen and my external examiner Dr. Mojgan Nejad for their valuable suggestions and revisions in preparing this thesis. I would also like to thank both faculty and the staff members of the Department of Chemistry for their assistance, especially Dr. Christine Gottardo and Dr. Robert Mawhinney for their guidelines in my chemistry challenges and Dr. Brenda Magajna for her technical support. I also wish to extend my sincere thanks to Dr. Guoseheng Wu, Mr. Michael Sorokopud, and Mr. Greg Krepka, LUIL department, Lakehead University for helping me with the analytical instruments. I thank all the previous and current lab members for encouraging me and providing me an ideal workplace environment. I, specially thank Dr. Weijue Gao, Dr. Samira Gharehkhani, Dr. Mohan Konduri and Dr. Agha Hassan for their continues assistance and guidelines in the lab. I would also like to thank my beloved parents and siblings for their overwhelming support and encouragement during this journey. Special gratitude and appreciation to my husband, Ali, to stay by my side all the way and pushed me and supported me to move forward every day. The financial assistant from FPInnovations, and NSERC, Canada is also much appreciated.

Table of Contents

List of Figures

List of Tables

Chapter 1: Introduction

1.1 Overview

Lignin is the first most abundant aromatic bio-polymer on earth, consisting of 20 to 40% of the dry mass of wood.[1,2] As a result of an increase in papermaking production in the 19th century, the commercial production of lignin increased globally. In the 19th century, lignin was known to be an obstacle to the papermaking process because of its dark color and deteriorating effect on the strength of the paper. While 1/3 of the mass of lignocellulose, the precursor to paper is lignin; therefore, lignocellulose needed to be delignified, which produced large scale amounts of by-product annually.[3] For decades, the solution to this problem was as simple as burning it as fuel.

By the 1930s, sulfite pulping had become the dominant means of producing wood pulp. In this process, lignin is removed from wood pulp, and lignosulfonates are a water-soluble by-product.[4] Many applications have been proposed.[5] Lignosulfonates (LS) have been used in a vast range of applications as dispersants, emulsion stabilizers, binders and sequestrants (water treatment).[6] Currently, LS utilization in mentioned applications encountered major drawbacks primarily because of the limited worldwide production of LS, which counts for only *ca*. 2% of the total worldwide production of chemical pulp.[7] Therefore, considering the worldwide availability of kraft pulping process,[8] a new trend in valorizing kraft lignin was introduced over the past decades. Lignin had been treated traditionally as a low-quality, low-value side stream of product processing that gained substantial consideration as an abundant raw material to be employed in a wide variety of processes and applications, gaining the potential to displace traditional fossil-based chemicals and products.[9] For these reasons, lignin is predicted to play a crucial role in the Canadian bio-economy value chain.[10]

To find out the most suitable modification route of lignin-based on the desired application, an initial comprehensive understanding of the physicochemical structure of unmodified lignin is required. Lignin consists of polyphenolic material arising from an enzyme-mediated dehydrogenative polymerization of three phenylpropanoid monomers, coniferyl, sinapyl, and *p*-coumaryl alcohols.[11] However, lignin is viewed as a macromolecule of physically and chemically heterogeneous materials whose structure and consequence of monomers could be unique based on the origin, the types of plants (softwood, hardwood, and non-wood), and isolation methods (sulfite, kraft, organosolv, soda and hydrolysis).[12,13] Therefore, the first step for lignin valorization is to quantify lignin functional groups , internal linkages, molecular weight, and other physicochemical

properties that could affect its modification routes. Different modification pathways have been conducted on lignin to alter its properties and make it useful for specific applications. These modifications could be categorized in polymerization,[14] catalytic reactions,[15] depolymerization,[16] oxidation,[17] and grafting[18] on the lignin. Modification reactions can occur on aromatic, aliphatic, or both parts, which would result in unique properties. The focus of this thesis is on the polymerization and grafting methods on lignin to produce adsorbents, dispersants, and emulsifiers for application in variable colloidal systems.

The main goal of this dissertation was to synthesize lignin-based dispersants or adsorbents that are renewable, biodegradable, and non-toxic. In this chapter **(chapter 1)**, a brief summary of the subsequent chapters in this thesis is provided. First, the objectives of this research work are summarized.

1.2 The overall objectives of this study are to:

1. Synthesize and characterize physicochemical properties of kraft lignin-polystyrene macromolecules via free-radical polymerization in aqueous solutions.

2. Assess the adsorption affinity of lignin-polystyrene substrate compared to lignin and polystyrene in isolating copper ions from the aqueous system.

4. Synthesize a novel sulfo-functionalized lignin macromolecule and evaluate its potential as an emulsifier in the form of polymeric or particle surfactants and analyze the pH-dependent changes and the viscoelastic properties in the Pickering and non-Pickering emulsion systems.

3. Investigate the fundamental dynamic interfacial analysis and emulsion properties of the polymeric lignin surfactant at different oil/water interfaces.

5. Characterize the physicochemical properties of various hydrolysis lignin and their chemical reactivity toward various sulfo-functionalization processes.

6. Systematically compare dispersion properties of various sulfo-functionalized hydrolysis lignins considering the differences in charge density, and physical properties.

The following chapters are presented in this thesis in order to address the proposed objectives.

Chapter 2 provides a brief introduction to the lignin resources and isolation methods, chemistry, chemical valorization, applications and methodologies. The Literature review is structured into sections discussing the functionalization and polymerization methods implemented previously to add value to lignin-based biopolymers. The second section discusses various methods identified

in the literature and in this study to evaluate the properties of lignin-based polymers for potential applications such as adsorbents and dispersants.

Chapter 3 presents a comprehensive literature review relevant to the production and application of a variety of plant-based polymers and particles implemented for use as an emulsifier in oil/water systems. This section reviews publications related to the resources, modification, chemical properties of polymeric or particles of plant-based materials including lignin. Moreover, the emulsion knowledge, strategies of stabilization, and properties of plant-based emulsifiers on micro and macroscopic properties of emulsions are discussed.

Chapter 4 introduces the polymerization of lignin and styrene (St) to produce kraft lignin-styrene (KL-PS) copolymers. Further, lignin copolymers were characterized to confirm their properties. Degree of polymerization and functional groups alteration were examined. The production of homopolymers of PS was also illustrated; further, the surface energy of KL, KL-PS and PS were assessed and compared. As a potential application, adsorption of copper ions from aqueous solution was compared for KL, KL-PS and PS.

Chapter 5 describes the synthesis of a novel water-soluble sulfo-functionalized polymeric lignin (SEKL) with further discussion on its application as emulsifiers for Pickering/non-Pickering emulsion stabilization under influence of pH alteration with unique properties. The SEKL properties with pH alteration, emulsion formulation, micro and macro-observation of emulsions, short-term and long-term stabilities and reversibility of stabilization were analyzed.

Chapter 6 illustrates the behavior of sulfoethylated lignin at different oil interfaces as a polymeric surfactant. Through a systematic approach, the dynamic kinetic adsorption of SEKL polymer were examined at the interfaces of xylene, cyclohexane and decane as the oil phase. The effect of polymer concentration and ionic strength on the adsorption of polymers at different oil interfaces and kinetic studies was investigated. The physical stability analysis of the emulsions was further correlated to their adsorption analysis.

Chapter 7 reports on a comprehensive physicochemical characterization of seven different hydrolysis lignin including their various chemical composition, sugar content, hydroxyl group content, internal linkages, surface area, and size of particles in suspension. Further, their chemical reactivity toward 3 distinctive sulfo-functionalization routes of grafting was conducted and their reactivity was compared. In addition, the correlations between unmodified lignin properties and DS of produced polymers were assessed. As the final assessment of polymers potential application,

their effectiveness in dispersing clay suspensions were compared and the best application for each modification was introduced.

Chapter 8 provides conclusions and suggestions for future research.

1.3 References

[1] A. P. de Candolle, A. de Candolle, Exposition of the principles of natural classification and the art of describing and studying plants. Roret, **1844**.

[2] A. McDonald, L. Donaldson, Wood, Constituents of, Elsevier **2001**.

[3] P. Fatehi, J. Chen, Extraction of technical lignins from pulping spent liquors, challenges and opportunities, Production of biofuels and chemicals from lignin, Springer **2016**, 35-54.

[4] P. Bajpai, Biermann's Handbook of Pulp and Paper: Raw Material and Pulp Making, Elsevier **2018**.

[5] R. Flatt, I. Schober, Superplasticizers and the rheology of concrete, Understanding the rheology of concrete, Elsevier **2012**, 144-208.

[6] A. Macfarlane, M. Mai, J. Kadla, Bio-based chemicals from biorefining: Lignin conversion and utilisation, *Advances in Biorefineries*, Elsevier **2014**, 659-692.

[7] M. Österberg, M. H. Sipponen, B. D. Mattos, O. J. Rojas, *Green Chem.* **2020**, *22*(9), 2712-2733.

[8] M. Alekhina, O. Ershova, A. Ebert, S. Heikkinen, H. Sixta, *Ind. Crops Prod.* **2015**, *66*, 220-228.

[9] J. Zakzeski, P. C. Bruijnincx, A. L. Jongerius, B. M. Weckhuysen, *Chem. Rev.* **2010**, *110*(6), 3552-3599.

[10] M. K. Awasthi, S. Sarsaiya, A. Patel, A. Juneja, R. P. Singh, B. Yan, S. K. Awasthi, A. Jain, T. Liu, Y. Duan, *Renew. Sust. Energ. Rev*. **2020,** *127*, 109876-109894.

[11] S. Gharehkhani, Y. Zhang, P. Fatehi, *Prog. Energy Combust. Sci.* **2019,** 72, 59-89.

[12] S. H. Ghaffar, M. Fan, *Biomass Bioenerg* **2013,** *57*, 264-279.

[13] F. S. Chakar, A.J. Ragauskas, *Ind. Crops Prod.* **2004**, *20*(2), 131-141.

[14] B. M. Upton, A. M. Kasko, *Chem. Rev.* **2016**, *116*(4), 2275-2306.

[15] C. Li, X. Zhao, A. Wang, G.W. Huber, T. Zhang, *Chem. Rev.* **2015,** *115*(21), 11559-11624.

[16] Z. Sun, B. Fridrich, A. de Santi, S. Elangovan, K. Barta, *Chem. Rev.* **2018**, *118*(2), 614-678.

[17] S. Gillet, M. Aguedo, L. Petitjean, A. Morais, A. da Costa Lopes, R. Łukasik, P. Anastas, *Green Chem.* **2017**, *19*(18), 4200-4233.
[18] A. E. Kazzaz, Z. H. Feizi, P. Fatehi, *Green Chem.* **2019**, *21*(21), 5714-5752.

Chapter 2: Literature review

2.1 Lignin resources and isolation

Lignin forms 25-30% of plant cell walls along with the other two major polymeric components, cellulose and hemicellulose. The main role of lignin is to act as a matrix material to bind the plant polysaccharide microfibrils and fibers together, which imparts strength and rigidity to the plant stem.[1] In addition, due to the antioxidant and antimicrobial properties associated with lignin chemical structure,[2,3] lignin functions as a shield to protect against biological attack and assists in the transportation mechanism of water by sealing plant cell walls against water leaks.[4]

Technical lignin can be extracted from pulping chemical processes that use either sulphur or are sulphur-free. There are five different types of classified technical lignins with distinctive properties including kraft, lignosulfonate, soda, organosolv and hydrolysis lignin with variable physicochemical properties that are summarized in Table 1.[5]

This thesis is centered around kraft lignin as the most available technical lignin and hydrolysis lignin as the most recent technology and the least investigated of the two. In the kraft process, via using white liquor, a strong alkali solvent of aqueous sodium hydroxide and sodium sulphide, the bonds between lignin and cellulose are broken. The linkages between the phenylpropane units of lignin macromolecules are cleaved into smaller chains, which makes kraft lignin soluble in the pulping liquor system and is called black liquor.[6] Black liquor is used mainly as the fuel in the recovery process of kraft pulp mills and supplies the energy need of the mills.[7] Different isolation methods from black liquor have been introduced to generate the technical Kraft lignin commercially. LignoBoost™ and LignoForce™ technologies are the common processes. [8,9] As shown in Table 1, added aliphatic thiol groups make kraft lignin a high sulphur content (1 to 2 wt%) with hydrophobic properties.[10]

In the hydrolysis process of biomass, lignocellulosic biomass is separated where fractionated cellulose and hemicellulose are hydrolyzed to monomer sugars using acid, base or enzyme. For the production of enzymatic lignin, which was used in this research thesis, the raw material is first processed by mechanical refining and then treated with enzymes for 15-72 h at a temperature below 50 °C.[11] Cellulose would be separated from lignin in the form of monomer sugars. Although HL is not a sulfur free by-product, its content is much lower (≤1%) than KL or LS (1-8%), and due to the less chemical consumption, it is considered a greener process.[12] Hydrolysis lignin has distinctive properties compared to kraft lignin with a light color, odor free and high

content of sugar (10-30 wt.%), which makes its structure closer to that of native lignin.[13] Lignin-carbohydrate internal linkages, called LCCs, added more complexity to hydrolysis lignin structure and less availability of functional groups.

Table 2.1. Chemical and physical properties of different commercial lignin. (Adapted from Ref. [5] with permission of Elsevier).

Type	Sulfur content (wt.%)	Sugar content (wt.%)	Molecular weight (g/mol)	Ash content (wt.%)	Moisture content (wt.%)	Poly-disperibility
Kraft	1-3	1-2.3	<25,000	0.5-3	3-6	2.5-4
Lignosulfonate	3.5-8	-	<15,000	4.5-8	5.8	4.2-9
Soda	0	1.5-3	<15,000	0.7-2.3	2.5-5	2.5-3.5
Hydrolyzed lignin	0-1	10-22.4	5,000-10,000	1-3	4-9	1.5-3
Organosolv	0	1-3	<5000	1.7	7.5	1.5-2.4

2.2 Lignin chemistry

Lignin chemical structure is shaped from irregular radical oxidative coupling of three basic phenylpropane monomers: p-coumaryl alcohol, coniferyl alcohol and sinapyl are referred to as "monolignols" in which the heterogenous repeating alcoholic units form p-hydroxyphenyl (H), guaiacyl (G) and syringyl (S) polymerized product, respectively [14] as shown in Figure 1. Different types of wood species and even distinctive parts of trees (softwoods, hardwoods and non-woods) could have remarkable chemical differences with unique molecular structures from the polymerization of mentioned monomers.[4] Softwoods lignins consist of mainly of guaiacyl with minimal amounts of hydroxyphenyl and syringyl contents.[15] Hardwood lignins contain both types of guaiacyl and syringyl lignins with small amounts of hydroxyphenyl lignin.[15] Non-wood lignins typically contain all three precursors, guaiacyl, syringyl and para-hydroxyphenyl with variable ratios.[16]

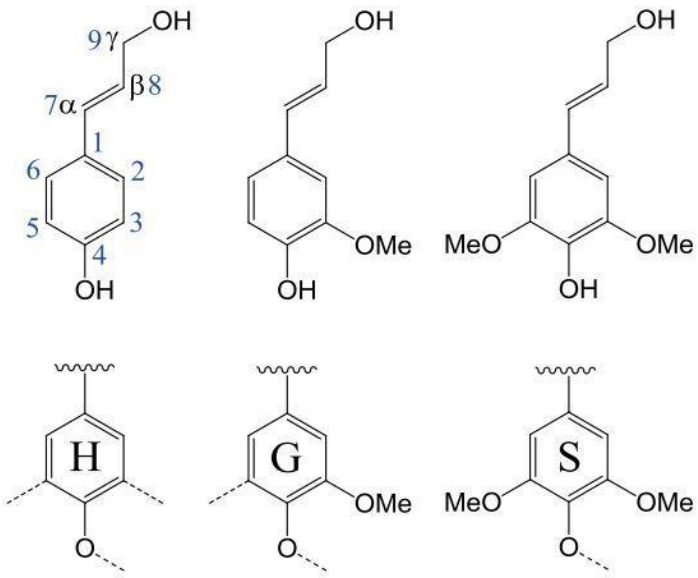

Figure 2.1: Lignin precursor monolignols p-coumaryl alcohol, coniferyl alcohol, and sinapyl alcohol (top row) and the corresponding p-hydroxyphenyl (H), guaiacyl (G), and syringyl (S) units of lignin. The aliphatic carbons 7-9 are referred to as α, β, and γ carbons, respectively, in this thesis. Adapted from [17].

The variable monomers are linked by carbon-carbon or ether bonds which form the final polymerized macromolecule.[18] Carbon-carbon bond with one-third and ether linkages with two-thirds form the most common linkage types in a lignin molecule that are β-O-4, α-O-4, β-5, 5-5, 4-O-5, β-1, β-β and dibenzodioxocin shown in Figure 2 within lignin structure.[19-22]

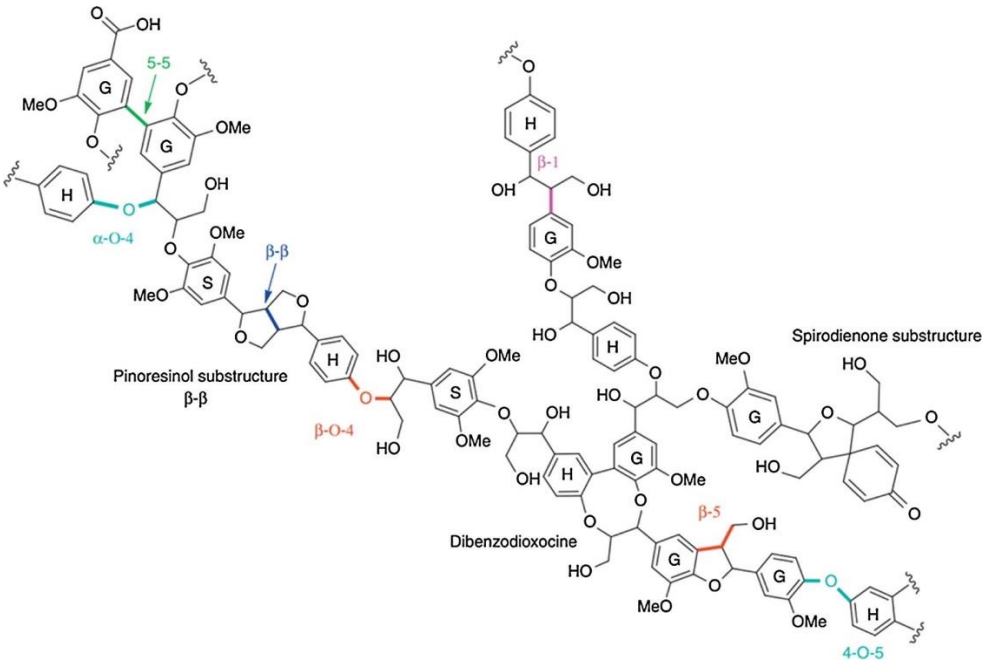

Figure 2.2: Representation of the lignin structure with the main linkages. (Adapted from Ref. [22] with permission of Elsevier).

Due to the large and complicated structure of lignin with excessive internal linkages and the difficulties in lignin analysis, a complete structure of a lignin has not yet been identified, while available structure models in literature are only illustrations of each linkage and their lignin unit types.

Delignification and isolation processes would modify the chemical structure of lignin by changing the internal linkages. During the kraft process, the majority of β-O-4 and α-O-4 linkages are cleaved and produce non-etherified phenolic hydroxyl groups in lignin; however, due to the very mild conditions in the hydrolysis process, limited cleavage would occur that indeed increases the percentage of etherified linkages.[23]

The more cleavage of etherified linkages would associate with elevated content of free hydroxyl functional groups. The major functional groups of lignin are aliphatic hydroxyl, phenolic hydroxyl, methoxyl, carbonyl, and uncondensed guaiacyl groups.[24]

The content of phenol in lignin directly controls the reactivity of lignin in chemical pulping.[25] Therefore, it shows the importance and critical role of the delignification and isolation process which could ultimately define the reactivity of isolated lignin.

Another important factor for the reactivity of lignin to be considered is the connection to carbohydrate segments and sugar content. There are eight different types of lignin-carbohydrate (L-C) bonds, i.e., benzyl ether, benzyl ester, glycosidic or phenyl glycosidic, hemiacetal or acetal linkages, and ferulate or diferulate esters that are linked to lignin at 4-OH and 4-O positions,[26] which are shown in Figure 3. It should be mentioned that the ratio of these linkages could again vary depending on the source and isolation process, although Benzyl ether (BE), ester, and phenyl glycoside (PhyGlc) are considered as the most typical lignin-carbohydrate linkages.[27]

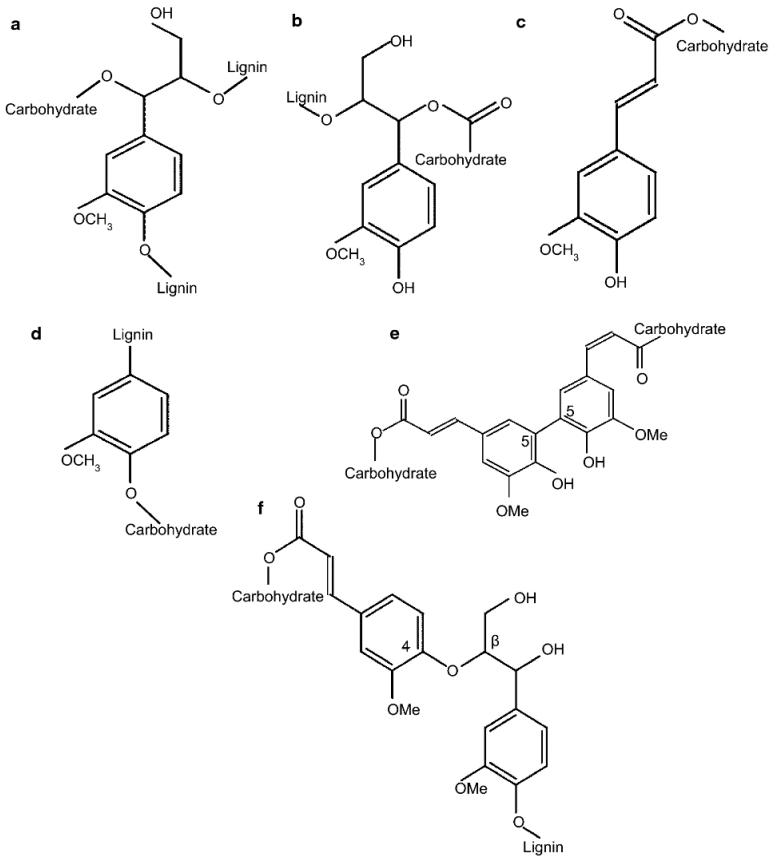

Figure 2.3: Major types of LCC linkages: **a** benzyl ether; **b** benzyl ester; **c** ferulate ester; **d** phenyl glycoside; **e** diferulate ester (5′–5′ linkage) **f** diferulate ester (4-O-β linkage). Adapted from [26].

2.3 Value-added product from lignin

Due to the excessive advantages of lignin, such as easy availability, high energy density (kJ/g), active chemical structure, and sustainability, many researchers have tried to make lignin more compatible and applicable in different industries. One of the uplifting facts was to make products that could replace petroleum-based materials for green and sustainable substitutions.[29]

Over the past decades, lignin was utilized for variable applications based on three different strategies: 1) employing lignin without or with less modification, 2) degradation of lignin to other materials, and 3) modification of lignin with altering its properties.[30] Based on the first strategy with no modification, technical lignin could be implemented in a particular application by having the desired properties. However, most of the isolated lignins require further modifications to be useful in variable applications. Degradation of lignin to produce small chemical compounds such as vanillin was investigated by many researchers as well.[31] Further chemical changes to degraded

lignin materials such as lower molecular weight, less steric hindrance, increased reactive sites, and increased content of phenolic hydroxyl put in extra advantages to lignin for the synthesis of lignin-phenol-formaldehyde resins.[32] The last category is associated with engineering the properties of the lignin by chemical modification on the active sites to produce more hydrophobic or hydrophilic polymers with variable molecular weights, charge densities, wettability, surface, and interfacial properties.[30]

The polymers from natural resources offer great potential for the preparation of novel and advanced applications. This section discusses the two common techniques to produce lignin polymers via chemical modifications that have been followed to develop advanced materials from lignin to be used in variable applications.

2.3.1 Free radical polymerization

Free radical polymerization is considered as the simplest, most economical, efficient, and appropriate method for industrial purposes [33] compared to other types of polymerization such as RAFT or condensation polymerization. Polymerization of lignin with cationic, anionic, amphoteric, and non-ionic monomers are feasible and were reported in the past.[34] The functionalization was reported to impart valuable properties to lignin, making it more hydrophilic, hydrophobic or thermally stable.

The polymerization mechanism follows via the formation of phenoxy and alkoxy radicals on lignin through the initiator decomposition (e.g., ceric ammonium nitrate, potassium persulfate, or hydrogen peroxide) under heating. Polymerization would be initiated following the attack of phenoxy radicals to the vinyl group of monomers to form a graft chain of homopolymer on the lignin backbone.[35]

Many polymers were produced using water-soluble monomers. Fang et al. [36] synthesized enzymatically hydrolyzed lignin-grafted-acrylamide polymers using acrylamide as an uncharged monomer. Kong et al. [37] polymerized acrylic acid (i.e., anionic monomer) and kraft lignin via free radical polymerization to produce water-soluble lignin-grafted-acrylic acid polymers. Cationic kraft lignin (CKL) macromolecules were produced via polymerizing kraft lignin (KL) with [2-(acryloyloxy) ethyl] trimethyl ammonium chloride (ATAC) or [2-(methacryloyloxy) ethyl] trimethylammonium methyl sulfate (METAM).[38] Another study reported to produce a water soluble lignin- poly (acrylamide)-poly (2-methacryloyloxyethyl) trimethyl ammonium) copolymer

via polymerizing kraft lignin (KL) with acrylamide (AM) and (2-methacryloyloxyethyl) trimethyl ammonium chloride (DMC) as two monomer system in an aqueous solution.[39]

Using insoluble monomers in water makes the polymerization more challenging in aqueous-based systems. Insoluble monomers such as styrene and divinylbenzene would produce water-insoluble polymers with distinct properties compared to water-soluble ones. Styrene and divinylbenzene are among the most popular polymeric sorbents.[40] Because of their hydrophobic character, interactions through van der Waals forces and π-electron interaction of their aromatic ring are possible.[40] Chapter 4 states the emulsion polymerization of lignin and styrene in aqueous medium following free radical polymerization technique. Polymerization of lignin and styrene have been reported previously following different techniques, including atom transfer radical polymerization[41,42] radiation induced graft polymerization,[43] or emulsion suspension polymerization.[40] Atom transfer radical polymerization (ATRP) technique was implemented to polymerize styrene and methyl methacrylate on lignin to produce lignin composites.[41] Graft polymerization of styrene and divinylbenzene monomers on kraft lignin was conducted in a mixture of water and organic solvents (i.e., toluene and 1-decanol) in an emulsion polymerization system to synthesize porous adsorbent.[40] The purpose and novelty of this thesis was also to incorporate lignin into polystyrene via radical polymerization to increase PS porosity and add functionality to its structure to form an adsorbent for the separation of metal ions from aqueous system.

2.3.2 Graft functionalization

Different methods of graft functionalization on lignin have been reported over the past ten years. This process gained popularity due to its simple chemical process, effectivity, high grafting and solubility of the final polymers. The functionalization can happen either on the phenolic, aliphatic hydroxyl groups or directly on the ring. Some examples are oxidation,[44] oxyalkylation [45] halogenation,[46] amination,[47] carboxyalkylation,[48] and sulfoalkylation.[49] These polymers, due to their solubility and controllable charge density and molecular weight, were applied in the variable application as dispersant,[50] flocculant,[51] binder,[52] thickener,[53] emulsifier, and detergent.[54]

Chapters 5 and 6 are focused on a simple and facile process to produce sulfoethylated lignin as a novel lignin derivative.

Grafting mechanism could follow different pathways depending on the reagent used and the medium (aqueous/solvent, acidic/basic). The most probable mechanisms are nucleophilic substitution with the hydroxy groups of lignin and electrophilic addition to the double bonds of the lignin or aliphatic segment. Therefore, the strength of the lignin as a nucleophile in the SN2 mechanism or as electrophile in electrophilic addition could be crucial. In chapter 7, three variable routes of sulfo-alkylation (sulfonation, sulfomethylation and sulfoethylation) of lignin with different modification mechanisms were compared and their degree of substitution were correlated to their physicochemical properties of unmodified lignin samples. So far, a systematic comparison of different sulfo-alkylation reactions has not been reported.

2.4 Applications

Various polymers with different properties were reported to be produced using lignin as the precursor. However, each of them might be suitable for a specific application due to their distinct properties after modifications.[36-56] For example, polymers with high molecular weight and charge density obtained from polymerization of lignin and acrylic acid showed promising results as a potential wastewater treatment flocculant.[37,55] While a high molecular weight polymer without surface charges and lack of solubility like lignin-styrene-divinylbenzene could be an efficient adsorbent.[40] On the other hand, low molecular weight polymers with high charge density are suitable dispersants for coal slurry,[56] while lower charge density would be an ideal emulsifier to adsorb at oil interface as a polymeric surfactant. Therefore, such polymers could be a good alternative for oil-based additives in different applications.

2.4.1 Adsorbents

Water pollution by heavy metal ions is a worldwide concern due to the high toxicity and irreversible detrimental effects of heavy ions on human, animal, and marine systems.[57] In recent years, extensive research was conducted to find new cost-effective adsorbents originating from biomass.[58] Utilization of adsorbents is considered as a promising method for the removal of heavy metal ions in water with an easy form of operation, great removal efficiency, and the high availability of various adsorbents.[59] The potential of lignin as a bio-based adsorbent has been discussed in previous studies. Lignin was reported to adsorb metal ions such as Pb (II), Zn (II), Cu (II) and Cd (II) from aqueous systems. [58,60] As an example, saturated adsorption of 26 mg/g of Cu (II) on wheat straw lignin was previously reported as an adsorbent.[61]

Guo et al. [62] described that a lignin isolated from black liquor adsorbed ions from an aqueous system via interactions through two main sites of carboxylic and phenolic groups identified via potentiometric (acid-base) titrations and complexation model calculations in which the phenolic sites showed a higher affinity for metal ions.

Polystyrene, PS, is also well recognized for its dispersive intermolecular interactions, which is widely used as the building block to produce adsorbent for water treatment.[40] Different methods of functionalization or cross-linking were applied to make a more effective PS. The examples include the activation of its active sites [63] via Schiff base,[64] sulfonate groups [65] or amine groups.[66] The objective and novelty of this study was to use lignin instead of chemicals to add functionality to PS.

Chapter 4 in this thesis shows the effective incorporation of KL into PS for improving its ion metal uptakes as a green substitution. In addition to the functional groups anchored on PS, which are capable of adsorbing ions, the aromatic electron-rich system of PS is also capable of interacting with ions, as previously reported in literature. [67,68]

Quadrupolar characteristic of the aromatic system is responsible for the adsorptive properties of PS for cations in water. The uneven distribution of π-electron above and below the face of an aromatic system forms a quadrupolar system (e.g., benzene ring).[69] Several non-covalent interactions are therefore associated with this system namely; polar- π interactions,[70] self-stacking,[71] hydrogen- π, [72] and cation- π interactions.[67] Therefore, the contribution of Kl and PS as a united polymer segment is expected to improve both properties of Kl and PS for effective interactions with metal ions.

2.4.2 Surfactants

Surfactants have a crucial role in the chemical industry by modifying different phases. They can be used as emulsifiers for stabilizing liquid-liquid mixtures or applied as dispersants for solid-liquid systems. With their variety of applications, they are key portions to produce foods, agrochemicals, pharmaceuticals, personal care and/or detergents in the industry.[73] All surfactants are constituted of a hydrophilic head and a hydrophobic tail and are categorized into 3 main subgroups of anionic, cationic, and amphoteric surfactants.[74]

Anionic surfactants would form in the presence of carboxylates, sulfonates, sulfates, or phosphates in which sulfonate ones due to their wide range of solubility and tolerance against hydrolysis at a low or high pH have a wide range of applications in different industries.[75]

Despite their wide application, the synthesis of sulfonate based anionic surfactants are complex and costly.[73] Therefore, there is a surge for producing more environmentally friendly surfactants with a simpler production process. Over the past decades, polymeric surfactants have shown considerable advantages over traditional small-molecule surfactants due to their distinctive features, such as multiple functional groups, complex conformational changes at oil interface, and viscosity enhancement of emulsions.[76] Among them, biobased polymeric materials have attracted substantial interest due to their great biocompatibility, biodegradability, renewability, and long-term stability.[77] In this context, the development of novel bio-based polymers with surface activity is in high demand.[73]

Lignin with the large availability and sustainability has been widely used as polymeric surfactants in the form of lignosulfonate to disperse pesticides, dyes, carbon black and in enhanced oil recovery (EOR) over the past decades.[78] However, there are some obstacles in using LS as surfactants, for one thing, LS has limited ability to reduce the surface tension of the water; therefore, other synthetic surfactants are required to be used with LS as co-surfactants.[79] For another reason, LS production is only 2% of the whole production of lignin worldwide; therefore, a limited supply is available to be used on a large scale.[80] Thus, kraft lignin with large availability could be a better substitution with slight chemical modifications.

Lignin already owns the hydrophobic segment due to the aromatic and aliphatic carbon chains, with limited functional groups such as aliphatic and phenolic OH and carboxylate groups.[73] However limited solubility and charge density (CD) are the main barriers to be effectively implemented as surfactants.

Grafting functionalization with simple processes is suggested as effective alternatives to improve the properties of lignin.[81] Many research studies investigated the effectiveness of such polymers, namely: carboxylated, carboxyethylated, sulfonated, and sulfomethylated lignins as emulsifiers or dispersants in variable systems.[73] Previously, lignin tannic acid (KL-TA)[44] and carboxymethylated lignin (CML)[82] were implemented as polymeric surfactants to stabilize oil-water systems; however, KL-TA and CML had limited affinity to lower the surface tension of water. Therefore, a novel modification to address this issue was needed for better compatibility of lignin-based surfactants at the oil-water interface. In addition, the fundamental understanding of the mechanism and kinetic of adsorption of polymeric lignin surfactants have not been investigated so far.

In this thesis, we introduced a novel polymeric surfactant called SEKL as an effective emulsifier at the oil-water interfaces. Its surface and interfacial properties and behaviors at different systems with variations in polymer dosage, ionic strength and pHs have been investigated comprehensively in this thesis and the reports are available in chapter 5 and 6. A comprehensive literature review on this subject regarding emulsion types and currently used plant-based emulsifiers are provided in chapter 3 as a review paper.

Dispersants are required to be used in clay suspensions to improve their dispersibility and stability of colloidal systems over time.[56] A stable clay colloidal system is critical in various mining, chemical and mineral processing industries as the base material for many formulations such as cosmetics, ceramics paints and coating.[83] The choice of the right dispersant is very crucial since there are many factors that may influence the stability of the suspension. Well-known factors are molecular weight, charge density, and particle size, which could affect the system in many ways.[84] Evaluating the adsorption of polymers at the surface of colloidal particles is the first step of monitoring its performance. Other factors, such as zeta potential of suspension, is important to be considered.

The performance of SEKL as a dispersant for the clay system was also compared with already tested dispersants such as sulfonated and sulfomethylated lignin in chapter 7. Table 1 summarized the already established grafted lignin samples from different sources and modification routes as dispersants for different aqueous suspensions. The most common modification routes for synthesizing effective dispersants are sulfonation and sulfomethylation using kraft or alkali lignin resources. [85-91] However, there is no report for correlating the physicochemical properties and reactivity of HL toward various chemical sulfo-functionalization. The main objective of the last study in this thesis is to correlate the physicochemical properties of different HL samples toward sulfonation, sulfomethylation, and sulfoethylation and the comparison of their performance as clay dispersants.

Table 2.2. Summary of grafted lignin polymers from different sources and modification routes as dispersants for different aqueous suspensions.

Source	Modification	Application	Ref.
Washed aqueous slurry	Sulfonation	Dispersant in dye	[85]
Alkali lignin	Sulfonation	Dispersant for cement particles	[86]

Enzymatic hydrolysis	Sulfomethylation	Dispersion for graphite suspension	[50]
Alkaline, and enzymatic hydrolysis	Sulfomethylation	Dispersant for concrete paste	[87]
Oxidized softwood kraft	Sulfomethylation	Dispersant for cement	[88]
Hardwood kraft	Sulfomethylation	Dispersant for cement	[49]
Alkali	Sulfomethylation	Dispersant for coal–water slurry	[89]
Alkali-corn stalk	Sulfomethylation	Dispersant for dye	[90]
Wheat straw alkali	Sulfomethylation	Dispersion for tio_2	[91]
Alkali	Sulfobutylation	Dispersant for coal-water slurry	[92]
Eucalyptus kraft	Sulfobutylation	Dispersant for dye	[93]
Harwood kraft	Carboxymethylation	Dispersant for clay suspension	[56]
Wheat straw alkali	Carboxymethylation	Dispersant	[94]

2.5 Methodology

2.5.1 Characterization

Proton-1 nuclear magnetic resonance (^{1}H-NMR) analysis of unmodified and modified samples was conducted by dissolving ≈30 mg of each sample and 8 mg of trimethylsilyl propanoic acid (TSP) as an internal standard in 500 mL of appropriate solvent based on solubility (e g. $CDCl_3$, D_2O, DMSO-d_6 or a mixture). After stirring solutions overnight at room temperature, the spectra of samples were recorded by INOVA-500 MHz instrument (Varian, USA) at a 45˚ pulse width with 64 number of scans using 1 s relaxation delay. If required, the areas under the spectra were used for quantitative analysis.

The same method of sample preparation and instrument adjustments were followed for 2D 1H–1H COSY analysis.

The phosphorus-31 NMR (^{31}PNMR) analysis was used for quantitative analysis of phenolic and aliphatic hydroxyl moieties of lignin and lignin-based products. The phosphitylation of samples were conducted with 2-chloro-4,4,5,5-tetramethyl-1,3,2- dioxaphospholane in a mixture of

pyridine and CCl_3D solvent (1.6/1). Cyclohexanol, with the known concentration of 0.20 mmol/mL as the internal standard, and chromium (III) acetylacetonate as the relaxation agent were added to the solution mixture. To acquire a spectrum, a 90 pulse with 5 s relaxation delay and 128 acquisitions with an inverse gated decoupling pulse were employed. Assignments and calculations were followed, as reported previously in the literature.[95] The area under the peaks ranging 150.4-145.5 and 140.3-138.3 ppm were assigned to aliphatic and phenolic hydroxyl moieties in samples, respectively.

2.5.2 Adsorption analysis

Quartz crystal microbalance with dissipation (QCM-D) technique was implemented in this thesis as a sensitive tool for investigating a real-time, label-free measurement of molecular adsorption and/or interactions on various surfaces. Fundamentally, QCM counts on the oscillation of a quartz crystal sensor at a specific frequency provided from an external voltage. It is known from the Sauerbrey relationship that further alterations of the mass on the quartz surface are linked to changes in the frequency of the oscillating crystal, as shown in equation 1:[96]

$$\Delta m = -C\Delta f \qquad (1)$$

where Δm and Δf refer to the mass and frequency changes and C is a constant value, which is related to the physical properties of the sensor (i.e., 0.177 mg/m Hz for a 5 MHz AT-cut quartz crystal). It should be noted that this relationship only applies to rigid, evenly distributed, and sufficiently thin adsorbed layers. In the case of a soft or viscoelastic layer, other methods (e g. Voigt) should be considered.

In addition to the sensitivity for adsorbed mass (ng/cm^2 sensitivity) based on changes in frequency of the quartz crystal, structural (viscoelastic) properties of adsorbed layers are also observable via changes in the dissipation parameter (D). Dissipation occurs when the driving voltage to the crystal is cut off and the energy from the oscillating crystal dissipates from the system. D is defined as:[97]

$$D = E_{lost} / 2\pi E_{stored} \qquad (2)$$

E_{lost} is the energy lost during one oscillation cycle and E_{stored} is the total stored energy in the oscillator.

The oscillating crystal with the changes in voltage is shown in Figure 4a. The high sensitivity of the instrument is associated with the repetition of voltage changes (voltage is applied and turned off) over 100 times per second. Figure 4b shows the signal generated by an oscillating crystal and the differences in signal decay between rigid and viscoelastic materials.

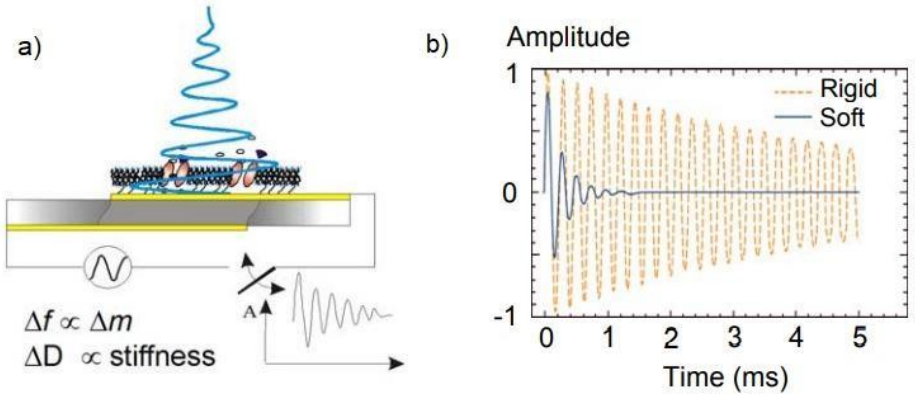

Figure 2.4: a) The oscillating crystal with applied voltage and the shear propagation wave penetrating the adsorbed molecular film, b) the difference in dissipation for rigid and soft (viscoelastic) films. Images from www.q-sense.com.

2.5.3 Surface and interfacial analysis

Surface properties, including wettability and surface energy, are two imperative aspects that express the compatibility of a polymer surface with the surrounding environment and key factors to understand the mechanism of surface-based phenomena. Characterizing the surface properties of polymers based on their thermodynamic properties e g., lifshitz-van der Waals and acid-base determination, hydrophobicity-hydrophilicity balance are important parameters to determine a suitable application. In many industries such as coatings, printing, adhesive, cosmetics, and pharmaceuticals, understanding the surface chemistry of polymers and surfaces is crucial.[98]

For the first-time, the surface energy of the lignin and lignin derivatives was calculated in this thesis, and the changes in surface energy components (polar/nonpolar or acidic/basic) in two different methods of Fowke's and Van Oss theory are compared for the unmodified and polymerized lignin.

In this work, two different methods, Fowke's theory, which explain the surface energy of a solid as containing two components, a "dispersive" and a "non-dispersive" and the Van Oss theory, which divides it into three components, was chosen. In van Oss theory, the dispersive component is the same as Fowke's theory but the non-dispersive one (polar) is divided into acidic and basic components.[99]

Fowke's theory is formed by the combination of three equations: young equation (equation 3), dupre's definition of adhesion energy (equation 4) and Fowke's theory; which describes the

adhesion energy between a solid and a liquid to be divided into the interaction between polar and non-polar components of two phases (equation 5). [100,101]

$$Young's\ equation\quad \sigma_S = \sigma_{SL} + \sigma_L \cos\theta \qquad (3)$$

$$Dupre's\ definition\ of\ adhesion\ energy\quad I_{SL} = \sigma_S + \sigma_L - \sigma_{SL} \qquad (4)$$

$$Adhesion\ energy\ with\ fowkes\ components\quad I_{SL} = 2\sqrt{(\sigma_L^D)(\sigma_S^D) + (\sigma_L^P)(\sigma_S^P)} \qquad (5)$$

In Young's equation, σ_L is the overall surface tension of the wetting liquid, σ_S is the overall surface energy of the solid, σ_{SL} is the interfacial tension between the solid and the liquid, and θ shows the contact angle between the wetting liquid and the solid. In the adhesion energy equation, components are divided based on Fowke's theory to σ_L^D and σ_L^P as the dispersive and polar components of the surface tension in the wetting liquid, and σ_S^D and σ_S^P the dispersive and polar components of the surface energy of the solid material, respectively. Finally, by rearranging these 3 formulas, the final equation for Fowke's theory would be obtained as shown in equation 6. Therefore, surface energy of a solid can be calculated by obtaining the contact angle between the coated solid surface and the polar and non-polar wetting liquids. [102,103]

$$\frac{\sigma_L\,(coscos\,\theta+1)}{2} = \sqrt{(\sigma_L^D)(\sigma_S^D) + (\sigma_L^P)(\sigma_S^P)} \qquad (6)$$

The Van Oss theory is attained by dividing the polar components of the surface to acidic (+) and basic (-), meaning that interaction of the solid surface with the wetting liquid through polar interaction is based on their acidity and basicity. The basic component originates from the ability of the surface to act as a basic by donating electron density through dipole-dipole and hydrogen bonding. However, the acidic component shows the desire of the surface in accepting electron density. By modifying equation 6 by dividing the polar components into acidic and basic, equation 7 is obtained in Van Oss theory as shown in equation bellow. [104-106]

$$\frac{\sigma_L\,(coscos\,\theta+1)}{2} = \sqrt{(\sigma_L^D)(\sigma_S^D) + (\sigma_S^+)(\sigma_L^-) + (\sigma_S^-)(\sigma_L^+)} \qquad (7)$$

Hence, by measuring contact angle values between coated surfaces of lignin and polymerized lignin with the wetting liquids with known dispersive, acidic and basic surface tension values, the solid surface energy can be calculated based on both Fowke's and Van Oss theories. [107,108]

The contact angle analysis was conducted via placing 5µL of liquid droplets on the coated surfaces following static contact angle with the sessile drop and the analysis was performed using a theta optical tensiometer attention (Biolin Scientific) at 25 °C for 30 sec.

For determining the three-phase (OCA) contact angles of a solid surface at an oil-water interface the slides with the water droplet on top of them were transferred to a glass chamber filled with purified oil and the contact angle (i.e., three-phase contact angle) of surface at the oil-water interface was measured accordingly following the work of[109] as depicted in Figure 5.

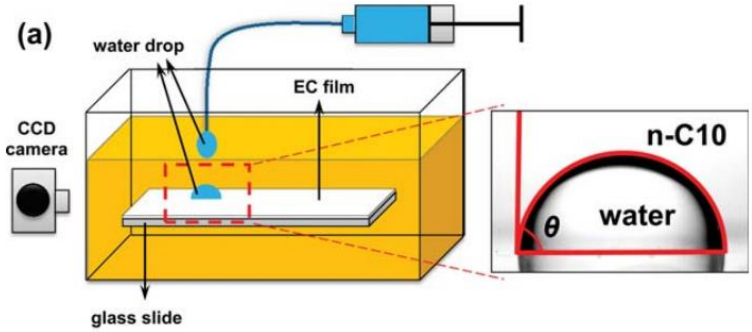

Figure 2.5: measuring the three-phase contact angle of coated slide at oil interface. (Adapted from [109] Copyright © 2017, American Chemical Society).

An Attension Theta Biolin optical tensiometer was implemented following the pendant drop method to measure the dynamic interfacial tension (γ) between lignin derivative as a polymeric surfactant of different concentrations and organic phase.[110] Precisely, 3 mL of organic solvent (i.e., xylene, cyclohexane, decane) was charged to a Quartz cuvette and sealed to minimize volume loss. The SEKL solution with different concentrations was charged to the syringe that was connected to a stainless-steel needle with an inner diameter of 0.84 mm. Before each experiment, the needle was cleaned with Milli-Q water and dried. The needle was submerged 1 mm into the oil phase, and an aqueous SEKL droplet with a constant volume of 5 µL was generated at the tip of the needle. While the chamber was illuminated from the back side with an optic lamp, a video camera captured the images from the front side over 3600 sec at a frame rate of 10 images per second in the first 600 sec and 1 image per minute in the last 3000 sec. The interfacial tensions were calculated from the shapes analysis of droplets using the Young-Laplace equation.[110]

2.5.4 Stability analysis

The destabilization behaviour of the emulsion systems in this thesis was studied using a centrifugal separation analyser (CSA) LUMiSizer 6100-29 (L.U.M. GmbH Berlin). This instrument simultaneously detects the intensity of the transmitted light of a NIR light source (λ of 880 nm) as a function of time and position over the entire sample cell length, while being subjected to centrifugation using STEPtechnology (space and time-resolved extinction profiles technology). A

CCD-line detector within the instrument records the distribution of local transmission over the entire sample length to define the stability of the system. Finally, space and time-resolved transmission profiles are obtained, from which the integral value indicates the sedimentation progress with time.[111]

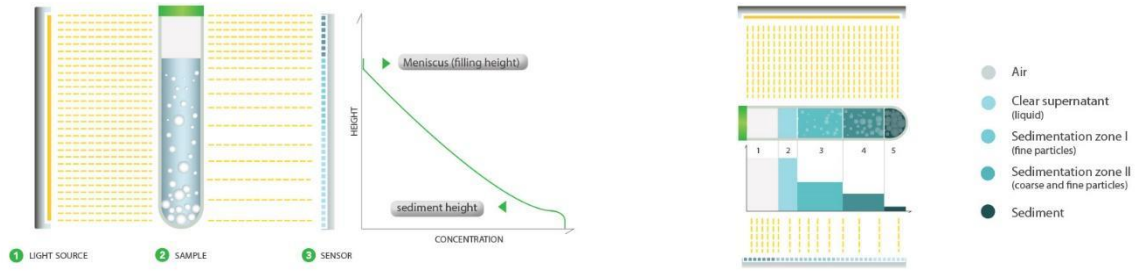

Figure 2.6: STEP-Technology basic scheme from https://www.lum-gmbh.com/

A vertical scan analyzer (Turbiscan Lab Expert, Formulaction, France) was also used to monitor the stability of emulsions and clay suspensions. The samples were prepared inside the glass container of the instrument and subjected to analysis. The entire height of the sample was scanned with a pulsed near-infrared light (λ = 880 nm) and the transmitted and backscattered lights were record by the detectors in which a microscopic fingerprint of the samples could be presented at a given time.

The stability of samples can be presented quantitively by term of instability index (TSI), where both coalescence and settling phenomena are considered in TSI evaluation. The TSI is determined by equation 8.

$$TSI = \sqrt{\frac{\sum_{i-1}^{n} (x_i - x_{bs})^2}{n-1}} \qquad (8)$$

Where n, xi, xbs, refer to the number of scanning, an average of the backscattered light intensity at the scanning time, and the average of x_i, respectively. The higher the TSI, the lower the stability is.[44]

2.6 References

[1] W. Boerjan, J. Ralph, M. Baucher, *Annu. Rev. Plant Biol.* **2003**, *54*(1), 519-546.

[2] W. Yang, E. Fortunati, D. Gao, G. M. Balestra, G. Giovanale, X. He, L. Torre, J. M. Kenny, D. Puglia, *ACS Sustainable Chem. Eng.* **2018**, *6*(3), 3502-3514.

[3] J. L. Espinoza-Acosta, P. I. Torres-Chávez, B. Ramírez-Wong, C. M. López-Saiz, B. Montaño-Leyva, *Bioresources* **2016**, *11*(2), 5452-5481.

[4] J. Ralph, K. Lundquist, G. Brunow, F. Lu, H. Kim, P. F. Schatz, J. M. Marita, R. D. Hatfield, S.A. Ralph, J. H. Christensen, *Phytochem Rev.* **2004**, *3*(1-2), 29-60.

[5] A. E. Kazzaz, P. Fatehi, Technical lignin and its potential modification routes: A mini-review, *Ind. Crops Prod.* **2020**, *154*, 112732-112745.

[6] F. S. Chakar, A. J. Ragauskas, *Ind. Crops Prod.* **2004**, *20*(2), 131-141.

[7] A. Van Heiningen, *Pulp Pap. Canada* **2006,** *107*(6), 38-43.

[8] A. E. Rodrigues, P. C. d. O. R. Pinto, M. F. Barreiro, C. A. E. da Costa, M. I. F. da Mota, I. Fernandes, Chemical Pulp Mills as Biorefineries, An Integrated Approach for Added-Value Products from Lignocellulosic Biorefineries, Springer **2018**, 1-51.

[9] L. Dessbesell, M. Paleologou, M. Leitch, R. Pulkki, C. C. Xu, *Renew. Sust. Energ. Rev.* **2020,** *123*, 109768-109779.

[10] D. Kai, M. J. Tan, P. L. Chee, Y. K. Chua, Y. L. Yap, X. J. Loh, *Green Chem.* **2016,** *18*(5), 1175-1200.

[11] Y. Sun, J. Cheng, A review, *Bioresour. Technol.* **2002**, *83*(1), 1-11.

[12] J. Cho, S. Chu, P.J. Dauenhauer, G.W. Huber, *Green Chem.* **2012**, *14*(2), 428-439.

[13] F. Menezes, G. Rocha, R. Maciel Filho, *Chem. Eng. Trans.* **2016**, *50*, 397-402.

[14] F. Xu, Structure, ultrastructure, and chemical composition, Cereal straw as a resource for sustainable biomaterials and biofuels. Amsterdam, the Netherlands: Elsevier **2010**, 9-47.

[15] K. M. Holtman, An Investigation of the Milled Wood Lignin Isolation Procedure by Solution- and Solid-State NMR Spectroscopy, Dissertation **2004**.

[16] O. Derkacheva, D. Sukhov, *Macromol. Symp.* **2008**, *265*(1), 61-68.

[17] M. Sipponen, Effect of lignin structure on enzymatic hydrolysis of plant residues, Dissertation **2015**.

[18] B. M. Upton, A. M. Kasko, *Chem. Rev* **2016**, *116*(4), 2275-2306.

[19] C. Xu, R. A. D. Arancon, J. Labidi, R. Luque, *Chem. Soc. Rev.* **2014**, *43*(22), 7485-7500.

[20] C. Li, X. Zhao, A. Wang, G. W. Huber, T. Zhang, *Chem. Rev* **2015**, *115*(21), 11559-11624.

[21] P. Azadi, O. R. Inderwildi, R. Farnood, D. A. King, A critical review, *Renew. Sust. Energ. Rev.* **2013**, *21*, 506-523.

[22] P. Figueiredo, K. Lintinen, J. T. Hirvonen, M. A. Kostiainen, H. A. Santos, *Prog. Mater. Sci.* **2018**, *93*, 233-269.

[23] I. Norberg, Carbon fibres from kraft lignin, KTH Royal Institute of Technology, **2012**.

[24] B. Joffres, D. Laurenti, N. Charon, A. Daudin, A. Quignard, C. Geantet, A review, *Oil Gas Sci. Technol. 68*(4) (2013) 753-763.

[25] M. Ek, G. Gellerstedt, G. Henriksson, Wood chemistry and biotechnology, Walter de Gruyter **2009**.

[26] D. Tarasov, M. Leitch, P. Fatehi, A review, *Biotechnol. Biofuels* **2018**, *11*(1), 269-297.

[27] M. Balakshin, E. Capanema, H. Gracz, H. m. Chang, H. Jameel, Planta **2011**, *233*(6), 1097-1110.

[28] P. Albersheim, A. Darvill, K. Roberts, R. Sederoff, A. Staehelin, Plant cell walls, Garland Science **2010**.

[29] J. Zakzeski, P.C. Bruijnincx, A.L. Jongerius, B.M. Weckhuysen, *Chem. Rev* **2010**, *110*(6), 3552-3599.

[30] S. Laurichesse, L. Avérous, *Prog. Polym. Sci* **2014**, *39*(7), 1266-1290.

[31] A. Mathias, A. Rodrigues, *Holzforschung* **1995**, *49*(3), 273-278.

[32] S. Kalami, N. Chen, H. Borazjani, M. Nejad, *Ind. Crops Prod.* **2018**, *125*, 520-528.

[33] R. Fang, X. Cheng, X. Xu, *Bioresour. Technol.* **2010**, *101*(19), 7323-7329.

[34] D. Bajwa, G. Pourhashem, A. Ullah, S. Bajwa, *Ind. Crops Prod.* **2019**, *139*, 111526-111537.

[35] F. Kong, S. Wang, W. Gao, P. Fatehi, *RSC adv* **2018**, *8*(22), 12322-12336.

[36] R. Fang, X. S. Cheng, J. Fu, Z. B. Zheng, *J. Nat. Sci.* **2009,** *1*(1), 17-22.

[37] F. Kong, S. Wang, J. T. Price, M. K. Konduri, P. Fatehi, *Green Chem.* **2015,** *17*(8), 4355-4366.

[38] S. Sabaghi, P. Fatehi, *Biomacromolecules* **2019**, *20*(10), 3940-3951.

[39] A. Hasan, P. Fatehi, *J. Appl. Polym. Sci.* **2018**, *135*(23), 46338-46349.

[40] B. Podkościelna, M. Sobiesiak, Y. Zhao, B. Gawdzik, O. Sevastyanova, *Holzforschung* **2015**, *69*(6), 769-776.

[41] C. Wang, R. A. Venditti, *ACS Sustainable Chem. Eng.* **2015,** *3*(8), 1839-1845.

[42] S. L. Hilburg, A. N. Elder, H. Chung, R. L. Ferebee, M. R. Bockstaller, N. R. Washburn, *Polymer* **2014**, *55*(4), 995-1003.

[43] A. Ayoub, R. A. Venditti, H. Jameel, H. M. Chang, *J. Appl. Polym. Sci.* **2014**, *131*(1) 39743-39753.

[44] S. Gharehkhani, N. Ghavidel, P. Fatehi, *ACS Sustainable Chem. Eng.* **2018**, *7*(2), 2370-2379.

[45] I. Kühnel, B. Saake, R. Lehnen, *Macromol. Chem. Phys.* **2018**, *219*(7), 1700613-1700619.

[46] A. Sequeiros, L. Serrano, J. Labidi, *J. Chem. Technol. Biotechnol.* **2016,** *91*(6), 1809-1815.

[47] T. Zheng, D. Zheng, X. Li, C. Cai, H. Lou, W. Liu, X. Qiu, *ACS Sustainable Chem. Eng.* **2017**, *5*(9), 7743-7750.

[48] K. Bahramia, P. Fatehi, *ChemSusChem* **2018**, *11*(17), 2967-2980.

[49] M. K. Konduri, P. Fatehi, *ACS Sustainable Chem. Eng.* **2015**, *3*(6), 1172-1182.

[50] B. Zhang, D. Yang, H. Wang, Y. Qian, J. Huang, L. Yu, X. Qiu, *ACS Sustainable Chem. Eng.* **2018**, *7*(1), 1120-1128.

[51] J. Tian, S. Ren, G. Fang, Y. Ma, Q. Ai, *Bioresources* **2014,** *9*(4), 6290-6303.

[52] Y. Chen, H. Zhang, Z. Zhu, S. Fu, *Int. J. Biol. Macromol*. **2020,** *152*, 775-785.

[53] E. Cortés-Triviño, C. Valencia, M.A. Delgado, J.M. Franco, *Polymers* **2018**, *10*(6), 670-684.

[54] C. Chen, M. Zhu, M. Li, Y. Fan, R. C. Sun, *Biotechnol. Biofuels* **2016,** *9*(1), 1-15.

[55] M. Ataie, K. Sutherland, L. Pakzad, P. Fatehi*, Sep. Purif. Technol.* **2020,** *247,* 116944-116954.

[56] M. K. Konduri, F. Kong, P. Fatehi, *Eur. Polym. J.* **2015**, *70,* 371-383.

[57] M. Vafaeezadeh, M. M. Hashemi, N. Ghavidel, *RSC adv* **2016,** *6*(17), 14128-14133.

[58] Y. Ge, Z. Li, A review, *ACS Sustainable Chem. Eng.* **2018,** *6*(5), 7181-7192.

[59] F. Fu, Q. Wang, A review, *J. Environ. Manage.* **2011,** *92*(3), 407-418.

[60] W. Jin, Z. Zhang, G. Wu, R. Tolba, A. Chen, *RSC Adv* **2014,** *4*(53), 27843-27849.

[61] T. Todorciuc, L. Bulgariu, V.I. Popa, *Cell Chem Technol* **2015**, *49*, 439-447.

[62] X. Guo, S. Zhang, X. q. Shan, *J. Hazard. Mater.* **2008,** *151*(1), 134-142.

[63] J. Chen, G. Cheng, Y. Chai, W. Han, W. Zong, J. Chen, C. Li, W. Wang, L. Ou, Y. Yu, *Colloids Surf. B: Biointerfaces* **2018,** *161*, 480-487.

[64] J. Zhou, F. Gao, T. Jiao, R. Xing, L. Zhang, Q. Zhang, Q. Peng, *Colloids Surf. A Physicochem. Eng. Asp.* **2018,** *545,* 60-67.

[65] Z. Yang, C. Zhou, H. Yang, T. Cai, J. Cai, H. Li, D. Zhou, B. Chen, A. Li, R. Cheng, *Ind. Eng. Chem. Res.* **2012,** *51*(27), 9204-9212.

[66] Y. Zhang, Y. Chen, C. Wang, Y. Wei, *J. Hazard. Mater.* **2014**, *276*, 129-137.

[67] L. J. Barbour, S. L. De Wall, E. S. Meadows, G. W. Gokel, *Ind. Eng. Chem. Res.* **2000,** *39*(10), 3436-3441.

[68] N. Javkhlantugs, H. Bayar, C. Ganzorig, K. Ueda, *Int. J. Nanomedicine* **2013,** *8,* 2487-2496.

[69] M. Keiluweit, M. Kleber, *Environ. Sci. Technol.* **2009**, *43*(10), 3421-3429.

[70] W. Chen, L. Duan, L. Wang, D. Zhu, *Environ. Sci. Technol.* **2008,** *42*(18), 6862-6868.

[71] W. L. Jorgensen, D. L. Severance, *J. Am. Chem. Soc.* **1990**, *112*(12), 4768-4774.

[72] S. C. Ringwald, J. E. Pemberton, *Environ. Sci. Technol.* **2000,** *34*(2), 259-265.

[73] N. Alwadani, P. Fatehi, *CRC* **2018**, *1*(2), 126-138.

[74] L. L. Schramm, E. N. Stasiuk, D. G. Marangoni, *Annu. Rep. Prog. Chem., Sect. C: Phys. Chem.* **2003,** *99*, 3-48.

[75] E. L. Crepaldi, P. C. Pavan, J. Tronto, J. B. Valim, *J. Colloid Interf. Sci.* **2002**, *248*(2), 429-442.

[76] C. C. Chang, R. Letteri, R. C. Hayward, T. Emrick, *Macromolecules* **2015,** *48*(21), 7843-7850.

[77] S. Kalliola, E. Repo, V. Srivastava, F. Zhao, J. P. Heiskanen, J. A. Sirviö, H. Liimatainen, M. Sillanpää, *Langmuir* **2018,** *34*(8), 2800-2806.

[78] S. Hong, J. Bae, G. Lewis, *SPE Reserv. Eng.* **1987**, *2*(01), 17-27.

[79] L. I. Tolosa, A. J. Rodríguez-Malaver, A. M. González, O. J. Rojas, *J. Colloid Interf. Sci.* **2006,** *294*(1), 182-186.

[80] M. Österberg, M. H. Sipponen, B. D. Mattos, O. J. Rojas, *Green Chem.* **2020**, *22*(9), 2712-2733.

[81] A. E. Kazzaz, Z. H. Feizi, P. Fatehi, *Green Chem.* **2019**, *21*(21), 5714-5752.

[82] S. Li, J. A. Willoughby, O. J. Rojas, *ChemSusChem* **2016**, *9*, 2460-2469.

[83] A. Hasan, P. Fatehi, *Appl. Clay Sci.* **2018,** *158,* 72-82.

[84] D. Y. Hopa, P. Fatehi, *Polymers* **2020**, *12*(9), 2046-20647.

[85] P. Dilling, Selective crosslinking of low molecular weight sulfonated lignins and lignosulfate products produced thereby, Google Patents, **1985**.

[86] X. Ouyang, L. Ke, X. Qiu, Y. Guo, Y. Pang, *J Dispers. Sci. Technol.* **2009,** *30*(1), 1-6.

[87] C. Huang, J. Ma, W. Zhang, G. Huang, Q. Yong, *Polymers* **2018,** *10*(8), 841-853.

[88] W. He, P. Fatehi, *Rsc Adv* **2015,** *5*(58), 47031-47039.

[89] Y. Qin, D. Yang, W. Guo, X. Qiu, *Ind. Eng. Chem. Res* **2015,** *27*, 192-200.

[90] H. Wu, F. Chen, Q. Feng, X. Yue, *Bioresources* **2012,** *7*(3), 2742-2751.

[91] H. Zhou, Y. Chang, X. Wu, D. Yang, X. Qiu, *ACS Sustainable Chem. Eng.* **2015,** *3*(3), 518-523.

[92] X. Qiu, W. Zeng, W. Liang, Y. Xue, N. Hong, Y. Li, *J Dispers. Sci. Technol.* **2016,** *37*(4), 472-478.

[93] H. Zhang, B. Yu, W. Zhou, X. Liu, F. Chen, *Int. J. Biol. Macromol.* **2018,** *109*, 1232-1238.

[94] L. H. Gan, M. S. Zhou, X. Q. Qiu, *Adv. Mater. Res., Trans Tech Publ,* **2012,** 55, 1293-1298.

[95] Y. Pu, S. Cao, A. J. Ragauskas, *Energy Environ. Sci.* **2011**, *4*(9), 3154-3166.

[96] E. Irwin, J. Ho, S. Kane, K. Healy, *Langmuir* **2005,** *21*(12), 5529-5536.

[97] F. Höök, B. Kasemo, T. Nylander, C. Fant, K. Sott, H. Elwing, *Anal. Chem.* **2001,** *73*(24), 5796-5804.

[98] M. Żenkiewicz, J. Achiev. *Mater. Manuf. Eng.* **2007,** *24*(1), 137-145.

[99] C. Della Volpe, D. Maniglio, M. Brugnara, S. Siboni, M. Morra, *J. Colloid Interf. Sci.* **2004,** *271*(2), 434-453.

[100] F. M. Fowkes, W. A. Zisman, Contact angle, wettability, and adhesion, **1964**.

[101] D. E. Packham, *Int J Adhes Adhes* **2003,** *23*(6), 437-448.

[102] G. Navascues, *Rep. Prog. Phys* **1979,** *42*(7), 1131-1190.

[103] J. Spelt, D. Absolom, A. Neumann, *Langmuir* **1986,** *2*(5), 620-625.

[104] D. K. Owens, R. Wendt, *J. Appl. Polym. Sci.* **1969,** *13*(8), 1741-1747.

[105] G. Fourche, *Polym. Eng. Sci.* **1995,** *35*(12), 957-967.

[106] C. Van Oss, R. Good, M. Chaudhury, *J. Colloid Interf. Sci.* **1986**, *111*(2), 378-390.

[107] C. Van Oss, R. Good, M. Chaudhury, *Langmuir* **1988,** *4*(4), 884-891.

[108] C. J. Van Oss, M. K. Chaudhury, R. *J. Good, Chem. Rev* **1988,** *88*(6), 927-941.

[109] N. Bizmark, M. A. Ioannidis, *Langmuir* **2017**, *33*(40), 10568-10576.

[110] J. Bi, F. Yang, D. Harbottle, E. Pensini, P. Tchoukov, S.b. Simon, J. Sjöblom, T. Dabros, J. Czarnecki, Q. Liu, *Langmuir* **2015**, *31*(38), 10382-10391.

[111] U. Staudinger, B. Krause, C. Steinbach, P. Pötschke, B. Voit, *Polymer* **2014**, *55*(24), 6335-6344.

Chapter 3: Strategies for emulsion stabilization using polymers and particles of plant-based biomaterials

3.1 Abstract

As the main aim of this review chapter, we articulated the recent progress in the use of plant-based polymers and particles for the stabilization of Pickering and non-Pickering emulsion systems. Due to their availability and promising performance, we discussed how the source, modification, and formulation of cellulose, starch, protein, and lignin-based polymers and particles would impact their emulsion stabilization. Special attention was given toward the material synthesis in two forms of polymeric surfactants and particles and the corresponding formulated emulsions. Also, the effects of particle size, degree of aggregation, wettability, degree of substitution, and electrical charge in stabilizing oil/water systems and micro and macro structures of oil droplets were discussed. The wide range of applications using such plant-based stabilizers in different technologies, and their challenge and future perspectives were described.

3.2 Introduction

Emulsions play a major role in the formulation of processed foods, personal care goods, agrochemical, and pharmaceutical products. Emulsifiers have been utilized in a wide range of industries to create such stable emulsions with appropriate shelf lives and functional features. The industrial stabilizers are mostly synthetic surfactants, such as tweens and spans,[1] or animal-based emulsifiers for food purposes such as gelatins, egg protein, and whey protein.[2] Due to the worldwide demand and strong motivation for plant-based natural ingredients, many manufacturers have been reformulating their products to replace synthetic[3] or animal origin surfactants with green alternatives,[4,5] while biocompatibility of the green surfactants is increasingly regarded as a major challenge.[6]

The most common and available plant-based resources that have been implemented for emulsion stabilization are polysaccharides, such as cellulose and starch; aromatic macromolecules, such as lignin; and polypeptides, such as proteins. These materials are considered biocompatible due to their natural origin and have shown promising capability in stabilizing emulsions as reported in several review papers dealing with natural emulsifiers,[7] particles of biological origin,[8] naturally derived or biodegradable particles,[9] or plant-based particles intended for food applications. However, sensible progress has been achieved on this topic recently, and the prevision articles lack the latest development on this area.[10] Other review papers using natural emulsifiers are do not

include discussion on the material source and application, e.g., lignocelluloses[11] cellulose[12] protein[13] or food Pickering application.[14]

With given such attention to plant-based emulsifiers, there is still a gap in material production mainly through chemical modifications and particle formulations. Many of the potential materials, such as proteins and lignin, have been undermined for years in emulsion systems due to their poor aqueous dispersibility and strong aggregation tendency.[14] However, surface modification, functionalization, and particle formulation have altered their functionality for different applications.[15-17] Despite their long history as emulsifiers; starch and cellulose, can be further modified to enhance their emulsifying properties and long-term stability. The main reason for the modification of such materials is to alter their particle size, wettability, and dispersibility in the continuous phase to optimize their interaction at the interface and provide stability to the system.

Therefore, the focus of this chapter is to articulate a comprehensive overview of the chemical modification of plant-based polymeric compounds and particles and their direct effects on the stabilization of emulsions. The attention of this article is on both Pickering/non-Pickering emulsions.[18] The chapter starts with a brief introduction about the different methods of droplet stabilization (Pickering/non-Pickering), and the sources and isolation methods for the four different plant-based materials. Furthermore, we directed our attention to how two types of polymer and particle formulations would impact the oil droplet size, phase separation, coalescence, viscosity, or interfacial tension changes of emulsions. In the end, the application of formulated emulsions in different technologies is reviewed.

3.3 Pickering/Non-Pickering Theory of Stabilization

3.3.1 Non-Pickering Emulsions

Mixing two immiscible phases, i.e., oil and water, requires high energy to create an interface; otherwise, the two phases tend to reduce their contact to make the system thermodynamically stable. The Gibbs free energy of the system (ΔG, J) is defined as (Equation 1):[10]

$$\Delta G = \gamma . \Delta A \quad (1)$$

Where γ (N/m) is the interfacial tension between oil and water, and ΔA (m^2) is the total interfacial area in the system. To obtain a stable oil and water mixture, i.e., emulsion, emulsifiers are required to decrease the interfacial tension between the two phases, thereby lowering the free energy of the system (equation 1). The role of emulsifiers is to first adsorb at the oil-water interface and then lower the interfacial tension to facilitate the generation of fine droplets. Then, it should maintain

the stability of oil/water droplets once they have been formed by generating a coating layer at the oil droplets.[7,19] This layer could prevent the aggregation of oil droplets via electrostatic interactions (in this case charged emulsifiers) and/or from physical steric barrier interactions, as displayed in Fig. 1.[7, 20,21] Insufficient or short-lasting repulsive forces would cause weak flocculation, strong flocculation, or coalescence depending on the nature of the emulsifier layer at the interface and its resistance to disruption. Electrostatically stabilized emulsions are known to be highly sensitive to the changes in pH and ionic strength, e.g., proteins, phospholipids, and ionic surfactants.[10,22] On the contrary, those, such as amphiphilic polysaccharides, primarily stabilized by steric repulsion are less sensitive to changes in environmental conditions.[7,23]

Natural-based polymers, such as proteins[24,25] or macromolecules, like starch and lignin, are polymers with a strong affinity for one of the phases (soluble in one phase) and can bring electrostatic and steric repulsion or both for oil droplets.[26,27] The emulsion formulated using the above emulsifiers is called non-Pickering or conventional emulsions.

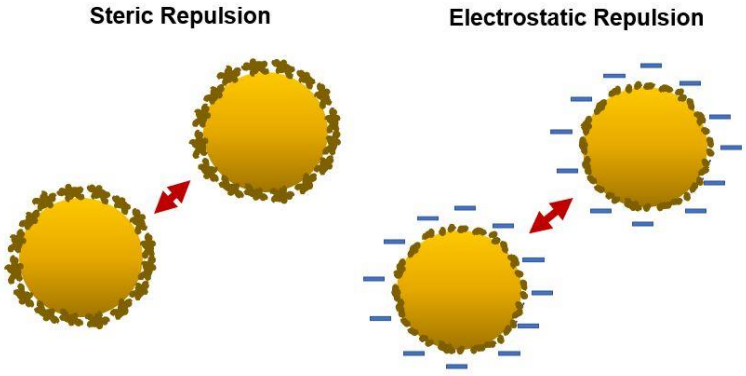

Figure 3.1: Two different mechanisms of oil droplet stabilization with uncharged and charged natural polymers. (Adapted from Ref. [7] with permission of Elsevier).

3.3.2 Pickering Emulsion

The other category of emulsions is called Pickering emulsions and they are stabilized in the presence of solid colloidal particles that are partly wetted by oil and water (Ramsden[28] and Pickering[29]). Considerable interests have been rising over the past decade for the use of particles as stabilizers due to the substantial stabilizations they introduced to the system.[30,31]

A distinctive characteristic of Pickering emulsions, compared to the conventional emulsion, is the formation of a flexible but robust layer upon the adsorption of solid particles at the liquid-liquid

interface,[6] which makes its attachment irreversible due to the considerable energy associated with its adsorption according to Equation 2:[30]

$\Delta E = \pi r^2 \gamma (1 - |\cos \theta|)^2$ (2)

where r is the particle radius (m), γ is the interfacial tension between pristine oil and water (N/m), and θ is the contact angle of particles at the oil-water interface.[30] As depicted in Fig. 2a, if the solid particle has a contact angle below 90˚, they become wet preferably by the water phase, leading to an oil-in-water (O/W) emulsion. By contrast, if the particles have a contact angle larger than 90˚, they are primarily located in the oil phase and a water-in-oil emulsion (W/O) is obtained.[32,33] Based on equation 2 and as depicted in Fig. 2b, the magnitude of this energy is dependent on the particle size and wettability.[10,34,35] The contour plot of adsorption energies in Fig. 2b depicts that various combinations of the contact angle and the size of the particles are feasible to optimize the adsorption energy, and it is not restricted to neutral contact angle (θ=90˚) and nanometer-size particles.[35,36] However, generally too hydrophobic or too hydrophilic particles are not of interest, because it requires large size particles to obtain high detachment energy, which ultimately increases the size of emulsion droplets that are unlikely to stay stabilized.[6,10,35] Based on the stokes law, a larger droplet size is strongly correlated with lower emulsion stability.[10,37,38] Also, generating particles of small size is often an objective as it reduces the amount of emulsifier required for stabilizing droplets.[6,35]

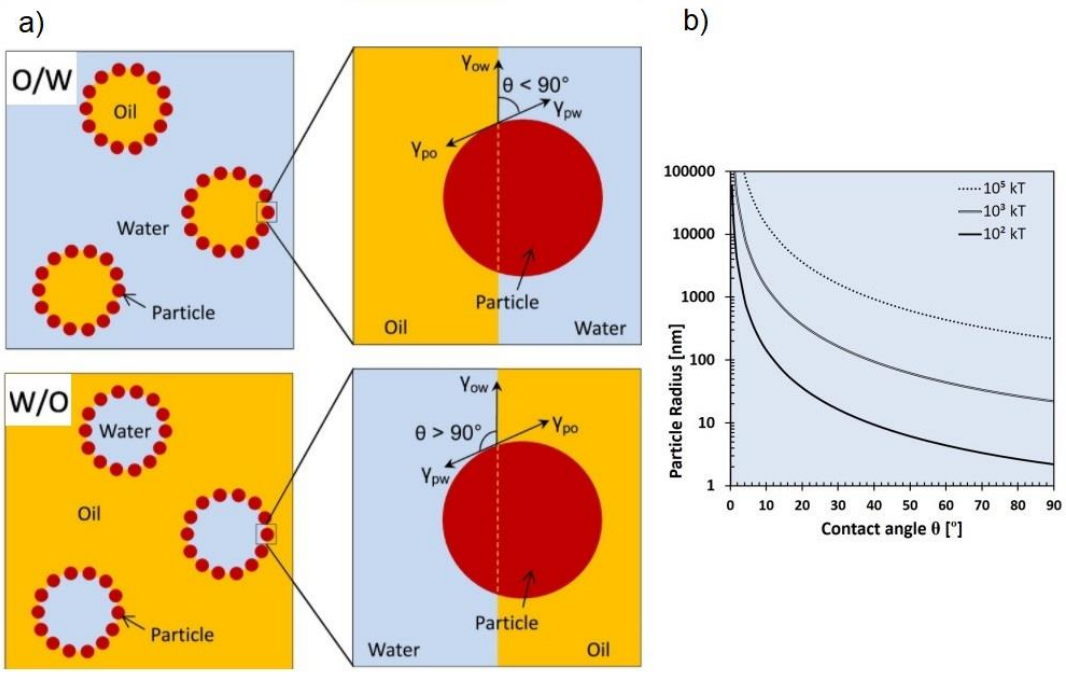

Figure 3.2: (a) Schematic representation of an O/W and a W/O Pickering emulsion at microscopic, and nanoscopic scales (Adapted from Ref. [33] with permission of Elsevier). (b) Contour plot of equal detachment energy (ΔG/kT) for various particle radii and contact angle combination (Adapted from Ref. [35] with permission of Elsevier).

3.4 Plant-Based Biomaterials-Resources and Structural Characteristics

3.4.1 Nanocellulose materials

Plant-based nano cellulose can be classified into two main categories namely: cellulose nanofibers (CNFs) and cellulose nanocrystals (CNCs).[39,40] Plant-based natural sources of cellulose are wood and agricultural processing wastes.[41,42] Chemically, the crystalline regime of cellulose is formed of a linear homopolymerized monomer, named anhydro glucose unit (AGU), bearing three hydroxyl groups that are linked by β-1-4-linkages with a varying degrees of polymerization (DP).[43-45]

Cellulose nanofibers (CNFs) are isolated using a mechanical disintegration process of cellulose fibers, such as high-pressure homogenization, micro fluidization, grinding, and ultrasonication.[46-48] Generally, the mechanical deconstruction process of pulp is often used in combination with some pre-treatments to reduce the energy requirements, which could be an optional (2,2,6,6-tetramethylpiperidine-1-oxyl radical) TEMPO-mediated oxidation or chemical/enzymatic processes to facilitate fibrillation.[49-51] The CNFs contain crystalline and amorphous areas with flexible fibrous with a diameter of less than 100 nm and a length of 500 nm or longer.[52,53]

As the second category, cellulose nanocrystals (CNCs), also named nanocrystalline cellulose, are obtained via the cleavage of the amorphous domains of cellulose fibers through acidic hydrolysis (H_2SO_4, HCl, H_3PO_4, HNO_3) or enzymatic treatment.[54-57] Produced particles are highly crystalline (with the degree of crystallinity between 54 and 88%) with broadly rod- or needle-shape particles with the size of 10-30 nm in diameter and several hundred nanometers in length.[52,58-60]

The use of CNC and CNF in different applications is associated with distinctive results, which makes them ideal candidates for a variable application such as, foods, cosmetics, pharmaceutics, and composites.[61-64]

3.4.2 Starch

Starch is the most abundant polysaccharide synthesized naturally as insoluble, semi-crystalline granules in plant roots, stalks, crop seeds, and staple crops such as rice, corn, wheat, tapioca, and potato.[65] The commercial isolation process of starch from botanical sources consists of extraction and refining by wet grinding, sieving, and drying.[66,67] Chemically, the polymers of starch, i.e., amylose and amylopectin, are composed of several monosaccharides or sugar (glucose) molecules that are linked together with -α-D-(1-4) and/or -α-D-(1-6) linkages.[68] Starch can be used either as is, which is called "native starch", or undergoes chemical modifications to reach specific properties, which is called "modified starch".[68,69]

Synthesis of starch nanoparticles (SNPs) and nanocrystals (SNCs) gained attention along with recent interests in nanomaterials formulation, which further enhanced starch application.[70,71] Starch nanocrystals (SNCs) form from the disruption of amorphous domains from semi-crystalline granules by physical treatments and acid hydrolysis.[72] The main differences between the SNCs and SNPs are the relative crystallinity and morphology.[73] The crystallinity of the SNCs is significantly higher than the crystallinity of the native starch, while the crystallinity of the SNPs is lower than that of native starch.[73] In addition, SNP is spherical, while SNC is platelet-like.[74] Starch has a long history in human diet patterns as it is non-toxic, non-irritant, and edible.[75] As a result, it has a wide application in the food industry as an ingredient, emulsifier, and thickener.[65,69,71]

3.4.3 Proteins

Plant-based proteins are naturally produced in soybeans, pulses (e.g., pea, chickpea, and lentil), and cereals (e.g., wheat, barley, and zein) for the storage of amino acids.[76] The strings of amino acid units covalently linked by peptide bonds create proteins, which are physiochemically varied depending on the type, number, and sequence of amino acids in the polypeptide chain.[7,77] The extraction of plant proteins is followed according to the classical method of Osborne, which is based on the sequential extraction of proteins in water (albumins), dilute salt solutions (globulins), alcohol-aqueous mixtures (prolamins), and dilute acids or alkalis (glutelins).[10,14,78]

Proteins extracted from crops, such as soybeans, corn, and wheat, are commonly generated as by-products of edible oil, starch, or other food processing products.[13] Most proteins are amphiphilic molecules containing a mixture of polar and non-polar amino acids, which are applied in emulsification, gelation, foaming, and as ingredients in the food industry.[13,79-81] The preparation

of protein particles for altered applications, such as drug delivery, encapsulation, and food emulsions, has gained popularity over the past few years.[82-87]

3.4.4 Lignin

Lignin is a natural aromatic and heterogeneous biomacromolecule that accounts for 20-30% of dry weight of biomass, which is produced as a by-product from the chemical liberation of wood fibers (cellulose and hemicellulose) in the pulping process.[88,89] Polymeric lignin is commonly known to shape from the irregular radical oxidative coupling of three basic phenylpropane monomers: p-coumaryl alcohol, coniferyl alcohol and sinapyl alcohol. The repeating alcoholic units[90] form p-hydroxyphenyl (H), guaiacyl (G) and syringyl (S) polymerized products, respectively.[91] Lignin structure depends on the source (hardwood, softwood or non-wood) as well as the applied pulping and isolation process (sulfite, kraft, soda and organosolv pulping processes).[92-95] The main differences in the isolated lignin products appear in its functional group contents, such as the phenolic and aliphatic hydroxyl, carboxyl, and sulfonate groups.[96-98] Recently, nano-scaled lignin particles have gained considerable interest as solutions to overcome many of the obstacles that have impeded the efficient and broad utilization of lignin.[99-101]

3.5 Strategies for Emulsion Stabilization

3.5.1 Polymeric Surfactants

Two main components of polymeric surfactants are hydrophilic and hydrophobic moieties that provide them with surface-active properties.[102,103] The water-soluble polymers effectively reduce intermolecular forces between solvent molecules, thereby reducing surface or interfacial tension upon their adsorption at the interface.[104] In this section, the latest modifications of polymeric plant-based materials, which were used in emulsifications studies, are reviewed. Also, the impact of their properties, such as polymer size, grafting ratio, and solubility, on the emulsion properties including droplet size, zeta potential, viscosity, or interfacial tension alterations are evaluated.

3.5.1.1 Cellulose Derivatives

Cellulose was proved to be a potentially efficient emulsifier.105 The most common derivatives of cellulose implemented as emulsifiers are the cellulose ethers, e.g., methyl cellulose (MC), ethyl cellulose (EC), hydroxyethyl cellulose (HEC), hydroxypropyl cellulose (HPC), hydroxyethyl methylcellulose (HEMC), hydroxypropyl methylcellulose (HPMC) and carboxymethyl cellulose (CMC) (Fig. 3) that are currently produced commercially.[105-107] In this case, their synthesis and chemistry has been widely reviewed previously.[108-110] The derivatives with different alkyl chains

are most often water-soluble and, therefore, useful as stabilizers for immiscible oil-water systems.[106,111] Latest studies on the application of such emulsifiers are summarized in Table 1 and discussed below.

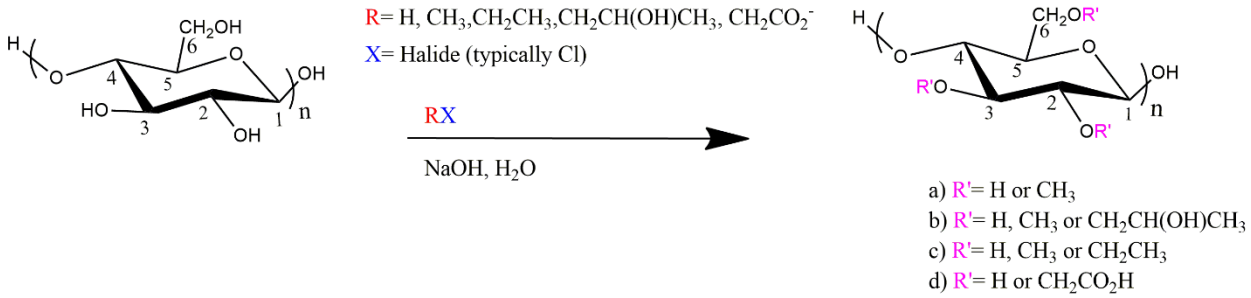

Figure 3.3: structure of cellulose derivatives with (a) methyl, (b) hydroxypropyl methyl, (c) methyl ethyl, and (d) carboxymethyl groups reacted with different alkyl halides. Reprinted with permission from [108]. Copyright (2020) American Chemical Society.

Cellulose ethers are usually used as additive emulsifiers and are known to effectively enhance viscosity, which is associated with oil droplet stabilization through the steric mechanism.[112] For instance, sodium carboxymethylcellulose (CMCNa) was reported to be used as an additive emulsifier in the presence of Tween 20, Tween 80 or sodium caseinate for emulsion formulations,[113-115] which greatly inhibited creaming and coalescence by decreasing oil droplet size and improving emulsion viscosity.[113]

Hydroxypropyl methylcellulose, HPMC, was shown to be an effective emulsifier in the absence of any other additives comprising of both hydrophobic methyl and hydrophilic hydroxypropyl substituents that combines surface activity and viscoelastic properties.[116] The molecular weight and degree of methyl and hydroxypropyl substitutions are described to alter the emulsion properties including droplet size and viscosity.[117,118] HPMC with a lower molecular weight produces smaller droplet diameters while that with the higher molecular weight is associated with the elevated viscosity of the emulsions, which effectively minimizes the creaming and flocculation processes.[117,118] In addition, the higher DS:MS grafting ratio of HPMC is also associated with the greater physical stability of emulsions with an improved viscosity.[118,119]

The hydrophobic cellulose derivatives, ethyl(hydroxyethyl)-cellulose (HM-EHEC) reported to dramatically improve the stability of macroemulsions compared to hydrophilic hydroxyethyl

cellulose (HEC) due to the better effectiveness of HM-EHEC in lowering the interfacial tension and improving the viscosity.[120]

In addition to the use of etherified cellulose as emulsifiers, regenerated cellulose pulps (RCP) without any further modification showed significant amphiphilicity via decreasing the interfacial tension (IFT) between oil and water.[121] In this case, the effectiveness of RCP in reducing the IFT was directly associated with its M_w (25 to 7 kg/mol).[121] This observation proposed the fact that the interfacial activity of cellulose derivatives is not only related to the grafted alkyl chain but a large extent associated with the cellulose backbone.[121]

Despite progress in utilizing cellulose derivatives as emulsifiers, they are still mainly considered as thickener [108,122,123] or additive emulsifiers [105] in industrial emulsion systems due to their incapability to generate emulsions with long term stability.

Table 3.1. Properties of cellulose derivatives as emulsifiers.

Emulsifier-dosage	Grafting ratio (mol/mol)	Emulsion composition	droplet size (µm)	Zeta potential (mv)/ IFT (mN/m)	Viscosity (mPa.s)	Ref.
Tween 20-1.5% w/w	-	Corn oil, 70%	bimodal distribution (0.2 to 12/ 2 to 80)	- 54.83	2.02	[113]
Tween 20-1.5% w/w +CMCNa-1% w/w			0.2 to 12	- 56.3	257.5	
HPMC-2wt.%	DS+MS=2.16 Mw (2 to 90 kg/mol)	Sunflower, 10%	1.44 to 3	+0.291 to +0.239	0.34 to 67	[117]
HPMC-1wt.%	DS= 1.37 and 2, MS= 0.23 and 0.85, M_w=250 and 670 kg/mol.	Sunflower, 10%	1.5 and 1.7	-1.1 and -1	0.12 and 2.69	[118]
HPMC-1wt.%	DS=0.28, MS=0.64 to 0.94	Medium chain triglycerides, 15%	1.38 to 1.96	-	0.05 to 0.4	[119]
HEC-1.0 wt.%	HM=0.01	Paraffin, 50%	.	IFT 31	0	[120]
HMHEC-1.0 wt.%			10	IFT 27	0.35	
RCP-0.1 wt.%	Aged from 24 h to 360 h produced RCP with M_w 25 to 7 kg/mol	Paraffin, 15%	10 to 1	IFT 20 to 18	1 to 0.1	[121]

DS; degrees of substitution of methoxy groups,

MS; mass molar substitutions of hydroxypropoxy groups

IFT; interfacial tension

3.5.1.2 Starch Derivatives

Native starch cannot function as an ideal stabilizer due to the poor hydrophobicity and large size.[124] The size of starch granules is dependent on their botanical sources varying in a wide range of 0.3-100 µm.[124-126] The emulsifying properties of starch granules could be improved by chemical or physical modifications. The different chemical modifications of starch including esterification, etherification, oxidation, acid treatment, hydroxypropilation, and crosslinking have been carried out.[70,127,128] The esterified starch at OH¬ group of carbon 2, 3, and 6 in the glucose molecule with alkyl halides or alkenyl succinyl anhydrides (-SA) is the most common starch derivative with enhanced emulsifying properties due to the enhanced amphiphilic and surface-active properties (Fig. 4).[69,127-130]

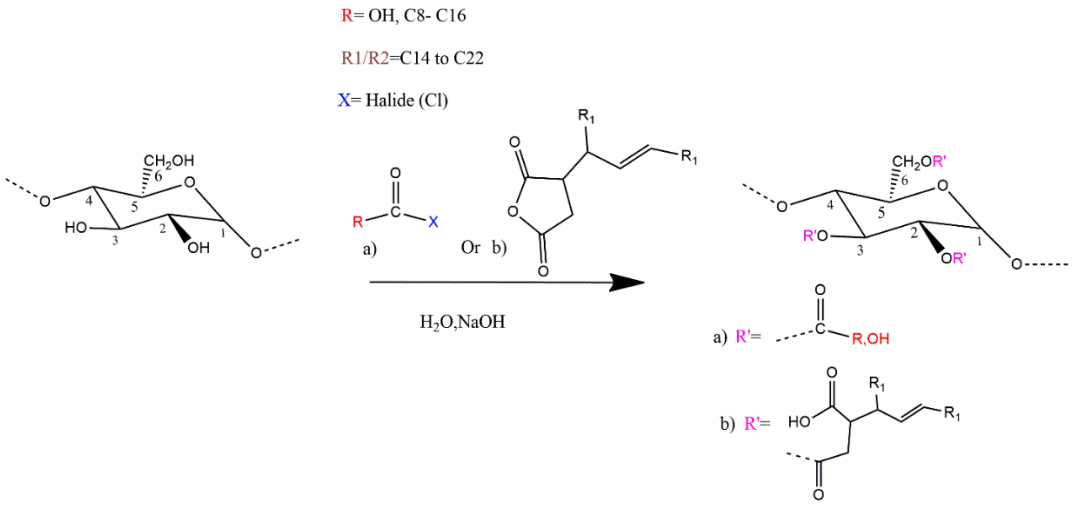

Figure 3.4: Structure of starch derivatives with (a) alkyl halides or chloroacetic acid and (b) alkenyl succinyl anhydrides (-SA) groups. (Adapted from Ref. [69] with permission of Elsevier).

Depending on the use of starch granules or water-soluble starch derivatives of octenyl succinic anhydride (OSA), both Pickering and non-Pickering emulsions are reported to be produced from starch derivatives and a summary of recent studies is shown in Table 2. The use of OSA-starch granules as Pickering emulsifiers from various sources and sizes including native rice starch (5-10 µm), waxy maize starch (10-20 µm), waxy potato starch (20-30 µm), Quinoa~2 and Amaranth~1.4 are available.[126,131,132] It was elaborated that emulsion properties (emulsifying capacity and storage stability) were influenced by DS and particle size of starch granules. While starch with a higher DS was more effective at similar DS values, the particle size of OS-starch granules was the key factor, as the smaller particles of OS-starch granules from varied sources exhibited a smaller oil droplet size and lower creaming index.[126,131,132]

Water-soluble esterified starch (DOSA) offered better emulsification activity than insoluble granules (GOSA) with a similar DS by generating greater ζ-potential, smaller particle size, and long-term stability.[133] The contributing factors in the stabilization properties of water-soluble OS-starch derivatives are reported as R_h, DS, M_w, and branch length.[134,135] In this case, however, it was depicted that a satisfactory correlation could not be proven between the degree of esterification and emulsion stability.[136] Similarly, a comparison between three water-soluble OSA-modified waxy maize starches with different R_h (15-78 nm) and DS (0.016-0.028) depicted that the lowest DS with a medium R_h sample generated the most stable droplets over time due to the finest oil droplets and the highest viscosity.[137] As another effective parameter, the chain-length distribution (CLD) or the degree of branching of commercial OSA-starches was altered by hydrolysis processes, which demonstrated that the larger molecular size and longer chains at the constant DS resulted in larger emulsion droplets, which could negatively affect the stability of emulsions.[138] Other starch derivatives, such as acetylated, phosphorylated,[139] alkylated,[140,141] and carboxymethylated starch[142,143] were also produced to improve the emulsifying capabilities of starch via adding charged or hydrophobic groups. The produced derivatives typically showed stronger emulsifying properties, lower surface tension, and better amphiphilic properties than unmodified starch. For instance, the negatively charged phosphate starch and the hydrophobic starch acetates improved the emulsifying capabilities of the starch derivatives more effectively than unmodified starch, however, their stability was less efficient compared to OSA-S stabilized emulsions with high oil retention of 94.75%.[139] Laurate starches acted as a better stabilizer compared to hydrolyzed starch, which was associated with greater solubility and lower zeta potential that caused a more effective electrostatic repulsion between starch granules to effectively stabilize oil-in-water emulsions.[140] Amphiphilic starch (CMS-LS) from etherified carboxymethyl starch (CMS) had better emulsifying properties than starch and CMS, as it showed higher surface activity by reducing the surface tension of water.[142] Despite noticeable progress in implementing modified micro-scale starch and starch granules as stabilizers, emulsions have poor stability against gravity force due to their large size.[144]

Table 3.2. Properties of starch derivatives as emulsifiers.

Emulsifier-dosage	Modification route	Source /DS	Properties/ Particle size (μm)	Emulsion type and composition	Oil droplet size (μm)	Other properties	Ref.

(OSA)-Starch granule-800 mg/mL	Esterification with octenyl succinic anhydride (OSA)	Rice, Quinoa, and Amaranth-3%	Rice 6.92, Quinoa 2.44 and Amaranth 1.48 µm	Pickering - Miglyol 812- 5% v/v	Rice 26 / Quinoa 17 / and Amarant 8	-	[126]
(OSA)-Starch granule-3% w/v	Esterification with octenyl succinic anhydride (OSA)	Spherulites, Rice, Waxy maize and Waxy potato-~0.0180	OS-SS 3.8, OS-NRS 7.5, OS-WMS14.5, OS-WPS 24	Pickering - Orange oil- 30% v/v	14-18-23-35	Creaming index %=42, 60, 70 and 100	[131]
(OSA)-sweet potato starch granule	Esterification with octenyl succinic anhydride (OSA)	Sweet potato - DS 0,0.0095 to 0.0230	15.47	Pickering - Canola oil- 50% v/v	~100 to 10	Emulsifying capacity 0 to 0.57	[132]
GOSA/ DOSA-1 wt %	Esterification with octenyl succinic anhydride (OSA)	Waxy maize starch-DS=0.016-0.028	GOSA-20	MCT-10 wt %	0.9-0.76/ after storage 2.5-1	Z=-(8-15)/IFT:20-19.4 mN/m	[133]
	Heat treatment and a spray drying		DOSA- 78.6 nm		0.34-0.33/ after storage 0.9-0.7	Z=-(25-28)/19.3-16.5	
OSA-CFG-0.5, 1, and 1.5%, w/w	Esterification with octenyl succinic anhydride (OSA	Corn fibre-DE 0, 0.3, 2.4, 3.4 and 6.1%	2×10^5 kg/mol	Non-Pickering -Soybean oil- 5.0% w/w	2.7 to 1 to 1.5	IFT= 48 To 25 mN/m / IS= 0.8 to 0.2 to 0.4	[136]
OSA-starch-1% (w/w)	Esterification with octenyl succinic anhydride (OSA)	waxy maize W1-0.025	11.5 nm	Non-Pickering - MCT 5% g/g	0.19	IFT=38 ΔT 2.9%	[137]
		W2-0.031	48 nm		0.2	IFT=35 ΔT 0.2%	
		W3-0.038	3.7 nm		0.17	IFT=24 mN/m ΔT 26.2%	
OSA-starch	Commercials-debranched using isoamylase	Waxy maize varieties~ DS=0.023/	~0.2 nm to ~12 nm / DB=4.7 to 6.8 (%)	Non-Pickering - MCT 15% w/w	0.2 to 0.4	Viscosity ~100 to ~20 mpa.s	[138]
Phosphorylated waxy maize starches	Hydrolysis with HCl (5% v/v) +Sodium tripolyphosphate	Waxy maize starch-0.046	WI=56%	Non-Pickering - Orange peel oil 20% w/w	-	Oil retentions 55.75%	[139]
Acetylated starch	Hydrolysis with HCl +Acetylation with acetic anhydride	Waxy maize starch-0.033	WI=63%	Non-Pickering - Orange peel oil 20% w/w	-	Oil retentions 61.31%	[139]
Lauroylated starch - 20 and 30 wt.%	Hydrolysis (H)	Rice starch-1.86	H1-3/ WI= 3.44%	-Non-Pickering - Canola oil 30% w/w	H-18.2	TSI 2.20	[140]
	+Esterification with lauroyl chloride (HL)		HL-4.9/ WI= 53%		HL-13.2	TSI 2	
Lauroylated starch	Esterification with lauroyl chloride	Amaranth-0.01	1.09	Pickering	7-9	-	[141]

Carboxymethyl Starch Sodium Laurate Starch	Carboxymethylation with chloroacetic acid + Lauric acid	Potato Starches- 0.386+ 0.164	30 amphiphilic	Pickering - - Soybean oil 1%	-	Surface tension 29.5	[142]

WI: water solubility index

IS: instability index

ΔT: gravitational stabilities

Z: Zeta potential

DB: Degree of branching

TSI: destabilization index

3.5.1.3 Protein Derivatives

Proteins from diverse sources with variable molecular and physicochemical characteristics can greatly affect their abilities to form and stabilize oil-in-water emulsions.[4] Due to their amphiphilic structures, the balance between polar and non-polar groups at the surface of proteins control their surface activity, [7] while an optimum level of surface hydrophobicity governs whether the protein could be a good emulsifier.[145-147] Unmodified pea (Pisum sativum), lentil (Lens culinaris), and faba bean (Vicia faba) protein demonstrated to be efficient emulsifiers for forming and stabilizing oil-in-water emulsions with small oil droplets ($d < 0.3$ μm) at higher emulsifier levels (5% protein).[148] However, in some cases, the proteins need to be physically or enzymatically modified to uncover their buried interior active functions to make them effective emulsifiers as summarized in Table 3.

The surface and interfacial properties of proteins were improved using physical treatment by unfolding the aggregates. For instance, more hydrophobic residues of lotus seed protein were exposed by microwave treatment, which improved the solubility of the samples.[149] Thus, the stable solution improved the emulsifying properties of lotus seed protein by reducing the oil droplet size. In addition, the solubility, surface hydrophobicity, and emulsifying activity of soybean β-conglycinin,[150] vegetable proteins (pea, rice protein isolate),[151] peanut protein isolate,[152] and jackfruit seed protein isolate [153] were enhanced by the high-intensity ultrasound treatment due to the reduced particle sizes.

The particle size and polydispersity of protein reported to be increased by enzymatic cross-linking, which led to elevated emulsion stability and elastic gel-like properties (compared to the non-crosslinked emulsion that showed phase separation after two weeks).[154] Other thermal or acidic

treatments of proteins were also effective in forming gel-like emulsions with elevated emulsion stability.[155]

Proteins with high molecular weights and extended structures are often better at preventing aggregation by generating stronger steric repulsion in emulsions.[7] One of the proposed reasons[13] for unstable emulsions using globular proteins is associated with their structural unfolding at the oil interface, which causes the loss of interfacial film thickness and exposure of more reactive groups.[156,157]

Table 3.3. Properties of protein derivatives as emulsifiers.

Emulsifier-dosage	Modification route	Source	Particle size nm/M_w	Emulsion composition	Oil droplet size (μm)	Other properties	Ref.
LSPIs-10 mg/mL	Microwave-vacuum treatment-ranging from 0 to 200 W for 3 min	Lotus seed- WI 49.2% (untreated) to 76.2% at 100 w opt	500 (untreated) to 50	Corn oil-25%	Creaming to 0.366 after 28 days	-	[149]
Soybean β-conglycinin-0.5%	Ultrasound treated-20 kHz at 400 W-0 to 40 min	Defatted 7B soy flour- WI 85 (untreated) to 93%	75 (untreated) to 50	Corn oil 25%	-	ESI 9.7 to 57.5 min	[150]
PPI-0.1 wt.%	Ultrasound treated-20 kHz, ~34 W cm^{-2} for 2 min	Pea	5250 (untreated) to 222	Rapeseed oil-10 wt.%	0.8 (untreated) to 0.5 μm after 28 days	IFT 5 mN/m	[151]
PPI- 1%	Ultrasound treated-20 kHz 0-1020 W for 1 min	Peanut protein powder	Native PPI 474.7 to 255.8	Soybean oil-33 wt.%	-	ESI 35 to 60 min	[152]
Crosslinked-chickpea protein-6% w/w	Enzymatic crosslinking with ACTIVA®TI TG	Chickpea protein- high solubility at pH 10	M_w=50 to 240 kg/mol	Corn oil-40%	1 (untreated) to 10-100 (gel-like)	Emulsions were stable for more than a month	[154]

WI: Water solubility index

ESI: Emulsion stability index

3.5.1.4 Lignin Derivatives

Almost all isolated lignin products tend to aggregate in neutral aqueous environments; thus they are not suitable for stabilizing emulsions as polymeric emulsifiers.[92-95] Lignosulfonate is the only by-product of the pulp and paper industry that is dispersible in water and acts as a polyelectrolyte, thus it may stabilize emulsions through repulsion via an electrical double layer. Still, after several decades, lignosulfonate is an appealing biomaterial that is applied as a surfactant in many research

studies.[158-160] However, lignosulfonate faces some disadvantages: 1) its limited capability in reducing the interfacial tension in emulsion systems, which requires supplements, such as synthetic co-surfactants,[161] and 2) the limited availability of lignosulfonate (only 2% of the total lignin production worldwide).[100] Therefore, the valorization of other insoluble lignin sources via grafting or polymerization reactions were implemented to imply surface activity to lignin, which produced anionic,[162] amphoteric,[163] and non-ionic derivatives with interfacial activity as stated in Table 4.

The anionic derivatives of lignin, such as carboxyalkylated,[164-166] sulfoalkylated,[167] and acylated lignin,[168] were reported as effective emulsifiers to increase the interfacial activity of lignin. The mutual trend was a decline in surface and interfacial tension with the polar groups, as was reported for carboxymethylated lignin (CML), which was further decreased by increasing the DS of CML,[165] lignin-tannic acid,[166] and sulfoethylated lignin derivatives.[167] The stabilized emulsion with carboxyalkylated and sulfonated lignin derivatives showed pH-responsive performance. This behaviour is believed to be a result of surface charge elimination via the protonation of functional groups.[165,166,169] Acylated lignin derivatives synthesized from modification of lignin with succinic anhydride (SA) and dodecylsuccinic anhydride (DSA) also showed more surface tension depletion compared to the unmodified lignin, while the longer chain derivatives showed better emulsifying properties.[168]

Amphoteric derivatives were also effective in improving the surface and interfacial properties of lignin. Hydrophilic sulfonic groups and lipophilic long carbon chains of modified alkali lignin (ASAL) with amination, sulfonation, and acylation, efficiently were reported to reduce the oil-water interfacial tension.[170]

Non-ionic polymeric lignin derivatives were reported to comparably perform as non-ionic industrial surfactants.[171] Lignin-PEO (poly ethylene oxide) was successfully used for the emulsion polymerization of styrene, while that with a lower molecular weight demonstrated higher stabilizing efficiency.[172] Similarly, the surface activity (surface tension decline) and emulsifying properties of OZ-PEGylated lignin derivatives (polyethylene glycol) were dependent on the length of grafted PEG, as the medium DS showed the better properties.[173]

Moreover, a stable water-in-oil emulsion was achieved using hydrophobized lignin derivatives with butyric anhydride (BA) as the emulsifier.[174] The lignin-BA was found to be completely

soluble in organic monomers, as it maintained water-in-oil emulsion stable over 30 days via steric and electrokinetic effects.

Table 3.4. Properties of lignin derivatives as emulsifiers.

Emulsifier-dosage	Modification route	Source /DS	Properties/ Particle size (nm)	Emulsion composition	Oil droplet size (μm)	Other properties	Ref.
CML- 2%	Carboxymethylation with monochloroacetic acid	Pine kraft/ organosolv-DS 35%	Mw 5-6 kg/mol, D=3.5-4	Kerosene- 30-70%	< 2.5	Surface tension 34 mN/m	[164]
CMLs	Carboxymethylation with chloroacetic acid	Indulin AT-DS 24-30%, Solubility 1.3-2 g/100 g	-	Kerosene- 30-70%	~2.5	Surface tension 65-62 mN/m	[165]
KL-TA-1.5%	Carboxyalkylation with Tannic acid	Softwood kraft lignin-100%-CD=-2.8 mmol/g	8-15	Cyclohexane-50%	6-12 / emulsion fraction 75-98%	IFT 21.7 mN/m	[166]
SEKL-0.25-1.5 wt.%	Sulfoethylation with 2-bromoethane sulfonate salt	Softwood kraft lignin-100%-CD=-1.3 mmol/g	21	Xylene, Cyclohexane, and Decane-50%	X~7, C ~5 and D ≤ 2.5	IFT:X 10.7, C 12.2, D 14 mN/m	[167]
SA/DSA-lignin-1% wt/v	Acylation with succinic anhydride (SA), and dodecyl-succinic anhydride (DSA)	Alkali lignin-soluble	-	Xylene- 50%	**SI:** AL=1.6 ALSA=5 ALDSA =12 h	Surface tension 42 to 38 mN/m	[168]
ASAL-5%.	Amination with Diethylenetriamine and CH2O+ Sulfonation with Na2SO3 and CH2O Acylation with palmitoyl chloride	Alkaline lignin	-	-	-	IFT to 5 mN/m	[170]
m-Lig-PEO-1%	Oxyanionic polymerization of EO	Softwood kraft lignin-yield 40-90# solubility 2.02 mg L^{-1}	Mw 2.5-9 kg/mol-251 and 398	Styrene-20%	Latex of 0.322-0.405	Surface tension 54-62 mN/m / SE: 4.98-2.37 10^6 cm^2/g	[172]
OzEL-PEGs	Ozone oxidation +Esterification with melted polyethylene glycol (PEG)	Enzymatic lignin DS (0.47, 1.13, 1.86)	2, 4, 17 kg/mol/ $Đ$ =1.3-2.2	Edible oil- 10%	3 (at DS 1.13)	Surface tension 55.42, 52.87, 57.48 mN/m	[173]
BA-KL-0.5 and 5 wt%	Esterification with butyric anhydride with Methylimidazole catalyst	Kraft lignin	2.7 kg/mol	Styrene- 50%	0.499-0.363	Decrease the interface energy from 35 to 15 J/m^2	[174]

SI stability index

SE Stabilizer efficiency

EC: Emulsifying capacity

3.5.2 Particle Stabilization

Pickering emulsions usually display a longer lifetime when compared to surfactant-based emulsions, which is due to the higher steric resistance against droplet coalescence induced by the solid particles adsorbed at the O/W interface.[30] The particle preparation can be classified into "top-down" and "bottom-up" methods.[175] If the preparation follows a breakdown of larger particles via improvement in the structure and size, it is called "top-down" process. On the other hand, "bottom-up" process is based on combining atoms or molecules in a controlled manner to produce particles.[175] In the following section, different methods of particle formulation based on the most common plant-based biomaterials and their use in the Pickering stabilization of oil/water system are reviewed. The attention was given to the surface charges, size, and wettability of particles and their effect on emulsion properties including oil droplet size and physical stability.

3.5.2.1 Nanocellulose particles

Cellulose nanocrystals (CNCs) and cellulose nanofibers (CNFs) are the two main particle forms of nanocellulose materials, in which their methods of production were explained in section 3.1 and further, their properties on emulsion formulation are discussed here. Within the nano cellulosic materials as particle stabilisers, CNCs gained the main spotlight.[176,177,178] Most recently, the introduction of novel resources such as defatted rice bran (DRB),[179] asparagus,[180] and non-bleached fine fractions of carton pulp,[181] were given extra attention in order to propose more sustainable fiber supplies. Latest studies on the use of nanocellulose particles in Pickering emulsion stabilization are provided in Table 5.

The CNCs are usually negatively charged due to the presence of ester sulfate or carboxyl groups, which could promote repulsions at the interface while the edges of the nanocrystals are hydrophobic allowing for their adsorption at the O/W interface. Adding salt to water (50 mM) or removing the sulfate groups from the surface of the CNCs may decrease electrostatic repulsion and enhanced emulsion stability.[182-185] For instance, the lower the surface charges by de-sulfation, the higher the stability of the formulated emulsions with smaller oil droplet size would be.[184,186] A comparison between CNCs and de-sulfated CNCs showed that a porous and multilayer interface formed at the oil interface using de-sulfated CNCs, would cause a larger tendency for aggregation compared to a denser layer with charged CNCs.[187] However, higher surface charges were also

shown to enhance the emulsification efficiency of produced CNCs with longer hydrolysis time, which increased CNC charges and reduced its particle size.[180]

Therefore, it seems that a combination of the nature of the charges at the surface and particle size would ultimately alter CNC's emulsifying properties, which are all dependant on the source, crystalline organization and morphology of particles and the methods of treatment of CNCs (e.g., de-sulfation in the acidic or alkaline system). In addition, the non-adsorbed CNCs in the continuous phase is also reported to affect the emulsion's final stabilization.[186]

Other factors rather than surface charges were shown to have a dominant role in the properties of emulsions. For instance, different crystalline allomorph and particle sizes altered the hydrophilicity and morphologies of CNCs and consequently affected their ability to stabilize O/W Pickering emulsions.[188] Needle-like particles (CNCs-I, length 200 nm) with lower crystallinity and hydrophilicity were a better stabilizer compared to individual ellipsoid shape granules (CNCs-II, length 18.8 nm) with similar surface charges by showing larger emulsion ratio, two-time smaller droplet size, and superior stability performance.[188] In addition, the aspect ratio of cellulose particles is known to directly influence the coverage ratio of droplets in emulsions. For example, CNCs with a low aspect ratio (short nanocrystals) could form monodispersed oil droplets with a high surface coverage ratio (coverage >80%), while a higher aspect ratio (longer nanocrystals) was associated with an interconnected network of low covered droplets (40%).[189,187]

Yet, creaming occurs for stabilized emulsions with CNCs over time. To address this problem, water-soluble CNC derivatives (CNC-HEC and CNC-MC) were mixed with CNC particles, which led to the smaller oil droplet in the emulsion that stabilized them over a longer time.[190] A lower surface coverage was reported for the mixture of stabilizers in emulsions, which revealed the important role of HEC and MC to stabilize the interface with fewer CNCs.[190] The effective influence of polymers was also shown on the formation of dried and re-dispersible CNC-based emulsions.[191]

The hydrophilic nature of CNCs with abundant hydroxyl groups makes it difficult to disperse in hydrophobic polymer matrices and consequently hampers its practical applications, e.g., stabilizing W/O emulsions. The hydrophobic particles of CNC derivatives such as acylated CNC with an excess of cinnamoyl chloride, [192,193] alkylated,[194-197] and reductive aminated CNC[181,198] had higher compatibility with organic solvents yielding the formulation of reverse water-in-oil Pickering emulsions.[197]

In addition to CNCs, physically or chemically treated CNF particles are reported as Pickering stabilizers in many studies.[199-201] CNFs can form entangled networks due to their longer fibers, which form a shield around the oil droplets, preventing them from coalescing; while the shorter length and aspect ratio of CNC was shown to be more effective in preventing the coalescence phenomenon.[199] For instance, TEMPO-CNFs with a shorter length than untreated CNF formed a larger volume of emulsions with small and homogeneous oil droplets, which also showed good stability after storage for 30 days.[201]

Several studies also focused on the comparison between CNC and CNF, while the latter one formed much larger oil droplets (20 μm) compared to CNC (4-6 μm).[202] On the other hand, oxidized (TEMPO)-CNF showed to be as effective as CNC-stabilized emulsions by effectively reducing both the particle size and oil droplet size.[202] However, the stability was more significant for CNF and T-CNF stabilized emulsions due to the longer networks of fibrils formed around droplets resulting in a physical barrier against coalescence.[202-204]

Table 3.5. Properties of nanocellulose particles as Pickering stabilizers.

Emulsifier -dosage	Preparation	Source /DS	Properties/ Particle size (nm)	Emulsion composition	Oil droplet size (μm)	3-phase CA˚/other properties	Ref.
CNCs/de-sulfated CNCs	De-sulfated by acidic treatment (HCl) Time 0 to 10 h	Cotton (CCN)/Surface charges (0.123 to 0.019 e/nm^2)	189 to 117	Hexadecane-30%	Unstable to 3.8	E: 0 to 70%	[184]
CNCs/desulfated CNCs- 0.8 to 5 g/L	Sulfuric acid hydrolysis/ de-sulfated by acidic treatment (HCl)	Whatman filters-0.16 e/nm^2/0	Rod-like 195 long, 23 width and 6 thick	Hexadecane 10, 20, and 30%	S=4.7-2.1	Thickness=7 nm/ Coverage of the droplet =85%	[187]
					D=5-2.8	18 nm/ 45%	
CNC	Sulfuric acid hydrolysis (T 1.5-3.5 h)	Cellulose fibers asparagus	261.8 to 180	Palm oil 30%	3 μm /E: 15-32 %	Zp= -31.2 to -52 mV	[180]
CNCs-0 to 3 g/l	Sulfuric acid hydrolysis	Unmodified 50 μm and mercerized microcrystalline cellulose (MCC)-Surfac charge, 0.12 and 0.1 e/nm^2	CNCs-I (length 200, width 16.4, and L/W = 13) CrIs: 70.9%	Hexadecane- 25%	50 to 5/ E:0.25 to 0.46	44˚	[188]
			CNCs-II (length 18.8, width 10.9, and L/W = 1.7) CrIs 72.8%		70 to 10/ E:0.22 to 0.40	26.9˚	
CNC 0.3+ polymer 0.2 wt %	Sulfuric acid hydrolysis	Cotton filter aid+ MC+ HEC	-	Dodecane 50%	CNC 12/ Over time to 30	SC%=80/ coalescence	[190]

					HEC or MC 6 Over time to >30 μm	Significant coalescence	
					Mixed 2-3/ minimal droplet change	SC%=20% / mild creaming	
Cin-CNC-0.5-4 mg/mL	Esterification with cinnamoyl chloride	Commercial	CNC-rod-like length of 110.3 and width 4.8	Toluene 70%	-	14˚	[192]
			Cin-CNC length of 138.9 and width 8.1		60 to 5	75.9˚ / SC%= 62%	
CNC-C18-0.3 to 0.05 wt %	Hydrazone reaction with hydrazinium hydroxide and amidation reaction EDC/NHS	Cellulose filters	Length of 84 and width of 4.9	n-Hexane 50%	206 to 11	IFT 55.5 to 39.5 mN/m	[194]
CNC-NH_2-0.1-1 wt.%	Amination with epichlorohydrin	Commercial CNC	200	Cyclohexane- 75%	50 to 32	-	[198]
CNF-0.01-0.09 wt%	TEMPO oxidized with NaClO at pH 10	Kelp (seaweed)	Non-uniform >3 μm	Sunflower oil- 25%	~20	E: 16.2-26.1%- not stable	[201]
			Length 0.6-1 μm, width 10-20		~10	8.2-21.9% stable	
CNC, CNF and TCNF-8 mg/mL	-	Wood CNCs, wood CNFs, TEMPO- CNFs	CNCs 50-250	Hexadecane 20%	CNCs 4-6	Flowing	[202]
			CNFs and TCNFs few micrometers		CNFs 30	Gel-like behavior	
					TCNF 1		

E: emulsion volum/ratio

SC: Droplet surface coverage%

CrIs: Crystallinity index

EDC: N-(3-(dimethylamino)- propyl)-N′-ethylcarbodiimide hydrochloride

NHS: N-hydroxysuccinimide

3.5.2.2 Starch Particles

The nanoparticles from starch (SNPs) are produced using various techniques of chemical treatments with acid hydrolysis, emulsion-crosslinking, nanoprecipitation, and physical treatments with high-pressure homogenization, ultrasonication, reactive extrusion, and gamma irradiation or a combination of them.[70,205,206] There are several review articles available for starch modification and particle formulation.[70,207] Briefly, Table 6 summarized studies in the past 5 years in producing Pickering emulsions using starch nanoparticles.

The use of esterified or cross-linked starch for particle formulation via nanoprecipitation or alkali-freezing/freeze-drying was reported to enhance the wettability of particles (θ closer to 90˚), which produced narrowed-sized oil droplets.[208,209] Functionalized starch nanoparticles produced via graft polymerization were reported to increase the hydrophilicity of particles at a higher grafting ratio, which increased the oil droplet size.[210,211]

The importance of particle size and their wettability, $\theta_{ow,}$ as the two main variables for Pickering emulsion stability were investigated in several studies.[30,212,213] For instance, the three-phase contact angle (θ) of particles increased from 53.3˚ to 73.4˚ with the increase in the size of the SNPs, inferring the higher hydrophilicity of the smaller particles.[212] In addition, these particles were all strongly attached to the water-oil interface, independent of their θ due to the large adsorption energy, which was increased with the larger particles (-5.6×10^4 to -1.65×10^6 K_BT).[212] However, the importance of the wettability of the particles and their direct correlation with the oil droplet size was emphasized. For instance, medium-sized nanoparticles (100-220 nm) showed near-neutral wettability (θ_{ow} ~90˚) that produced the smallest oil droplets. However, other particle size ranges (<100 nm or >220 nm) were associated with further discrepancies from θ_{ow} ~90˚ that formed larger oil droplets.[213]

Starch nanocrystals (SNCs) are considered as the second category of starch particles with variable sizes, depending on the starch source.[207] SNCs produced from H_2SO_4 hydrolysis was successfully implemented to form stable gel-like O/W Pickering emulsions in which by increasing concentration of particles, oil droplet size decreased, and creaming stability increased.[214,215]

Modified or treated SNCs were effective in improving the stability of Pickering emulsions. For instance, the acetylated SNC particles improved the emulsifying capacity due to the enhanced electrostatic repulsion created among the droplets, which reduced the size of oil droplets.[216] Moreover, the particle size of SNCs from different sources was effectively reduced by alkaline treatment, which ultimately improved the Pickering-stabilizing capacity of starch particles.[217] However, a major variation in droplet size, storage stability, and viscosity properties of emulsions were reported to be dependent on the starch source. For instance, structural differences between the two kinds of maize starch with similar particle sizes played a vital role in the physicochemical properties of particles.[217]

Table 3.6. Properties of starch particles as Pickering stabilizers.

Emulsifier-dosage	Preparation method	Source	Particle size (nm)	Emulsion composition	Oil droplet size (μm)	3-phase CA˚	Ref.
Amphipathic SNP-0.5-2 wt.%	Acetic anhydride and phthalic anhydride+ Nanoprecipitation	Acidified corn	150	Ethyl acetate- 30-40%	34-10	104˚	[208]
CSTNs crosslinked SNP 1 wt.%	Alkali-freezing dispersions+ freeze-drying+ crosslinking thermal elimination	Corn 2-10 μm	140	Sunflower oil- 30%	1.8-3	Native 45, CSTN 78˚	[209]
CMS-g-DMAEMA-1% (w/v)	Gelatinization+ polymerization + ethanol precipitation	Carboxymethyl maize- G R:14-33%	~100	Grape oil-50%	12 to 31	119 to 80˚	[210]
SNP-g-PNIPAM-0.5 mg/mL	Precipitation of initiator-attached SNP -graft radical polymerization SET-LRP	Acidified corn-conversion 33-85 (%)	190-400	*n*-hexane, toluene	30 to 100	103 to 65˚	[211]
SNP	Nanoprecipitation	*	100, 210, 320	Hexane-water interface	-	53.3 to 73.4˚	[212]
SNP-1 wt%	Nanoprecipitation/ enzymolysis and recrystallization Method	Corn, Sweet Potato	<100	Soybean oil 50%	48.34	84.3˚	[213]
			100-220		29.33	89.1-94.8˚	
			>220		48.76	105.5-129.4˚	
SNC-0.5-4 wt.%	Sulfuric acid hydrolysis	Waxy maize	750	Soy oil-80%	60 to 30	78˚	[214]
Sago-SNC 0.5-4% (w/v)	Sulfuric acid hydrolysis	Sago	20-100	Corn oil-50%	*	Creaming decreased	[215]
Acetylated SNC-0.2-2 wt.%	Acid hydrolysis+ acetylation	Corn 15 μm-DS= 0.11-0.41)	SNC 86	Olive oil-20%	1.85-1.21	*	[216]
			ACSNC 92		0.78		
Alkaline treated SNC-3%, w/v	Acid hydrolysis+ alkaline treatment	Waxy maize starch/ Normal maize starch	300/400	Sunflower oil-50%	5/70	95/78˚-viscosity 23/13 mpa.s	[217]

3.5.2.3 Protein Particles

The different methods of self-assembling, enzymatic cross-linking, thermomechanical treatments (e.g., ultrasonication, or stirring-heating),[218,219] high-pressure homogenizer[220,221] and solvent-induced precipitation[222] are introduced as effective techniques for producing protein particles. Additional references are available for more details on these methods of particle formulation.[86,81] Studies in the past 5 years in producing Pickering emulsions using protein nanoparticles are summarized in Table 7.

Using acetylated protein for particle formulation was reported to advance the hydrophobicity of particles with neutral wettability (θ=86.7˚) that enhanced its emulsifying properties.[223,224] The aggregation of proteins can also be induced by adding divalent ions (Na^+ and Ca^{2+})[225,226] and/or crosslinking using transglutaminase, peroxidase or tyrosinase.[227,227] The Ca^{2+}-induced aggregation of soy protein isolate (SPI) produced nanosized particles (130 nm), and its crosslinking with glutaraldehyde (GAD) increased the particle size to 150 nm.[225] As demonstrated in Fig.5, the GAD crosslinking of SPI nanoparticles was associated with the formation of larger oil droplets compared to Ca^{2+}-induced SPI nanoparticles. However, the extent of creaming was lowered using GAD compared to the uncross-linked nanoparticles. The crosslinking was suggested to bring stronger internal integrity that resisted more against droplet flocculation and coalescence.[225]

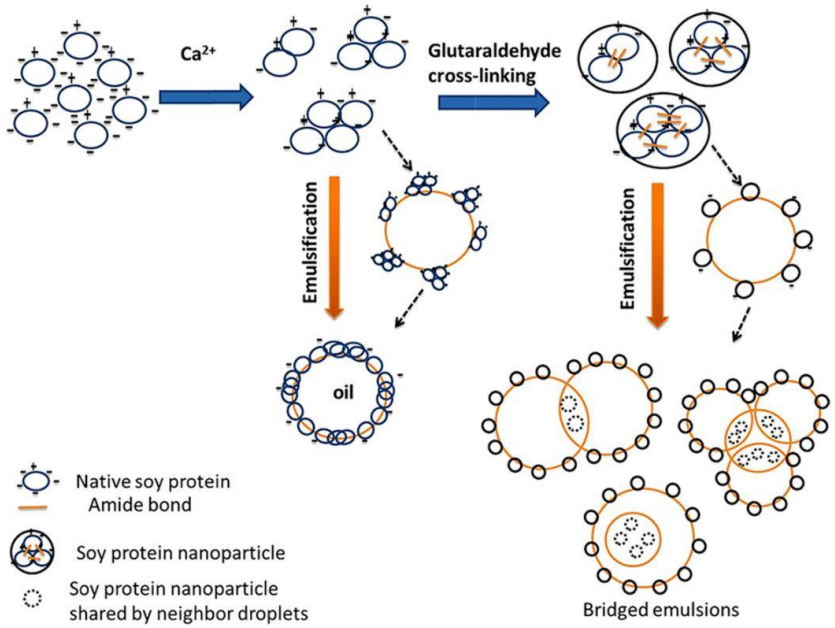

Figure 3.5: Ca^{2+}-induced soy protein nanoparticles formulation with or without cross-linking for Pickering stabilization of oil droplets. (Adapted from Ref. [225] with permission of Elsevier).

Protein from different sources may have a high hydrophobic (zein or rapeseed) or hydrophilic nature with variable sizes, which restrict their effective adsorption at the oil-water interface. Several studies produced stable Pickering emulsion with the incorporation of other hydrophilic or hydrophobic components, such as anthocyanins (CAN),[228] chitosan,[229] sodium caseinate,[230] tannic acid[231] or octenyl succinic anhydride[232] with tuning the wettability and size of particles.

A protein nanoparticle complex (SPI-CAN) was formed by covalent complexation between SPI (soy protein isolate) and ACN (anthocyanins), which was initiated by heating with added NaCl (300 mM) and leading to a decrease in the particle size compared to SPI alone. SPI-ACN complex nanoparticles with smaller particle size and increased repulsion forces formed smaller oil droplets with enhanced creaming index by 50%.[228]

A zein/TA complex colloidal particle (ZTP) was produced following the antisolvent approach based on the hydrogen-bonding interaction between zein and TA. A near-neutral wettability (θ_{ow}∼86˚) resulted in a complex particle (ZTP/TA) compared to θ_{ow}∼110˚ for unmodified particles that resulted in elevated Pickering stability due to the smaller particle size and enhanced interfacial reactivity.[222,233]

On the other hand, amphiphilic (neutral wettability) gliadin nanoparticles (OSA-GNPs) were produced by esterified hydrophilic gliadin nanoparticles (GNPs) to improve the emulsifying nature of GNPs via improving their hydrophobicity, which ultimately decreased the oil droplet size.[232]

Table 3.7. Properties of protein particles as Pickering stabilizers.

Emulsifier-dosage	Preparation method	Source	Particle size (nm)	Emulsion composition	Oil droplet size (μm)	3-phase CA˚/other properties	Ref.
ARPI-0.2-0.8% w/v	Thermal processing	Rapeseed	170	Rapeseed oil-30%	1.3 to 0.4	RPI 58˚	[224]
						ARPIT 86.7˚	
SPI-0.02-0.4% (w/v)	Ca^{2+} (5mM) induced aggregation+ crosslinking with GAD (0-200%)	Soy flour	SPI 130	Soy oil-50%	100-50	SC: 3.8 %	[225]
			CSPI 150		450-50	8.7-12.6 %	
PPI-0.5-2%	Thermal and Na^{+} (500 mM) induced aggregation	Peanut	178	Corn oil-20-70%	124 to 36	45˚	[83]
			260			66˚	
SPI-ACN complex	Thermal and Na^{+} (300 mM) induced aggregation- 0.2%	Soy flour/ rice extract powder	SPI 675	Soy oil-20%	15-20	CI 34%	[228]
			SPI-ACN 186			CI 17%	
ZTPs-0.25-1.5	Heating / Antisolvent	Corn/ zein/TA ratio of 1:0.2	∼200	Corn oil > 50%	43 to 12	110˚	[222]
			~ 90			86˚	
OGNPs-1.5%	Ultrasound treatment+ Anti-solvent +OSA	Gluten/DOS 2% to 10%	122.97	Corn oil 10%	20.72	39.1˚	[232]
			233 to 379		7-4	59.1 to 99.4˚	

Kafirin based nanoparticle-1.5%	Anti-solvent precipitation	Sorghum grain	Mean value 206	Soybean oil- 30, 50, 70%	75	125˚	[234]

CI: Creaming Index

SC: Surface coverage

3.5.2.4 Lignin Particles

There are different techniques for lignin nanoparticle (LNP) preparation, which can be found either in a spherical or irregular shape.[100] There are several review publications that focused either on LNP formulation[101,235,236] and applications.[100,237] Briefly, such methods involve the controlled solvent evaporation of atomized droplets of lignin solution,[238] the post-drying of dispersed particles formed by microemulsions[239] or solvent shifting techniques that will form spherical lignin particles.[240] Other methods of acidification or uncontrolled drying, e.g., oven-drying, result in a network of aggregated, irregular, and heterogeneous precipitates.[100] A summary of the lignin particles used for Pickering stabilizations over the past 5 years is provided in Table 8.

The properties of particles can be directly affected by their preparation methods, which would ultimately affect the stability of emulsions. For instance, particles formed from the solvent shifting (SS) method were generally smaller and more hydrophilic than larger and more hydrophobic particles produced via the direct dialysis (DD) method. This SS method was associated with the gentle self-assembly of lignin polymers via dialysis against a rapid transformation.[240] Consequently, the Pickering emulsions stabilized by LNP were the least stable due to hydrophilic and small size particles produced in the SS method.[240]

The source of lignin (kraft, organosolv, or alkali lignin) was revealed to directly affect the size and wettability of particles and consequently the stability of emulsions.[238,240] Generally, the particles formulated from kraft (KL) or alkali lignin (AL), due to higher hydrophilicity, are smaller than hydrophobic organosolv (OL) lignin source.[238,240] Accordingly, KL-stabilized Pickering emulsions were found to be more stable compared to OL-stabilized emulsions.[238] In addition, AL-Pickering emulsions were more stable compared to OL-stabilized emulsions.[240]

Surface-active particles could also be formed using polymerization techniques [241] while grafting degree showed an influential effect on the LNP performance as a stabilizer. For instance, polymer-grafted lignin nanoparticles (PGLNs) with a lower grafting density (100 μmol/g) led to a greater decline in interfacial tension, higher concentration at the oil-water interface, and smaller oil droplet size compared to higher grafting particles (700 μmol/g).[242]

Table 3.8. Properties of lignin particles as a Pickering stabilizer.

Emulsifier-dosage	Preparation method	Source	Particle size (nm)	Emulsion composition (w/w) or (v/v)	Emulsion droplet size (μm)	3-phase CA˚/Others	Ref.
LNP-0.6 and 0.2 wt.%/	Lignin alkaline solution+ Microemulsions	Kraft lignin	Controllable size -90 nm to 1 μm	Hexadecane- 30%	7.7 and 22.3	-	[239]
Colloidal LNP-0.5 mg/mL	Solvent-exchange or dialysis	Organosolv lignin	SS 300	Olive oil, toluene and silicone oil 4:1	Least stable/phase separation	23.1˚	[240]
			DD 680		Stabilized emulsion	56.0˚	
LNP-0.1-0.6%	DMF-Aerosol Flow Reactor at 153 °C	Kraft	356, 1019	Kerosene-50%	5-17	57˚ /Cream layer 0.7, stable	[238]
		Organosolv lignin	679, 189		-	69 ˚ / not stable-flocculated	
Colloidal LNP-0.5 mg mL^{-1}	Dialysis	Alkali	300	0.1% curcumin-containing sunflower oil 25%	73% oil retain	31˚	[240]
		Organosolv lignin	680		65% oil retain	56˚	
AL-g-PNIPAM- 0.1 wt %	ARTP polymerization+ solvent shifting	Alkali lignin/Organosolv lignin	~152	Palm oil 1:2	204	Thermoresponsive behavior	[241]
PGLNs-1 mg/mL	RAFT polymerization	Kraft lignin/ Grafting:100 700 μmol/g	100	Cyclohexane 40%	19	IFT: 24.5 mN/m	[242]
					24	26.5 mN/m	
Cationic-CLPs-5 g/L	Solvent shifting + coated with cationic KL with GTMAC	Kraft lignin	250	Toluene 50%	Bimodal; 5-10 and 50-100	ES 90-100% at pH<6	[243]
N-SEKL-0.25%	Acidification	Kraft lignin	12 polymeric	Xylene 50%	11	22˚/TSI: 20	[169]
			750 particles		~4	50˚/5	
Colloidal LNP-0.1 to 1wt.%	Solvent-exchange	Lignoboost kraft lignin	200	Rapeseed oil 50%	Uniform oil droplets	Stabilized emulsion	[244]
LNP-0.60 wt. %	Acid precipitation dialyzed and ultrasonication	Sulfur-free alkaline pulping liquor	~100	Rapeseed oil- 10 %	1	TSI 50 after 21 days	[245]
LNP- 2 g/L	Nanoprecipitation with injection or dialysis	Alkaline lignin- yield 80%	250-750	Essential oil- 10%	2-8	Oil decay index reduced by 15-25% compared to lignin suspension	[246]

TSI: Destabilization index

ES: Emulsion stability

One of the challenges of using lignin nanoparticles as an oil stabilizer is their less compatibility with food-grade oils. Sipponen et al.[243] revealed that compared to toluene in-water emulsions, a less stable system was formed with olive oil-in-water emulsions (as a polar oil) using cationic colloidal lignin particles (c-CLP). The better correlation with organic toluene was suggested to originate from attractive forces, such as π-π and cation-π interactions, with the aromatic rings of lignin and its cationic moieties at pH<6.[243] Hence, it may be predicted that more attention would be given to enhance the adaptation of lignin nanoparticles toward food-grade emulsion systems in the future.

The advantage of LNPs compared to polymeric lignin surfactants was evaluated in chapter 5 of this thesis.[169] Sulfo-functionalized lignin particles (N-SEKL) formed a gel-like and ultra-stable Pickering emulsion due to considerable viscosity enhancement of the emulsion (24 Pa.s) compared with the unstable liquid-like emulsions (0.24 Pa s) using polymeric surfactants.[169]

Lignin nanoparticles bring unique advantages of antimicrobial, antioxidant and UV-shielding properties over the synthetic particles to emulsion.[247-249] Currently, research on the development of an organic solvent-free or industrially scalable nanoparticle production is on-going.[244-246]

3.5.3 Mixed-plant Emulsifiers

Recently, a new trend for the formulation of entirely green products using only plant-based biomaterials gained interest to improve the properties of the aforementioned emulsifiers. In this case, the same mentioned plant-based surfactants or particles would be jointly utilized to elevate their properties without any chemical reactions. A summary of the available complexation and emulsion properties is summarized in Table 9.

At a certain pH, due to the opposite charges of the biopolymers, complexes could be formed via electrostatic interaction. These complexes are relatively stable due to their surface charges, which allow their interaction with solvent molecules making them water-soluble. By designing the conditions of the biopolymer self-assembly, such as pH, protein to polysaccharide ratio, total concentration, and ionic strength, the complex bioparticles with controlled sizes can be produced.[250] Polysaccharides and proteins could be linked either through Maillard (i.e., a chemical reaction between amino acids and reactive carbonyl groups of sugars) or electrostatic interactions to fabricate surface-active complexes with advantages of both biopolymers.[250]

It was stated that pH adjustment plays a crucial role in such complexation. For instance, variable properties were associated with the complexation between Pea protein isolate (PPI) and gum Arabic (GA) mixtures as a function of pH, which resulted in the formation of soluble (pH 4.23) or insoluble (pH 3.77) complexes, maximum biopolymer interactions (pH 3.60), and dissolution of complexes (pH 2.62).[251] In another study, it was shown that the sequence of adjusting pH and homogenizing soy oil with soy proteins isolate (SPI) solution with/without GA greatly influenced the formation of the interface layer, droplet size, and the stability of the formulated emulsions.[252] Naturally available plant-based surfactants are reported to increase the emulsifying properties of proteins through different combinations, such as soy lecithin/quillaja saponin (QS),[253] gum Arabic (GA)/QS, GA/tannic acid (TA)[254] and zein/TA,[222] yielding higher emulsion stability with smaller oil droplet sizes.[255] For instance, a natural plant-based surfactant, quillaja saponin (QS), which is isolated from the bark of the Quillaja Saponaria tree, was used to successfully improve the properties of hydrolyzed Rice glutelin (RG) protein as a deficient emulsifier.[256] In this case, the size of the oil droplets decreased as the QS-to-HRG ratio increased, while no creaming was observed after 24 h of storage. Similarly, the physical stability of almond protein isolate (API) stabilized emulsions was improved by the addition of camellia saponin (CS), another natural plant-based surfactant at pH=3 and pH=7 via reducing the oil droplet size.[257]

Tannic acid (TA) as a natural polyphenol and food-grade material with a long history of the industrial application was also reported to well control the self-assembly and hydrophobicity of wheat starch (WS). The complexes of TA/WS at pH 4 were reported to inhibit the creaming of soybean oil-based emulsions by forming a thick interfacial network around oil droplets or obtaining smaller-sized droplets with tuned wettability.[258]

The improvement in the stabilization of Pickering emulsions using modified particles with natural emulsifiers is also reported.[259,260] The complexation of pectin with hydrophobic zein particles (ZP) improved its wettability (84-86˚) and particle size, which resulted in a smaller oil droplet size and prevented coalescence of oil droplets at pH 3. As illustrated in Fig 6, exceeding the isoelectric point of ZP at pH 6 caused the desorption of pectin from the surface of ZP due to the electrostatic repulsive force, resulting in unstable emulsions similar to ZP particles alone at the interface.[261]

The complexation of flaxseed protein particles (FP) and the soluble fraction of flaxseed mucilage (SFM) at pH 3 enhanced interfacial activity (IFT=10 mM/m) and tuned wettability of particles. While using native FP or its particles alone resulted in poorly stable emulsions, stabilized Pickering

emulsion was formed using FP-SFM complex with no variation in the droplet size during storage.[262]

Table 3.9. Combination of different plant-based stabilizers for emulsion stabilization.

Emulsifier -dosage	Complex combination	Source	Particle size (nm)	Emulsion composition	Emulsion droplet size (μm)	CA˚/Other properties	Ref
Soy lecithin/ QS-0.25-2%	Mixing 1% SI and (0.25 to 2%) QS stock solutions.	Soy lecithin and Quillaja saponin	-	MCT-50 wt.%	Lecithin=0 3-1	5-20 mPa.s	[253]
					0.75-0.25	20-35 mPa.s	
HRG-QS-1wt.%	Mixing HRG (0.5%) and QS (0.5%) stock solutions. QS-to-HRG ratio 1:4 to 1:1 pH 7	Rice glutelin and Quillajasaponin	-	Refined rice bran oil-10 wt.%	QS=0 5-10	creamed	[256]
					0.24 to 0.18	no creaming	
API- CS-1.5 wt.%	Mixing API (2wt.%) and CS (1/2 wt.%) stock solutions. pH 7 / pH 3	Almond and tea saponins	-	Walnut oil-5 wt. %l	CS=0 4.5 / 20	-	[257]
					1 /7-8	-	
TA/WS at 0.25-1% WS	2 % (w/v) WS, TA (5 %, w/v)- TA/WS=0.05- pH 4	Wheat grains	-	Soybean oil-30%	9.99 to 2.7	TA=0 38˚	[258]
						86˚	
ZPHP	Mass ratios of pectin-to-zein particle 1:10, 2:10, and 5:10 at pH =3	Zein, pectin from citrus peel	116	Corn oil- 75%	unstable	Pectin=0 110˚	[261]
			583- 659		230-105	86-84˚	
FP- SFM-0.45%	FP and SFM stock solutions 0.45 wt.% (ratio50:50) acidification at pH 3	Brown flaxseeds	Super micron aggregates	Tricaprylin oil- 2.5 wt.%	SFM=0: 10 <	FP=0, 28˚	[262]
			Around 300		5-6	67˚	

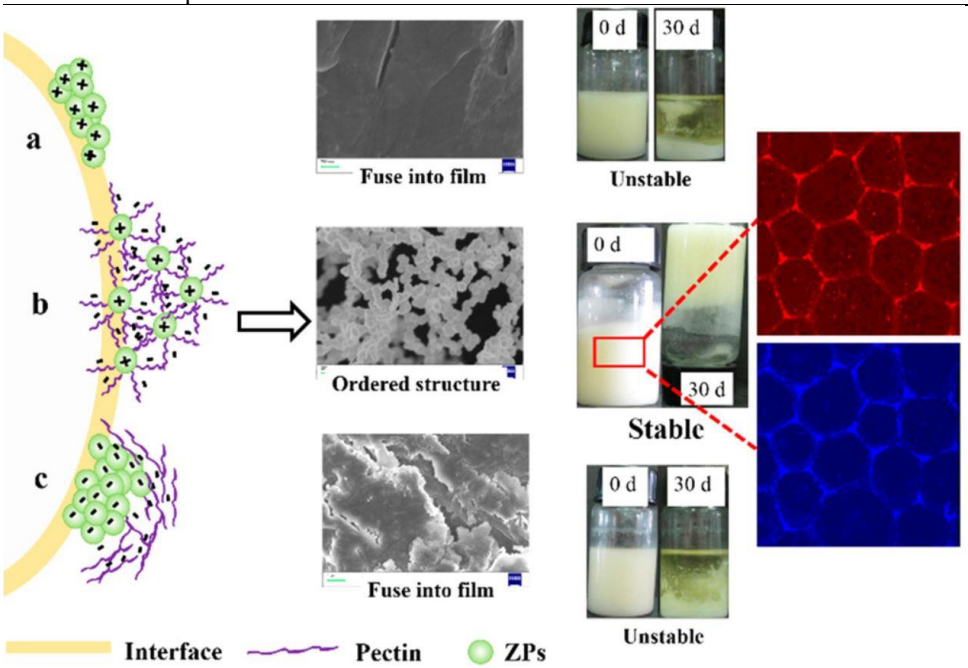

Figure 3.6: Schematic illustration for the formation of interfacial structure by ZPs at pH 3.8 (a), ZPHPs at pH 3.8 (b), and ZPHPs at pH 6.0 (c) and corresponding emulsion stability observation. Adapted with permission from [261]. Copyright (2020) American Chemical Society.

3.6 Application

Pickering/non-Pickering emulsions stabilized by plant-based particles and emulsifiers are sustainable and biocompatible systems that can be applied as foods, drug delivery mediums, hybrid materials, crude oil recuperation, and emulsion polymerization. Several review articles have focused particularly on the application of lignin,[263] starch,[264] proteins,[265] and cellulosic[176] in different technologies using stabilized emulsions. Here, we summarized mostly targeted applications of stabilized emulsions using plant-based polymers and particles studied over the past 5 years.

3.6.1 Encapsulating agents

Loaded microcapsules with active ingredients that are soluble in organic phase cores of capsules dispersed in aqueous media or vice versa can be attained in the form of emulsions or Pickering emulsions.[263] These capsules have a wide range of applications in thermal energy, in situ polymerization, or controlled loading and releasing of drugs or pesticides in pharmaceutical and agricultural technologies.[266,267] A list of plant-based stabilizers implemented as an encapsulating agent in such applications is summarized in Table 10.

CNCs and CNFs were applied for the microencapsulation of phase change materials (PCMs) for thermal energy storage. PS/CNC was employed as a shell to encapsulate paraffin wax as an organic PCM material leading to the much higher heat capacities of PW@PS/CNC slurries (31.9 J/g) than water.[268] Similar thermal regulation properties were obtained via encapsulated paraffin by CNF to further consolidate into a PCM composite with high enthalpy (139 J/g), which was proposed to be implemented in energy-efficient smart buildings construction.[269] In addition, the application of microcapsule for crop protection is reported using cinnamoyl chloride modified cellulose nanocrystals (CNC-CC) to stabilize polydopamine (DA) microcapsules with the controlled release over a longer time.[270]

Encapsulation in the medical application is reported via oil-in-water Pickering emulsion stabilized by aminated nanocellulose (ANC) particles, encapsulating coumarin and curcumin, which showed to inhibit microbial growth and prevented the favored killing of cancer cells compared to normal cells with the sustainable release.[271] Moreover, the encapsulation of various water-soluble or

water-insoluble drugs using LNPs is reported with low toxicity (cell viability of 90%) compared to many other biomaterials with improved release profile[272-274] and reduced cell viability of cancer cells.[275] Antibacterial Ag/lignin micro PCMs with both high transition enthalpy (177.6 J/g), good thermal stability, durability, and antibacterial activity are formulated.[276] Starch granule, pea protein, soy glycinin, and kafirin particles were also used to encapsulate curcumin with high efficiency and storage stability.[277-279] Starch-based emulsion successfully simulated oral and simulated gastric digestion.[277]

The OS-starch particles with an amphiphilic character were applied for encapsulating bioactive ingredients into foods while protecting them from water, oxygen, heat, etc.[280] As a general approach, after preparation of the OS-starch stabilized emulsion with encapsulated ingredients, solid capsules are obtained by spray-drying (or freeze-drying) in a powder form that can be used in food formulations.[281] The encapsulated active ingredients are released when the OS-starch is digested by the enzyme α-amylase.[280] For instance, spray-dried microcapsules of OSA/XG with encapsulated octadecadienoic acids (CLA) showed 64% reduced oxidation and enhanced control release of CLA in simulated small intestinal conditions.[282] As another interesting application of starch particles in food capsulations, sodium salt was loaded within emulsions of W1/O/W2 to enhance saltiness sensitivity into the oral cavity as a promising approach for the reduction of salt or sugar in emulsion-based foods.[283]

Table 3.10. Plant-based materials used for the encapsulation of active substances.

Emulsifier	Active substance	Encapsulation efficiency	Purpose	Performance	Suggested application	Ref.
PS/CNC	PCM (paraffin)	83.5%	Thermal energy storage	Thermal stability, 99.4%	Isothermal thermoses or electric chargeable hand warmers	[268]
CNF	PCM (paraffin)	72 wt%	Thermal regulation nanocomposites	Pure PCM showed no tensile strength/ PCM/CNF: Tensile strength 30 MPa and strain to failure of 12%.	Smart buildings construction	[269]
CNC-CC	Polydopamine DA	90%	Crop protection	Controlled the DA release to 80% over 50 h	Delivery of agrochemicals for pest control	[270]
ANC	Curcumin and coumarin PE	93 and 96% for curcumin and coumarin	Drug systems	Sustained release of 98% and 48% for coumarin and curcumin at pH 3.5 over 8 days	Antimicrobial and anticancer targeted sites	[271]
LNCs (AL)	Coumarin 6	70-90%	Targeted drug delivery	Complete release over 2 h	-	[272]

APS-LNPs	Gatifloxacin (G FLX) and doxorubicin (DOX)	40 and 90%	Drug/bioactive macromolecule loading	Controlled release of 50% over 50 h- cell viability of 90%	Biomedical field	[274]
pLNPs	Different drug loadings/ Benzazulene (BZL), Sorafenib (SFN)	77 BZL and 68% SFN	Drug delivery and biomedical applications	BZL release of 90 and 95 %/ SFN 61 and 100% at pH 5.5 and 7.4- reducing the cell viability of cancer cells from about 90% to 0%.	-	[275]
Ag/lignin	PCMs	69.0%	Thermal resistant and antibacterial	Energy-storage efficiency 69%, thermal storage capability 99%-100th heating-cooling cycle	Biomedical, textile and construction areas.	[276]
OSA-starch granule	Curcumin	80%/24 h storage stability	Delivery system s	Encapsulation stability of 95.3% and 86.3% during oral and intestinal simulated digestions	Delivery of bioactive compounds	[277]
OSA/XG	Octadecadienoic acids (CLA)	89.25%	Food delivery system	Enhanced CLA release to 12.1%-50.1%.	A wide range of bioactive components for various applications	[282]

3.6.2 Foods formulated emulsions

The use of plant-based stabilizer, mainly protein and starch have grown considerably as an emulsion stabilizer in food applications due to their availability, nontoxicity, and functional qualities, such as pasting and slow digestibility, nutrition values and ultimately their emulsifying properties. Several review articles directed on the food application by Pickering particles composed of polysaccharides, proteins, or polyphenols are available.[14,284,285]

OS-starch found a wide application in the food industry mainly as an emulsifier and fat replacer due to its colorless, tasteless, low-cost.[280] It should be stated that OS-starch with a DS <3% was approved as a food additive in the United States, members of the European Union, and China.[286] Mayonnaise-like emulsions without egg yolk were formulated using OSA-starch as the stabilizer, which formed a pseudoplastic system (shear thinning behavior) similar to the conventional mayonnaise.[287] In this case, the oil content of up to 60 wt.% was feasible to emulsify, while the long-term stability remained a problem.[287] Alternatively, egg yolk was partially (75%) substituted by (OSA)-modified starch resulting in the maximum emulsion stability of >95% after two months of storage.[288]

Plant-based proteins as emulsifiers are also known to be less allergenic compared to animal-derived proteins.[265] They can also act as antioxidants, implying that they are capable of inhibiting lipid oxidation, which made them suitable for lipid stabilization in food application.[289,290] For

instance, water-soluble legume proteins (lentil, pea, faba bean, and almond) effectively reduced lipid oxidation as the oil phase (flaxseed, ycopene, walnut, and fish oils) by 25-30% compared to animal-based protein stabilizers.[257,291,292]

A report is also available for the use of nano cellulosic emulsifiers in food-grade emulsions with edible oil.[293] In this case, designing food and beverage with cellulose particle stabilized-Pickering emulsions with the enhanced bioavailability of functional nutrients is growing.[294] The combinations of CNF, guar gum, and CMC in low-fat mayonnaise, with improved stability over commercial emulsifiers for O/W emulsion was also reported.[295]

3.6.3 Composites and other applications

Plant-based/polymer nanocomposite films can be prepared by polymerizing monomer droplets of O/W emulsions stabilized by plant-based polymers or particles, which is very similar to conventional suspension polymerization.[296] Several examples are summarized in Table 11, which reports the improved properties of composites in the presence of such polymers/particles. Composites formed via Pickering polymerization of PS or PBuMA stabilized by CNF or CNCAs, respectively, showed enhanced mechanical and thermal properties compared to CNF/CNCAs free composites.[297,298] Regenerated cellulose (RC)[299] and LNPs[300] were also incorporated into PLA composites via oil-in-water Pickering emulsion stabilized by RC and LNPs, respectively. The RC/PLA composites showed enhanced crystallization and thermomechanical properties including storage modulus and tensile strength compared with the native PLA.[299] The introduction of lignin particles improved crystallinity, stiffness, and thermal properties of PLA, which would have an advantage in industrial applications compared to the dispersed lignin particles in the usual melt blending material.[300]

As another application, the water-expandable beads of PS were formed by polymerization with cross-linked starch nanoparticles (CSTN) as a Pickering emulsion stabilizer, which improved the expandability of beads by 7 times with extended shelf life.[301]

Table 3.11. Plant-based emulsifiers used for composites and beads formation.

Emulsifier	Application	Product	Improved property	Ref
TEMPO CNF	Reinforcing fillers-12%	(PS)/CNF composites	Young's modulus 88%- Tensile strength 30%- high optical transparency 88%	[297]
CNCAs	Reinforcing fillers-0.5 wt%	PBuMA-CNCAs nanolatexes composites	Young's modulus 550%- fracture strength 115%	[298]

RC	Reinforcing fillers- 1-2 wt.%	RC/PLA composites	The crystallinity 159%- storage modulus 15%- tensile strength 34%	[299]
LNPs	Reinforcing fillers - 5.0 wt%	PLA/lignin composites	The crystallinity 10%- Young's modulus 15%- decomposition temperature improved by about 10 °C	[300]
CSTN	Water-stabilizing agent-1 wt. %	Water-expandable polystyrene beads (CSTNWEPS)	Expansion ratio of ~7 for as-synthesized beads and ~3 after 3 months- Preserved water content after 3 months was 88% compared to 2.6% without CSTN incorporation	[301]

In terms of water-soluble emulsifiers, a widely used application for lignosulfonate has been in a chemical injection process of EOR (Enhanced Oil Recovery) for the oil industry.[302,303] Carboxymethylated lignin has shown promising emulsifier properties by decreasing the viscosity of crude bitumen and refined oil,[164] stabilizing high internal phase ratio emulsions (70:30 fuel-to-water) for application in a compression-ignition diesel engine[304] and indicated a potential alternative for use in fuel emulsions.[165]

As a promising approach to managing large-scale oil spills with a detrimental impact on the environment and marine life, a mixture of lignin nanoparticles and 1-pentanol worked effectively for oil spill recovery with the effective adsorption of LNPs to the oil-water interface.[305]

Ojala et al.[306] also studied the stabilization of marine diesel O/W emulsions with bi-functionalized CNC (But-CNCs) for such applications as oil-spill response agents.

3.7 Future Perspectives and Challenges

The swift growth in research topics of Pickering stabilization by plant-based particles was inevitable over the past 5 years, and the rise would continue. However, still conventional emulsions using polymers have their places in research, and it is predicted that more attention would be given to the combination of polymers and particles as stabilizers for improved stability of emulsion systems. The optimization of surface and morphological properties by modifying particle size, wettability, aggregation, and surface chemistry were shown to be the underlying parameters on altering emulsion properties that will remain a big challenge to overcome for different materials. Despite all the progress on research and development of Pickering emulsions using plant-based resources, no commercialized product based on Pickering emulsions is available.[33] Some significant challenges to the commercialization of Pickering emulsions remained to be overcome. In all the discussed plant-based stabilizers, the composition, structure, and physicochemical properties of the isolated raw materials could be easily affected by the source of the material and

formulation process, which might remain the greatest challenge for their commercialization. The scale-up production of particles will need to be addressed to facilitate the industrialization of Pickering emulsion applications. The scale-up processes should be economically viable, sustainable, and reproducible. Maintaining a constant composition of the ingredients from batch-to-batch production could be a real challenge considering the inevitable role of variables (e.g., weather and soil conditions, time of harvest, and extraction methods) on the molecular and functional properties of plant-based materials.[7] The storage stability and biodegradability rate of particles should be improved and controlled for a particular application. In addition to the production challenges, expanding the research area on the fundamental studies of the stabilization processes should be given more attention. The target of research on such sustainable plant-based emulsifying agents is to partially or completely replace the synthetic or animal-based particles and emulsifiers with them. Therefore, for future research, it may be suggested that more application-oriented studies on the use of plant-based polymers and particles be implemented. Alternatively, more attention can be paid to the combination and/or modification of plant-based polymers or particles from different sources for generating impactful Pickering and Non-Pickering emulsifiers.

3.8 Conclusions

Many plant-derived materials are poorly soluble in water, but they can be effectively functionalized for higher solubility or be used as insoluble particles in variable sizes from nanometers to micrometers that can stabilize oil/water systems. This paper comprehensively reviewed various modification and formulation routes for functionalizing and producing plant-based polymers and particles and their utilization in stabilizing emulsion systems (Pickering/non-Pickering). The main properties that affected the behavior of polymeric surfactants as emulsifiers were molecular weight, surface charge, functional groups, and solubility, while surface charge, size, and wettability properties were the influential factors for nanoparticles. The formulated emulsions showed a wide range of applications in various technologies, which could be further expanded. In conclusion, exploring and modifying underutilized plant-based materials as sustainable resources could pave the way for developing green substitutes for oil-based and animal-based materials to be used in various processes and technologies.

3.9 References

[1] I. Kralova, J. Sjöblom, *J. Dispersion Sci. Technol.* **2009**, *30*, 1363-1383.

[2] T. del Castillo-Santaella, J. M. Peula-García, J. Maldonado-Valderrama, A. B. Jódar-Reyes, *Colloids surf. B: Biointerfaces* **2019**, *173*, 295-302.

[3] D. Baines, R. Seal, *Natural food additives, ingredients and flavourings*, Elsevier, **2012**.

[4] A. C. Karaca, N. Low, M. Nickerson, *Trends Food Sci. Technol.* **2015**, *42*, 5-12.

[5] A. Nesterenko, I. Alric, F. Silvestre, V. Durrieu, *Ind. Crops Prod.* **2013**, *42*, 469-479.

[6] L. E. Low, S. P. Siva, Y. K. Ho, E. S. Chan, B. T. Tey, *Adv. Colloid Interface Sci.* **2020**, *277*, 102117-102140.

[7] D. J. McClements, C. E. Gumus, *Adv. Colloid Interface Sci.* **2016**, *234*, 3-26.

[8] S. Lam, K. P. Velikov, O. D. Velev, *Curr. Opin. Colloid Interface Sci.* **2014**, *19*, 490-500.

[9] V. Calabrese, J. C. Courtenay, K. J. Edler, J. L. Scott, *Curr. Opin. Green Sustain. Chem.* **2018**, *12*, 83-90.

[10] C. C. Berton-Carabin, K. Schroën, *Annu Rev Food Sci. Technol.* **2015**, *6*, 263-297.

[11] K. S. Mikkonen, *Green Chem.* **2020**, *22*, 1019-1037.

[12] H. Dai, J. Wu, H. Zhang, Y. Chen, L. Ma, H. Huang, Y. Huang, Y. Zhang, *Trends Food Sci. Technol.* **2020**, *102*, 16-29

[13] C. H. Tang, *Food Hydrocoll.* **2020**, *103*, 105664-105679.

[14] A. Sarkar, E. Dickinson, *Curr. Opin. Colloid Interface Sci.* **2020,** *49*, 69-81.

[15] S. Sabaghi, P. Fatehi, *Biomacromolecules* **2019**, *20*, 3940-3951.

[16] N. Ghavidel Darestani, A. Tikka, P. Fatehi, *Polymers* **2018**, *10*, 928-945.

[17] B. Wildt, P. Mali, P. C. Searson, *Langmuir* **2006**, *22*, 10528-10534.

[18] M. W. Boehm, F. J. Warren, S. K. Baier, M. J. Gidley, J. R. Stokes, *Food Hydrocoll.* **2019**, *96*, 475-480.

[19] D. J. McClements, *Adv Nutr.* **2015**, *6*, 338S-352S.

[20] J. N. Israelachvili, *Intermolecular and surface forces*, Academic press, **2011**.

[21] D. J. McClements, *Food emulsions: principles, practices, and techniques*, CRC press, **2015**.

[22] E. Dickinson, *Colloids surf. B: Biointerfaces* **2010**, *81*, 130-140.

[23] C. Qian, E. A. Decker, H. Xiao, D. J. McClements, *J. Am. Oil Chem.' Soc.* **2011**, *88*, 47-55.

[24] M. Zembyla, A. Lazidis, B. S. Murray, A. Sarkar, *Langmuir* **2019**, *35*, 13078-13089.

[25] Z. M. Gao, X. Q. Yang, N. N. Wu, L. J. Wang, J. M. Wang, J. Guo, S. W. Yin, *J. Agric. Food Chem.* **2014**, *62*, 2672-2678.

[26] J. Ma, C. Gan, Q. Xu, J. Zhou, J. Zhang, *Colloids Surf. A Physicochem. Eng. Asp.* **2015**, *471*, 65-72.

[27] H. Ajiro, Y. J. Hsiao, H. T. Tran, T. Fujiwara, M. Akashi, *Macromolecules* **2013**, *46*, 5150-5156.

[28] W. Ramsden, *Proc. R. Soc. Lond.* **1904**, *72*, 156-164.

[29] S. U. Pickering, *J. Chem. Soc., Trans.* **1907**, *91*, 2001-2021.

[30] B. P. Binks, *Curr. Opin. Colloid Interface Sci.* **2002**, *7*, 21-41.

[31] S. Tcholakova, N. Denkov, A. Lips, *Phys. Chem. Chem. Phys.* **2008**, *10*, 1608-1627.

[32] I. Capron, O. J. Rojas, R. Bordes, *Curr. Opin. Colloid Interface Sci.* **2017**, *29*, 83-95.

[33] C. Albert, M. Beladjine, N. Tsapis, E. Fattal, F. Agnely, N. Huang, *J Control Release* **2019**, *309*, 302-332.

[34] N. Bizmark, M. A. Ioannidis, D. E. Henneke, *Langmuir* **2014**, *30*, 710-717.

[35] M. Rayner, D. Marku, M. Eriksson, M. Sjöö, P. Dejmek, M. Wahlgren, *Colloids Surf. A Physicochem. Eng. Asp.* **2014**, *458*, 48-62.

[36] J. Bergfreund, Q. Sun, P. Fischer, P. Bertsch, *Nanoscale Adv.* **2019**, *1*, 4308-4312.

[37] M. Shields, R. Ellis, B. R. Saunders, *Colloids Surf. A Physicochem. Eng. Asp.* **2001**, *178*, 265-276.

[38] M. M. Robins, *Curr. Opin. Colloid Interface Sci.* **2000**, *5*, 265-272.

[39] D. Klemm, B. Heublein, H. P. Fink, A. Bohn, *Angew. Chem., Int. Ed.* **2005**, *44*, 3358-3393.

[40] J. M. Raquez, Y. Habibi, M. Murariu, P. Dubois, *Prog. Polym. Sci.* **2013**, *38*, 1504-1542.

[41] N. Lavoine, I. Desloges, J. Bras, *Carbohydr. Polym.* **2014**, *103*, 528-537.

[42] R. J. Moon, A. Martini, J. Nairn, J. Simonsen, J. Youngblood, *Chem. Soc. Rev.* **2011**, *40*, 3941-3994.

[43] D. Klemm, F. Kramer, S. Moritz, T. Lindström, M. Ankerfors, D. Gray, A. Dorris, *Angew. Chem., Int. Ed.* **2011**, *50*, 5438-5466.

[44] N. Lavoine, I. Desloges, A. Dufresne, J. Bras, *Carbohydr. Polym.* **2012**, *90*, 735-764.

[45] Y. Habibi, L. A. Lucia, O. J. Rojas, *Chem. Rev.* **2010**, *110*, 3479-3500.

[46] S. Alila, I. Besbes, M. R. Vilar, P. Mutjé, S. Boufi, *Ind. Crops Prod.* **2013**, *41*, 250-259.

[47] M. Jonoobi, R. Oladi, Y. Davoudpour, K. Oksman, A. Dufresne, Y. Hamzeh, R. Davoodi, *Cellulose* **2015**, *22*, 935-969.

[48] H. A. Khalil, Y. Davoudpour, M. N. Islam, A. Mustapha, K. Sudesh, R. Dungani, M. Jawaid, *Carbohydr. Polym.* **2014**, *99*, 649-665.

[49] Z. Karim, S. Afrin, Q. Husain, R. Danish, *Crit. Rev. Biotechnol.* **2017**, *37*, 355-370.

[50] R. Aaen, S. Simon, F. W. Brodin, K. Syverud, *Cellulose* **2019**, *26*, 5483-5496.

[51] L. Alves, E. Ferraz, A. Lourenço, P. Ferreira, M. Rasteiro, J. Gamelas, *Carbohydr. Polym.* **2020**, *237*, 116109-116116.

[52] H. Du, W. Liu, M. Zhang, C. Si, X. Zhang, B. Li, *Carbohydr. Polym.* **2019**, *209*, 130-144.

[53] R. Mu, X. Hong, Y. Ni, Y. Li, J. Pang, Q. Wang, J. Xiao, Y. Zheng, *Trends Food Sci. Technol.* **2019**, *93*, 136-144.

[54] O. V. Surov, M. I. Voronova, N. V. Rubleva, L. A. Kuzmicheva, D. Nikitin, A. Choukourov, V. A. Titov, A. G. Zakharov, *Cellulose* **2018**, *25*, 5035-5048.

[55] R. Rohaizu, W. Wanrosli, *Ultrason Sonochem.* **2017**, *34*, 631-639.

[56] F. Ferreira, M. Mariano, S. Rabelo, R. Gouveia, L. Lona, *Appl. Surf. Sci.* **2018**, *436*, 1113-1122.

[57] H. Hasegawa, Y. Horikawa, T. Shikata, *Macromolecules* **2020**, *53*, 2677-2685.

[58] F. V. Ferreira, C. G. Otoni, J. Kevin, H. S. Barud, L. M. Lona, E. D. Cranston, O. J. Rojas, *Mater. Today* **2020**, *37*, 126-141.

[59] P. Bertsch, M. Arcari, T. Geue, R. Mezzenga, G. Nyström, P. Fischer, *Biomacromolecules* **2019**, *20*, 4574-4580.

[60] P. Bertsch, M. Diener, J. Adamcik, N. Scheuble, T. Geue, R. Mezzenga, P. Fischer, *Langmuir* **2018**, *34*, 15195-15202.

[61] K. J. De France, T. Hoare, E. D. Cranston, *Chem. Mater.* **2017**, *29*, 4609-4631.

[62] Y. Dong, H. Paukkonen, W. Fang, E. Kontturi, T. Laaksonen, P. Laaksonen, *Int. J. Pharm.* **2018**, *548*, 113-119.

[63] A. Dufresne, *Curr. For. Rep.* **2019**, *5*, 76-89.

[64] Z. H. Feizi, P. Fatehi, *Cellulose* **2020**, *27,* 1-14.

[65] M. G. Sajilata, R. S. Singhal, P. R. Kulkarni, *Compr. Rev. Food Sci. Food Saf.* **2006**, *5*, 1-17.

[66] P. R. Correia, M. L. Beirão-da-Costa, *Food Bioprod. Process* **2012**, *90*, 309-316.

[67] P. R. Correia, M. L. Beirão-da-Costa, *Starch-Stärke* **2010**, *62*, 421-428.

[68] R. F. Tester, J. Karkalas, X. Qi, *J. Cereal Sci.* **2004**, *39*, 151-165.

[69] M. C. Sweedman, M. J. Tizzotti, C. Schäfer, R. G. Gilbert, *Carbohydr. Polym.* **2013**, *92*, 905-920.

[70] J. Kaur, G. Kaur, S. Sharma, K. Jeet, *Crit. Rev. Food Sci. Nutr* **2018**, *58*, 1097-1107.

[71] J. Marto, A. Ascenso, S. Simoes, A. J. Almeida, H. M. Ribeiro, *Expert Opin. Drug Deliv.* **2016**, *13*, 1093-1107.

[72] S. B. Haaj, W. Thielemans, A. Magnin, S. Boufi, *ACS Appl. Mater. Interfaces* **2014**, *6*, 8263-8273.

[73] Y. Chen, Y. Hao, K. Ting, Q. Li, Q. Gao, *Food Chem.* **2019**, *286*, 467-474.

[74] C. Xu, C. Chen, D. Wu, *Carbohydr. Polym.* **2018**, *182*, 115-122.

[75] M. Matos, A. Timgren, M. Sjöö, P. Dejmek, M. Rayner, *Colloids Surf. A Physicochem. Eng. Asp.* **2013**, *423*, 147-153.

[76] D. J. McClements, L. Bai, C. Chung, *Annu Rev Food Sci. Technol.* **2017**, *8*, 205-236.

[77] J. W. Brady, *Introductory Food Chem.*, Comstock, **2013**.

[78] N. Diovisalvi, N. R. Calvo, N. Izquierdo, H. Echeverría, G. A. Divito, F. García, *J. Agron.* **2018**, *110*, 1532-1543.

[79] R. S. Lam, M. T. Nickerson, *Food Chem.* **2013**, *141*, 975-984.

[80] D. R. Holding, *Front. Plant Sci.* **2014**, *5*, 276-285.

[81] M. Tarhini, H. Greige-Gerges, A. Elaissari, *Int. J. Pharm.* **2017**, *522*, 172-197.

[82] M. Evans, I. Ratcliffe, P. A. Williams, *Curr. Opin. Colloid Interface Sci.* **2013**, *18*, 272-282.

[83] F. Ning, Z. Ge, L. Qiu, X. Wang, L. Luo, H. Xiong, Q. Huang, *Food Hydrocoll.* **2020**, *99*, 105308-105316.

[84] Z. Ren, Z. Chen, Y. Zhang, X. Lin, B. Li, *Food Hydrocoll.* **2019**, *96*, 322-330.

[85] H. Malekzad, H. Mirshekari, P. Sahandi Zangabad, S. Moosavi Basri, F. Baniasadi, M. Sharifi Aghdam, M. Karimi, M. R. Hamblin, *Crit. Rev. Biotechnol.* **2018**, *38*, 47-67.

[86] A. G. Wouters, J. A. Delcour, *Curr. Opin. Food Sci.* **2019**, *25*, 19-27.

[87] D. Ercili-Cura, A. Miyamoto, A. Paananen, H. Yoshii, K. Poutanen, R. Partanen, *Food Hydrocoll.* **2015**, *44*, 183-190.

[88] M. Norgren, H. Edlund, *Curr. Opin. Colloid Interface Sci.* **2014**, *19*, 409-416.

[89] W. Boerjan, J. Ralph, M. Baucher, *Annu. Rev. Plant Biol.* **2003**, *54*, 519-546.

[90] J. Ralph, K. Lundquist, G. Brunow, F. Lu, H. Kim, P. F. Schatz, J. M. Marita, R. D. Hatfield, S. A. Ralph, J. H. Christensen, *Phytochem Rev.* **2004**, *3*, 29-60.

[91] S. Gharehkhani, Y. Zhang, P. Fatehi, *Prog. Energy Combust. Sci.* **2019**, *72*, 59-89.

[92] R. Alén, in *Industrial biorefineries & white biotechnology*, Elsevier, **2015**, 91-126.

[93] H. Shi, P. Fatehi, H. Xiao, Y. Ni, *Bioresour. Technol.* **2011**, *102*, 5177-5182.

[94] T. Aro, P. Fatehi, *ChemSusChem* **2017**, *10*, 1861-1877.

[95] Z. Liu, Y. Ni, P. Fatehi, A. Saeed, *Biomass Bioenerg* **2011**, *35*, 1789-1796.

[96] S. Laurichesse, L. Avérous, *Prog. Polym. Sci.* **2014**, *39*, 1266-1290.

[97] B. M. Upton, A. M. Kasko, *Chem. Rev.* **2016**, *116*, 2275-2306.

[98] W. Zhao, B. Simmons, S. Singh, A. Ragauskas, G. Cheng, *Green Chem.* **2016**, *18*, 5693-5700.

[99] P. Tableueiredo, K. Lintinen, J. T. Hirvonen, M. A. Kostiainen, H. A. Santos, *Prog. Mater. Sci.* **2018**, *93*, 233-269.

[100] M. Österberg, M. H. Sipponen, B. D. Mattos, O. J. Rojas, *Green Chem.* **2020**, *22*, 2712-2733.

[101] W. Gao, P. Fatehi, *Can. J. Chem. Eng.* **2019**, *97*, 2827-2842.

[102] A. S. Nerurkar, K. S. Hingurao, H. G. Suthar, *J Sci Ind Res India* **2009**, *68*, 273-277.

[103] D. K. F. Santos, R. D. Rufino, J. M. Luna, V. A. Santos, L. A. Sarubbo, *Int. J. Mol. Sci.* **2016**, *17*, 401-432.

[104] R. Jahan, A. M. Bodratti, M. Tsianou, P. Alexandridis, *Adv. Colloid Interface Sci.* **2020**, *275*, 102061-102083.

[105] S. Cox, A. Sandall, L. Smith, M. Rossi, K. Whelan, *Nutr. Rev.* **2020,** *0(0)*, 1-16.

[106] K. Jedvert, T. Heinze, *J Polym Eng.* **2017**, *37*, 845-860.

[107] H. Thielking, M. Schmidt, *Ullmann's encyclopedia of industrial chemistry* **2000**.

[108] H. C. Arca, L. I. Mosquera-Giraldo, V. Bi, D. Xu, L. S. Taylor, K. J. Edgar, *Biomacromolecules* **2018**, *19*, 2351-2376.

[109] T. Heinze, O. A. El Seoud, A. Koschella, in *Cellulose derivatives*, Springer, **2018**, 429-477.

[110] M. Kostag, M. Gericke, T. Heinze, O. A. El Seoud, *Cellulose* **2019**, *26*, 139-184.

[111] Y. Habibi, L. A. Lucia, *Polysaccharide building blocks: a sustainable approach to the development of renewable biomaterials*, John Wiley & Sons, **2012**.

[112] A. Torcello-Gómez, T. J. Foster, *Carbohydr. Polym.* **2016**, *144*, 495-503.

[113] J. Teixé-Roig, G. Oms-Oliu, G. Velderrain-Rodríguez, I. Odriozola-Serrano, O. Martín-Belloso, *Food Bioproc Tec.* **2018**, *11*, 2229-2241.

[114] M. Matos, G. Gutiérrez, J. Coca, C. Pazos, *Colloids Surf. A Physicochem. Eng. Asp.* **2014**, *442*, 69-79.

[115] A. Schuch, C. Helfenritter, M. Funck, H. Schuchmann, *Colloids Surf. A Physicochem. Eng. Asp.* **2015**, *475*, 2-8.

[116] G. Sun, L. Lei, H. Chen, B. Li, Y. Cao, Y. Li, *Food Funct.* **2018**, *9*, 3657-3664.

[117] N. A. Camino, A. M. Pilosof, *Food Hydrocoll.* **2011**, *25*, 1051-1062.

[118] R. T. Shimada, M. S. Fonseca, D. F. Petri, *Colloids Surf. A Physicochem. Eng. Asp.* **2017**, *529*, 137-145.

[119] H. O. Akinosho, L. Wicker, *LWT-J. Food Sci. Technol.* **2015**, *63*, 582-589.

[120] W. Sun, D. Sun, Y. Wei, S. Liu, S. Zhang, *J. Colloid Interface Sci.* **2007**, *311*, 228-236.

[121] C. Costa, I. Mira, J. W. Benjamins, B. Lindman, H. Edlund, M. Norgren, *J. Mol. Liq.* **2019**, *292*, 111325-111332.

[122] H. C. Arca, Virginia Tech, Doctoral dissertation, **2016**.

[123] A. P. Imeson, *Thickening and gelling agents for food*, Springer Science & Business Media, **2012**.

[124] C. Li, Y. Li, P. Sun, C. Yang, *Colloids Surf. A Physicochem. Eng. Asp.* **2013**, *431*, 142-149.

[125] A. Timgren, M. Rayner, P. Dejmek, D. Marku, M. Sjöö, *Food Sci. Nutr.* **2013**, *1*, 157-171.

[126] A. Marefati, B. Wiege, N. Haase, M. Matos, M. Rayner, *Carbohydr. Polym.* **2017**, *175*, 473-483.

[127] E. Agama-Acevedo, L. A. Bello-Perez, *Curr. Opin. Food Sci.* **2017**, *13*, 78-83.

[128] A. C. Eliasson, B. Bergenståhl, L. Nilsson, M. Sjöö, *Cereal Chem.* **2013**, *90*, 326-334.

[129] S. Simsek, M. Ovando-Martinez, A. Marefati, M. Sjöö, M. Rayner, *Food Res. Int.* **2015**, *75*, 41-49.

[130] H. Namazi, F. Fathi, A. Dadkhah, *Sci. Iran.* **2011**, *18*, 439-445.

[131] S. Li, C. Li, Y. Yang, X. He, B. Zhang, X. Fu, C. P. Tan, Q. Huang, *Food Chem.* **2019**, *283*, 437-444.

[132] J. Li, F. Ye, L. Lei, Y. Zhou, G. Zhao, *J. Agric. Food Chem.* **2018**, *66*, 4541-4550.

[133] W. Liu, Y. Li, H. D. Goff, J. Nsor-Atindana, J. Ma, F. Zhong, *Langmuir* **2019**, *35*, 4702-4709.

[134] M. C. Sweedman, C. Schäfer, R. G. Gilbert, *Carbohydr. Polym.* **2014**, *111*, 918-927.

[135] M. C. Sweedman, J. Hasjim, C. Schäfer, R. G. Gilbert, *Carbohydr. Polym.* **2014**, *112*, 85-93.

[136] Y. Wei, Y. Xie, Z. Cai, Y. Guo, M. Wu, P. Wang, R. Li, H. Zhang, *J. Colloid Interface Sci.* **2020,** *580*, 480-492.

[137] S. Zhao, G. Tian, C. Zhao, C. Lu, Y. Bao, X. Liu, J. Zheng, *Food Hydrocoll.* **2018**, *85*, 248-256.

[138] H. Zhang, C. Schäfer, P. Wu, B. Deng, G. Yang, E. Li, R. G. Gilbert, C. Li, *Food Hydrocoll.* **2018**, *74*, 168-175.

[139] B. Murúa-Pagola, C. Beristain-Guevara, F. Martínez-Bustos, *J. Food Eng.* **2009**, *91*, 380-386.

[140] Y. García-Tejeda, E. Leal-Castañeda, V. Espinosa-Solis, V. Barrera-Figueroa, *Carbohydr. Polym.* **2018**, *194*, 177-183.

[141] E. J. Leal-Castañeda, Y. García-Tejeda, H. Hernández-Sánchez, L. Alamilla-Beltrán, D. I. Téllez-Medina, G. Calderón-Domínguez, H. S. García, G. F. Gutiérrez-López, *Food Hydrocoll.* **2018**, *80*, 177-185.

[142] X. He, X. Gong, W. Li, W. Cao, J. Yan, R. Guo, B. Niu, L. Jia, *Starch-Stärke* **2019**, *71*, 1900089-1900097.

[143] M. Xie, Y. Duan, F. Li, X. Wang, X. Cui, U. Bacha, M. Zhu, Z. Xiao, Z. Zhao, *Starch-Stärke* **2017**, *69*, 1600061-1600070.

[144] X. Song, Y. Pei, M. Qiao, F. Ma, H. Ren, Q. Zhao, *Food Hydrocoll.* **2015**, *45*, 256-263.

[145] E. Dickinson, *Food Hydrocoll.* **2003**, *17*, 25-39.

[146] J. Sirison, K. Matsumiya, M. Samoto, H. Hidaka, M. Kouno, Y. Matsumura, *Biosci. Biotechnol. Biochem.* **2017**, *81*, 790-802.

[147] Y. Li, M. Zhong, F. Xie, Y. Sun, S. Zhang, B. Qi, *Food Chem.* **2020**, *309*, 125579-125588.

[148] C. E. Gumus, E. A. Decker, D. J. McClements, *Food Biophys.* **2017**, *12*, 186-197.

[149] Y. Zheng, Z. Li, C. Zhang, B. Zheng, Y. Tian, *Food Chem.* **2020**, *311*, 125932-125941.

[150] H. Hu, I. W. Cheung, S. Pan, E. C. Li-Chan, *Food Hydrocoll.* **2015**, *45*, 102-110.

[151] J. O'sullivan, B. Murray, C. Flynn, I. Norton, *Food Hydrocoll.* **2016**, *53*, 141-154.

[152] Q. T. Zhang, Z. C. Tu, H. Xiao, H. Wang, X. Q. Huang, G. X. Liu, C. M. Liu, Y. Shi, L. L. Fan, D. R. Lin, *Food Bioprod. Process* **2014**, *92*, 30-37.

[153] J. Resendiz-Vazquez, J. Ulloa, J. Urías-Silvas, P. Bautista-Rosales, J. Ramírez-Ramírez, P. Rosas-Ulloa, L. González-Torres, *Ultrason Sonochem.* **2017**, *37*, 436-444.

[154] J. Glusac, S. Isaschar-Ovdat, A. Fishman, *Food Chem.* **2020**, *315*, 126301.

[155] S. Ben-Harb, M. Panouille, D. Huc-Mathis, G. Moulin, A. Saint-Eve, F. Irlinger, P. Bonnarme, C. Michon, I. Souchon, *Food Hydrocoll.* **2018**, *77*, 75-84.

[156] D. J. McClements, *Curr. Opin. Colloid Interface Sci.* **2004**, *9*, 305-313.

[157] M. Makeri, K. Muhammad, H. Ghazali, A. Mohammed, *J. Food Meas. Charact.* **2019**, *13*, 97-106.

[158] G. Neale, V. Hornof, C. Chiwetelu, *Can. J. Chem.* **1981**, *59*, 1938-1943.

[159] S. Farad, M. A. Manan, N. Ismail, H. K. Nsamba, E. Galiwango, I. Kabenge, *Am. J. Sci. Technol.* **2016**, *3*, 63-72.

[160] C. Xu, F. Ferdosian, in *Conversion of Lignin into Bio-Based Chemicals and Materials*, Springer, **2017**, 81-90.

[161] N. Alwadani, P. Fatehi, *CRC* **2018**, *1*, 126-138.

[162] C. Z. Chen, M. F. Li, Y. Y. Wu, R. C. Sun, *RSC Adv.* **2014**, *4*, 16944-16950.

[163] M. Zhou, W. Wang, D. Yang, X. Qiu, *RSC Adv.* **2015**, *5*, 2441-2448.

[164] S. Li, D. Ogunkoya, T. Fang, J. Willoughby, O. J. Rojas, *J. Colloid Interface Sci.* **2016**, *482*, 27-38.

[165] S. Li, J. A. Willoughby, O. J. Rojas, *ChemSusChem* **2016**, *9*, 2460-2469.

[166] S. Gharehkhani, N. Ghavidel, P. Fatehi, *ACS Sustain. Chem. Eng.* **2018**, *7*, 2370-2379.

[167] N. Ghavidel, P. Fatehi, *RSC Adv.* **2019**, *9*, 17639-17652.

[168] N. Delgado, F. Ysambertt, G. Chávez, B. Bravo, D. E. García, J. Santos, *Waste Biomass Valori.* **2019**, *10*, 3383-3395.

[169] N. Ghavidel, P. Fatehi, *ChemSusChem* **2020,** *13*(17), 4567-4578.

[170] J. Zhang, Y. Ge, L. Qin, W. Huang, Z. Li, *J. Dispersion Sci. Technol.* **2018**, *39*, 1140-1143.

[171] K. M. Perkins, C. Gupta, E. N. Charleson, N. R. Washburn, *Colloids Surf. A Physicochem. Eng. Asp.* **2017**, *530*, 200-208.

[172] B. V. Schmidt, V. Molinari, D. Esposito, K. Tauer, M. Antonietti, *Polymer* **2017**, *112*, 418-426.

[173] C. Shi, S. Zhang, W. Wang, R. J. Linhardt, A. J. Ragauskas, *ACS Sustain. Chem. Eng.* **2019**, *8*, 22-28.

[174] Z. Zhang, Y. Zhang, Z. Lin, A. Mulyadi, W. Mu, Y. Deng, *Chem. Eng. Sci.* **2017**, *165*, 55-64.

[175] H. Saari, K. Heravifar, M. Rayner, M. Wahlgren, M. Sjöö, *Cereal Chem.* **2016**, *93*, 116-124.

[176] L. Bai, S. Lv, W. Xiang, S. Huan, D. J. McClements, O. J. Rojas, *Food Hydrocoll.* **2019**, *96*, 699-708.

[177] L. Bai, S. Lv, W. Xiang, S. Huan, D. J. McClements, O. J. Rojas, *Food Hydrocoll.* **2019**, *96*, 709-716.

[178] J. Shin, K. Na, S. Shin, S. M. Seo, H. J. Youn, I.-K. Park, J. Hyun, *Biomolecules* **2019**, *9*, 799-812.

[179] T. Angkuratipakorn, A. Sriprai, S. Tantrawong, W. Chaiyasit, J. Singkhonrat, *Colloids Surf. A Physicochem. Eng. Asp.* **2017**, *522*, 310-319.

[180] W. Wang, G. Du, C. Li, H. Zhang, Y. Long, Y. Ni, *Carbohydr. Polym.* **2016**, *151*, 1-8.

[181] J. Ojala, J. A. Sirviö, H. Liimatainen, *Cellulose* **2018**, *25*, 293-304.

[182] J. Tang, M. F. X. Lee, W. Zhang, B. Zhao, R. M. Berry, K. C. Tam, *Biomacromolecules* **2014**, *15*, 3052-3060.

[183] S. Varanasi, L. Henzel, L. Mendoza, R. Prathapan, W. Batchelor, R. Tabor, G. Garnier, *Front. Chem.* **2018**, *6*, 409-418.

[184] I. Kalashnikova, H. Bizot, B. Cathala, I. Capron, *Biomacromolecules* **2012**, *13*, 267-275.

[185] F. Cherhal, B. Cathala, I. Capron, *Nord Pulp Paper Res J.* **2015**, *30*, 126-131.

[186] A. Pandey, M. Derakhshandeh, S. A. Kedzior, B. Pilapil, N. Shomrat, T. Segal-Peretz, S. L. Bryant, M. Trifkovic, *J. Colloid Interface Sci.* **2018**, *532*, 808-818.

[187] F. Cherhal, F. Cousin, I. Capron, *Biomacromolecules* **2016**, *17*, 496-502.

[188] X. Li, J. Li, J. Gong, Y. Kuang, L. Mo, T. Song, *Carbohydr. Polym.* **2018**, *183*, 303-310.

[189] I. Kalashnikova, H. Bizot, P. Bertoncini, B. Cathala, I. Capron, *Soft Matter* **2013**, *9*, 952-959.

[190] Z. Hu, T. Patten, R. Pelton, E. D. Cranston, *ACS Sustain. Chem. Eng.* **2015**, *3*, 1023-1031.

[191] Z. Hu, H. S. Marway, H. Kasem, R. Pelton, E. D. Cranston, *ACS Macro Letters* **2016**, *5*, 185-189.

[192] Z. Zhang, K. C. Tam, X. Wang, G. Sèbe, *ACS Sustain. Chem. Eng.* **2018**, *6*, 2583-2590.

[193] C. Tang, Y. Chen, J. Luo, M. Y. Low, Z. Shi, J. Tang, Z. Zhang, B. Peng, K. C. Tam, *Cellulose* **2019**, *26*, 7753-7767.

[194] W. Du, J. Guo, H. Li, Y. Gao, *ACS Sustain. Chem. Eng.* **2017**, *5*, 7514-7523.

[195] H. M. Ahsan, X. Zhang, Y. Liu, Y. Wang, Y. Li, B. Li, J. Wang, S. Liu, *Food Hydrocoll.* **2020**, *104*, 105742-105754.

[196] N. Bizmark, M. A. Ioannidis, *Langmuir* **2017**, *33*, 10568-10576.

[197] A. G. Cunha, J. B. Mougel, B. Cathala, L. A. Berglund, I. Capron, *Langmuir* **2014**, *30*, 9327-9335.

[198] M. Qiao, X. Yang, Y. Zhu, G. Guerin, S. Zhang, *Langmuir* **2020,** *36*, 6421-6428.

[199] A. L. R. Costa, A. Gomes, H. Tibolla, F. C. Menegalli, R. L. Cunha, *Carbohydr. Polym.* **2018**, *194*, 122-131.

[200] S. Yokota, K. Kamada, A. Sugiyama, T. Kondo, *Carbohydr. Polym.* **2019**, *226*, 115293-115300.

[201] J. Wu, W. Zhu, X. Shi, Q. Li, C. Huang, Y. Tian, S. Wang, *Carbohydr. Polym.* **2020**, *236*, 115999-116009.

[202] C. Jiménez Saelices, I. Capron, *Biomacromolecules* **2018**, *19*, 460-469.

[203] M. Gestranius, P. Stenius, E. Kontturi, J. Sjöblom, T. Tammelin, *Colloids Surf. A Physicochem. Eng. Asp.* **2017**, *519*, 60-70.

[204] Y. Lu, X. Qian, W. Xie, W. Zhang, J. Huang, D. Wu, *Food Hydrocoll.* **2019**, *94*, 114-127.

[205] Y. Tan, K. Xu, L. Li, C. Liu, C. Song, P. Wang, *ACS Appl. Mater. Interfaces* **2009**, *1*, 956-959.

[206] X. Ma, R. Jian, P. R. Chang, J. Yu, *Biomacromolecules* **2008**, *9*, 3314-3320.

[207] H.-Y. Kim, S. S. Park, S.-T. Lim, *Colloids surf. B: Biointerfaces* **2015**, *126*, 607-620.

[208] K. Zhai, X. Pei, C. Wang, Y. Deng, Y. Tan, Y. Bai, B. Zhang, K. Xu, P. Wang, *Nt. J. Biol. Macromol.* **2019**, *131*, 1032-1037.

[209] P. Sufi-Maragheh, N. Nikfarjam, Y. Deng, N. Taheri-Qazvini, *Colloids surf. B: Biointerfaces* **2019**, *181*, 244-251.

[210] Z. Xiao, L. Wang, C. Lv, S. Guo, X. Lu, L. Tao, Q. Duan, Q. Yang, Z. Luo, *Nt. J. Biol. Macromol.* **2020**, *143*, 401-412.

[211] X. Pei, K. Zhai, C. Wang, Y. Deng, Y. Tan, B. Zhang, Y. Bai, K. Xu, P. Wang, *Langmuir* **2019**, *35*, 7222-7230.

[212] X. Pei, K. Zhai, X. Liang, Y. Deng, Y. Tan, P. Wang, K. Xu, *Langmuir* **2017**, *33*, 3787-3793.

[213] S. Ge, L. Xiong, M. Li, J. Liu, J. Yang, R. Chang, C. Liang, Q. Sun, *Food Chem.* **2017**, *234*, 339-347.

[214] T. Yang, J. Zheng, B. S. Zheng, F. Liu, S. Wang, C. H. Tang, *Food Hydrocoll.* **2018**, *82*, 230-238.

[215] A. Azfaralariff, F. F. Fazial, R. S. Sontanosamy, M. F. Nazar, A. M. Lazim, *J. Food Eng.* **2020**, *280*, 109974.

[216] X. Qian, Y. Lu, W. Xie, D. Wu, *Carbohydr. Polym.* **2020**, *230*, 115575-115585.

[217] K. Wang, Y. Hong, Z. Gu, L. Cheng, Z. Li, C. Li, *Nt. J. Biol. Macromol.* **2020,** *155*, 273-285.

[218] F. Liu, C. H. Tang, *Food Hydrocoll.* **2016**, *60*, 606-619.

[219] K. Matsumiya, B. S. Murray, *Food Hydrocoll.* **2016**, *60*, 206-215.

[220] B. Jiao, A. Shi, Q. Wang, B. P. Binks, *Angew. Chem. Int. Ed.* **2018**, *130*, 9418-9422.

[221] Z. Ren, Z. Chen, Y. Zhang, X. Lin, B. Li, *Nt. J. Biol. Macromol.* **2020**, *151*, 247-256.

[222] Y. Zou, J. Guo, S. W. Yin, J. M. Wang, X. Q. Yang, *J. Agric. Food Chem.* **2015**, *63*, 7405-7414.

[223] Z. Wang, R. X. Zhang, C. Zhang, C. Dai, X. Ju, R. He, *J. Agric. Food Chem.* **2019**, *67*, 887-894.

[224] Z. Wang, N. Zhang, C. Chen, R. He, X. Ju, *J. Agric. Food Chem.* **2020**, *68*, 3607-3614.

[225] F. Liu, S. Y. Ou, C. H. Tang, *Food Hydrocoll.* **2017**, *65*, 175-186.

[226] A. Shi, X. Chen, L. Liu, H. Hu, H. Liu, Q. Wang, D. Agyei, *RSC Adv.* **2017**, *7*, 53247-53254.

[227] S. K. Dhayal, R. J. Delahaije, R. J. de Vries, H. Gruppen, P. A. Wierenga, *Soft matter* **2015**, *11*, 7888-7898.

[228] M. Ju, G. Zhu, G. Huang, X. Shen, Y. Zhang, L. Jiang, X. Sui, *Food Hydrocoll.* **2020**, *99*, 105329-105337.

[229] L. J. Wang, Y. Q. Hu, S. W. Yin, X. Q. Yang, F. R. Lai, S. Q. Wang, *J. Agric. Food Chem.* **2015**, *63*, 2514-2524.

[230] Y. Feng, Y. Lee, *Food Hydrocoll.* **2016**, *56*, 292-302.

[231] Y. Zou, C. van Baalen, X. Yang, E. Scholten, *Food Hydrocoll.* **2018**, *80*, 130-140.

[232] X. M. Li, J. Zhu, Y. Pan, R. Meng, B. Zhang, H. Q. Chen, *Food Hydrocoll.* **2019**, *90*, 19-27.

[233] Y. Zou, Z. Wan, J. Guo, J. Wang, S. Yin, X. Yang, *Food Hydrocoll.* **2017**, *63*, 364-371.

[234] J. Xiao, A. J. P. Gonzalez, Q. Huang, *Food Hydrocoll.* **2016**, *54*, 30-39.

[235] M. Ago, B. L. Tardy, L. Wang, J. Guo, A. Khakalo, O. J. Rojas, *MRS Bull.* **2017**, *42*, 371-379.

[236] P. S. Chauhan, *Bioresour. Technol. Reports* **2020**, *9*, 100374-100374.

[237] A. Henn, M. L. Mattinen, *Recent Prog. Mater* **2019**, *1*, 1-1.

[238] M. Ago, S. Huan, M. Borghei, J. Raula, E. I. Kauppinen, O. J. Rojas, *ACS Appl. Mater. Interfaces* **2016**, *8*, 23302-23310.

[239] T. E. Nypelö, C. A. Carrillo, O. J. Rojas, *Soft Matter* **2015**, *11*, 2046-2054.

[240] M. R. Bertolo, L. B. B. de Paiva, V. M. Nascimento, C. A. Gandin, M. O. Neto, C. E. Driemeier, S. C. Rabelo, *Ind. Crops Prod.* **2019**, *140*, 111591-111603.

[241] L. Dai, Y. Li, F. Kong, K. Liu, C. Si, Y. Ni, *ACS Sustain. Chem. Eng.* **2019**, *7*, 13497-13504.

[242] K. S. Silmore, C. Gupta, N. R. Washburn, *J. Colloid Interface Sci.* **2016**, *466*, 91-100.

[243] M. H. Sipponen, M. Smyth, T. Leskinen, L.-S. Johansson, M. Österberg, *Green Chem.* **2017**, *19*, 5831-5840.

[244] K. Lintinen, Y. Xiao, R. B. Ashok, T. Leskinen, E. Sakarinen, M. Sipponen, F. Muhammad, P. Oinas, M. Österberg, M. Kostiainen, *Green Chem.* **2018**, *20*, 843-850.

[245] M. B. Agustin, P. A. Penttilä, M. Lahtinen, K. S. Mikkonen, *ACS Sustain. Chem. Eng.* **2019**, *7*, 19925-19934.

[246] L. Chen, Y. Shi, B. Gao, Y. Zhao, Y. Jiang, Z. Zha, W. Xue, L. Gong, *ACS Sustain. Chem. Eng.* **2019**, *8*, 714-722.

[247] D. Ye, S. Li, X. Lu, X. Zhang, O. J. Rojas, *ACS Sustain. Chem. Eng.* **2016**, *4*, 5248-5257.

[248] J. D. Nguyen, B. S. Matsuura, C. R. Stephenson, *J. Am. Chem. Soc.* **2014**, *136*, 1218-1221.

[249] M. Farooq, T. Zou, G. Riviere, M. H. Sipponen, M. Österberg, *Biomacromolecules* **2018**, *20*, 693-704.

[250] E. Dickinson, *Soft Matter* **2008**, *4*, 932-942.

[251] S. Liu, C. Elmer, N. Low, M. Nickerson, *Food Res. Int.* **2010**, *43*, 489-495.

[252] X. Kong, C. Jia, C. Zhang, Y. Hua, Y. Chen, *RSC Adv.* **2017**, *7*, 31875-31885.

[253] X. Luo, Y. Zhou, L. Bai, F. Liu, R. Zhang, Z. Zhang, B. Zheng, Y. Deng, D. J. McClements, *Food Res. Int.* **2017**, *96*, 103-112.

[254] R. Li, Y. Tan, T. Dai, R. Zhang, G. Fu, Y. Wan, C. Liu, D. J. McClements, *Food Funct.* **2019**, *10*, 7239-7252.

[255] L. Amagliani, J. O'Regan, A. L. Kelly, J. A. O'Mahony, *Trends Food Sci. Technol.* **2017**, *64*, 1-12.

[256] X. Xu, Q. Sun, D. J. McClements, *Food Hydrocoll.* **2019**, *89*, 396-405.

[257] S. Zhang, L. Tian, J. Yi, Z. Zhu, E. A. Decker, D. J. McClements, *Food Hydrocoll.* **2020**, *109*, 106136-106146.

[258] X. Wei, J. Li, M. Eid, B. Li, *Food Hydrocoll.* **2020**, *17*, 105728-105743.

[259] S. Soltani, A. Madadlou, *Carbohydr. Polym.* **2016**, *136*, 738-743.

[260] Y. Jiang, D. Wang, F. Li, D. Li, Q. Huang, *Nt. J. Biol. Macromol.* **2020**, *148*, 1280-1289.

[261] F. Z. Zhou, X. N. Huang, Z. l. WU, S. W. Yin, J.H. Zhu, C. H. Tang, X. Q. Yang, *J. Agric. Food Chem.* **2018**, *66*, 11113-11123.

[262] M. N. Nasrabadi, S. A. H. Goli, A. S. Doost, B. Roman, K. Dewettinck, C. V. Stevens, P. Van der Meeren, *Colloids Surf. A Physicochem. Eng. Asp.* **2019**, *563*, 170-182.

[263] M. H. Sipponen, H. Lange, C. Crestini, A. Henn, M. Österberg, *ChemSusChem* **2019**, *12*, 2039-2054.

[264] C. Wang, X. Fu, C.-H. Tang, Q. Huang, B. Zhang, *Food Chem.* **2017**, *227*, 298-304.

[265] Y. H. Cho, O. G. Jones, in *Adv. Food Nutr. Res.* **2019**, *88*, 47-84.

[266] V. Mikulcová, R. Bordes, V. Kašpárková, *Food Hydrocoll.* **2016**, *61*, 780-792.

[267] B. D. Mattos, B. L. Tardy, W. L. Magalhães, O. J. Rojas, *J Control Release* **2017**, *262*, 139-150.

[268] B. Zhang, Z. Zhang, S. Kapar, P. Ataeian, J. da Silva Bernardes, R. Berry, W. Zhao, G. Zhou, K. C. Tam, *ACS Sustain. Chem. Eng.* **2019**, *7*, 17756-17767.

[269] Y. Li, S. Yu, P. Chen, R. Rojas, A. Hajian, L. Berglund, *Nano Energy* **2017**, *34*, 541-548.

[270] C. Tang, Y. Li, J. Pun, A. S. M. Osman, K. C. Tam, *Colloids Surf. A Physicochem. Eng. Asp.* **2019**, *570*, 403-413.

[271] F. A. Ngwabebhoh, S. I. Erdagi, U. Yildiz, *Carbohydr. Polym.* **2018**, *201*, 317-328.

[272] E. D. Bartzoka, H. Lange, K. Thiel, C. Crestini, *ACS Sustain. Chem. Eng.* **2016**, *4*, 5194-5203.

[273] D. Yiamsawas, S. J. Beckers, H. Lu, K. Landfester, F. R. Wurm, *ACS Biomater. Sci. Eng.* **2017**, *3*, 2375-2383.

[274] L. Chen, X. Zhou, Y. Shi, B. Gao, J. Wu, T. B. Kirk, J. Xu, W. Xue, *Chem. Eng. J.* **2018**, *346*, 217-225.

[275] P. Figueiredo, K. Lintinen, A. Kiriazis, V. Hynninen, Z. Liu, T. Bauleth-Ramos, A. Rahikkala, A. Correia, T. Kohout, B. Sarmento, *Biomaterials* **2017**, *121*, 97-108.

[276] X. Li, Y. Wang, B. Wang, X. Feng, Z. Mao, X. Sui, *Nt. J. Biol. Macromol.* **2020**, *144*, 624-631.

[277] A. Marefati, M. Bertrand, M. Sjöö, P. Dejmek, M. Rayner, *Food Hydrocoll.* **2017**, *63*, 309-320.

[278] F. Liu, C. H. Tang, *Food Hydrocoll.* **2016**, *56*, 434-444.

[279] J. Xiao, C. Li, Q. Huang, *J. Agric. Food Chem.* **2015**, *63*, 10263-10270.

[280] L. Altuna, M. L. Herrera, M. L. Foresti, *Food Hydrocoll.* **2018**, *80*, 97-110.

[281] S. Y. Cheuk, F. F. Shih, E. T. Champagne, K. W. Daigle, J. A. Patindol, C. P. Mattison, S. M. Boue, *Food Chem.* **2015**, *174*, 585-590.

[282] H. He, Y. Hong, Z. Gu, G. Liu, L. Cheng, Z. Li, *Carbohydr. Polym.* **2016**, *147*, 243-250.

[283] N. Chiu, A. Tarrega, C. Parmenter, L. Hewson, B. Wolf, I. D. Fisk, *Food Hydrocoll.* **2017**, *69*, 450-458.

[284] S. Qamar, Y. J. Manrique, H. Parekh, J. R. Falconer, *Crit. Rev. Food Sci. Nutr* **2019**, 1-21.

[285] S. N. Warnakulasuriya, M. T. Nickerson, *J. Sci. Food Agric.* **2018**, *98*, 5559-5571.

[286] B. Mahadevan, B. A. Thorsrud, G. P. Brorby, H. E. Ferguson, *Food Chem. Toxicol.* **2014**, *72*, 83-89.

[287] P. Chivero, S. Gohtani, H. Yoshii, A. Nakamura, *LWT-J. Food Sci. Technol.* **2016**, *69*, 59-66.

[288] S. Ghazaei, M. Mizani, Z. Piravi-Vanak, M. Alimi, *J. Food Sci. Technol.* **2015**, *35*, 150-156.

[289] A. G. Samaranayaka, E. C. Li-Chan, *J. Funct. Foods* **2011**, *3*, 229-254.

[290] F. Z. Zhou, L. Yan, S. W. Yin, C. H. Tang, X. Q. Yang, *J. Agric. Food Chem.* **2018**, *66*, 1461-1471.

[291] K. K. Ho, K. Schroën, M. F. San Martín-González, C. C. Berton-Carabin, *Food Struct.* **2017**, *12*, 34-42.

[292] C. E. Gumus, E. A. Decker, D. J. McClements, *Food Res. Int.* **2017**, *100*, 175-185.

[293] L. Bai, W. Xiang, S. Huan, O. J. Rojas, *Biomacromolecules* **2018**, *19*, 1674-1685.

[294] F. Niu, B. Han, J. Fan, M. Kou, B. Zhang, Z.-J. Feng, W. Pan, W. Zhou, *Carbohydr. Polym.* **2018**, *199*, 314-319.

[295] L. Golchoobi, M. Alimi, S. Shokoohi, H. Yousefi, *J. Texture Stud.* **2016**, *47*, 403-412.

[296] K. A. Dubey, C. V. Chaudhari, Y. K. Bhardwaj, L. Varshney, in *Advances in Biomaterials for Biomedical Applications*, Springer, **2017**, 1-44.

[297] A. Werner, G. Sèbe, V. Héroguez, *Polym. Chem.* **2018**, *9*, 5043-5050.

[298] S. Fujisawa, E. Togawa, K. Kuroda, *Biomacromolecules* **2017**, *18*, 266-271.

[299] Y. Zhang, Y. Jiang, L. Han, B. Wang, H. Xu, Y. Zhong, L. Zhang, Z. Mao, X. Sui, *Carbohydr. Polym.* **2018**, *179*, 86-92.

[300] X. Li, N. Hegyesi, Y. Zhang, Z. Mao, X. Feng, B. Wang, B. Pukánszky, X. Sui, *Eur. Polym. J.* **2019**, *110*, 378-384.

[301] N. Nikfarjam, M. Sabzi, Y. Deng, N. T. Qazvini, *Ind. Eng. Chem. Res.* **2015**, *54*, 6627-6633.

[302] R. Setiati, S. Kasmungin, S. Siregar, T. Marhaendrajana, D. Wahyuningrum, *Yang Dinilai Reviewer I Reviewer II* **2017**, *101*, 157.

[303] Z. Q. Lim, N. A. A. Aziz, A. K. Idris, N. A. M. Akhir, *Petrol Res,* **2019**, *5(2),* 154-163.

[304] D. Ogunkoya, S. Li, O. J. Rojas, T. Fang, *Appl. Energy* **2015**, *154*, 851-861.

[305] J. G. Lee, L. L. Larive, K. T. Valsaraj, B. Bharti, *ACS Appl. Mater. Interfaces* **2018**, *10*, 43282-43289.

[306] J. Ojala, J. A. Sirviö, H. Liimatainen, *Chem. Eng. J.* **2016**, *288*, 312-320.

Chapter 4: Synergistic effect of lignin incorporation into polystyrene for producing sustainable superadsorbent

4.1 Abstract

Lignin has gained intensive interest as an excellent raw material for the generation of advanced green products. Polystyrene (PS) is known for its worldwide application in water purification processes. To induce a more sustainable polymer (KL-PS) compared to PS, kraft lignin (KL) and styrene were polymerized via free radical polymerization in a facile aqueous emulsion process. KL enhanced surface area and porosity of KL-PS. The physicochemical properties of induced KL-PS were analyzed, and the fate of lignin in KL-PS was discussed fundamentally. Wettability and surface energy analyses were implemented to monitor the surface properties of KL, PS and KL-PS. Incorporation of KL in PS (40 wt%) boosted its surface energy and oxygen content, which led to KL-PS with better compatibility than PS with copper ions in aqueous systems. A quartz crystal microbalance with dissipation (QCM-D) confirmed the noticeably higher adsorption performance of copper ions on KL-PS than on PS and KL. The sorption mechanism, which was revealed by FTIR studies, was primarily attributed to the coordination of Cu (II) and hydroxyl groups of KL-PS as well as the quadrupolar system of KL-PS.

4.2 Introduction

Water contamination with heavy metals is considered as a serious concern for environmental safety due to its threatening consequences for human and ecosystem health.[1] Industrial effluents and human activities are known as major producers of materials contaminated with heavy metals.[2] Among the extensive heavy metals, copper sequestering gained global attentions because of its widespread presence in industrial effluents.[3] Adsorption process is an efficient approach for contaminant removals. Various alternative adsorbents including activated carbon, [4,5] silica-based materials,[6] aniline-based composites,[7] polystyrene-based nanocomposites,[3] metal oxides[8] and biomass[9,10] were previously applied for cleanup of copper ions dissolved in industrially produced effluents.

Lignin, as an abundant renewable, nontoxic and environmentally friendly resource, has gained an intensive attention globally.[11] Lignin is known as a bio-based amorphous polymer with a 3-dimensional structure containing different functional groups.[12] Owing to its functional groups, lignin exposes surface activity, which makes its reaction and interaction with other materials possible.[13,14] In the past, lignin was used in composite production to improve composite's

sustainability. For example, lignin was incorporated into poly (lactic acid) (PLA) and the product showed excellent antioxidant activities and good biocompatibility, which has the potential to be used in biomedical applications.[15] It has also been shown that adding lignin to quercetin can produce a green alternative to the synthetic antioxidants that are in use in food, cosmetics, and pharmaceuticals.[16] In a recent study, a stable nanodrug carrier was formed by self-assembly of alkali lignin (AL) with the bioactive molecule resveratrol (RSV) and Fe_3O_4 magnetic nanoparticles which strongly supported the AL NPs application as a new and highly efficient nanodelivery.[17] Different studies examined the potential of lignin as a bio-based adsorbent.[18-22] Adsorption of Pb(II), Zn(II), Cu(II) and Cd(II) on kraft lignin was reported in the past.[18] As an example, Todorciuc and coworkers reported a saturated adsorption of 26 mg g^{-1} for Cu(II) on lignin generated from wheat straw.[19] Adsorption affinity of lignin for metal ions was suggested to proceed through its carboxylate and phenolate groups.[20] Although an explicit mechanism for the adsorption of metals on lignin is still unknown, surface adsorption[21] and ion-exchange[22] are directed.

Polystyrene, PS, as a hydrophobic polymer with recognized dispersive intermolecular interactions, is widely used as the building block for the production of adsorbent for water purification. However, it requires functionalization or cross-linking to improve its surface properties.[23] Different types of modifier, such as $CaCO_3$,[24] schiff base,[3] sulfonate groups,[25] or amine groups[26] were anchored onto PS to improves its compatibility with ions. It is well-known that introducing functional groups such as sulfonate, amine or hydroxyl groups on the PS' surface plays an important role in enhancing its compatibility with ions. However, the electron-rich π system of PS is also capable of interacting with ions. Lu and coworkers investigated the adhesive force between electron- rich π system of poly-l-tryptophan (PTrp), poly-l-tyrosine (PTyr) and polystyrene (PS) and the adjacent cations (NH_3R^+) in water.[27] They stated that cation–π interactions occur between positively charged groups and aromatic groups of polymers.[27] In another research, Javkhlantugs and coworkers postulated that positively charged guanidine group of arginine would closely contact with the benzene ring of the PS, which would indicate the existence of cation-π interaction between them.[28] Quadrupolar characteristic of the aromatic system enables polystyrene to offer adsorption for cations in water. A quadrupolar is originated from the uneven distribution of π-electron above and below the face of an aromatic system (e.g., benzene ring).[29] The polystyrene quadrupolar system, owing to its π-donors, has the potential to

participate in series of non-covalent interactions namely; polar-π interactions,[30] self-stacking,[31] hydrogen-π interactions[32] and cation-π interactions.[27] The latter is a non-covalent interaction between a cation and planar surface of an aromatic π-donor system, which will be studied in this work.

Decoration of PS for the production of a functionalized, porous and sustainable bio-adsorbent using lignin was the main objective of the present study. Lignin as a green biomacromolecule [33] was embedded in PS to enhance its physicochemical properties. The reported product, KL-PS, was synthesized via radical polymerization in a facile aqueous emulsion system. Special attention was paid to the physicochemical properties of KL-PS and its performance as an adsorbent. Wettability and surface energy are two imperative aspects that express the compatibility of polymer's surface with surrounding.[34] Jiang and coworkers depicted that treating lignin film with a non-ionic surfactant (i.e., Tween 80) resulted in higher polar surface energy as well as the hydrophilicity of lignin film.[35] Despite its potential use, the surface chemistry of KL-PS was yet to be studied. For the first time, the surface energy of KL-PS polymer was studied and the changes in surface energy components (polar/nonpolar and acidic/basic) of the polymer was compared with those of lignin and polystyrene following Fowkes' and van Oss theories. The presence of hydroxyl functional groups in KL-PS was monitored following phosphorus nuclear magnetic resonance (P-NMR). Furthermore, the interaction of the functionalized PS (i.e., KL-PS) with copper ions in an aqueous medium was monitored by means of a quartz crystal microbalance with dissipation (QCM-D). FT-IR was also implemented as a tool to fundamentally distinguish the chemical interactions between copper and PS, KL and KL-PS polymers.

4.3 Materials and methods

4.3.1 Materials

Softwood kraft lignin was used as received from FPInnovations' pilot plant facilities in Thunder Bay, ON. Dioctyl sulfosuccinate sodium salt (DOSS), α,α′-azoiso-bis-butyronitrile (AIBN), 1-decanol, toluene, tetrahydrofuran, d_6-dimethyl sulfoxide (d_6-DMSO), chloroform-d ($CDCl_3$), trimethylsilyl propanoic acid (TSP), deuterated chloroform, pyridine, cyclohexanol, chromium (III) acetylacetonate, NaOH, calcium chloride, 2-chloro-4,4,5,5-tetramethyl-1,3,2-dioxaphospholane, diiodomethane, glycerol, $Cu(NO_3)_2.3H_2O$, 30% ammonium hydroxide solution and hydrogen peroxide, all analytical grades, were purchased from Sigma-Aldrich and used as received. MiliQ H_2O was used instead of distilled water in all QCM experiments. Styrene,

analytical grade, was purchased from Sigma-Aldrich and purified following available procedures.[36]

4.3.2 Lignin styrene polymerization.

Anionic surfactant, DOSS (0.75 g, 1.68 mmol), was added to 150 mL of deionized water in a 250 mL three neck flask and the mixture was stirred for 0.5 h at 80 °C to dissolve the surfactant in water in a nitrogen environment. At the same time, styrene (12 mL, 105 mmol) was charged to 1/1 (v/v) mixture of 1-decanol and toluene in a separate beaker and was deoxygenated by purging with N_2 for 0.5 h. The mixture was then transferred to the three-neck flask. One hour was given for the oil micelles to form. Lignin (3 g, 16.6 mmol) was separately dispersed in 10 mL of deionized water, and initiator, AIBN (based on 1 wt.% of lignin), was added to the lignin suspension while stirring and purging with nitrogen for 0.5 h at room temperature. In the last step, the lignin suspension with initiator was added to the three-neck flask to initiate the polymerization. The mixture was stirred at 350 rpm for 18 h at 80 °C in an oil bath. The lignin-polystyrene (KL-PS) polymer was agglomerated upon completion of the reaction and was floated in the polystyrene micelles. The mixture was filtered by a filter paper and the precipitate was washed with excess amounts of hot water (1L). Soxhlet extraction (using boiling acetone) was applied for purifying the product from solvent and remained homopolymer of PS. The purified polymer was dried in the vacuum oven at 60 °C for 48 h. The final lignin-polystyrene polymer was denoted as KL-PS in this study.

4.3.3 Polystyrene production.

The styrene homopolymer, PS, was produced following the same steps of the KL-PS polymerization but in the absence of lignin. Upon completion of the reaction, as filtration was ineffective in separating the PS particles, they were precipitated in 400 mL of ethanol. The PS was dried in a vacuum oven at 60 °C for 48 h.

4.3.4 NMR analysis.

In this set of experiments, 27 mg of KL or KL-PS and 8 mg of trimethylsilyl propanoic acid (TSP) were dissolved in 500 µL of DMSO-d_6 and 27 mg of PS was dissolved in 500 µL of $CDCl_3$ stirring overnight and ^{1}H-NMR spectra of samples were recorded by INOVA-500 MHz instrument (Varian, USA). A 45° pulse width after 64 number of scans with 1 s relaxation delay were adjusted to obtain the spectra. The areas under the spectra were used for quantitative analysis.

For quantitative analysis of phenolic and aliphatic hydroxyl moieties of lignin-based products, the phosphitylation of KL and KL-PS with 2-chloro,4455-tetramethyl-1,3,2-dioxaphospholane was followed.[37] A mixture of pyridine and CCl_3D solvent was used to dissolve the samples, and the quantification analysis was conducted with a known concentration of internal standard (cyclohexanol 0.20 mmol/mL) via following the procedure stated previously.[37] To acquire a spectrum, a 90° pulse with 5 s relaxation delay and 128 acquisitions with an inverse gated decoupling pulse were employed. Assignments and calculations were followed as reported previously in the literature.[37] The area under the peaks ranging 150.4-145.5 ppm was assigned to aliphatic hydroxyl moieties in samples. Phenolic moieties have peaks at 140.3-138.3 ppm.[37]

4.3.5 Molecular weight analysis

The molecular weights of KL and KL-PS samples were determined using a gel permeation chromatography technique, Malvern GPCmax VE2001 Module + Viscotek TDA305 with multi-detectors (UV, RI, viscometer, low angle and right-angle laser) by dissolving samples in THF as eluent. Columns of PAS106M, PAS103 and PAS102.5 were used at a fixed flow rate of 1.0 mL/min and 35 °C. The molecular weight of PS was analyzed using a static light scattering, SLS, an analyzer (BI-200SM Brookhaven Instruments Corp., Holtsville, NY, USA). Polystyrene solutions in the concentration range of 1 and 5 g/L were prepared in toluene. Maximum solid state laser power of 35 mW at the wavelength of 637 nm was applied, and the measured data was further analyzed using Zimm plot software (Holtsville, NY, USA) to obtain the absolute molecular weight of the polymers.[38]

4.3.6 Elemental and surface area analyses.

Elemental analysis of KL, PS and KL-PS was conducted using an Elementar Vario EL Cube, Germany, elemental analyzer. The specific surface areas and pore diameter distributions of KL, KL-PS and PS were determined using a Quantachrome surface area analyzer, Nova2200e (USA). The ground samples were dried in an oven at 105 °C overnight prior to analysis. Then, 0.05 g of each sample was initially pretreated for 4 h at 100 °C. Branuer-Emmett-Teller (BET) method via adsorption-desorption isotherms using nitrogen gas at -180 °C in the relative pressure range of 0.01 to 0.99 were applied to measure the specific surface areas of the samples. The total pore volume of the samples (V_p, cm^3/g) was calculated at the relative pressure of 0.99.[39]

4.3.7 Spin coating of polymer films.

KL, PS and KL-PS were coated on clean dried glass substrates using a spin coater (WS-400B-NPP) spin-processor (Laurell Technologies Corp). In this set of experiments, KL and KL-PS were dissolved in 1,4-dioxane (4 wt.% concentration) followed by stirring at 300 rpm overnight at room temperature, while the PS solution was prepared in toluene under the same conditions. Subsequently, the solutions were spin-coated on glass substrates at 2000 rpm over 40 s under a nitrogen environment. The coated samples were kept covered prior to analysis.[40]

4.3.8 Contact angle and surface energy measurements.

The contact angles of deionized water, diiodomethane and glycerol on the coated surfaces were determined for surface energy measurements. The analysis was conducted via placing 5 µL of liquid droplets on the coated surfaces following static contact angle measurement with the sessile drop method using a theta optical tensiometer attention (Biolin Scientific) at 25 °C for 30 s. Nine measurements were conducted on each solid coated surface, and the average values of the readings were fitted into Young-Laplace equation.[34] Fowke's model equation 1 was followed using contact angle results of water and diiodomethane as the polar and non-polar wetting liquids to calculate the surface energy of KL, PS and KL-PS coated films:[41]

$$\frac{\boldsymbol{\sigma_L}\,(\boldsymbol{\cos\theta}+\mathbf{1})}{\mathbf{2}} = \sqrt{(\boldsymbol{\sigma_L^D})(\boldsymbol{\sigma_S^D}) + (\boldsymbol{\sigma_L^P})(\boldsymbol{\sigma_S^P})} \qquad (1)$$

where θ is the contact angle between the wetting liquid and the solid surface. Also, $\boldsymbol{\sigma_L}$, $\boldsymbol{\sigma_L^D}$ and $\boldsymbol{\sigma_L^P}$ are surface tension, as well as dispersive and polar components of $\boldsymbol{\sigma_L}$, respectively[42] (Table A1.1, appendix information) and $\boldsymbol{\sigma_S^D}$ and $\boldsymbol{\sigma_S^P}$ stand for the dispersive and polar components of solid and liquid through polar interaction is based on surface acidity and basicity, which can be analyzed by dividing the polar components of the surface into acidic ($\boldsymbol{\sigma_S^+}$) and basic ($\boldsymbol{\sigma_S^-}$). The basic component originates from the ability of the surface to act as a basic by donating electron density through dipole-dipole and hydrogen bonding.[43] However, the acidic component shows the desire of the surface in accepting electron density. By fitting contact angle results, which were obtained for the interaction of the coated films and deionized water, diiodomethane and glycerol, into equation 2, $\boldsymbol{\sigma_S^+}$ and $\boldsymbol{\sigma_S^-}$ can be determined.

$$\frac{\boldsymbol{\sigma_L}\,(\boldsymbol{\cos\theta}+\mathbf{1})}{\mathbf{2}} = \sqrt{(\boldsymbol{\sigma_L^D})(\boldsymbol{\sigma_S^D}) + (\boldsymbol{\sigma_S^+})(\boldsymbol{\sigma_L^-}) + (\boldsymbol{\sigma_S^-})(\boldsymbol{\sigma_L^+})} \qquad (2)$$

In this equation, $\boldsymbol{\sigma_L^-}$ and $\boldsymbol{\sigma_L^+}$ are the acidic and basic surface tension components of the test liquids, respectively.

4.3.9 Adsorption experiment.

Adsorption experiment was conducted in order to measure and compare the capability of KL, PS and KL-PS surfaces for copper uptake from aqueous solution. In this set of experiment, 50 mg/L Cu (II) solution was prepared by dissolving 190 mg of Cu $(NO_3)_2.3H_2O$ (M_W of 241.6 g mol^{-1}) in 1L of deionized water and the pH was adjusted to 4.5 by diluted HNO_3 solution. This pH was selected because Cu (II) forms solid particles of Cu $(OH)_2$ at pH ≥ 6.[44] At first, 0.01 g of KL, PS and KL-PS were mixed in 50 mL of prepared Cu (II) solution. The suspensions were then stirred at 150 rpm and room temperature for 12 h. The particles were separated from the solution through filtration using a filter paper. They were then collected from the filter paper for FT-IR analysis. The treated solutions were collected and after dilution were analyzed for quantitative detection of Cu (II) by a Varian (Agilent) Vista Pro Radial inductively coupled plasma (ICP) at the wavelength 327.395 1/cm with plasma flow rate of 15.0 L/min with 3 replicates.

Adsorption capacity was calculated following equation 3:

$$q = \frac{C_i - C_f}{m} \times V \qquad (3)$$

Wherein, q represents the adsorption mass, C_i and C_f express the initial and final Cu (II) concentration based on ICP results, V is Cu (II) solution volume and m stands for the adsorbent mass

4.3.10 Substrate preparation for QCM analysis.

KL, KL-PS and PS substrates were coated on the gold-coated crystals sensors (Q Sense). The sensors were cleaned by immersing in a solution of $H_2O/NH_4OH/H_2O_2$ at the ratio of 10/2/2 v/v/v for 10 min at 60 °C. Then, the sensors were rinsed with water, dried with nitrogen and irradiated with the UV/ozone oxidation cleaner (PSD Series, digital UV ozone system, NOVASCAN) for 10 min prior to use. Then, 1.4 dioxane was used to prepare a 2.5 wt.% of KL or KL-PS solution, while toluene was used to prepare a 2.5 wt.% of PS solution. The solutions were stirred at 300 rpm overnight at room temperature. Afterward, 50 µL of the solutions were considered for preparing 3 different substrates of KL, KL-PS and PS via spin coating on the cleaned gold crystals for 45 s at 3000 rpm. The coated sensors were dried in oven at 105 °C for 15 h to improve their stability.[35]

4.3.11 QCM-D experiments.

In this study, the adsorption of Cu (II) onto KL, KL-PS and PS substrates was studied by means of Quartz crystal microbalance with dissipation (QCM-D). Variation in resonant frequency, Δf, and dissipation, ΔD, upon the adsorption of adsorbate, Cu (II), on the substrate oscillating gold

sensors of the instrument will pertain to the real time detection of mass and viscoelasticity changes of the adsorbed layer, as comprehensively explained earlier.[45] Two different adsorption models were used to evaluate the obtained data from the instrument. Sauerbrey equation is practical when a rigid layer forms on the sensor, whereas Voigt model is suitable for a softer film.[46] The magnitude of ΔD defines which model will fit better into data for Δm (mass) and Δd (thickness) evaluation. Low dissipation changes relate to the Sauerbrey equation, but higher ΔD will refer to the Voigt model.[46] Formulation of adsorbed mass and thickness based on Sauerbrey model is shown in equations 4 and 5:[47]

$$\mathbf{\Delta m_{Sauerbrey}} = -\frac{\mathbf{C\Delta f}}{\mathbf{n}} \qquad (4)$$

$$\mathbf{d_{Sauerbrey}} = \frac{\mathbf{\Delta m_{Sauerbrey}}}{\mathbf{\rho}} \qquad (5)$$

where $\mathbf{\Delta m}$ and $\mathbf{\Delta f}$ refer to the mass and frequency changes and C is a constant value, which is related to the physical properties of the sensor (i.e., 0.177 mg/mHz for a 5 MHz AT-cut quartz crystal).[48] Voigt model has been explained in detail in the available literature[49] and was applied by Q-Tools software (Q-Sense) in this study to estimate the thickness and mass of coated layer of KL-PS in adsorbing copper ions from the aqueous solution. These results were compared with those of KL and PS films. In this set of experiment, 50 mg/L Cu (II) solution was prepared by dissolving 190 mg of $Cu(NO_3)_2.3H_2O$ (M_W of 241.6 g/mol) in 1L of Mili-Q water and the pH was adjusted to 4.5 by diluted HNO_3 solution. This pH was selected because Cu (II) forms solid particles of $Cu(OH)_2$ at pH ≥ 6.[44] Coated sensors were installed in a QCM cell and the adsorption study was conducted in a real time via monitoring the mass uptake on the coated gold sensors. All measurements were started after obtaining a stable baseline for a buffer solution, i.e., Mili-Q water with controlled pH of 4.5 (prepared via using HNO_3). It approximately took 15 min to reach a stable baseline in each experiment, which was then followed by flushing Cu (II) solution at 50 mg/L concentration at pH 4.5. All experiments were conducted at 22 °C and a constant flow rate of 0.15 mL/min. When the changes in frequency for the 5th overtone was less than 2 Hz/h, the adsorption was considered equilibrated (in almost 140 min). The buffer solution was applied after the experiments to wash any loosely adsorbed Cu (II) from the substrate. The adsorption experiments were terminated after 20 min of buffer rinsing. For mass and thickness calculations, the bulk viscosity and density were assumed to be 1.05 mPa.s and 0.99 g/cm^3 for KL and PS using

Sauerbrey equation,[50] respectively, while the adsorbed layer viscosity was approximated to be the same as the bulk solution viscosity to fit the data into the Voigt model for KL-PS.[51]

4.3.12 FTIR analysis.

The filtered polymers from the batch experiment were used in this set of analysis. After air drying, they were placed on the zinc selenide (ZnSe) crystal element of a Fourier transform infrared spectroscopy (FTIR) (Bruker Tensor 27) equipped with an ATR assembly. The measurements were performed in the 550−4000 1/cm region with a resolution of 0.6 1/cm. To compare the absorption wavenumbers shifting, the spectra was also obtained for polymers (KL-KL-PS and PS) without copper adsorption.

4.3.13 SEM analysis.

The morphology and elemental composition of coated substrates on gold sensors before and after ion adsorption were investigated with a scanning electron microscope (SEM) Hitachi field emission SU-70 with energy dispersive X-Ray (EDX) Oxford AZtec with the adjusted voltage of 10 kV.

4.4 Results and discussion

4.4.1 Polymer characterization.

In this study, modified PS (KL-PS) and PS were produced using an emulsion polymerization technique. The incorporation of lignin in PS following free radical polymerization can be described via formation of phenoxy and alkoxy radicals on lignin through the initiator decomposition under heating.[52] AIBN molecule is unstable under heating and decomposes to one nitrogen molecule and two radicals of 2-cyanoprop-2-yl. These radicals then produce hydroxyl radicals by capturing hydrogens of aliphatic and aromatic OH groups or would directly promote the homo-polymerization of styrene.[53] Polymerization would be initiated following the attack of phenoxy radicals to the vinyl group of styrene, which led to the integration of lignin into PS's building block.[52] The proposed structure of KL-PS and ^{1}H-NMR spectra of PS, KL and KL-PS are depicted in Figure 1. The aromatic ring and aliphatic signals of PS are observable in the PS spectrum. KL's spectrum also depicts the aromatic moieties, accompanied with a wide signal (region of 3.45-4.05 ppm) corresponding to methoxy group.[54] The chemical shifts between 8 and 9.5 ppm belonging to phenolic hydroxy group is also observable in the spectrum of KL. After polymerization, the signature signals of PS and KL are both appeared in the spectrum of KL-PS. However, the intensity of peaks is different. The peaks at 0.88 (2') and 1.26 ppm (1') possibly indicates the first styrene

molecule attached to a hydroxyl group (-O-CH_2-CH-) of lignin and the peak at 2.12 ppm (3') is assigned to the other styrene segments attached to the first styrene molecule (2' in Figure 1), which corresponds to 3 hydrogen (-CH_2- CH-).[54] The H-NMR analysis provides evidence for the successful incorporation (grafting) of KL in PS polymerization. The quantitative analysis of NMR results confirms the incorporation of 40 wt.% of lignin into KL-PS polymer.

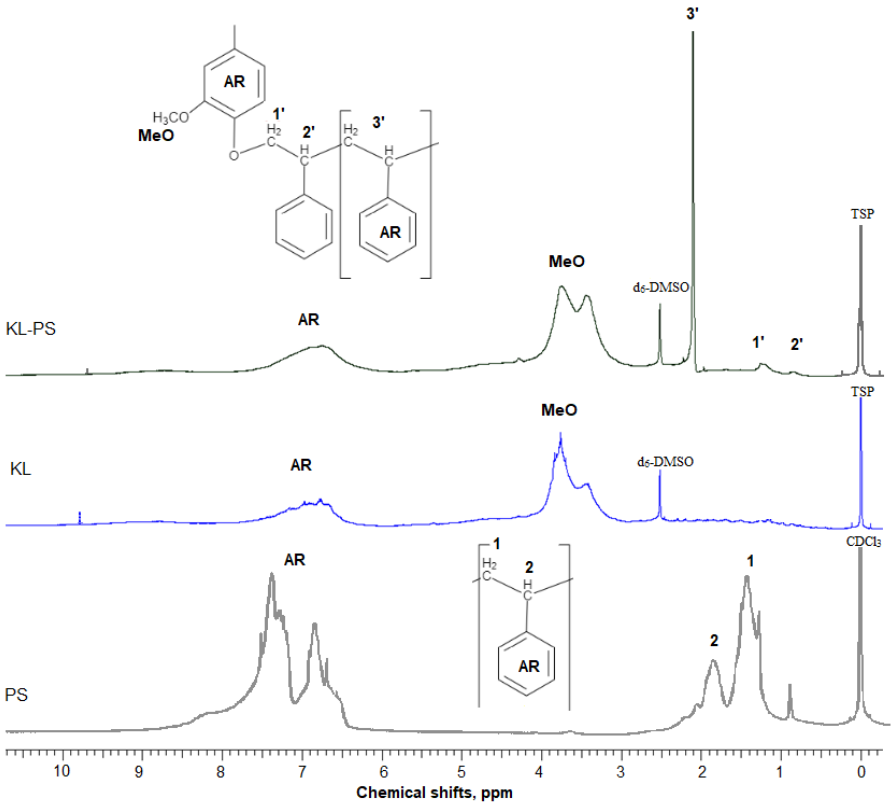

Figure 4.1: H-NMR spectra of PS, KL and KL-PS. AR stands for aromatic ring. The polymerization is shown only on the phenol groups of lignin.

Table A1.1 lists the properties of KL, KL-PS and PS. The surface area analysis illustrates variable physical properties for KL, KL-PS and KL. Analysing the phosphorylated KL and KL-PS with ^{31}P-NMR would help monitor the hydroxyl groups of lignin integrating in KL-PS.[55] The quantitative data on various -OH groups[56] of KL and KL-PS are listed in Table 1, while the ^{31}P-NMR spectra for the samples are available in Figure A1.1 . Kraft lignin in this study contains 1.62 mmol/g aliphatic hydroxyl group, 2.2 mmol/g phenolic group, and 0.14 mmol/g carboxylate group, which are in agreement with previously reported values for kraft lignin.[57] Less than half (40%) of the total measured hydroxyl groups are composed of aliphatic hydroxyl groups in KL. The rest

of the hydroxyl groups (56%) in KL originated from phenolic moieties consisting 63% Ph-OH guaiacyl and 37% C5-substituted hydroxyl groups.

After polymerization, the amount of aliphatic and aromatic hydroxyl groups present in KL-PS are 0.93 and 1.1 mmol/g, respectively. This elaborates that the polymerization was proceeded through participation of hydroxyl groups in radical polymerization, however, almost half of the hydroxyl groups remained intact. Based on ^{31}P-NMR results, it is observable that 51 and 43% of total phenolic and aliphatic hydroxyl groups participated in the polymerization reaction with styrene, respectively.

KL has a limited surface area of 24 m^2/g with the pore volume of 0.035 cm^3/g. PS is also known to have a limited surface area (in this case 15 m^2/g) and pore volume (0.021 cm^3/g), which requires co-monomers, cross-linkers or further modifications in order to improve its porosity.[58] KL-PS has a larger surface area of 44 m^2/g with pore volume of 0.053 $cm^{3/}g$, implying that the polymerization of KL and styrene generated a heterogeneous polymer (KL-PS) with larger porosity than the polymerization of a homopolymer (PS).

Aliphatic and phenolic hydroxyl groups of lignin selectively participate in polymerization with PS (proven by P-NMR analysis in table1), implying that the polymerization of PS on lignin is heterogeneous in nature. As lignin does not have homogenous surface characteristics, this heterogenous chain expansion will contribute to the creation of an uneven coating layer on lignin and ultimately a more porous material. It should be stated that the purpose of this study was to compare the surface area of these polymers with themselves. The increase in the surface area for improved adsorption is outside the scope of this study, and it can be persuaded in the future via the following pathways suggested in the literature.[9,59]

The integration of lignin onto PS occurred from three different positions of lignin molecules that are shown in Figure 2. Also, the carboxylate group content of KL-PS remained almost unchanged.

Table 4.1. Hydroxyl groups (mmol/g) of KL and KL-PS studied by means of ^{31}P-NMR

sample	Aliphatic -OH	C5-substituted	Ph-OH guaiacyl (G)	Total cond. phenolate	Carboxylate
KL	1.62±0.10	0.80±0.06	1.40±0.06	2.2±0.08	0.14±0.01
KL-PS	0.93±0.05	0.46±0.01	0.61±0.03	1.1±0.04	0.10±0.01

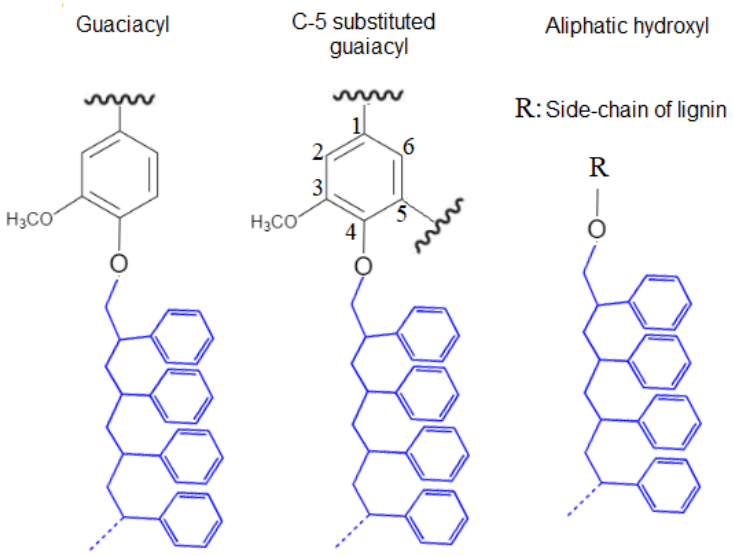

Figure 4.2**:** Proposed positions for the PS graft polymerization on KL's hydroxyl groups.

4.4.2 Surface properties of PS, KL and KL-PS substrates.

The surface tension of the test liquids in Table A1.2 and contact angle results for water, diiodomethane and glycerol droplets on the films (Table A1.3) were fabricated in Fowke's and Van Oss's equations for determining the polar σ_S^P, dispersive (nonpolar) σ_S^D, acidic σ_S^+ and basic σ_S^- components of the surface energy of PS, KL and KL-PS which are listed in Table 2.[60,61] The contact angle of water droplets on reported surfaces is also shown in Figure 3.

Lignin shows the highest surface energy among tested substrates. Notley and coworkers also reported surface energy of 57.1 mN/m^2 for kraft lignin.[62] The results of surface energy in Table 2 show the significantly more contribution of nonpolar components than the polar component of the substrates to the surface energy development. KL has σ_S^P of 12.9 mN/m^2 following Fowke theory. Van Oss theory rationales the polar characteristic of surface energy to be 0.66 mN/m^2 for σ_S^{P+} (acidic) and 18.3 mN/m^2 for σ_S^{P-}(basic). Interestingly, the majority of the polar component is dedicated to the basic rather than acidic component (Table 2), which is related to the electron-donating property of substrates. Basic component is related to the phenolic and aliphatic hydroxyl and methoxy groups of lignin.[57] The electron-donating capacity of these moieties enables such surfaces to interact with acidic species, i.e., electron acceptors.[57] Comparatively, Kraft lignin's high basicity can be justified by its functional groups and oxygen content comparably determined by ^{31}P-NMR and elemental analysis (Table A1.1).

On the other hand, PS has low surface energy with less contribution of polar components. This is mainly because of the benzene ring's existence that is closely associated with dispersive and hydrophobic forces. Low surface energy of a material is a barrier for its interaction with the surrounding environment.[62] Therefore, modifying PS with a material with higher surface energy would improve its compatibility with its surrounding environment. Grafting of KL and PS resulted in an increment in the polar component of surface energy for PS. As can be seen in Table 2, the σ_S^- value was increased from 6.23 mN/m^2 for KL to 10.7 mN/m^2 for KL-PS, which arises from the increment in oxygen content of the surface for KL-PS compared to that for PS (Table A1.1). Also, the wettability of PS surface was improved by lignin incorporation. This is because more oxygen atoms are associated with lignin's functional groups than with styrene. Addition of polar functional groups is well-known to increase the surface energy of polymers, and as a result, it would enhance polymer's interaction with metals.[63] For example, oxidation is known to enhance metal-polymer adhesion.[63]

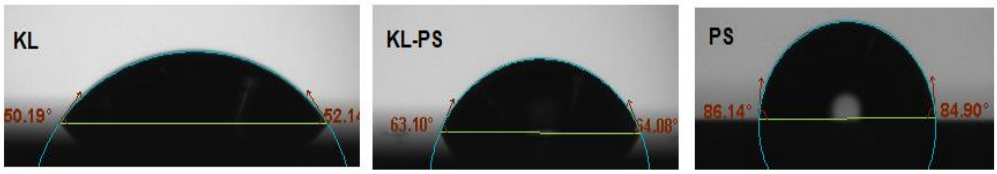

Figure 4.3: Contact angle images of water droplet on KL, KL-PS and PS coated substrates.

Table 4.2. Surface energy of KL, KL-PS and PS substrates determined following Fowke's and van Oss's theories with their dispersive and polar components.

	Fowke theory			van Oss theory			
	σ_S mN m^{-2}	σ_S^D mN m^{-2}	σ_S^PmN m^{-2}	σ_SmN m^{-2}	σ_S^DmN m^{-2}	σ_S^+mN m^{-2}	σ_S^-mN m^{-2}
KL	60±1	47±1	12.9±1	65.86±3	46.9±2	0.66±0.1	18.3±2
KL-PS	53.5±2	46.9±2	6.6±1	57.75±1	46.9±2	0.15±0.1	10.7±1
PS	46.8±1	41.9±1	4.9±1	50.9±1	41.8±1	1.9±0.4	6.23±1

4.4.3 Adsorption analysis.

KL, PS and KL-PS samples adsorbed 22, 15 and 45 mg/g of Cu (II) following equation 3, respectively. The adsorption capacity of these three polymers are in harmony with their physical properties, as KL-PS has the highest surface area of 44 m^2/g and pore volume of 0.053 cm^3/g. However, the adsorption experiment does not provide any information regarding the chemical interactions of the polymers and the cation ion. To fundamentally examine such an interaction, the QCM and FT-IR analyses were performed.

4.4.4 QCM analysis.

Figure 4 shows changes in the frequency (*Δf)* and dissipation (*ΔD*) of the QCM sensors coated with KL, KL-PS and PS as a function of time. Switching the influent solution from buffer to Cu (II) led to a drop in frequency, implying the adsorption of Cu (II) onto the substrates. At equilibrium, *Δf* values for KL, KL-PS and PS were -7.2, -24.4 and -7.1 Hz at the 5^{th} overtone, respectively. KL-PS showed the highest adsorption affinity with a noticeable decrease in *Δf*. Different trends in *Δf* are related to the interaction between coated solid substrate and the bulk solution. KL coated sensor showed faster adsorption at the beginning of the experiment with a steeper *Δf* change (i.e., it reached the saturation point almost in 60 mins). The PS coated sensor had slower adsorption with saturation reaching in 120 min. KL-PS with the maximum *Δf* seemed to have adsorption performance between KL and PS, which showed a fast uptake in the first 60 min and then slower interaction afterward. Surprisingly, rinsing with a buffer solution made a major difference in the interactions of the coated surfaces with the bulk solution. In this case, KL coated surface lost copper ions, while KL-PS and PS coated surfaces were not affected by buffer rinsing. *ΔD* changes are also illustrated in Figure 4. Interestingly, both KL and PS show low dissipation values. KL shows a rapid *ΔD* increase, while PS depicted a slower change (i.e., similar to their frequency changes). It was postulated previously that magnitude of changes in dissipation is related to the properties of the adsorbed layer.[64] Figure 4 also shows different overtones of 5, 7 and 9 with similar trends for coated sensors. In Figure 4a and 4b; overlapping different frequency overtones with minor increment in *ΔD* ($> 2 \times 10^{-6}$) would imply that a rigid layer of copper ions was formed on the KL and PS coated sensors.[50] In Figure 4c; the higher *ΔD* magnitude of 8.7×10^{-6} for KL-PS with segregated frequency lines for different overtones would reveal that the adsorbed layer was more nonrigid.[65]

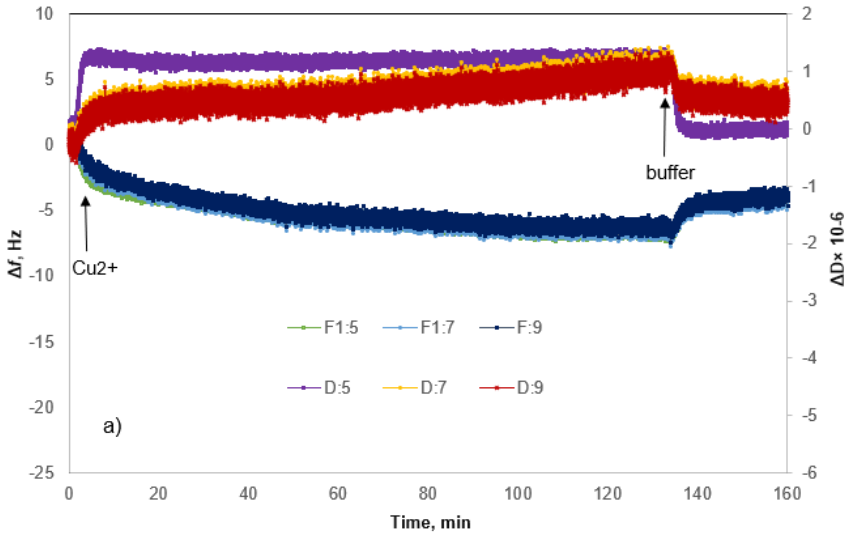
Δf, Hz
ΔD× 10-6
Time, min
Cu2+
buffer
F1:5
F1:7
F:9
D:5
D:7
D:9
a)

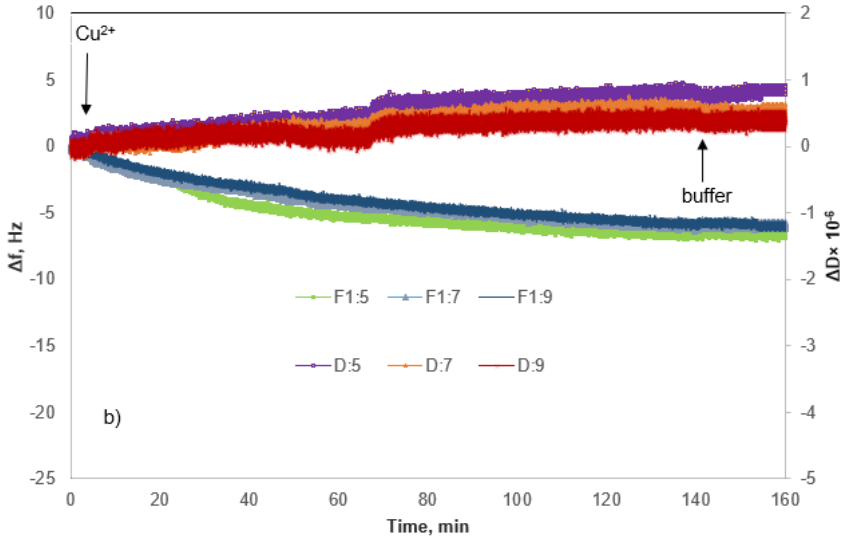
Δf, Hz
ΔD× 10-6
Time, min
Cu2+
buffer
F1:5
F1:7
F1:9
D:5
D:7
D:9
b)

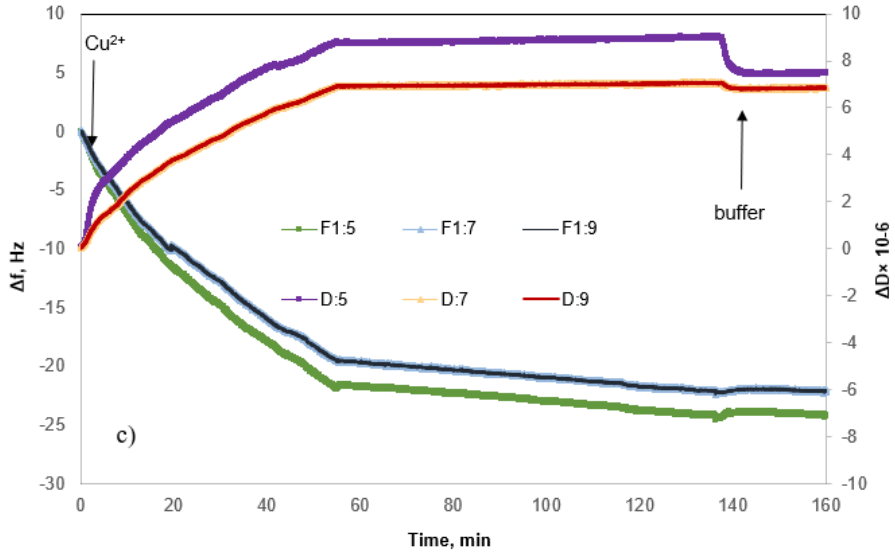
Δf, Hz
ΔD× 10-6
Time, min
Cu2+
buffer
F1:5
F1:7
F1:9
D:5
D:7
D:9
c)

Figure 4.4: Changes in frequency (*Δf)* and dissipation *(ΔD)* as a function of time for Cu (II) adsorption on sensors coated with a) KL b) PS c) KL-PS. The arrows indicate a switch in the solution feed. The corresponding *Δf* and *ΔD* for the 5th, 7th and 9th overtones are illustrated.

The ratio of *ΔD/Δf* in Figure 5 was also studied to understand the structural properties of adsorbed layers. The higher slope represents a dissipative layer, implying that higher energy is bound in each frequency change unit while copper ion adsorbs on the surface.[46] In addition, a higher ratio implies a more mobile and viscoelastic layer and a lower slope reflects a compact and elastic film.[66] In Figure 5, *ΔD/Δf* ratio for the PS-coated sensor at 5th overtone showed almost zero slope at the beginning of the adsorption, which reflects that the adsorbed layer did not change the viscoelastic behaviour of the surface,[67] which originates from a large mass growth with a minor dissipation variation. Further changes in *ΔD* results in a slight increase in the *ΔD/Δf* ratio for PS. On the other hand, KL shows a steeper slope at the beginning of the adsorption, but it reaches a plateau upon saturation, implying a stiff layer formation on the KL coated sensor.[68]
KL-PS illustrates a different slope (*ΔD/Δf* ratio) and it had a larger *ΔD* and *Δf* magnitudes, yielding a loose and viscoelastic structure.[51] Based on the elasticity and viscoelasticity of the adsorbed layer, the degree of Cu (II) adsorption can be determined using Sauerbrey model ($\Delta m_{Sauerbrey}$) for KL and PS, and the Voigt model (Δm_{Voigt}) for KL-PS.[67,68] Model fits for the adsorption of Cu(II) on the KL-PS is shown in Figure A1.2 in the appendix materials.
The calculated adsorbed mass and thickness of Cu (II) layer on KL, KL-PS and PS substrates after buffer rinsing are summarized in Table 3. There is not a distinguishable difference between the fitted adsorbed mass for KL and PS in both models, but a deviation is noticeable for Δm_{Voigt} from $\Delta m_{Sauerbrey}$ for KL-PS. This designates that the adsorbed layer onto KL-PS is not rigid and is mostly viscoelastic, whereas the adsorbed layer onto KL and PS is rigid,[49] which is in accordance with previous discussion on the structure of adsorbed layers. The adsorbed mass on KL-PS substrate was determined to be 434 ng/cm^2 following the Sauerbrey model and 4378 ng/cm^2 following the Voigt model. The reason for this noticeable variation in mass uptake between QCM and adsorption experiments would be the adsorption of water molecules on the coated layer of KL-PS that resulted in a thicker and loose structure. It may also be implied that the KL-PS film possesses higher porosity after coating on the QCM sensor.

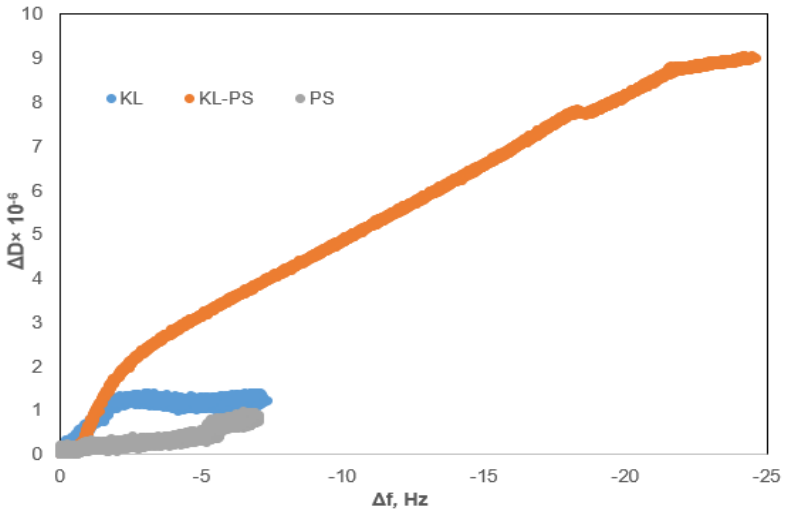

Figure 4.5: Changes in dissipation (ΔD) as a function of changes in frequency (Δf) for the KL, KL-PS and PS substrates in the Cu (II) adsorption experiment at 5th overtone (total time=140 min).

Table 4.3. The adsorbed mass and thickness of Cu (II) layer on KL, KL-PS and PS substrates using Sauerbrey and Voigt models.

Substrate	$\Delta m_{Sauerbrey}$ (ng/cm^2)	$\Delta d_{Sauerbrey}$ (nm)	Δm_{Voigt} (ng/cm^2)	Δd_{Voigt} (nm)
KL	81	0.67	77	0.77
PS	120	1.08	97	0.97
KL-PS	434	3.94	4378	4.38

4.4.5 FT-IR analysis.

This tool was implemented to compare vibrational changes of the molecules of KL, PS and KL-PS before and after Cu(II) adsorption in Figure 6.[69,70] The FT-IR absorption spectra in Figure 6a shows different absorption wavelengths associated with KL structure, in which the wide peak at 3100-3550 1/cm contributes to the hydroxyl functional groups of KL, and the signal at 1647 1/cm is related to the C=O stretching vibration.[71] Figure 6b and 6c illustrate the wavelengths relating to the structures of PS and KL-PS. Two characteristic absorption peaks of 746 and 690 1/cm are observable in the PS spectrum and peaks at 2821 and 2930 1/cm were observed due to $-CH_2$ stretching vibrations.[72] KL-PS spectrum in Figure 6c represents the peaks that are observable on the spectra of both KL and PS, confirming the integration of KL in PS substrate.

The second spectra (blue line) in each panel illustrates the changes in FTIR absorption vibration after copper ion adsorption. A difference in KL absorption signals is observable after copper adsorption, which in fact illustrates the movement of hydroxyl group signal from 3400 to 3410 1/cm (Figure 6a). This may be caused by the formation of dipole bonds between Cu (II) and hydroxyl groups of lignin owing to their negative dipole moments, resulting in an increase in energy and a blue shift in absorption.[69,73] Figure 6b represents that there is not a noticeable variation in absorption by Cu (II) adsorption on PS. This, in fact, justifies the limited adsorption capacity of PS as experienced in the QCM experiment (Figure 4b). PS did not show effective interaction with copper ions mainly because of a shortage of functional groups as well as low surface area and surface energy as shown in Tables S1 and 3. Therefore, neither chemical nor physical adsorption occurs effectively in this case and only a minor variation in the characteristic signal of PS (from 746 to 749 1/cm) was obtained, which will be explained later.

On the other hand, KL-PS showed the highest adsorption mass both in batch and QCM experiments, which resulted in noticeable changes in the FT-IR vibrational absorption in Figure 6c. The visible difference is observable for the vibrational band at 746 1/cm (the same signal in PS), which is assigned to out-of-plane bending of aromatic C-H bonds, δ_{C-H}.[74] The out-of-plane bending in aromatic structure is visible when all 5 C-H bonds bend at the same time and in the same direction perpendicular to the aromatic ring, which is illustrated in Figure 6c (the bending may happen in or out of paper, which is shown as + and -).[75] In the absence of copper (grey line in Figure 6c), light with a wavenumber of 746 1/cm is needed to excite δ_{C-H} vibration for KL-PS. After the adsorption of copper by KL-PS (Figure 6c), light at a higher wavenumber (754 1/cm) was required for the δ_{C-H} vibration absorption, representing a constraint effect of copper ions on aromatic C-H bond's bending. These results would suggest that a copper ion might be above the aromatic ring of KL-PS. This orientation corresponds to the formation of cation-π interaction between copper ions and the aromatic structure of KL-PS. The copper cations with a low electron density interact with the high electron density in the π system of aromatic ring, resulting in higher excitation energy, which was stemmed from the δ_{C-H} vibration absorption band.[76]

The solvation of cations also plays an important role in the strength of the cation-π interaction. Solvation of the cations extends the distance between cation and π system, thus lessening the energy associated with the cation-π interaction.[77] Although hydration of cations in aqueous system might be a barrier to π-system interactions, significant bonding strength (33 kJ/mol) is

simulated to exist within the π-system and cations surrounded with water molecules.[78] Wang and coworkers introduced δ_{C-H} band shifts (4 1/cm) in FTIR analysis as an indicator of the cation-π interaction between mineral surfaces and aromatic hydrocarbons.[75] Along with the observed vibrational movement at 746 1/cm, KL-PS-Cu wavelengths illustrate another visible signal alteration at the characteristic peak of residual hydroxy moieties (3100-3550 1/cm) in Figure 6c. The mentioned signal depicted a blue shift from 3371 to 3388 1/cm, which is identical to the same signal change observed in KL-Cu spectrum, suggesting the participation of residual functional groups in adsorbing Cu (II) ions.

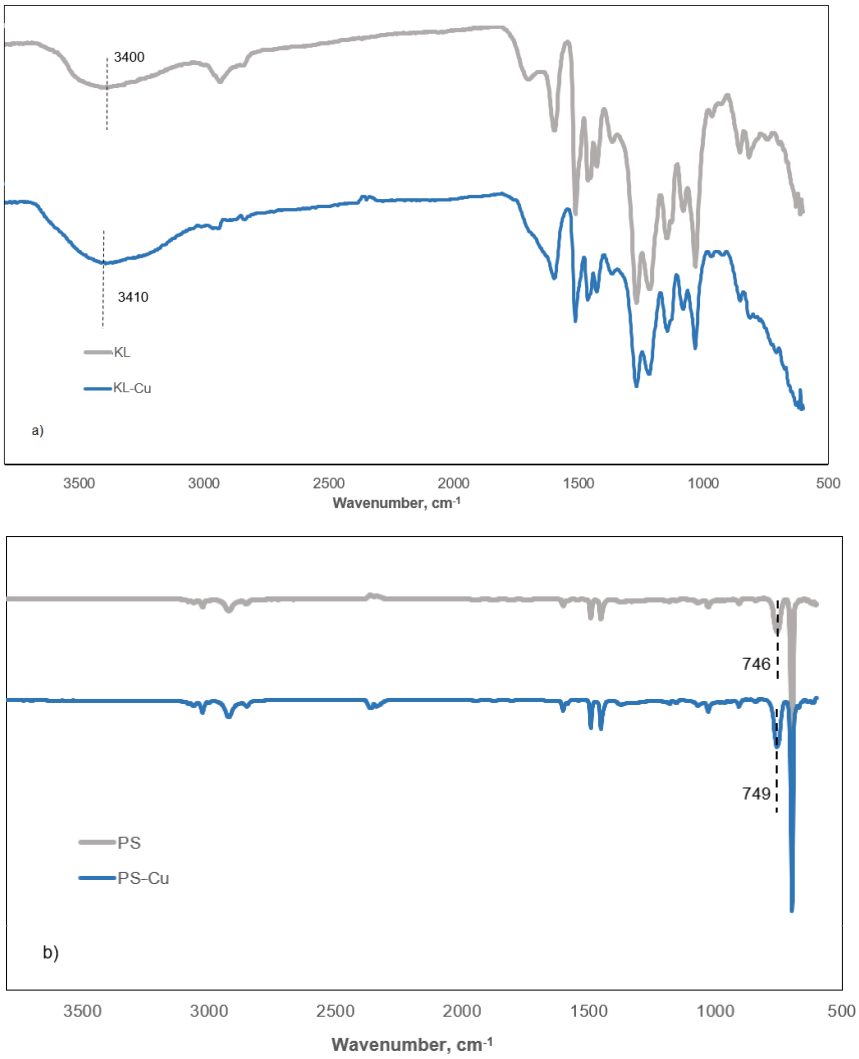

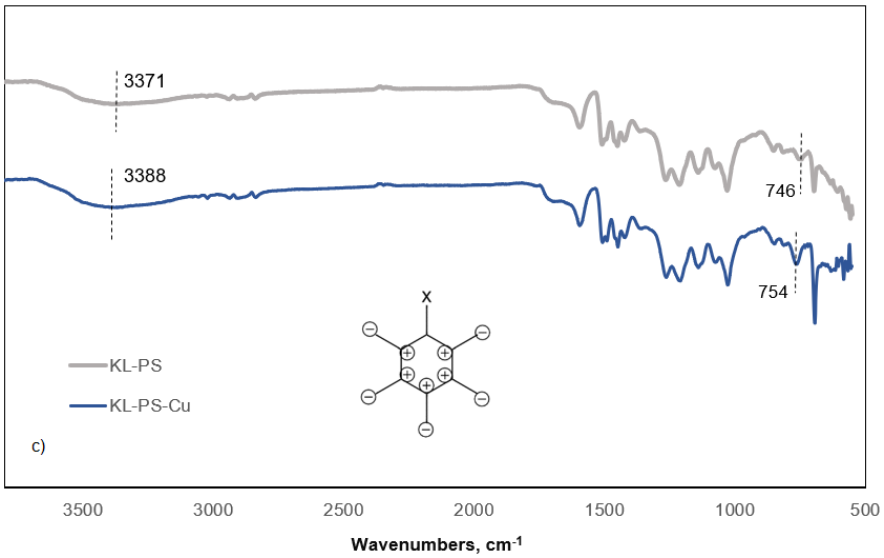

Figure 4.6: FTIR spectra of a) KL, b) PS and c) KL-PS before (grey) and after (blue) Cu (II) adsorption.

4.4.6 Adsorption mechanism.

Based on the obtained data, it is possible to propose the adsorption mechanism involved in adsorption. The schematic chemical interactions are suggested in Figure 7. KL has limited surface area of 24 m^2/g, which is a limitation for effective physical adsorption. Therefore, the most probable interaction between KL and Cu (II) would be the ion-dipole interaction between Cu (II) and polar functional groups of lignin, such as phenolate, aliphatic hydroxy and carboxyl groups, owing to their negative dipole moments (Figure 7a), which were proven by FT-IR results. The adsorption process observed by steep changes in ΔD and Δf in QCM experiment for KL (Figure 4a) would also imply that the interaction of KL's surface with the ions is based on polar interactions. PS' limited surface area (15 m^2/g) would not make any advantage for its physical adsorption, although a paucity of chemical interaction is evident based on FT-IR results. Therefore, the most probable interaction between PS and copper ions is suggested to be the cation-π interaction, which is well recognized to be closely associated with dispersive and hydrophobic forces (Figure 7b).

Polystyrene lacks sufficient pore size and surface area (Table A1.1) accessible for copper ions, which justify its limited adsorption mass. However, the incorporation of KL into PS resulted in enhanced chemical and physical interactions for KL-PS polymers. The adsorption mechanism is more complicated for KL-PS as it seems to adsorb Cu (II) through physical interaction as well as more than one chemical interaction (Figure 7c). Its surface area is relatively larger than KL and

PS. Therefore, the physical interaction can play an important role in the adsorption mechanism. For chemical interactions, it is possible that both ion-dipole and cation-π interactions contribute to the isolation of Cu (II) from the bulk solution (Figure 6), as the polymer could have the advantages of both KL's and PS's chemical properties. Indeed, the higher surface area of KL-PS provided better possibility for the adhesion of copper ions through the chemical interaction mainly cation-π interactions.

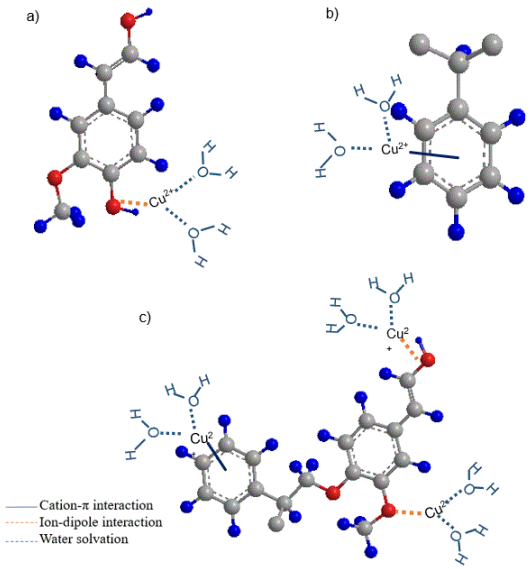

Figure 4.7: The possible interactions of copper ions and a) KL b) PS c) KL-PS substrates. Grey, red and blue balls represent carbon, oxygen and hydrogen atoms, respectively. For simplicity, only one unit of lignin or polystyrene is presented.

4.4.7 Visualization analysis.

The morphologies of KL, KL-PS and PS coated on QCM sensors were visualized by SEM/EDX before and after Cu (II) adsorption. The images before adsorption are available in Figure A1.3 in appendix information, while the images after the adsorption experiment are depicted in Figure 8. It is evident that a uniform layer is coated on each of the QCM sensors. The more porous structure of KL-PS than KL and PS is also observable. The EDX data provides elemental identification of surfaces. KL-PS is the only surface with detectable Cu (II) on its surface. The lack of N composition (from counter ion NO_3^-) also confirms that copper is adsorbed in the cation form and is distributed uniformly on the KL-PS surface (Figure A1.3).

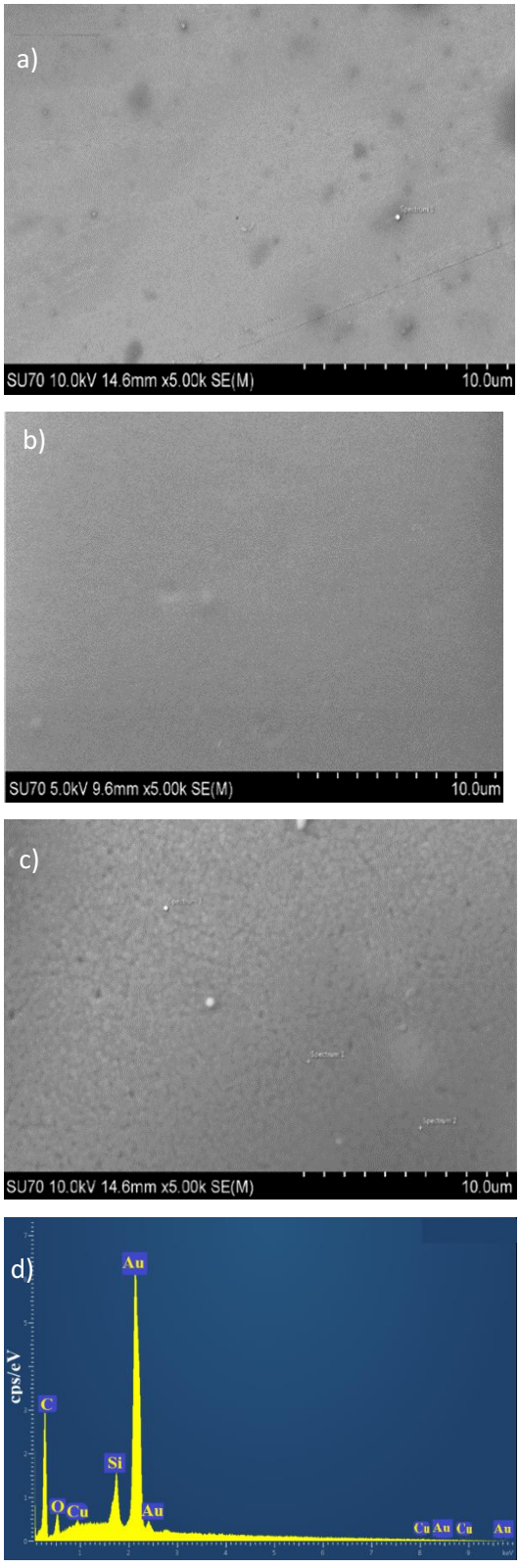

Figure 4.8**:** SEM/EDX images of coated gold sensors a) KL b) PS c) KL-PS d) EDX of KL-PS image after Cu (II) adsorption. The sharp Au signal comes from the gold sensor.

4.5 Development of a sustainable PS product.

Sustainability is a critical factor in the development of new products worldwide. This study reported a simple method to produce a more sustainable polystyrene matrix, which has the potential to be used as an adsorbent. The incorporation of lignin into PS not only improved its physicochemical properties but also decorated a greener and a sustainable polymer. The 40 wt% proportion of KL in KL-PS implies a 40 wt.% reduction in styrene monomer use for PS production and use. Due to the high adsorption capacity of KL-PS (Figure 5 and Table 2), the mass of KL-PS required for achieving a certain level of adsorption, e.g., 20 mg/g, will be significantly smaller than that of PS needed. In other words, KL incorporation in PS would not only reduce the mass of styrene needed for PS-based adsorbent production, but also decrease the overall mass of the induced KL-PS required as an adsorbent for ion removals. The extremely higher adsorption of KL-PS than PS (45 vs 15 mg/g Figure 5 and Table 3) suggest that KL-PS will have a much more cleaning effect in water and wastewater treatment processes. The results of this study provide solid evidence for the development of a new generation of sustainable PS-based adsorbent that is much more impactful than regular PS in ion removal for water and wastewater purification purposes. To further develop this new sustainable PS based adsorbent with a larger surface area, the production process of KL-PS should be investigated via developing the following techniques reported in the literature at larger scales.[9,56]

4.6 Conclusion

The incorporation of lignin, as a green and sustainable chemical, in polystyrene was reported as a facile process for producing a more efficient and sustainable polystyrene-based adsorbent. Successful incorporation of KL into polystyrene was confirmed by FT-IR and NMR characterization techniques. The ^{31}P-NMR analysis elucidated the participation of varied hydroxyl functional groups, such as aliphatic, guaiacyl and C5-substitied in the free radical polymerization with styrene. The surface area and image analysis confirmed the production of a more porous structure of KL-PS than PS and KL. We noted that the appearance of functional groups afforded solid surface energy increment and consequently enhanced interaction of KL-PS's surface with copper ions. QCM-D studies indicated better compatibility of KL-PS than KL and PS with copper ion, while showing a loose and viscoelastic structure of adsorbed ions with water entrapment. Both physical and chemical interactions contributed to copper ions adsorption, while implementing FT-IR analysis indicated that two mechanisms of ion-dipole and cationic-π interactions were

responsible for chemical uptake of copper ions. The modified polystyrene revealed a promising application as an adsorbent for copper ion uptake by KL-PS from an aqueous medium.

4.7 References

[1] Y. Yi, Z. Yang and S. Zhang, *Environ. Pollut* **2011**, *159*, 2575-2585.

[2] R. Gupta, N. Gupta and P. Rathi, *Appl. Microbiol. Biotechnol*. **2004**, *64*, 763-781.

[3] J. Zhou, F. Gao, T. Jiao, R. Xing, L. Zhang, Q. Zhang and Q. Peng, *Eng. Asp*. **2018**, *545*, 60-67.

[4] P. T. Yeung, P. Y. Chung, H. C. Tsang, J. C. Tang, G. Y. Cheng, R. Gambari, C. H. Chui and K. H. Lam, *RSC Adv.* **2014** ,*4*, 38839-38847.

[5] H. Gedam and R. S. Dongreb, *RSC Adv*. **2016**, *6*, 22639-22652.

[6] M. Vafaeezadeh, M. M. Hashemi and N. Ghavidel, *RSC Adv.* **2016**, *6*, 14128-14133.

[7] R. Gupta, R. Singh, S. Dubey, *Sep. Purif. Technol*. **2004**, *38*, 225-232.

[8] C. Jin, X. Zhang, J. Xin, G. Liu, G. Wu, Z. Kong and J. Zhang, *ACS Sustainable Chem. Eng.* **2017**, *5*(5), 4086.

[9] N. A. Awang, W. N. Wan Salleh, A. F. Ismail, N. Yusof, F. Aziz and J. Jaafar, *Ind. Eng. Chem. Res.* **2018**, *58*(2), 720-728.

[10] F. E. Soetaredjo, A. Kurniawan, L. K. Ong, D. R. Widagdyo and S. Ismadji, *RSC Adv.* **2014**, *4*, 52856-52870.

[11] T. Aro and P. Fatehi, *ChemSusChem* **2017**, *10*(9), 1861-1877.

[12] S. S. Chen, T. Maneerung, D. C. Tsang, Y. S. Ok and C. H. Wang, *Chem. Eng. J*. **2017**, *328*, 246-273.

[13] J. Xu, S. Zhu, P. Liu, W. Gao, J. Li and L. Mo, *RSC Adv***. 2017** ,*7* , 44751-44758.

[14] J. Joshua, B. A. Simmons and S. W. Singer, *RSC Adv*. **2016**, *6*, 54382-54393.

[15] D. Kai, W. Ren, L. Tian, L. Chee, Y. Liu, S. Ramakrishna and X. J. Loh, *ACS Sustainable Chem. Eng*. **2016**, *4*(10), 5268-5276.

[16] D. Liu, Y. Li, Y. Qian, Y. Xiao, S. Du and X. Qiu, *ACS Sustainable Chem. Eng*. **2017**, *5*(9), 8424-8428.

[17] L. Dai, R. Liu, L. Q. Hu, Z. F. Zou and C. L. Si, *ACS Sustainable Chem. Eng*. 2017, *5*(9), 8241-8249.

[18] Y. Ge and Z. Li, *ACS Sustainable Chem. Eng.* **2018**, *6*(5), 7181-7192.

[19] T. Todorciuc, L. Bulgariu and V. Popa, I. *Cell Chem. Technol*. **2015**, *49*(5-6), 439-447.

[20] X. Guo, S. Zhang and X. Q. Shan, *J Hazard Mater*. **2008**, *151*, 134-142.

[21] W. Jin, Z. Zhang, G. Wu, R. Tolba and A. Chen, *RSC Adv.* **2014**, *4*, 27843-27849.

[22] R. H. Crist, J. R. Martin and D. R. Crist, *Environ. Sci. Technol.* **2002**, *36*, 1485-1490.

[23] S. Fujisawa, E. Togawa and K. Kuroda, *Biomacromolecules*. **2016**, *18*(1), 266-271.

[24] J. Chen, G. Cheng, Y. Chai, W. Han, W. Zong, J. Chen, C. Li, W. Wang, L. Ou and Y. Yu, *Colloid Surf. B Biointerf*. **2018**, *161*, 480-487.

[25] Z. Yang, C. Zhou, H. Yang, T. Cai, J. Cai, H. Li, D. Zhou, B. Chen, A Li and R. Cheng, *Ind. Eng. Chem. Res.* **2012**, *51*(27), 9204-9212.

[26] Y. Zhang, Y. Chen, C. Wang and Y. Wei, *J. Hazard Mater*. **2014**, *276*, 129-137.

[27] L. J. Barbour, S. L. De Wall, E. S. Meadows and G. W. Gokel, *Ind. Eng. Chem. Res.* **2000**, *39*(10), 3436-3441.

[28] N. Javkhlantugs, H. Bayar, C. Ganzorig and K. Ueda, *Intl. J. Nanomedicine* **2013**, *8*, 2487.

[29] M. Keiluweit and M. Kleber, *Environ. Sci. Technol*. **2009**, *43*, 3421-3429.

[30] W. Chen, L. Duan, L. Wang and D. Zhu, *Environ. Sci. Technol*. **2008**, *42*, 6862-6868.

[31] W. L. Jorgensen and D. L. Severance, *J. Am. Chem. Soc*. **1990**, *112*, 4768-4774.

[32] S. C. Ringwald and J. E. Pemberton, *Environ. Sci. Technol* **2000**, *34*, 259-265.

[33] F. Yue, F. Lu, S. Ralph and J. Ralph, *Biomacromolecules* **2016**, *17*(6), 1909-1920.

[34] A. Elabbadi, H. A. Jerri, L. Ouali and P. Erni, *ACS Sustainable Chem. Eng*. **2015**, *3*(9), 2178-2186.

[35] F. Jiang, C. Qian, A. R. Esker and M. Roman, *J. Phys. Chem. B* **2017**, *121*, 9607-9620.

[36] D. La. Rosa, L. Varela, E. Sudol, M. El-Aasser and A. Klein, *J. Polym. Sci. A* **1999**, *37*, 4054-4065.

[37] Y. Pu, S. Cao and A. J. Ragauskas, *Energy Environ. Sci*. **2011**, *4*, 3154-3166.

[38] J. A. Lucey, M. Srinivasan, H. Singh and P. A. Munro, *J Agric Food Chem*. **2000**, *48*, 1610-1616.

[39] Y. Liu, X. Chen, X. Jia, X. Fan, B. Zhang, A. Zhang and Q. Zhang, *Ind. Eng. Chem. Res*. **2018**, *57*(50), 17259-17265.

[40] T. Tammelin, M. Österberg, L. S. Johansson and J. Laine, *Nord Pulp Pap Res J* **2006**, *21*(4), 444-450.

[41] J. Panzer, *J. Colloid Interf. Sci.* **1973**, *44*, 142-161.

[42] D. K. Owens and R. Wendt, *J. Appl. Polym. Sci.* **1969**, *13*(8), 1741-1747.

[43] C. J. Van Oss, R. Good and M. Chaudhury, *J. Colloid Interf. Sci*. **1986**, *111*(2), 378-390.

[44] T. W. J. Albrecht, J. Addai-Mensah and D. Fornasiero, Chemeca 2011: Engineering a Better World: Sydney Hilton Hotel, NSW, Australia, **2011**.

[45] K. Kubiak, Z. Adamczyk and M. Oćwieja, *Langmuir* **2015**, *31*, 2988-2996.

[46] R. Tanaka, T. Saito, T. Hänninen, Y. Ono, M. Hakalahti, T. Tammelin and A. Isogai, *Biomacromolecules* **2016**, *17*, 2104-2111.

[47] Y. Meng, L. Wang, H. Xiao, Y. Ma, L. Chao and Q. Xie, *RSC Adv.* **2016**, *6*, 33666-33675.

[48] F. L. Hatton, M. Ruda, M. Lansalot, F. D'Agosto, E. Malmström and A. Carlmark, *Biomacromolecules* **2016**, *17*(4), 1414-1424.

[49] K. Dutta, A. Nayak and G. Belfort, *J. Colloid Interf. Sci*. **2008**, *324*(1-2), 55-60.

[50] M. Rodahl and B. Kasemo, *Sens. Actuator A-Phys* **1996**, *54*, 448-456.

[51] M. Yan, C. Liu, D. Wang, J. Ni and J. Cheng, *Langmuir* **2011**, *27*, 9860-9865.

[52] M. Malow, K. D. Wehrstedt and M. Manolov, *Thermochim Acta* **2015**, *621*, 1-5.

[53] N. Ghavidel Darestani, A. Tikka and P. Fatehi, *Polymers* **2018**, *10*, 928-945.

[54] K. Barhpaima and P. Fatehi, *ChemSusChem* **2018**, *11*, 2967-2980.

[55] F. Monteil-Rivera, M. Phuong, M. Ye, A. Halasz and J. Hawari, *Ind Crop. Prod*. **2013**, *41*, 356-364.

[56] S. Yang, J. L. Wen, T. Q. Yuan and R. C. Sun, *RSC Adv*. **2014**, *4*, 57996-58004.

[57] S. M. Notley and M. Norgren, *Langmuir* **2010**, *26*, 5484-5490.

[58] V. Lee, R. G. Craig, F. E. Filisko and R. Zand, *J Biomed. Mat. Res*. **1996**, 31, 51-62.

[59] Q. Q. Liu, L. Wang, A. G. Xiao, H. J. Yu and Q. H. Tan, *Eur. Polym. J*. **2008**, *44*, 2516-2522.

[60] M. Norgren, S. M. Notley, A. Majtnerova and G. Gellerstedt, *Langmuir* **2006**, *22*, 1209-1214.

[61] R. Sukamanchi, D. Mathew and S. Kumar KS, *ACS Sustainable Chem. Eng.* **2016**, *5*(1), 252-260.

[62] E. Liston, L. Martinu and M. Wertheimer, *J Adhes. Sci. Technol*. **1913**, *7*(10), 1091-1127.

[63] K. L. Mittal, CRC Press: London, **1994**.

[64] C. Mensch, J. T. Buchman, C. L. Haynes, J. A. Pedersen and R. J. Hamers, *Langmuir* **2018**, *34*, 12369-12378.

[65] I. Schrader, L. Wittig, K. Richter, H. Vieker, A. Beyer, A. Gölzhäuser, A. Hartwig and P. Swiderek, *Langmuir* **2014**, *30*, 11945-11954.

[66] A. Doliška, V. Ribitsch, K. S. Kleinschek and S. Strnad, *Carbohydr. Polym*. **2013**, *93*, 246-255.

[67] K. S. Kontturi, T. Tammelin, L. S. Johansson and P. Stenius, *Langmuir* **2008**, *24*, 4743-4749.

[68] A. Garg, J. R. Heflin, H. W. Gibson and R. M. Davis, *Langmuir* **2008**, 24, 10887-10894.

[69] C. Jin, X. Zhang, J. Xin, G. Liu, J. Chen, G. Wu, T. Liu, J. Zhang and Z. Kong, *Ind. Eng. Chem. Res.* **2018**, *57*(23), 7872-7880.

[70] P. Duan, N. Yanai, H. Nagatomi and N. Kimizuka, *J. Am. Chem. Soc*. **2015**, *137*, 1887-1894.

[71] S. Gharehkhani, N. Ghavidel and P. Fatehi, *ACS Sustainable Chem. Eng.* **2018**, *7*(2), 2370-2379.

[72] D. Plackett, K. Jankova, H. Egsgaard and S. Hvilsted, *Biomacromolecules* **2005**, *6*(5), 2474-2484.

[73] C. Tian, J. Zhao, J. Zhang, S. Chu, Z. Dang, Z. Lin and B. Xing, *Environ Sci. Nano* **2017**, ***4***, 2134-2143.

[74] H. L. Luo, J. Sheng and Y. Wan, *Mater. Lett*. **2008**, *62*, 37-40.

[75] H. Wang, D. J. Grant, P. C. Burns and C. Na, *Langmuir* **2015**, *31*, 5820-5826.

[76] L. Drain, *Trans. Faraday Soc* **1953**, *49*, 650-654.

[77] S. Rao, H. Zipse and G. N. Sastry, *J. Phys. Chem. B*, **2009**, *113*, 7225-7236.

[78] Y. Xu, J. Shen, W. Zhu, X. Luo, K. Chen and H. Jiang, *J. Phys. Chem. B* **2005**, *109*, 5945-5949.

Chapter 5: Pickering/non-Pickering emulsions of nano structured sulfonated lignin derivative

5.1 Abstract

In this work, we produced sulfoethylated lignin (SEKL) polymeric surfactant and nano sulfoethylated lignin (N-SEKL) particles with the average size of 750±50 nm in a facile green process utilizing a solvent free reaction and acidification-based fractionation. SEKL formulated a liquid-like conventional emulsion with low viscosity that had temporary stability (5 h) at pH 7. However, N-SEKL formed a gel-like, motionless, and ultra-stable Pickering emulsion through a network of interaction between N-SEKL particles that created a steric hindrance among oil droplets at pH 3. The deposition of SEKL and N-SEKL on the oil surface was monitored by a Quartz crystal microbalance. Experimentally, it was shown that adsorption at pH 7 was reversible due to the low adsorption energy of SEKL on the oil droplet ($\Delta E \sim 15\ K_BT$), which was determined with the help of three-phase contact angle measurement. However, the high desorption energy ($\Delta E \sim 6.0\times10^{+5}\ K_BT$) of N-SEKL made it irreversibly adsorbed on the oil droplets. SEKL was too hydrophilic to attach to the oil interface ($\Delta E \sim 0$) and thus did not facilitate emulsion at pH 11. Therefore, it is feasible to apply SEKL for the formulation of Pickering or non-Pickering emulsions in the form of nanoparticle or polymeric surfactant, depending on the targeted application.

5.2 Introduction

The stabilization of emulsions by solid particles has gained substantial considerations over the past two decades because they not only possess most of the basic properties of conventional emulsions, but also they dramatically decrease the dosage of required emulsifier and exhibit long-term stability.[1] In conventional emulsions, an emulsifier forms an interfacial thin layer surrounding oil droplets that create interactions with hydrophilic and hydrophobic phases and is prone to gravitational separation and droplet coalescence.[2] While the adsorption of surfactant molecules is a reversible process ($\Delta E < 10\ K_BT$),[3] the desorption energy (ΔE) required to remove a solid particle from the oil-water interface is several orders of magnitude greater than the thermal energy.[4] It is suggested that the irreversible adsorption of particles at the oil interface in Pickering emulsions is due to the formation of a densely packed particle layer at the oil-water interface, which prevents both emulsion flocculation and coalescence by inducing a steric barrier.[5,6] The long-term stability of emulsions is an essential factor in many industries, such as food storage or cosmetic formulations.[7-8] However, for some other applications, the short-term stabilization of

emulsion or reversible adsorption of surfactant is the primary concern, including emulsion polymerization,[9] oil recovery[10] and interfacial catalysis for biphasic reactions.[11] Shifting on and off Pickering emulsions have been extensively studied applying variation in Ph,[12] temperature,[13] magnetic fields[14] or CO_2.[15] However, to the best our knowledge, using one emulsifier to produce both Pickering and non-Pickering (conventional) emulsions and to demulsify in a formulation is a novel approach.

Recently, a shift toward using biobased particles such as cellulose,[16] chitosan,[17] lignin,[18] modified starch[19] and soy protein[20] was observed in emulsion systems for responding to the environmental-friendly procedures.[21] Lignin is abundant biomass accounting for approximately 20-30% of plant weight and is considered as a natural three-dimensional macromolecule.[22] However, lignin is still considered as an underutilized material because only 1-2% of its vast production annually (50-70 million tons) is utilized for the production of value-added products.[23] Structurally, lignin is composed of both hydrophobic skeleton (phenylpropane monomers) and hydrophilic functional groups, such as carbonyl and phenolic hydroxyl groups.[24,25] Lignin extracted from pulp and paper industry was suggested to have potential for applications, such as bio-based adhesives, stabilizers, nano- and micro scaled carriers, via producing water dispersed lignin nanoparticle.[26,27] For example, Wei et al.[18] reported synthesizing lignin particles by adjusting the pH value of an aqueous lignin solution from an alkaline system, which was used for emulsion polymerization of styrene. However, partial Pickering emulsion was formed, which was stable only at pH<4 with a large oil droplet size (20-58.9 μm) and the 1:4 oil-water ratio. Unmodified lignin only contains limited surface-active groups, which restrict its function as an efficient emulsifier.[12] It is reported that a large amount of acid or alkali is required to activate lignin precipitation/dissolution, and the changes in emulsion properties is limited only to alkaline and acidic conditions. Also, increasing the oil to water ratio would limit its performance as an effective emulsifier.[12] Therefore, lignin functionalization gained considerable attention to promote the application of lignin as a polymeric emulsifier.[28] Increasing the dosage of emulsifier or salt and altering pH were among the techniques to improve emulsion properties [29] e.g., emulsion fraction, long-term stability or viscosity. Li et al. [30] formulated oil-in-water (O/W) fuel emulsions using carboxymethylated lignin (CML) as the emulsifier. They reported that smaller oil drop sizes (2.5 μm) were obtained with CML of increased degree of substitution, reduced pH, or

water-to-oil ratio. However, the use of high CML concentration (4 wt.%) and degree of substitution (DS=30%) makes its application unappealing.

In our previous study,[31] grafted lignin-tannic acid (KL-TA) emulsifiers were synthesized, which showed pH-responsive stability with varied emulsion fraction using 1.5 wt. % of KL-TA with the charge density of -2.8 mmol/g. In these studies, high-charged lignin surfactants were produced that were not appealing for emulsion formulation. This is due to the increased particle-oil and particle-particle electrostatic repulsion,[32] hence a higher dosage of lignin was used to improve the stability of conventional emulsions. Therefore, lower degrees of functionalization with limited surface charges were targeted in this study to overcome these obstacles. Comparatively, one of the simplest approaches to enhance emulsion properties is the use of solid particles for the formulation of Pickering emulsions via protonation/deprotonation of the functional groups of the emulsifiers, which is known to alter the wettability of the emulsifiers.[33] Such measures were previously reported by Kalliola et al. [34] via precipitation of carboxymethylated chitosan to prepare stable Pickering emulsions.

As the main novelty of the present study, we report on the production of a novel water-soluble lignin polymer by sulfo-functionalization of lignin using 2-bromoethanesulfonate salt (NaBES) in a facile and solvent free process without hazardous chemicals with low sulfonate content. In the next step, the formation of nanoparticles via acidifying the sulfoethylated kraft lignin solution (SEKL) was followed and denoted as N-SEKL. Furthermore, the formation of N-SEKL was visualized by TEM imaging.

The energy of adsorption of SEKL/N-SEKL at xylene, as the oil phase, was determined using the three-phase contact angle to predict the reversibility of their adsorption (Pickering/non-Pickering). The next objective of this study was to experimentally evaluate the performance of N-SEKL and SEKL for the formulation of Pickering/non-Pickering emulsion at the low dosage of 0.25 wt.%. For this reason, the fundamental understandings of the stabilization mechanism and the properties of the formulated emulsions, e.g., the rheological characteristics and their short and long-term stabilities, were thoroughly assessed.

5.3 Experimental Section

5.3.1 Materials

Softwood kraft lignin (KL) produced via the LignoForce^{TM} technology was received from FPInnovations. The analytical grades of 2-bromoethanesulfonate salt (NaBES), sodium hydroxide

(NaOH, 97%), potassium hydroxide (KOH, 97%), sulfuric acid (H_2SO_4, 98%), hydrochloric acid (HCl, 37%), phosphotungstic acid hydrate, sodium dodecyl sulfate salt (SDS), dimethyl sulfoxide-d6 (DMSO-d6), deuterium oxide (D_2O) deuterated chloroform, pyridine, cyclohexanol, chromium(III) acetylacetonate, 2-chloro-4,4,5,5-tetramethyl-1,3,2-dioxaphospholane, poly (ethylene oxide) and cellulose membrane (1000 g/mol cut off) were purchased from Sigma-Aldrich. Xylene ($C_6H_6(CH_3)_2$ ≥98.5%, ACS grade as a mixture of ortho, meta and para isomers, and Nile red dye were purchased from Fisher Scientific. All chemicals were used without further purification. HPLC-grade water was produced by a Milli-Q water purifier and used in QCM experiments. SiO_2-coated Q- Sense sensor crystals (QSX 303) were supplied from Q-Sense, Biolin Company, Gothenborg, Sweden.

5.3.2 Synthesis of sulfoethylated kraft lignin

Ground KL powder (1 g, 5.5 mmol) was dispersed in deionized water in three-neck flasks to make a 20 g/L suspension. The pH of the suspension was adjusted to 11 by adding 1M NaOH solution. The suspension was kept stirring for 1 h for a complete deprotonation of KL's functional groups (aliphatic and aromatic hydroxy groups). Then, 2-bromoethanesulfonate salt, NaBES (2.5 g, 11 mmol) with the molar ratios of 2:1 (NaBES): KL was fed to the reaction medium. The reaction was initiated by transferring the three-neck flask in a preheated water bath at 80 °C. Upon finalization of the reaction after 4 h, the reaction was cooled down to room temperature and was neutralized by adding 5 wt.% H_2SO_4. The sample was dialyzed using cellulose membrane for 2 days to purify the product from salts. The product solution was further dried in an oven at 105 °C.

5.3.3 SEKL Characterization

^{1}H-NMR and ^{1}H-^{1}H 2D-NMR analysis was conducted via dissolving KL and SEKL (35 mg) in DMSO-d_6 and D_2O (0.5 µL), respectively. The NMR spectra were recorded using INOVA A-500 MHz (Varian, USA) NMR instrument with a 45° pulse width, 64 scans, and a relaxation time of 1.0 or 4.0 s for 1D or 2D NMR, respectively.[35]

The molecular weight of SEKL was determined in the form of weight- and number-average molecular weights by the UV detector of a gel permeation chromatography (GPC) (Viscotek GPCmax, Malvern, UK) using PolyAnalytic columns, PAA206 and PAA203. A 0.1 mol/L $NaNO_3$ aqueous buffer solution was used as an eluent in the system and to prepare a 5 mg/mL sample solution. Poly (ethylene oxide) was used as a standard solution in the GPC.

SEKL functional groups from high to low pH (11-3) compared to acidified KL powder was identified via a Fourier transform infrared spectroscopy (FTIR) (Bruker Tensor 27) equipped with an ATRassembly. The measurements were performed in the 550-4000 1/cm region with a resolution of 0.6 1/cm. SEKL suspensions at varied pH ranges (11-3) were prepared using KOH or HCl 0.8N and after protonation/dissociation of functional groups were dried in the oven overnight for further FT-IR analysis.

Acid-base titrations were performed to determine functional groups content and their pKa's, using an automatic titrator (Metrohm, 905 Titrado, Switzerland) with a potentiometric endpoint determination, which was equipped with a syringe pump and pH meter. Typically, an aqueous suspension of SEKL (100 mg) in deionized water (100 mL) was used in the experiment, while its initial pH was adjusted to 2.5 by 0.1 N HCl. The samples were titrated with 0.1 N NaOH with continuous stirring with magnetic bar at a titration rate of 0.5 mL/min. The same procedure was repeated for the control sample that did not have SEKL. The comparison of the sample and control facilitated the functional group and pKa determination.[36]

5.3.4 N-SEKL formation and analysis using TEM

A SEKL aqueous solution (0.25 wt.%) was prepared at pH 7 and stirred overnight for fully dissolving SEKL in water. Nanoprecipitation was followed by acidifying the solution to pH 3±0.2 by adding a few drops of 0.8N HCl while slowly stirring the solution at 100 rpm and room temperature. After a short time, an opaque dispersed suspension of lignin particles was formed. One drop of N-SEKL suspension at pH 3 was placed on the carbon-coated sample holder grid of the TEM instrument and allowed to dry at room temperature overnight, then one drop of phosphotungstic acid hydrate solution (1wt.%) was placed on top of particles (N-SEKL) to provide electron beam conductivity [37] and allowed to dry at room temperature before imaging. The formed nanoparticles (N-SEKL) were imaged via transmission electron microscopy (TEM; Hitachi 7700, Japan) at the accelerating voltage of 100 kV and their sizes were determined based on the obtained images. The same procedure was followed for SEKL solutions for TEM analysis at pH 7 and 11.

5.3.5 Hydrodynamic size and zeta potential analysis

Dynamic light scattering analyzer (BI-200SM Brookhaven Instruments Corp., USA) equipped with a 35mW laser power source was used to obtain hydrodynamic diameters of SEKL at varied pH ranges. The operating conditions of this test were the wavelength of 637 nm, scattering angle of 90° and 25 °C. Six cells of 0.25 wt.% of SEKL solutions were prepared at pH 7, and their pH

was adjusted to various ranges of pH 3-11±0.2 using KOH or HCl 0.8N. After stabilizing for 2 h, their hydrodynamic size (R_h) was determined. The zeta potential of the prepared solutions was also measured using a ZetaPALS analyzer (Brookhaven Instruments Corp, USA).

5.3.6 Emulsion preparation

Stock aqueous solutions of SEKL (0.25 wt.%) at pH 7 and 11 and N-SEKL (0.25 wt.%) at pH 3 were prepared. Volumetric ratio of unity of aqueous SEKL solution or N-SEKL suspension and xylene, as the organic phase, were prepared in clean glass vials and emulsified using an ultrasonic machine (Omni-Ruptor 4000, Omni International Int.) at room temperature, 240 W power and 30 s for 3 s intervals.

5.3.7 Microscopic Structure

The dynamic changes in the microstructure of emulsions by pH changes were observed immediately after preparation by a Leica TCC-SP8 confocal laser scanning microscope (Leica Microsystems Inc., Germany) equipped with a WLL laser (563 nm excitation wavelengths) using a HC PL APO CS2 100×/1.40 oil immersion objective lens. After preparation of emulsion at pH 11 as explained above, emulsions at pH7 and pH3 were prepared accordingly by adding HCl (0.8N) dropwise to the system and further vortex mixing to observe the changes in microstructure of emulsions. In this set of experiments, 200 µL of emulsions without dilution were taken from the emulsion layer of the samples immediately after the pH adjustment and were stained by the 5 µL of Nile red dye suspension in water (0.5 wt.%). The stained samples were placed on a glass slide with cover glass slides on the top. Red fluorescence was used for observation of the samples with a 600-710 nm filter under a 563 nm laser illumination.

5.3.8 Rheological Properties

The rheological properties of formulated emulsions at pH 3 (using N-SEKL), 7 and 11 (using SEKL) were analyzed as described previously.[31] A hybrid rheometer (TA Instruments, Discovery HR-2) with a parallel plate geometry (8 mm, gap 500 µm) was used for carrying out the experiments at room temperature. Experiments were performed immediately after the preparation of the emulsion. Precisely, 1 mL of each emulsion was transferred by a pipet onto the lower plate of the instrument. A 3 min pre-shear at 100 1/s was applied on each sample prior to recording the data. The variations in viscosity were measured from 0.1 to 1000 1/s at 23 °C. To determine the linear viscoelastic region of SEKL, an amplitude sweep test was performed in the range of 0.01

and 100 1/s at frequency of 10 rad 1/s. A strain of 0.1% was chosen from the linear viscoelastic region to carry out frequency sweep measurements in the range of 0.1 and 1000 rad/s.

5.3.9 Stability measurements

A multi-sampling analytical centrifuge, a dispersion analyzer (LUMiSizer 611, LUM GmbH, Berlin, Germany) was used to investigate the separation behavior and long-term physical stability of the emulsions using SEKL or N-SEKL.[38] Undiluted formulated emulsions at pH 3, 7 and 11 were transferred into separate cells and subjected to a centrifugal force of the instrument. The operational parameters of the test were total emulsion volume of 0.4 mL; the wavelength of 865 nm; centrifugal rotation of 1000 rpm; experimental time of 1000 s with 1 s time interval between the recording, and temperature of 25 °C.

5.3.10 Contact angle analysis

The two- (WCA) and three-phase (OCA) contact angles of a solid surface (SEKL/N-SEKL) at an air-water and oil-water interface were determined using a theta optical tensiometer attention (Biolin Scientific). First, a 300 µL SEKL solution (0.25 wt.%) at pH 7 and 11 and N-SEKL suspension at pH 3 (0.25 wt.%) were coated on clean glass slides using a spin coater (WS-400B-NPP) spin-processor (Laurell Technologies Corp) at 1500 rpm for 20 s under nitrogen environment, and the films were dried in the oven at 105 °C overnight. Then, a drop of deionized (DI) water (5 µL) was placed on the coated glass slides, and the contact angle of SEKL/N-SEKL at the water-air interface (WCA) was determined following static contact angle (i.e., two phase contact angle) measurement with the sessile drop method at 25 °C for 10 s,[9] then the slides were transferred to a glass chamber filled with purified xylene and the contact angle (i.e., three phase contact angle) of SEKL/N-SEKL at the oil-water interface was measured accordingly.[39]

5.3.11 QCM-D measurements

The self-assembly of SEKL/N-SEKL at water-xylene interface was studied using a QCM-D and SiO_2-coated Q-Sense sensor (QSX 303), Sweden. We chose SiO_2 substrate for coating xylene due to the reported effective interaction between these two materials.[40]

To eliminate the presence of impurities on the surface, the SiO_2-coated sensor was first cleaned thoroughly by immersing it in SDS, sodium dodecyl sulfate solution (0.4 wt.%) for 2 h, and then it was extensively rinsed with MilliQ water. It was then dried with N_2 gas and treated with UV/ozone oxidation cleaner (PSD Series, digital UV ozone system, NOVASCAN) for 15 min. Afterward, it was rinsed again with MilliQ water and dried with N_2 before coating with xylene [41].

We followed a previously established procedure for coating silicon oil on Si substrate in this study on SiO_2-coated Q-Sense sensor with further modifications.[42] Xylene (5 µL) was spin-coated on the sensor at 3000 rpm for 30 s under N_2 environment with the acceleration rate of 200 m/s^2, followed by drying the sensor in the oven at 110 °C for 1 h. The coating procedure was repeated for 10 consecutive times while drying the sensor in the oven between each coating cycle.

The QCM-D adsorption experiments were started by rinsing the sensors with buffer solutions that were prepared by adjusting the pH of MilliQ water at 3, 7 or 11±0.2 by adding few drops of 0.8 N HCl or 0.8 N KOH (previously prepared solutions in MilliQ water), until the baseline was stabilised. Then, the adsorption experiment was initiated by replacing the buffer solutions with SEKL or N-SEKL solutions (500 mg/L) with the same pH as buffer. The temperature of 22 °C and a pump rate of 0.15 mL/min were maintained throughout all QCM-D experiments. The curves of resonance frequency (Δf) and dissipation factor (ΔD) were recorded accordingly over 20 minutes and the results at 7^{th} overtone were collected.

Another set of adsorption experiments at pH 3 was followed as explained above, however this time after adsorption completion, the N-SEKL sample was replaced by the buffer solution at the same pH and pumped into the chamber to observe the reversibility of the adsorbed layer which continued for an additional 10 mins.

5.3.12 SEM analysis

Scanning electron microscope (SEM) Hitachi field emission SU-70 was implemented to observe the SiO_2-QCM gold sensor before and after the formation of xylene film. The elemental composition of the substrates on the sensors before and after xylene coating was measured with energy dispersive X-ray (EDX) Oxford AZtec with the adjusted voltage of 10 kV at a ×200 magnification. In the second experiment, the coated sensors were air-dried after adsorption of SEKL or N-SEKL on a xylene-coated gold sensor, and the morphology of the adlayer was investigated by SEM with the voltage of 10 kV at a ×250 magnification.

5.3.13 pH-responsive behavior of emulsions

Stock solutions of SEKL (3 mL) at 0.25 wt.% concentration and pH 7 were fed to glass vials with 3 mL of xylene (oil/water ratio 1:1), and the emulsions were formed by ultrasonication at 240 W power and 30 s for 3 s intervals. The pH of the formulated emulsion at pH 7 was once changed to 3 by adding few droplets of 0.8 N of HCl and the emulsion was re-emulsified by ultrasonication for 10 s. In another set of experiments, the pH of the formulated emulsion was altered to 11 by

adding few droplets of 0.8N KOH and the mixing was conducted with a vortex mixer (VWR) at 2500 rpm for 10 s. The stability of emulsions was then visualized immediately after applying pH changes by a digital camera and monitored by a vertical scan analyzer (Turbiscan Lab Expert, Formulation, France) at room temperature for 24 h to obtain the stability index (TSI) of the emulsions at the bottom and top parts of the emulsion systems, where both coalescence and settling phenomena were considered in the TSI evaluation. The details for the operation of the vertical scan analyzer were previously explained,[31] and briefly, the TSI is determined following equation 1,

$$\mathrm{TSI} = \sqrt{\frac{\sum_{i=1}^{n}(x_i - x_{BS})^2}{n-1}} \qquad (1)$$

where n refers to the number of scans, x_i is the average of the backscattered light intensity at each scanning time, and x_{BS} is the average of x_i. Generally, the higher the TSI, the lower the stability.[43] The pH alteration was kept applying for another 5 cycles switching from pH 7 to 11 and vice versa and the TSI observations over 24 h were monitored by a vertical scan analyzer. The same trials were conducted by shifting pH of emulsions at pH 3 to 7 and 11 and vice versa.

5.3.14 Statistical Analysis

All experiments in this study were performed at least three times, and the data was expressed as mean ± standard deviation (SD).

5.4 Results and Discussion

5.4.1 SEKL production and dissolution

Water-soluble sulfoethylated kraft lignin (SEKL) polymer was produced through a substitution reaction for replacing phenolic hydroxyl groups of lignin with 2-bromoethansulfonate (Figure A2.1). The ^{1}H and ^{2}H-H-NMR spectra of the products and raw material confirmed the grafting of ethyl group on lignin structure (Figure A2.2) following the S_N2 reaction mechanism.[44] The GPC revealed the M_w and M_w/M_n (PDI) of 10±1 kg/mol and 1.80 for SEKL compared to 6.5±0.5 and 2.1 kg/mol for KL, and titration experiments showed the sulfonate group content of 1.2 and 0 meq/g for SEKL, and KL, respectively (Table A2.1). SEKL was highly stable at neutral pH without showing any sign of precipitation over three months (Figure A2.3). The system was also stable by alkalizing the solution to pH 11. However, acidifying the system to pH 3 disturbed its stabilization and resulted in aggregation and formation of nano-SEKL (N-SEKL) as shown in Figure 1a.

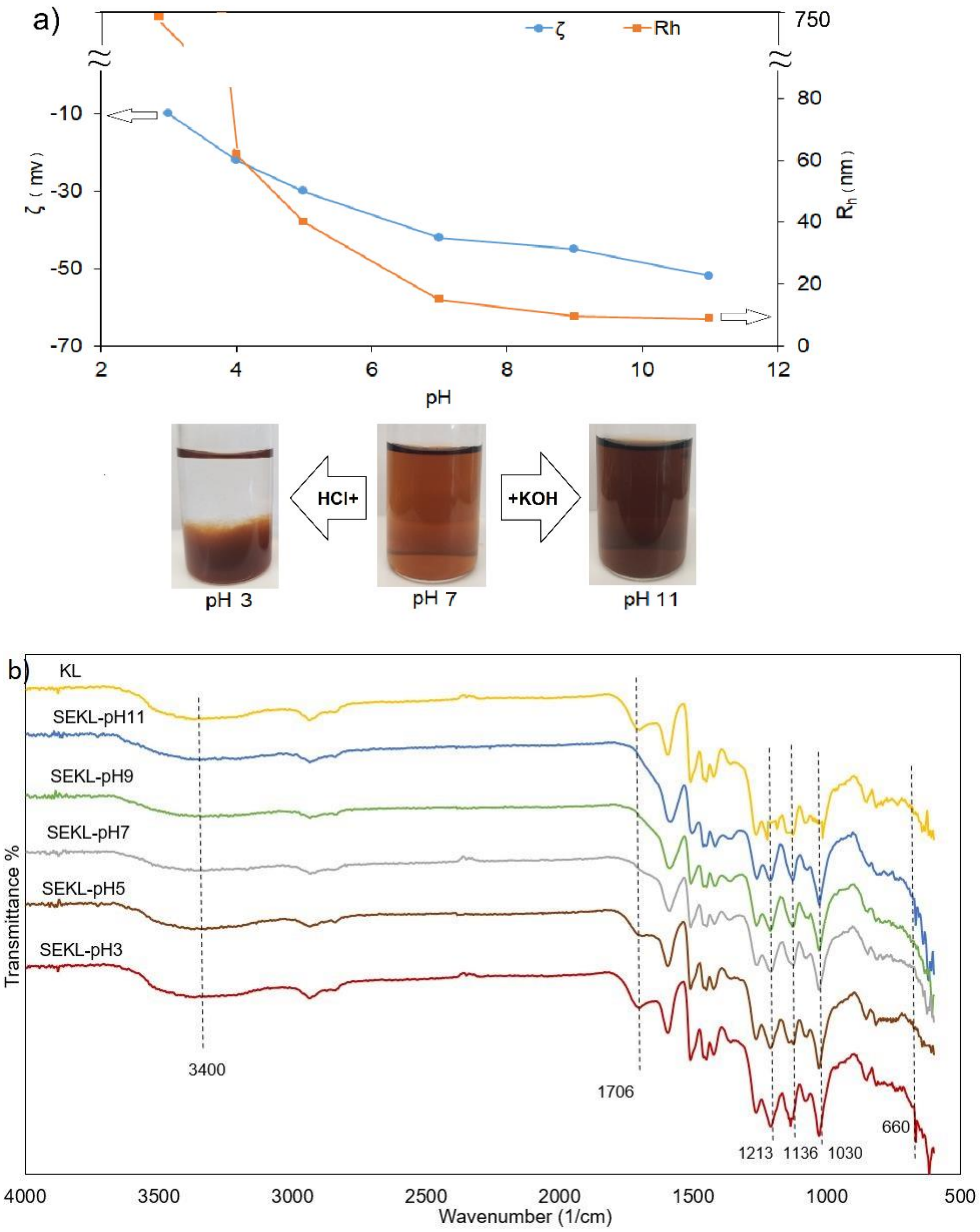

Figure 5.1: a) Zeta potential (ζ) and hydrodynamic size (R_h) of SEKL solution and b) FT-IR spectra of SEKL as a function of pH.

Quantitative measurements in Figure 1a show a continuous increase in ζ from -50 mV at pH 11 to -10 mV at pH 3 and the elevation in R_h from 9 to 750 nm, consequently. The higher stability at neutral and alkaline conditions is due to the sufficient electrostatic repulsion among the polymer segments originating from the charged sulfonate and carboxylate functional groups that were determined through FT-IR (Figure 1b) and titration analysis (Figure A2.4). Figure 1b presents the

FTIR spectra of KL and SEKL at different pH. The wide absorbances at 3400 1/cm in the FTIR spectra of KL and SEKL are the stretches of phenolic and aliphatic hydroxyl groups,[45] which is less strong at pH 11 and 9; suggesting the protonation of these functional groups on SEKL at lower pH. A sharp carboxyl group peak is presented for KL at 1706 1/cm. [46] This stretching vibration is strong under acidic pH for SEKL and is absent at higher pH, indicating its dissociation at pH >7. Compared to KL, SEKL has strong absorbance of S-O and S=O stretches at 1030, 1136 and 1213 1/cm,[45,47] which indicates the presence of sulfonate groups on SEKL. These peaks are present at all pH ranges, however, they moved toward a higher wavenumber by acidification due to the protonated acid groups. In addition, a new absorbance band at 660 1/cm is presented at pH 3, which is associated with the stretching vibration of S-OH band.[47]

The lignin polymer started to agglomerate at pH lower than 7. By acidifying the system, the functional groups were protonated at their pKa, which would result in the elimination of electrostatic repulsion. The first noticeable increment in R_h (40 nm in Figure 1) was observed at pH 5 and continued without precipitation till pH 4 for solution with the R_h of 60 nm. This first step of nano-aggregation of SEKL is associated with the protonation of carboxylate groups of lignin with pKa of 5±0.1 (Figure A2.4). The carboxylate group content of SEKL, which was originated from lignin, was quantified to be 0.25±01 mmol/g following the titration method (Figure A2.4), and 0.15±05 mmol/g following the P-NMR technique (P NMR analysis is described, and results are provided in Figure A2.5).

The amount of sulfonate group and its pKa were determined to be 1.2±01 mmol/g and at pH=2.8±0.1 (Figure A2.4), which promoted the nanoprecipitation of SEKL to produce sulfonated lignin nanoparticles (N-SEKL) by further acidification of solution to pH 3±0.2 (Figure 1). Indeed, the nanoprecipitation process occurred owing to 1) the lower solubility of SEKL at pH 3 as a result of the protonation of functional groups, that also weakened the electrostatic repulsion between the segments (ζ = -10 mv), and 2) superior attractive interaction between SEKL segments originating from the hydrogen-bonding, π-π interaction and hydrophobic forces[48,49] between alkyl chains and aromatic groups of SEKL at low pH.

Amorphous sulfonated Lignin nanoparticle (N-SEKL) was visualized with TEM, and its structure was shown in Figure 2 with a diameter of 533± 25 nm. Interestingly, a large cluster is formed of smaller nanoparticles in the range of 40-50 nm (Figure 2), which may also provide evidence for the aggregation of N-SEKL. The R_h of N-SEKL was 750± 50 nm at pH 3, which is fairly

comparable with the TEM image. However, the results are not completely comparable technically, mainly because R_h determines the hydrodynamic size of N-SEKL in solution, while TEM shows the size of particles in a dried state. The drying of polymeric precipitates is expected to affect the size and shape of the particles.[34]

It should be noted that nanoparticles were not observed for dried samples at pH 7 and 11 via implementing TEM visualization, and a uniform film of SEKL was formed in the dried state (Figure A2.6).

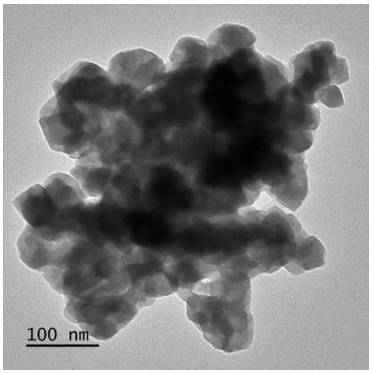

Figure 5.2: TEM image of a N-SEKL at pH 3 in a dried state (×100 nm).

5.4.2 Emulsions formulation

In this study, emulsions with varied stabilities and droplet sizes were formulated using SEKL/N-SEKL depending on the pH at the dosage of 0.25 wt.%. The dynamic changes in confocal images of formulated emulsions (from high to low pH by adding HCl) with their size distributions and long-time stability under centrifugal forces (shown as accelerated instability index) are depicted in Figure 3a-3d. Oil phase (xylene) was stained with Nile red, and is visualized by green color in the images.

The confocal images in Figure 3a and droplet size distribution graphs in Figure 3b for emulsions at pH 11 indicated the presence of a large and uneven droplet size at this pH. Most of the formed droplets are larger than 20 μm at pH 11. The dynamics of such emulsion was visualized by watching the motion of the droplets (Video V1), which exhibited a fast mobility of droplets at pH 11. Therefore, due to the higher collision of oil droplets, the likelihood of droplets' coalescence would increase by the accumulation of small droplets on the surface of large droplets, and thus the phase separation is highly probable. As a result, the instability index of 1 was obtained for emulsion at pH 11 (Figure 3c), implying a complete separation of oil and water phase after centrifuging (Figure 3d) that confirmed the poor emulsifying affinity of SEKL at pH 11. By adding HCl to the

system, formulated emulsion at pH 7 had smaller droplet sizes of 11 µm, and more even size distributions (Figure 3a and 3b) compared with that at pH 11. The motion of droplets has slightly decreased; however, still the obvious movements of droplets was recorded (Video V2). Hence, due to a more even droplet size distribution, less accumulation of oil droplets occurred and as a result, comparatively more stable emulsions are created at pH 7 compared with that at pH 11 (Instability Index of 0.6 in Figure 3c). Further decreasing the pH of the emulsion system to 3, confocal images showed different microscopic properties with considerable declines in the droplet size (to 4-5 µm) and motionless droplets under the microscope (Video V3). The stationary status of emulsions at pH 3 should be related to the formation of solid-like particles of N-SEKL at the oil interface. As a result of uniform and small droplet size and lack of collisions between them, ultra-stable emulsions were found at pH 3 (Instability Index of 0.1 in Figure 3c), with the minimum phase separation (Figure 3d).

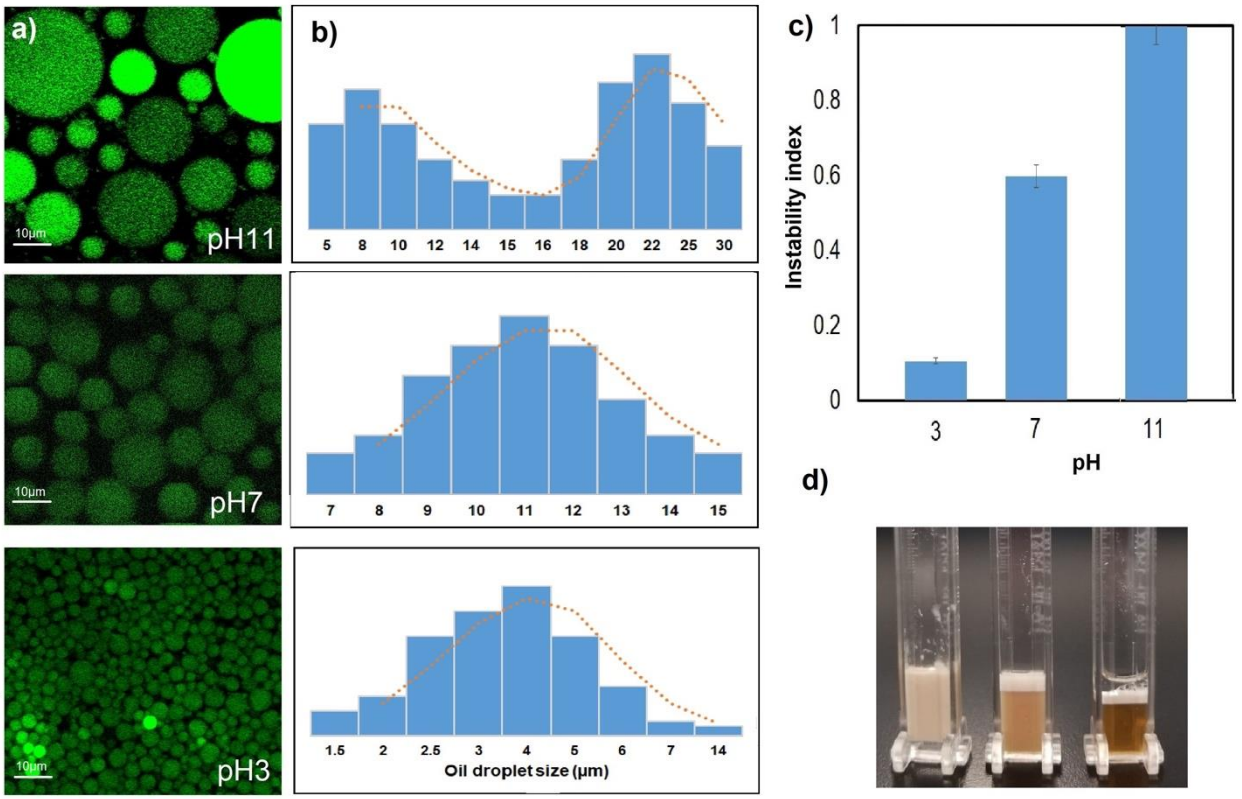

Figure 5.3: Dynamic changes in a) confocal images, b) droplet size of emulsions from high to low pH by adding HCl to pH11 emulsion after preparation and d) corresponding cell images after centrifuging. The scale bar is 10 µm in confocal images.

5.4.3 Rheological Characteristics

The rheological properties of formulated emulsions at different pHs were monitored by measuring their viscosity as a function of shear rates (Figure 4a). Evidently, there is a distinguishable viscosity difference among the emulsions at altered pH. The emulsion at pH 11 is more of a Newtonian fluid. However, emulsions at pH 7 and 3 are shear-thinning (i.e., a significant decrease in viscosity with increasing the shear rate).[50] Also, at the beginning of the measurements at a shear rate of 0.1 1/s, the viscosity of emulsions was 0.092, 0.24 and 24 Pa.s, at pH 11, 7 and 3, respectively (Figure 4a). Water and xylene are both Newtonian fluids with viscosities of approximately 0.001 and 0.0006-0.0008 Pa.s, respectively.[51] This implies that SEKL insignificantly impacted the fluid properties at pH 11 compared to other pHs.[31] The results may suggest that the adsorption of SEKL at the oil interface should be minimal, hence the oil droplets were relatively free (fewer inter-drop interactions) in the continuous phase (i.e., water).[30] As shown, we observed more viscosity increment at pH 7 and more markedly at pH 3. It has been previously reported that the changes in emulsion viscosity is generally affected by the interactions between the molecules/particles in the continuous phase and at the surfaces of the oil droplets.[52] For instance, Li et al.[30] suggested that the ion-dipole attraction between carboxymethylated lignin (CML) molecules and kerosene oil droplets elevated the fluid viscosity.[53] The same reason should be applicable for the elevated viscosity of water-xylene emulsion in the presence of SEKL at pH 7, however, the remarkable increase in the viscosity of the emulsion at pH 3 (24 vs 0.24 Pa.s) suggests a much stronger interaction (e.g., favourable hydrophobic interaction and π-π stacking)[54] between N-SEKL and xylene. In addition, a Pickering emulsion (formed from particles) generally has a high viscosity owing to the adsorption of solid particles at the oil interface that restrain the motion of oil droplets.[55] Based on Stokes' equation,[56] it is well-known that creaming is accelerated by a large droplet size and low viscosity of the continuous phase.[57] The enhanced viscosity at pH 3 slowed the droplet migration rate (V1 in appendix material) and the number of collisions between oil droplets (Figure 3). Therefore, lower viscosity along with smaller droplet size improved emulsion stability at pH 3. Accordingly, we observed less stability at pH 7 and unstable emulsion at pH 11 (Figure 3c).

Oscillatory measurements are helpful in demonstrating the viscoelastic properties of emulsions. The magnitudes of storage and loss modulus reflect two behaviors; namely, viscous or liquid-like behavior ($G' < G''$) or elastic or gel-like behavior ($G' > G''$).[58,59] Figure 4b shows the storage and loss modules as functions of angular frequency for emulsions at different pHs at fixed strain (1%)

and 0.25 wt.% SEKL/N-SEKL concentration. The results indicated that G′ was greater than G″ for all range of angular frequencies for emulsions stabilized at pH 3 in the presence of N-SEKL and a crossover was observed at the starting angular frequency point (0.1 rad/s); representing a gel-like behaviour. However, no crossover point was observed at pH 7 and pH 11 in the presence of SEKL, indicating a liquid-like behavior. The results indicated that stabilized emulsions with N-SEKL at pH 3 have a strong three-dimensional network structure, and the interfacial films formed at the oil-water interface are more elastic than the one stabilized at higher pHs.[50] However, the emulsion stabilized at pH 7 and 11 were not strong to form a network by increasing the angular frequency.[60,61]

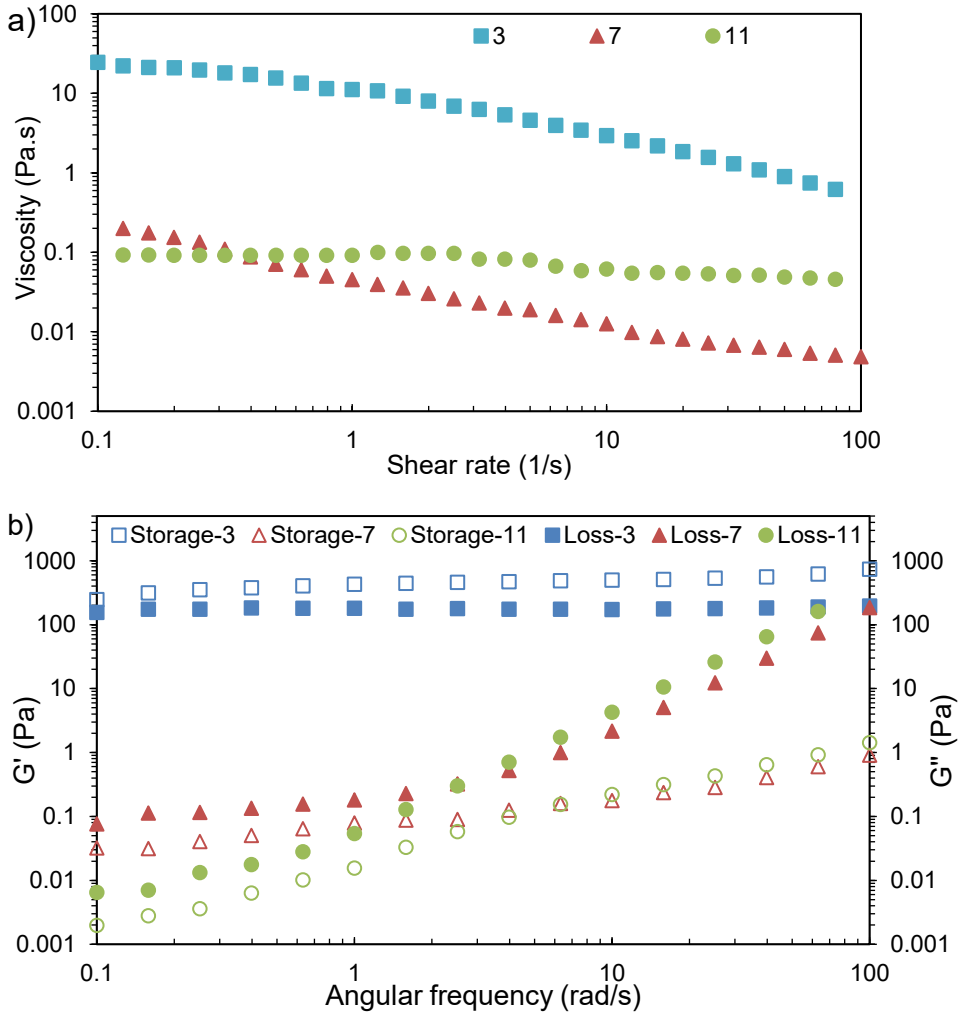

Figure 5.4: Rheological characteristics of emulsions at different pH values: (a) viscosity versus shear rate and (b) storage modulus G′ and loss modulus G″ versus angular frequency (G′ and G″ are represented as open and solid markers, respectively).

5.4.4 Wettability and adsorption energy

To predict the pH-dependence of adsorption of SEKL/N-SEKL at xylene interface, two- (WCA) and three-phase (OCA) contact angles of a solid surface (SEKL/N-SEKL) at an air-water and oil-water interface were determined, respectively.[62]

WCA would define the wettability of the SEKL surface in different pHs. The adsorption of SEKL/N-SEKL at the interface is possible only if the equilibrium of a three-phase contact angle θ exists.[63] The strong trapping of colloidal particles at fluid interfaces is a result of the significant decrease in surface free energy of the fluid upon adsorption of particles. The reduction in the detachment energy (ΔE) through the adsorption of a particle at the interface is known to associate with its radius (r or ½ R_h in our case) and 3-phase contact angle (θ) with following equation: [64,65]

$$|\Delta E| = \gamma_0 \pi r^2 (1 - \cos\theta)^2 \qquad (2)$$

where γ_0 denotes the interfacial tension of the pristine water-xylene interface (0.04 N/m)[66] and θ is the equilibrium contact angle of the oil-water interface in the presence of SEKL/N-SEKL.

Measuring the θ can help to predict the emulsion stability,[12] because the energy of adsorption at the interface based on eq 2 would be relatively small <10 k_BT if the particle is too hydrophilic (θ≤20˚) or too hydrophobic (θ ≥160).[67] The WCA and OCA images of SEKL/N-SEKL surface at pH 3, 7 and 11 are depicted in Figure 5. It is clear that the surface of coated SEKL is vastly wetted by water droplets when all the functional groups are deprotonated at pH 11 (WCA<10˚ and OCA=8˚). This confirms that SEKL is super hydrophilic at pH 11 with minimal compatibility toward the oil interface. The protonation of SEKL to pH 7 resulted in less wettability (WCA~20˚ and OCA~25˚), showing slightly better interaction of SEKL with the oil interface. The SEKL at pH 3 (i.e., N-SEKL) showed the highest compatibility with the oil interface with the WCA of 40˚ and OCA of 50˚. The elevated WCA/OCA at pH 3 would be associated with the reduction of electrostatic repulsion, which led to the dominance of hydrophobic features of lignin macromolecules.[48,68]

Adsorption free energy of the emulsion system, |ΔE|, was calculated following eq 1 via considering the results of ½ R_h (from Figure 1) and OCA (from Figure 5) to be 0.1, 14 and $6.0\times10^{+5}$ (k_BT) at pH 11, 7 and 3, respectively. Calculated |ΔE| at pH 11 is close to zero, which implies a considerable

hindrance toward the adsorption of SEKL at the xylene interface, yielding the complete separation of two phases and unstable emulsion at pH 11 (Figure 3). In addition, the |ΔE| at pH 7 is comparable with that of the adsorption of most surfactant molecules, however, they are easily detached and may not be effective over time.[4] On the other hand, one consequence of the very high adsorption energy at interfaces is the irreversibility of the adsorption.[4] The considerable enhancement of |ΔE| at pH 3 is associated with the enlarged particle size (Figure 1) and elevated OCA˚ (Figure 5). The magnitude of |ΔE| ($6.0\times10^{+5}$) at pH 3 proposes the formation of Pickering emulsion with an outstanding stability, which is comparable to the energy associated with the adsorption of solid nanoparticles at the oil interface. [69,70]

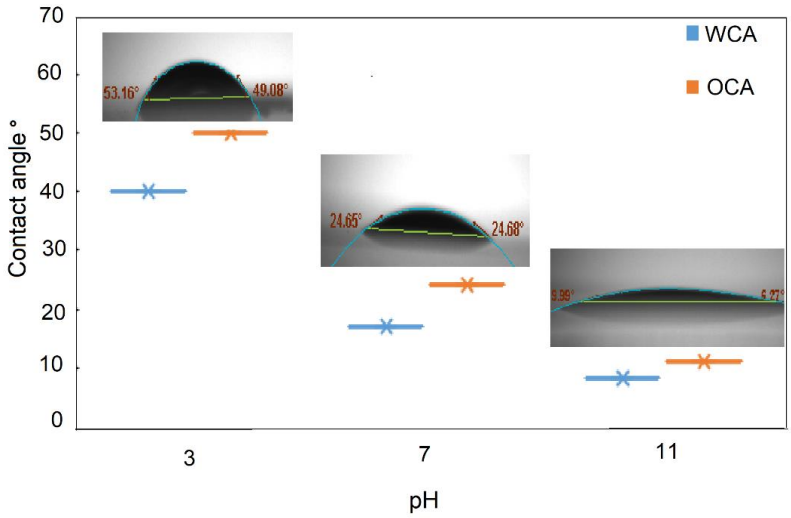

Figure 5.5: Contact angle of SEKL/N-SEKL surface at various pH for water-air (WCA) and oil-water (OCA) interface.

5.4.5 Adsorption analysis at the oil surface

Xylene-coated SiO_2 sensors were used in the adsorption experiment of SEKL/N-SEKL and the SEM/EDX images of SiO_2-sensors before and after xylene coating and the water contact angle of the surfaces are depicted in Figure A2.7. The assembly of SEKL/N-SEKL at oil-coated surface is summarized in Figure 6 at different pH, which represents the SEKL/N-SEKL adsorption affinity (Δf) and the viscoelasticity (ΔD) of the adlayer at xylene coated surface, respectively (Δf and ΔD plots vs time are presented in Figure A2.8a-b). It is observed that the adsorption of SEKL at the surface of xylene was only achievable at pH 3, when SEKL was in the form of N-SEKL, as seen as a considerable decrease in f (-7 Hz). The changes in D were limited to 0.3×10^{-6}, which illustrates the formation of a rigid N-SEKL adlayer at the oil surface. The surface morphology of the adlayer

on the xylene coated sensor is visualized by SEM (Figure 7), which illustrates the rough surface of the sensor, indirectly illustrating the assembly of solid particles on the xylene coated sensor. To find out whether the higher increment of frequency (f) at pH 3 was because of the adsorption or deposition of N-SEKL particles, the adsorption step (after 20 min) in QCM studies was followed by a buffer solution that had the same pH in a new adsorption experiment, and the results are presented in Figure A2.8c. It is seen that by washing the adlayer at pH 3 (after 20 min), desorption did not occur, and Δf remained constant. This was unsurprising since the adsorption of N-SEKL was anticipated to be irreversible due to the high adsorption energy ($6.0\times10^{+5}$ k_BT). Therefore, this test confirms that all the increment of f is indeed due to the adsorption at the oil surface rather than particles deposition, in which case the particles would have been washed off.

Interestingly, the adsorption experiment with SEKL solution at pH 7 resulted in an increment, rather than a decline in the f (Figure 6), which shows the desorption of SEKL from the surface, instead of adsorbing onto the surface.[71,72] This can happen when a hydrophobic segment of SEKL interacts with xylene. However, the higher hydrophilicity of SEKL (Figure 5) at this pH keeps it in the water phase and desorption of oil happens via the aqueous flow in the chamber. Indeed, SEKL functions as a detergent/surfactant in removing the oil droplets from the substrate. The fact that this removal happened at neutral pH would introduce SEKL as a potential biomaterial for the formulation of novel safe detergents. Furthermore, it was observed that there was no change in D (0, Figure 6) at pH 7, which suggests that SEKL did not change the viscoelasticity of the surface.[73] The SEM images of the surface after experiment may confirm the reduction in oil content of the coated sensor, which was confirmed by the reduction in the carbon content of coated xylene surface after desorption by X-ray (EDX) results (Figure A2.9).

A limited decline in f (-1.65 Hz) was observed at pH 11, which was coupled with an increase in D (0.64×10^{-6}, Figure 6). These changes can be attributed to the hydrophilic affinity of SEKL at pH 11 that penetrated through the oil film and attached to the hydrophilic SiO_2 surface. This indeed resulted in an increase in D that made a less rigid adlayer on top of the surface compared with the results at pH 3 ($0.64\times10^{-6} > 0.3\times10^{-6}$). A similar statement was reported while experimenting the slippery performance of lubricant coated surfaces (oil) on Si substrate, where the water molecules would come more into contact with the Si-substrate when there was no covalent bond formed between oil and Si surface.[42] Since the interaction of SEKL and the surface at pH 11 is in

nanometer range size (≤10 nm, Figure 1), there is no observable accumulation in the SEM analysis (Figure 7).

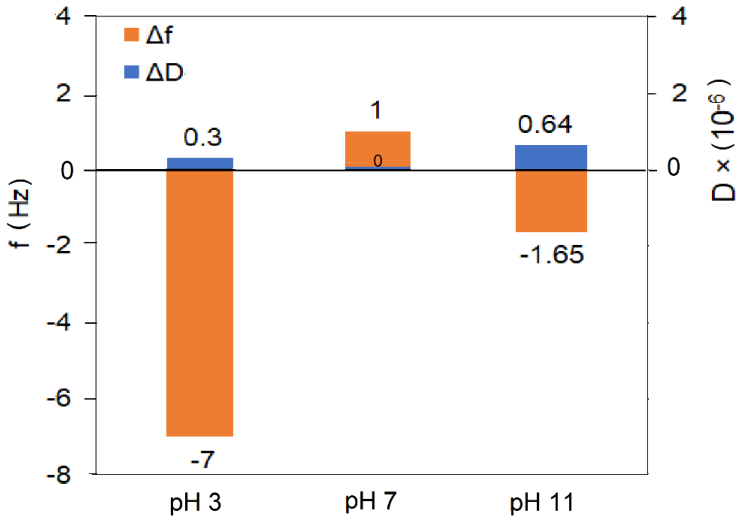

Figure 5.6: Equilibrium frequency and dissipation at 7th overtone after 20 min for the adsorption of SEKL/N-SEKL on xylene-coated SiO_2 sensor at pH 3, 7 and 11.

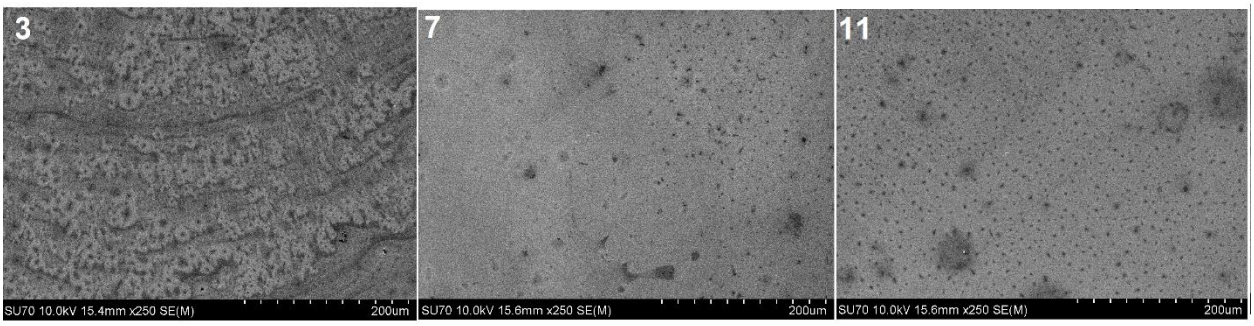

Figure 5.7**:** SEM images of adlayer from QCM-D experiment on xylene coated SiO_2 sensor at pH3, pH7 and pH11.

5.4.6 pH-responsive performance

To investigate whether the reversibility of emulsion is feasible with respect to pH, the pH responsive cycling experiments were conducted. Figure 8a and 8b shows the transformation of emulsions stability by changing pH from 7 to acidic or basic and vice versa. The 24-h stability of these samples was examined with a stability analyzer and visualized by a digital camera. In Figure 8, the instability of emulsions starting from pH 7 immediately after preparation depicted that the phase separation occurred at the same speed and level in the top and bottom zones of the emulsion,

and approximately the TSI of 20 was obtained in both zones after 24 h. It is evident that sedimentation and creaming happened in the bottom and top of the emulsion layer at pH 7 after 6h. Sedimentation corresponds to the excess of SEKL that sediment and form gel in the clarified phase over time, while creaming is known to be driven by the lower density of stabilized droplets.[74] Overall 50 % of the emulsion is remained stable after 24 h at pH 7 formulation as is squared by the red line in Figure 7b.

By adding a few drops of KOH to the emulsion at pH 7, an obvious sign of phase separation was immediately observed (Figure 8a and 8b). The phase separation was very fast (occurred in the first 30 minutes) and TSI reached 20 in both zones and increased over time to almost 40 and 50 for the top and bottom zones, respectively. Finally, a large clarified layer of aqueous SEKL solution on the bottom and coalescence oil on the top were visualized (Figure 8b). Only a small portion of 5% emulsion remained after 24-h observation at pH 11 formulation (squared red line).

By adding a few drops of HCl to emulsions of pH 7, phase separation was hindered, and stabilized emulsion was preserved with a minimum sign of phase separation over 24 h (only 15%). The destabilization only occurred in the bottom zone to TSI level of 10 with the formation of a thin clarified layer with no sign of sedimentation (no lignin color), which shows that SEKL segments participated in the emulsion formation in the form of N-SEKL, which had higher affinity toward oil phase rather than the aqueous phase. The emulsion remained macroscopically homogeneous with well distributed droplets that caused uniform backscattered light over the 24-h observation.

Alkalizing the emulsions of pH 3 to pH 7 and 11 did not initiate phase separation, and a stable and unseparated emulsion of pH 3 was preserved (the same TSI and visualization as shown in Figure 8a and 8b at pH 3 was observed). Hence, it is inferred that emulsion of pH 3 is irreversible as shown by red arrows in Figure 8b. This irreversibility should be due to their extreme gel-like properties (Figure 4b) and high desorption energy ($6.0\times10^{+5}$ K_BT) of N-SEKL at the oil interface. However, according to the work of Wei et al.,[18] Pickering emulsions stabilized by unmodified lignin particles are pH-responsive due to the dissolution of lignin particles in the alkaline system, and thus demulsification could occur. In this case, the nature of sulfonated lignin and acidified lignin particles would impact their behavior. Acidified lignin particles are agglomerated due to the strong π-π stacking and H-bonding developed among lignin segments. However, in addition to the mentioned interactions, the protonated sulfonic acid groups form additional intra- and intermolecular bonding via dipole-dipole and elevated H-bonding interactions. Moreover, there

are still partial sulfonate groups that are dissociated at pH3 (zeta=-10mv). Therefore, a network of ionic interactions would also form between positively protonated functional groups and anionic sulfonate groups that enhanced the compactness of the formed N-SEKL particles, which overall makes the interactions among N-SEKL stronger.[28] In addition, the size of unmodified lignin particles is generally smaller (around 200 nm)[18,27] than the size of N-SEKL (750 nm) in this study. Therefore, the functional groups are less accessible for deprotonation in the large particles of N-SEKL. The N-SEKL particles are also expected to form stronger intra interactions by strong ion-dipole associations between sulfonate groups on the adjacent oil droplets,[30] which is absent between lignin particles and oil droplets. The formulated Pickering emulsion by unmodified lignin particles are markedly larger (20-60 µm)[18] which yield lower inter-drop interactions[30] and make their adsorption reversible. Rather than chemical interactions, experimental conditions such as oil type, emulsifiers dosage and oil:water volume ratio that were respectively higher and smaller in previous studies for lignin particles[18] compared to this study would be influential factors in the pH-responsive behavior.

Further, the pH-responsive cycling was followed for 5 cycles between emulsification-demulsification between pH 7 and 11 as shown with green arrows in Figure 8b and the TSI alteration is presented in Figure A2.10 in appendix material.

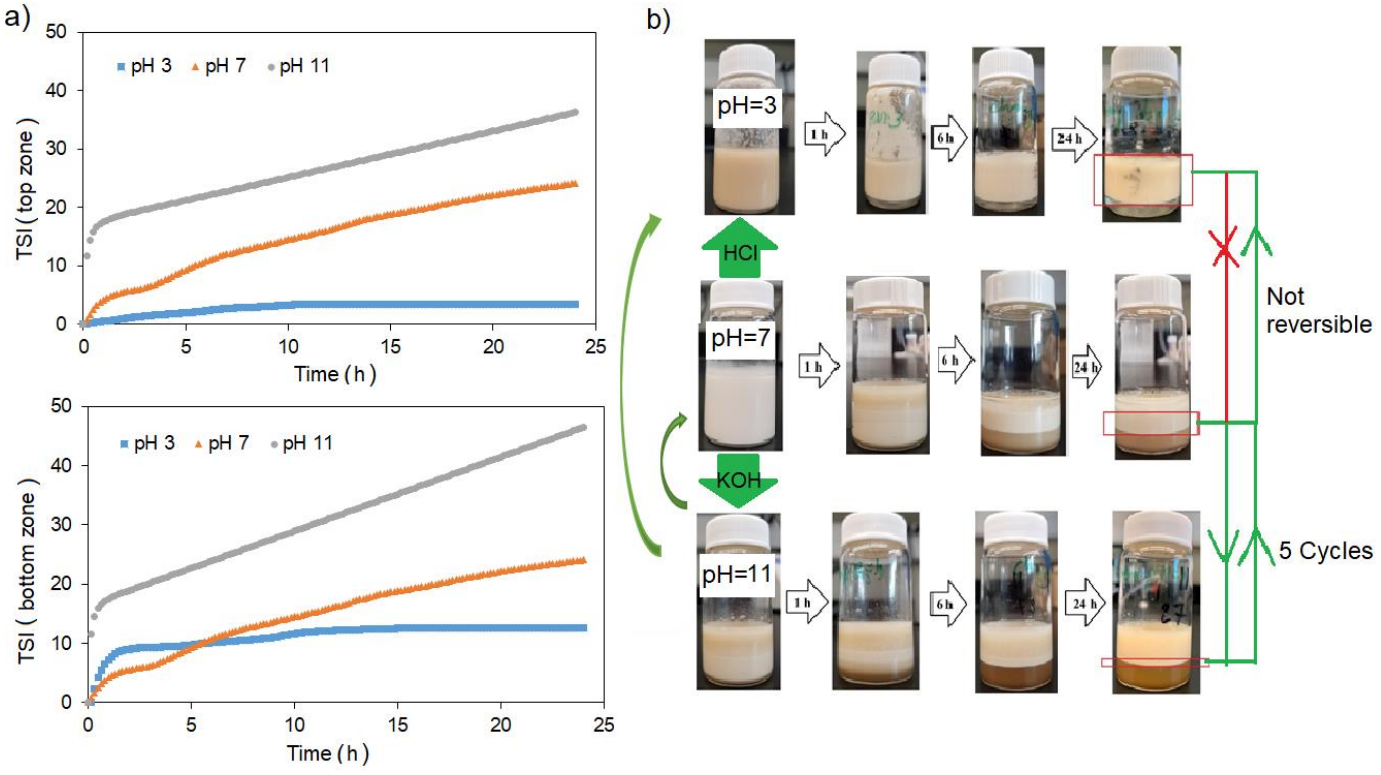

Figure 5.8: The 24-h emulsion observation upon pH alteration as a) TSI and b) visual observation.

5.4.7 Emulsification stability mechanism

The possible pH-dependent mechanism of Pickering/non-Pickering emulsions and de-emulsified oil-SEKL solution is presented in Figure 9. A typical property of Pickering emulsion is the large adsorption energy ($|\Delta E|$)[4] that was only obtained for emulsions formed at pH 3 ($6.0\times10^{+5}$ K_BT). Formation of N-SEKL at pH 3 (Figure 2) produced a strongly stable gel-like Pickering-emulsion with high viscosity (Figure 4), which assembled a rigid N-SEKL adlayer at the oil surface (Figure 6 and Figure 7). These properties suggested significant self-assembly of N-SEKL at the oil interface that bridges oil droplets together (Figure 9).[75] In this case, the hydrophobic interactions among N-SEKL and oil droplets made a network of interactions (e.g., van der Waals and π-π stacking). Indeed, due to the steric hindrance originating from the dense layer of N-SEKL at the oil interface, the aggregation of oil droplets was prevented, thus stabilized Pickering emulsions were formed.

The $|\Delta E|$ of SEKL at oil interface at pH 7 was fairly low (14 K_BT), which represents the adsorption of polymeric surfactants and formulation of conventional emulsions.[65] With using a water-soluble polymer (SEKL), the emulsion was not stable over time due to the liquid-like behaviour with lower viscosity (Figure 4) and higher mobility (V2) of the emulsions at pH 7. Although SEKL was able to interact with oil molecules (deposition occurred based on the results in Figure 6), the charge and solubility of SEKL hindered its effective self-assembly at the oil interface (Figure 9) due to electrostatic repulsion between SEKL-SEKL and SEKL-oil and higher affinity of SEKL toward water (WCA=15˚, Figure 5). Therefore, the oil droplets would tend to coalesce due to the lack of physical hindrance, the creaming of the oil droplets was promoted over time (Figure 8) and emulsion with short-term stability was formed.

At pH 11, fully charged SEKL molecules are too hydrophilic to wet the oil droplets (ζ=-50mv, Figure 1), hence the adsorption of SEKL at the interface was prevented thermodynamically ($|\Delta E| \cong 0$) and kinetically (Figure 6). Highly charged SEKL did not influence rheological properties of oil (i.e., low viscosity and liquid-like fluid, Figure 4), hence oil droplets would tend to coalescence very fast (blue arrows in Figure 9) and in a short period of time (Figure 8).[76] Consequently, emulsion formulation is prevented at this pH (Figure 8).

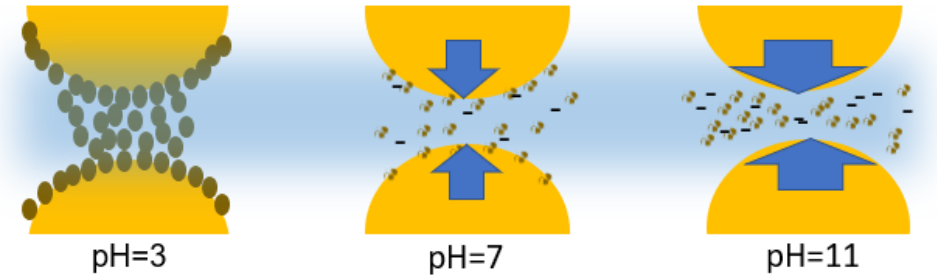

Figure 5.9: Schematic mechanism of emulsions stability at the xylene interface at different pHs in the form of Pickering at pH 3 or non-Pickering emulsion at pH 7 and demulsification at pH 11. The yellow half circle shows oil droplets, and the blue arrow shows the tendency for coalescence.

5.5 Application and future studies

It is feasible to use SEKL for the formulation of Pickering or non-Pickering emulsions depending on the targeted application in the form of nanoparticle or polymeric surfactant. While SEKL polymer is water-soluble at pH 7, non-Pickering emulsion can be formulated, which is completely stable in the first 5 h of formulation and then creaming and sedimentation happens slowly over time (Figure 8). The liquid-like properties of emulsion formulated by SEKL makes it suitable for application, such as emulsion polymerization, which requires fast mixing and short-term stability.[9] Accordingly, a complete demulsification can be followed by alkalizing the system.

Gel-form Pickering-emulsion can be formulated by either acidifying the emulsion of pH 7 or by adding N-SEKL directly to the system at pH 3. Therefore, N-SEKL can be utilized for the emulsion formulation with a long-term stability requirement. The adaptable feature of emulsion stabilization with pH is an interesting phenomenon for industrial applications, because it shows a flexible routine to transform the microstructure and rheological properties of a formulation.[74] For example, in food and cosmetics applications, a flexible and liquid like emulsion at pH 7 can be prepared during the production steps, which can later be adapted to a gel structure for the final desired product through a simple pH change. Interestingly, this final gel product can tolerate the subsequent pH alteration (in the case of acidic pH) or be reversed to liquid-like solution (in the case of alkaline pH). Another proposed application for SEKL is its use in detergent formulation. However, this needs further research and experimentation.

5.6 Conclusions

This work demonstrates the ability to carefully tailor emulsion properties with a green lignin-based emulsifier. A 100% green process without using solvent or hazardous chemicals was implemented

to synthesize sulfoethylated lignin polymer (SEKL) and a simple pH alteration to produce sulfonated lignin nanoparticles (N-SEKL). Non-Pickering (SEKL) and Pickering emulsions (N-SEKL) were formulated at pH 7 and pH 3 via mixing the respective lignin derivatives with xylene and water mixtures at the low dosage of 0.25 wt.%. While the emulsion containing SEKL showed liquid-like properties with low viscosity at pH 7, the presence of N-SEKL introduced solidity and gel-like properties with high viscosity to the Pickering emulsion. The adsorption analysis revealed the effective assembly of N-SEKL at pH 3 on the oil surface with a rigid adlayer on the oil surface. The bridging between oil droplets through a network of assembled particles with a high adsorption energy ($|\Delta E|=6.0 \times 10^5$ K_BT) yielded irreversible adsorption of N-SEKL at the oil interface, which was associated with an ultra-stable emulsion overtime at pH 3. At a higher pH, SEKL only partially interacted with the oil surface without effective assembly due to its higher surface charges. The formulated emulsion at pH 7 was temporarily (5 h) stable due to lack of steric hindrance between oil droplets and low adsorption energy of SEKL at oil interface (14 K_BT). It was also observed that a complete demulsification is feasible by alkalizing non-Pickering emulsions to pH 11. At pH 11, highly charged SEKL polymer was too hydrophilic (WCA<10˚) to adsorb at oil interface due to $|\Delta E|\sim 0$. As SEKL marginally influenced the Newtonian properties of the oil, fast oil coalescence happened. In opposition to non-Pickering emulsion, the Pickering emulsion using N-SEKL was not disturbed by pH alteration due to the network of rigid particle interaction. This adaptable system utilizing SEKL or N-SEKL can potentially be used for the preparation of oil-water emulsions with tunable physical properties depending on the targeted application in various industrial fields, e.g., cosmetics, pharmaceuticals or emulsion polymerizations. In this study, the sulfonation of lignin particles (N-SEKL) exhibited numerous advantages over unmodified acidic lignin particles for the formation of Pickering emulsions including, 1) lower dosage of emulsifier 2) stronger intra- and intermolecular interactions 3) larger nano-ranged particle size 4) use of more oil: water ratio 5) smaller oil droplet size 6) gel-like properties 7) tolerance to the subsequent pH alteration and 8) progressive control on the emulsion properties in an extended pH ranges.

5.7 References

[1] J. Wu, G. H. Ma, *Small* **2016**, *12*, 4633-4648.

[2] F. Goodarzi, S. Zendehboudi, *Can. J. Chem. Eng*. **2019**, *97*, 281-309.

[3] B. P. Binks, T. S. Horozov, Colloidal particles at liquid interfaces, Cambridge University Press, **2006**.

[4] B. P. Binks, *Curr. Opin. Colloid Interface Sci.* **2002**, *7*, 21-41.

[5] B. P. Binks, J. A. Rodrigues, *Angew. Chem. Int. Ed.* **2007**, *46*, 5389-5392.

[6] Z. Hu, T. Patten, R. Pelton, E. D. Cranston, *ACS Sustainable Chem. Eng.* **2015**, *3*, 1023-1031.

[7] J. Tang, P. J. Quinlan, K. C. Tam, *Soft Matter* **2015**, *11*, 3512-3529.

[8] X. Li, Y. Wang, B. Wang, X. Feng, Z. Mao, X. Sui, *Int. J. Biol. Macromol.* **2019**.

[9] N. Ghavidel, P. Fatehi, *RSC Adv.* **2019**, *9*, 17639-17652.

[10] L. Xia, S. Lu, G. Cao, *Sep. Sci. Technol.* **2003**, *38*, 4079-4094.

[11] M. Pera-Titus, L. Leclercq, J. M. Clacens, F. De Campo, V. Nardello-Rataj, *Angew. Chem. Int. Ed.* **2015**, *54*, 2006-2021.

[12] S. Lu, D. Yang, M. Wang, M. Yan, Y. Qian, D. Zheng, X. Qiu, *Colloids Surf. A* **2019**, 124158.

[13] J. O. Zoppe, R. A. Venditti, O. J. Rojas, *J. Colloid Interface Sci.* **2012**, *369*, 202-209.

[14] J. Zhou, X. Qiao, B. P. Binks, K. Sun, M. Bai, Y. Li, Y. Liu, *Langmuir* **2011**, *27*, 3308-3316.

[15] J. Jiang, Y. Zhu, Z. Cui, B. P. Binks, *Angew. Chem. Int. Ed.* **2013**, *52*, 12373-12376.

[16] I. Kalashnikova, H. Bizot, P. Bertoncini, B. Cathala, I. Capron, *Soft Matter* **2013**, *9*, 952-959.

[17] Z. Wei, C. Wang, S. Zou, H. Liu, Z. Tong, *Polymer* **2012**, *53*, 1229-1235.

[18] Z. Wei, Y. Yang, R. Yang, C. Wang, *Green Chem.* **2012**, *14*, 3230-3236.

[19] A. Yusoff, B. S. Murray, *Food Hydrocoll.* **2011**, *25*, 42-55.

[20] F. Liu, C. H. Tang, *J. Agric. Food Chem.* **2013**, *61*, 8888-8898.

[21] M. Sarker, N. Tomczak, S. Lim, *ACS Appl. Mater. Interfaces* **2017**, *9*, 11193-11201.

[22] S. Gharehkhani, Y. Zhang, P. Fatehi, *Prog. Energy Combust. Sci.* **2019**, *72*, 59-89.

[23] T. Aro, P. Fatehi, *ChemSusChem* **2017**, *10*, 1861-1877.

[24] S. Sabaghi, P. Fatehi, *Biomacromolecules* **2019**, *20*, 3940-3951.

[25] R. Gao, Y. Li, H. Kim, J. K. Mobley, J. Ralph, *ChemSusChem* **2018**, *11*, 2045-2050.

[26] M. H. Sipponen, H. Lange, C. Crestini, A. Henn, M. Österberg, *ChemSusChem* **2019**, *12*, 2039-2054.

[27] C. Frangville, M. Rutkevičius, A. P. Richter, O. D. Velev, S. D. Stoyanov, V. N. Paunov, *ChemPhysChem* **2012**, *13*, 4235-4243.

[28] Y. Pang, S. Wang, X. Qiu, Y. Luo, H. Lou, J. Huang, *J. Agric. Food Chem*. **2017**, *65*, 11011-11019.

[29] K. S. Silmore, C. Gupta, N. R. Washburn, *J. Colloid Interface Sci.* **2016**, *466*, 91-100.

[30] S. Li, J. A. Willoughby, O. J. Rojas, *ChemSusChem* **2016**, *9*, 2460-2469.

[31] S. Gharehkhani, N. Ghavidel, P. Fatehi, *ACS Sustainable Chem. Eng.* **2018**, *7*, 2370-2379.

[32] V. R. Dugyala, J. S. Muthukuru, E. Mani, M. G. Basavaraj, *Phys. Chem. Chem. Phys.* **2016**, *18*, 5499-5508.

[33] A. Morse, S. Armes, K. Thompson, D. Dupin, L. Fielding, P. Mills, R. Swart, *Langmuir* **2013**, *29*, 5466-5475.

[34] S. Kalliola, E. Repo, V. Srivastava, F. Zhao, J. P. Heiskanen, J. A. Sirviö, H. Liimatainen, M. Sillanpää, *Langmuir* **2018**, *34*, 2800-2806.

[35] N. Ghavidel Darestani, A. Tikka, P. Fatehi, *Polymers* **2018**, *10*, 928-945.

[36] J. Ederer, P. Janoš, P. Ecorchard, V. Štengl, Z. Bělčická, M. Šťastný, O. Pop-Georgievski, V. Dohnal, *React. Funct. Polym.* **2016**, *103*, 44-53.

[37] S. R. Yearla, K. Padmasree, *J. Exp. Nanosci.* **2016**, *11*, 289-302.

[38] C. Tan, M. C. Lee, A. Abbaspourrad, *ACS Sustainable Chem. Eng.* **2018**, *6*, 16657-16664.

[39] N. Bizmark, M. A. Ioannidis, *Langmuir* **2017**, *33*, 10568-10576.

[40] M. Hernández, J. Velasco, M. Asomoza, S. Solís, F. Rojas, V. Lara, *Ind. Eng. Chem. Res.* **2004**, *43*, 1779-1787.

[41] J. Penfold, E. Staples, I. Tucker, R. Thomas, *Langmuir* **2002**, *18*, 5755-5760.

[42] R. Pant, P. K. Roy, A. K. Nagarajan, K. Khare, *arXiv preprint arXiv:1508.00675* **2015**.

[43] Y. Lu, W. Kang, J. Jiang, J. Chen, D. Xu, P. Zhang, L. Zhang, H. Feng, H. Wu, *RSC Adv* **2017**, *7*, 8156-8166.

[44] K. Bahrpaima, P. Fatehi, *ChemSusChem* **2018**, *11*, 2967-2980.

[45] H. Lou, H. Lai, M. Wang, Y. Pang, D. Yang, X. Qiu, B. Wang, H. Zhang, *Ind. Eng. Chem. Res.* **2013**, *52*, 16101-16109.

[46] J. Huang, H. Xie, H. Ye, T. Xie, Y. Lin, J. Gong, C. Jiang, Y. Wu, S. Liu, Y. Cui, *Carbohydr. Polym*. **2016**, *138*, 301-308.

[47] X. Qiu, W. Zeng, W. Yu, Y. Xue, Y. Pang, X. Li, Y. Li, *ACS Sustainable Chem. Eng.* **2015**, *3*, 1551-1557.

[48] J. Wang, Y. Qian, L. Li, X. Qiu, *ChemSusChem* **2020,** *13*(17), 4420-4427.

[49] J. Mao, H. Tan, B. Yang, W. Zhang, X. Yang, Y. Zhang, H. Zhang, *Polymers* **2018**, *10*, 849.

[50] T. Sharma, G. S. Kumar, J. S. Sangwai, *Ind. Eng. Chem. Res.* **2015**, *54*, 1576-1584.

[51] Z. Fang, Y. Qiao, Z. Di, Y. Huo, P. Ma, S. Xia, *J. Chem. Eng. Data* **2008**, *53*, 2787-2792.

[52] C. A. Carrillo, D. Saloni, L. A. Lucia, M. A. Hubbe, O. J. Rojas, *J. Colloid Interface Sci.* **2012**, *381*, 171-179.

[53] J. Falco, R. Walker Jr, D. Shah, *AIChE J.* **1974**, *20*, 510-514.

[54] Y. Li, L. Yang, J. *Microencapsulation* **2015**, *32*, 255-272.

[55] Y. Zhang, S. Guo, X. Ren, X. Liu, Y. Fang, *Langmuir* **2017**, *33*, 12973-12981.

[56] G. Pi, Y. Li, M. Bao, L. Mao, H. Gong, Z. Wang, *ACS Sustainable Chem. Eng.* **2016**, *4*, 3095-3102.

[57] X. Zhao, G. Yu, J. Li, Y. Feng, L. Zhang, Y. Peng, Y. Tang, L. Wang, *ACS Sustainable Chem. Eng.* **2018**, *6*, 4105-4114.

[58] J. Xiao, X. a. Wang, A. J. P. Gonzalez, Q. Huang, *Food Hydrocoll.* **2016**, *54*, 30-39.

[59] C. Celia, E. Trapasso, D. Cosco, D. Paolino, M. Fresta*, Colloids Surf. B* **2009**, *72*, 155-160.

[60] Y. J. Kim, Y. D. Liu, Y. Seo, H. J. Choi, *Langmuir* **2013**, *29*, 4959-4965.

[61] R. Nigmatullin, R. Harniman, V. Gabrielli, J. C. Muñoz-García, Y. Z. Khimyak, J. s. Angulo, S. J. Eichhorn, *ACS Appl. Mater. Interfaces* **2018**, *10*, 19318-19322.

[62] T. Zeng, A. Deng, D. Yang, H. Li, C. Qi, Y. Gao, *Langmuir* **2019**, *35*, 11872-11880.

[63] V. Garbin, J. C. Crocker, K. J. Stebe*, J. Colloid Interface Sci.* **2012**, *387*, 1-11.

[64] P. Pieranski, *Phys. Rev. Lett.* **1980**, *45*, 569-574.

[65] N. Bizmark, M. A. Ioannidis, D. E. Henneke, *Langmuir* **2014**, *30*, 710-717.

[66] J. Bi, F. Yang, D. Harbottle, E. Pensini, P. Tchoukov, S. b. Simon, J. Sjöblom, T. Dabros, J. Czarnecki, Q. Liu, *Langmuir* **2015**, *31*, 10382-10391.

[67] B. P. Binks, J. H. Clint, *Langmuir* **2002**, *18*, 1270-1273.

[68] C. Fritz, C. Salas, H. Jameel, O. J. Rojas, *Nord. Pulp Pap. Res. J.* **2017**, *32*, 572-585.

[69] N. Bizmark, M. A. Ioannidis, *Langmuir* **2015**, *31*, 9282-9289.

[70] C. Tian, J. Feng, H. J. Cho, S. S. Datta, R. K. Prud'homme, *Nano lett.* **2018**, *18*, 4854-4860.

[71] O. Favrat, J. Gavoille, L. Aleya, G. Monteil, *J. Surfactants Deterg.* **2013**, *16*, 213-219.

[72] K. Olesen, C. van Leeuwen, F. I. Andersson, *Tenside Surfactants Deterg.* **2016**, *53*, 488-494.

[73] K. S. Kontturi, T. Tammelin, L. S. Johansson, P. Stenius, *Langmuir* **2008**, *24*, 4743-4749.

[74] L. Alison, A. F. Demirörs, E. Tervoort, A. Teleki, J. Vermant, A. R. Studart, *Langmuir* **2018**, *34*, 6147-6160.

[75] D. Wu, V. Mihali, A. Honciuc, *Langmuir* **2018**, *35*, 212-221.

[76] Y. Xi, Z. Luo, X. Lu, X. Peng, *J. Agric. Food Chem.* **2017**, *66*, 228-237.

Chapter 6: Dynamic interfacial and emulsion characterisation of polymeric lignin surfactant at different oil/water systems

6.1 Abstract

It is hypothesized that polymeric lignin surfactants have different affinities for stabilizing oil-water emulsions and that their emulsifying performance is highly affected by their adsorption performance at the oil-water interface. To validate the hypothesis, the adsorption performance of sulfoethylated lignin (SEKL) surfactant at different oil-water interfaces was examined by assessing the contact angle, dynamic interfacial tension depletion (surface pressure), and surface loading (Γ). Moreover, the interfacial adsorption kinetics of SEKL was comprehensively assessed at different oil-water systems to reveal the controlling mechanisms of the SEKL adsorption at the interface. Also, the impacts of SEKL concentration and ionic strength on the performance of SEKL as an effective emulsifier for the emulsions were assessed. Furthermore, the droplet size and instability index of the emulsions were systematically correlated with the adsorption performance of SEKL at the interface of oil and water. For the first time, by implementing a modified Ward Toradai diffusion model, two distinct early stages of the adsorption of SEKL at the oil interface were identified. Interestingly, the second stage was the determining stage of adsorption with the diffusion-controlled mechanism when polymers reconfigured at the oil/water interface. Salt screening facilitated the clustering of SEKL upon charge repulsion elimination, which removed the energy barrier in the first stage of adsorption ($\Delta Ep \rightarrow 0=0$), but it introduced a steric barrier upon the configuration of polymers at the oil interfaces in the second stage of adsorption. In addition to the kinetics of adsorption, satisfactory correlations were observed between surface pressure ($\Delta\gamma= \gamma\infty- \gamma0$), surface loading (Γ) of polymers, and contact angle at oil interfaces on one hand and the oil droplet size and emulsion stability on the other hand.

6.2 Introduction

Biobased polymeric materials such as lignocellulosic, starch, and chitosan macromolecules have attracted substantial interest due to their great biocompatibility, biodegradability, renewability.[1-4] They are applied as solubilizers, thickeners and stabilizers for emulsions systems due to their inherent features such as multiple functional groups, complex conformational changes at oil interface, and viscosity enhancement.[5,6]

Water-soluble lignin derivatives can be used as emulsifying agents to reduce the interfacial tension between oil and water and stabilize liquid-liquid mixtures by forming steric interfacial films.[7,8]

For instance, functionalized water-soluble lignin derivatives including carboxymethylated lignin,[9,10] kraft lignin-tannic acid,[11] sulfoethylated lignin[12] and polyacrylamide-grafted lignin[13] have been reported as efficient stabilizers for emulsions formation. Currently, methods for the characterization of emulsions using lignin derivatives mainly involve the analysis of destabilization, droplet size, and the rheological characterization of the emulsions.[9-13] In addition to such analysis, the knowledge of the kinetics of adsorbed mass at the interface of oil and water can shed lights on understanding the role of emulsifiers in such emulsion systems, especially in their long-term stability.[14-16]

Recently, substantial attention was devoted to exploring the interfacial behavior of natural-based emulsifiers including cellulose,[17] protein granule,[18] starch,[19] and chitosan[20] with different techniques, such as interfacial shear rheology, ellipsometry and dynamic interfacial tensiometry, to further determine their role in emulsion stability. For instance, Wei et al.[19] proposed a correlation between interfacial rheological properties of esterified fibre gum (CFG) and its emulsion stability. In another study, the surface loading of starch was determined by dual-wavelength methods to form a compact emulsifier layer at oil interface of n-hexane.[21] The impacts of structural and chemical properties of proteins on the interface properties of oil-water interfaces were also evaluated.[14,22,23] In our previous study, the use of sulfoethylated lignin (SEKL) as a polymeric surfactant was examined, even though the focus was on forming a Pickering stabilizer at altered pH.[12] However, the fundamental impacts of SEKL on the interfacial properties and emulsion stability of oil-water emulsions have not been evaluated.

The main objective of this study was to further understand the adsorption behavior and interfacial properties of the sulfoethylated lignin (SEKL) at different oil-water interfaces. In this work, decane, cyclohexane, and xylene were chosen as oil phases to explore the tendency of SEKL for stabilizing various oil-water emulsions.[24,25]

To predict and evaluate the compatibility and interfacial adsorption kinetics of SEKL at different oil-water interfaces, the contact angle of SEKL at water and oil interfaces and dynamic interfacial tension (γ) were measured. From the dynamic interfacial tension analysis, the important understandings of polymer behavior at the interface of different oils are plausible. Hence, the surface loading (Γ) was evaluated using Gibbs adsorption isotherms, as it was previously used for linking surface/interfacial tension to the surface concentration of polymers.[26-28] In addition, the modified Ward and Tordai diffusion model was implemented for the early stages of adsorption [29-

[31] to assess the diffusion performance of SEKL from the bulk system (i.e., water) to the interface and to further identify the mechanism of SEKL adsorption at different oil interfaces.[32]

In several studies, salt addition was found to facilitate the adsorption of polymers at the oil interface by screening polymer-oil and polymer-polymer electrostatic repulsion and thus facilitating the stability of emulsions.[33,34] For instance, the solubility and hydrophilicity of carboxymethylated lignin, CML, was reported to decrease with increasing the salt concentration, which improved the interaction of CML with the oil phase.[10] Similarly, the role of electrostatic interactions in the adsorption of SEKL at the oil-water interface was evaluated in this study.

Lastly, to find out whether there is a correlation between the interfacial properties and emulsions stability, emulsion stability was evaluated by means of confocal microscopy and accelerating centrifugal destabilization instruments.

6.3 Experimental Section

6.3.1 Materials

Softwood kraft lignin (KL) produced via the LignoForce^{TM} technology was received from FPInnovations. Also, 2-bromoethanesulfonate salt (NaBES 98%), sodium hydroxide (NaOH, 97%), potassium chloride (KCl), sodium nitrate ($NaNO_3$), sulfuric acid (H_2SO_4, 98%), hydrochloric acid (HCl, 37%), dimethyl sulfoxide-d6 (DMSO-d6), cyclohexane (C_6H_{12}), deuterium oxide (D_2O), polyethylene oxides and cellulose membrane (1000 g/mol cut off) were purchased from Sigma-Aldrich. Xylene ($C_6H_6(CH_3)_2$ ≥98.5%, ACS grade as a mixture of ortho, meta and para isomers, n-deacane ($C_{10}H_{22}$), and Nile red dye were purchased from Fisher Scientific. All chemicals were used without further purification.

6.3.2 Synthesis of Sulfoethylated Kraft Lignin

Dried KL powder was used as a precursor to synthesize sulfoethylated kraft lignin (SEKL) following our previously established method.[12] The alkalization of hydroxy groups of lignin (a 20 g/L aqueous system) was carried out in the presence of sodium hydroxide to form ionized nucleophiles. The phenol ions then reacted with 2-bromoethanesulfonate salt (NaBES) under the conditions of 2/1 mol/mol (NaBES/KL), 80 °C and 4 h reaction time in a three-neck glass flask to produce SEKL. Upon completion of the reaction, the reaction medium was cooled down to room temperature and then neutralized with 5 wt.% H_2SO_4. Afterward, it was dialyzed using a cellulose membrane for 4 days to purify the products from salts and unreacted reagents (i.e., Na^+, SO_4^{2-})

while changing the water every 12 h. The dried product, SEKL, was obtained after the evaporation of water in the oven at 105 °C.

6.3.3 Hydrodynamic Size Analysis

A dynamic light scattering analyzer (BI-200SM Brookhaven Instruments Corp., USA) equipped with a 35mW laser power source was used to obtain the hydrodynamic diameters of SEKL. Solutions of SEKL at 0.8 wt.% in a salt-free system and 10 and 100 mM KCl solutions were prepared at pH 7. After stabilizing for 24 h, the solutions were filtered by Whatman filters with a pore size of 0.45 μm. The R_h distribution of the samples was determined at the wavelength of 637 nm with a scattering angle of 90° at 25 °C.

The zeta potential of all solutions was also analyzed using a ZetaPALS analyzer (Brookhaven Instruments Corp, USA). Each sample was measured three times and the average values were reported.

6.3.4 Contact Angle Analysis

The contact angle of SEKL polymers at the air-water (WCA) and oil-water (OCA) interfaces was determined in two different experiments. Initially, the SEKL solution of 0.8 wt.% at pH 7 were coated on glass slides using a spin coater (WS-400B-NPP) spin-processor (Laurell Technologies Corp) at 1500 rpm for 20 s under nitrogen environment, and the films were dried in the oven at 105 °C overnight. In this experiment, a drop of deionized water (DI) was placed on the SEKL-coated glass slide and the contact angle of SEKL at the water-air interface (WCA) was determined following static contact angle measurement with the sessile drop method at 25 °C.[35] Then, following the Bizmark et al. procedure[24] the glass slide with the water droplet on its surface was introduced to a chamber filled with purified organic phase (i.e., xylene, cyclohexane or decane) to reflect the situation, in which emulsification occurs when SEKL polymers are dispersed in water first and then interacted with oil interface.[24] After the oil-water phase reaching its equilibrium (1 h), the OCA was measured accordingly. The same procedures were followed in different salinities at newly prepared coated glass slides. Aqueous droplets of 10 and 100 mM KCl were placed on the SEKL coated slides, and the WCA and OCA were obtained following the same steps explained above. All the measurements were repeated 3 times and the average of contact angle was reported in each experiment.

6.3.5 Dynamic Interfacial Tension Measurement

Dynamic interfacial tension (γ) between SEKL of different concentrations and the organic phase was measured using an Attension Theta Biolin optical tensiometer following the pendant drop method.[36] Precisely, 3 mL of organic solvent (i.e., xylene, cyclohexane, decane) was charged to a Quartz cuvette and sealed to minimize the volume loss. In one set of experiments, the SEKL concentration varied from 0.25 to 1.5 wt.% at 0 mM KCl ionic strength. Then, a droplet of SEKL solutions at variable concentrations with a constant volume of 5 µL was generated at the tip of a needle, which was submerged into the oil phase.[36] The images of the droplets were recorded over 3600 sec at a frame rate of 10 images per second in the first 600 sec and 1 image per minute in the last 3000 sec. The interfacial tensions were calculated from the analysis of the shape of droplets using the Young-Laplace equation.[37] In all calculations, density values (at 22 °C) were considered 997 kg/m^3 for water, 864 kg/m^3 for xylene, 730 kg/m^3 for decane and 779 kg/m^3 for cyclohexane.[38] The steady-state interfacial tensions (γ_∞) for all oil-water systems studied in this work were obtained from the intercepts of plots of γ against $1/\sqrt{t}$. A reference baseline for the γ of the oil-water systems was initially established (Figure A3.1). The value of γ_∞ of xylene, cyclohexane and decane against pure water (i.e., oil-water interface tension) was found to be 35, 44 and 47 mN/m, respectively, and the values were constant during the measurements. These results are comparable with reported values in other literature.[11,39,40] In another set of experiments, the concentration of SEKL was maintained constant at 0.8 wt.% in the presence of 10 and 100 mM KCl concentrations. Then, the above analysis was repeated to determine interfacial tensions in saline systems. Repeated measurements of the same experiment were in good correspondence with each other and generally lay within ±0.5 mN/m.

In addition to interfacial observations, the critical aggregation concentration (CAC) point of SEKL was determined to shape at 0.8 wt.% concentration and further details of surface tension analysis are provided in the appendix materials (Figure A3.2).

6.3.6 Emulsion Preparation

Different emulsion systems were prepared in this study using xylene, cyclohexane, and decane as the organic oil phase with varied chemical structures (Figure A3.3). Different stock solutions of SEKL at 0.25, 0.5, 0.8, and 1.5 wt.% concentrations in the salt-free system and at 0.8 wt.% SEKL in 10 and 100 mM KCl systems were prepared. The emulsions were prepared by mixing SEKL stock solutions and different oils in the volumetric ratio of 1/1 using an ultrasonic instrument

(Omni-Ruptor 4000, Omni International Int.) at 240 W power and 3 s interval for 30 s and room temperature.

6.3.7 Microscopic Structure

The microstructure of prepared emulsions was observed by a Leica TCC-SP8 confocal laser scanning microscope (Leica Microsystems Inc., Germany) equipped with a WLL laser (563 nm excitation wavelengths) using a HCPLAPOCS2 100×/1.40 oil immersion objective lens. In this set of experiments, 200 µL of all prepared emulsions without dilution was taken from the emulsion layer of the samples and were stained by the 5 µL of Nile red dye suspension in water (0.05 wt.%).[41] The stained samples were placed on a glass slide with a cover glass slide on the top. Red fluorescence was observed with a 600-710 nm filter under a 563 nm laser illumination.

6.3.8 Emulsion Stability

The accelerated stability of the emulsions using a dispersion analyzer (LUMiSizer 611, LUM GmbH, Berlin, Germany) was measured to determine the long-time storage stability of the emulsion in this study.[42] This instrument can reflect the movement of emulsion droplets through the sample. Undiluted emulsions were prepared as explained in the previous section, and they were placed in separate cells and subjected to a centrifugal force of this instrument. Upon the centrifugation, the heavier and lighter phases started to separate, and migration happened through the cell, which caused light transmission through the cells. Simultaneously, near-infrared light of the instrument (λ= 865 nm) was applied to illuminate the samples to determine the instability indices by the included software (SepView 6.0; LUM).[42] The dimensionless index was quantified by the clarification at a given separation time, divided by the maximum clarification.[43] The dramatic separation of phases is an indication of the instability of emulsions, which results in a larger instability index. The integration graphs were also generated and described as the "creaming rate", which showed the transmitted light in % over time. The higher creaming rate represents the lower stability of emulsions and vice versa. The operational parameters of the tests were the total sample volume of 0.4 mL of emulsion, the wavelength of 865 nm, rotational speed of 112 times compared to gravity, experimental time of 1000 s, the interval time (between recording) of 1 s and the temperature of 25 °C.

The zeta potential of the emulsion was measured with a ZetaPALS analyzer (Brookhaven Instruments Corp, USA). Samples were prepared following methodology stated in section 2.6. (Emulsion Preparation) and the samples were diluted 100 times in deionized water. The samples

were loaded into the cells and analyzed at the laser wavelength of 659 nm and the scattering angle of 90°. Zeta potential measurements was carried out as a function SEKL concentration, and oil type. At least three measurements were performed for each sample.

2.9. Statistical analysis

All measurements were implemented in triplicate and the results are reported as mean and standard deviation. Analyses were carried out in Excel 2016® for Windows® (Microsoft Office Home and Student®, 2016).

6.4 Results and Discussion

6.4.1 SEKL Formulation and Characterization

In this study, 2-bromoethanesulfonate (NaBES) was used to produce sulfoethylated kraft lignin (SEKL).[12] Briefly, the reaction followed a nucleophilic substitution mechanism (S_N2) where alkoxy ions from the dissociation of lignin's hydroxy groups in an alkaline medium substituted with brome ion on the NaBES salt (Figure A3.4). The ^1H and ^2H-H-NMR spectra of the products and raw material confirmed the grafting of the ethyl group on the lignin structure (Figure A3.5). The GPC revealed the M_w and M_w/M_n of 10±1 kg/mol and 1.80 for SEKL compared to 6.5±0.5 and 2.1 kg/mol for KL, and titration experiments showed the sulfonate group content of 1.2 and 0 meq/g for SEKL, and KL, respectively (Table A3.1), which confirmed the success of the sulfoethylation reaction.

6.4.2 Stability of SEKL Polymer Solution

As was shown previously, SEKL forms a stable solution at pH 7 in a salt-free system with no observable agglomeration or precipitation over time.[12] The effect of ionic strength on the stability of SEKL solutions was evaluated by monitoring the changes in electrostatic potential (ζ) and hydrodynamic size (R_h) at a constant concentration (Figure A3.6), and the results are summarized in Table 1. The charge screening lessened the magnitude of ζ from an initial value of -45 ±3 mV at 0.8 wt.% SEKL in the absence of salt to -31 ±2 mV and -20 ± 2 mV at elevated salinity, suggesting that salt screened some of the surface charges of the polymer (Table 1). The same behavior was previously reported for the grafted lignin polyacrylamide, as the ζ of its solution dropped from -40 to -22±2 mV when the NaCl concentration increased to 10 mM.[13]

The mean R_h of SEKL enlarged in higher salinity (Table 1), which suggests the aggregation of polymers at higher ionic strengths. Lignin is known to develop hydrophobic interactions, such as van der waals and π-stacking forces, which strongly contribute to the nano-aggregation of

polymers leading to a higher hydrodynamic size by screening the electrostatic repulsion between them.[44,45] These results agree with the DLVO theory,[46,47] which predicts the accumulation of polymers by a decrease in the double layer repulsion through salt screening that caused aggregation to a certain level. However, the SEKL solution was still stable with no observable precipitation (Figure A3.7) due to the sufficient electrostatic repulsion (ζ < -20 mv).[48] However, clusters with larger R_h are formed at elevated ionic strength.

Table 6.1. Physicochemical properties of SEKL solutions.

SEKL concentration (Wt.%)	KCl (mM)	Mean R_h (nm) (±2)	ζ potential (mV) (±3)
0.8	0	21	-45
0.8	10	35	-31
0.8	100	43	-20

6.4.3 Interfacial analysis

6.4.3.1 Wettability and compatibility of SEKL at Oil Interfaces

The contact angle of SEKL polymers at the air-water (WCA) and oil-water (OCA) interfaces was measured, and the results are shown in Figure A3.8. WCA at 0 mM (36.6˚) represents the hydrophilic nature of SEKL, which is associated with the functional groups, such as sulfonate moieties, anchored on lignin. The increased salinity resulted in an upsurge in WCA (39˚ and 43˚ at 10 and 100 mM KCl, Figure A3.8), verifying the elevated hydrophobicity of SEKL coated surface in saline systems. This is due to the partial neutralization of surface charges of polymers in the presence of counter ions (i.e., K+), which compressed the double layer and weakened electrostatic repulsive forces by reducing zeta potential (Table 1).[49,50]

The OCA is shown to be dependent on the oil system, which is the lowest (~25˚) at the xylene interface and greater at cyclohexane (~27˚) and decane (~36˚) interfaces. The lowest OCA at the xylene interface (Figures A3.8) implies the least favorable interaction between SEKL and xylene interface, despite the mutual structural aromaticity, which should be related to the higher polarity of xylene at the interface (2.5, Table A3.2).[51] On the other hand, the better compatibility of SEKL with cyclohexane and decane interfaces (i.e., larger OCA˚) with aliphatic structures should be

associated with the elevated hydrophobic interactions at the interface due to the limited oil polarity.[51]

In addition, charge screening effectively improved the OCA to (~35˚) independent of the oil type at 10 mM KCl (Figure A3.8) originating from the elimination of electrostatic repulsion and enrichment of hydrophobic interactions. At 100 mM KCl, the OCA at the xylene interface was raised to 53˚, while it was 42˚ and 44˚ for cyclohexane and decane interfaces, respectively (Figure A3.8). These superior hydrophobic interactions between xylene and SEKL structure probably originate from the π-π interactions associated with their mutual aromatic structure, which is absent in cyclohexane and decane systems.

6.4.3.2 Dynamic interfacial analysis

The dynamic interfacial tension (γ) is a fundamental quantity that is related to the assembly properties of adsorbed materials at interfaces and plays a crucial role in the process of emulsion formation and stabilization.[52] Polymeric surfactants reduce γ by migrating to the interface before their concentration reaches equilibrium at the interface.[53] In this study, the dynamic γ was measured via pendant drop tensiometry and drop-shape analysis for all systems at different SEKL concentrations over 3600 s, and the results are presented in Figure A3.9. The steady-state interfacial tensions (γ_∞) for all oil-water systems studied in this work were obtained from the intercepts of plots of γ against $1/\sqrt{t}$ (Figure A3.10) from data of t >1900 s in Figure 2, where a minimal alteration in γ is observed, and the results are summarized in Table 2.

As expected, the changes in γ for all systems at the oil-water interfaces depend on the concentration of SEKL in the aqueous solutions (Figure A3.9), as the higher dosages of SEKL in the bulk system (e.g., 1.5 wt% SEKL) yielded lower final γ values (γ_∞ in Table 2). Also, the rate of decline in γ varied over time, while changes were steeper in the first 250 s of the test, and it reached a plateau at the later stage of analysis (t >3000 s), suggesting that the polymers assembly reached an equilibrium.[21,54]

Paying attention to γ_∞ and γ_0 (pristine interfacial tension) at different oil interfaces (Table 2); the higher surface pressure ($\Delta\gamma_= \gamma_\infty - \gamma_0$) was obtained for the decane interface (33 mN/m) than for cyclohexane (31.8 mN/m) and xylene (24.3 mN/m) at the highest SEKL concentration, which implies a higher surface activity of SEKL at the decane interface. It is implied that the higher polarity of the oil at the interface was associated with fewer surface pressure variations, as was

also reported by Bergfreund et al.[55] on the adsorption of nanocrystals (CNCs) at different oil interfaces.

Table 6.2. The steady-state interfacial tensions (γ_∞) for aqueous solutions of SEKL at xylene, cyclohexane, and decane interfaces in salt-free systems.

SEKL (wt.%)	γ_∞ (mN/m) Xylene (±0.5)	γ_∞ (mN/m) Cyclohexane (±0.5)	γ_∞ (mN/m) Decane (±0.5)
0	35	44	47
0.25	12.1	17.3	16.5
0.5	11.9	14.6	15.5
0.8	11.0	13.7	15.0
1.5	10.7	12.2	14.1

Implementing the Gibbs adsorption isotherm (equation 1), surface loading of SEKL polymers per unit area at the interface was identified.[56]

$$\Gamma = \frac{1}{nRT}\frac{d\gamma_\infty}{d\ln c} \qquad (1)$$

In this equation, Γ stands for surface loading (mol/m^2), γ_∞ is the equilibrium interfacial tension obtained from Figure A3.9 and Table 2, c is the SEKL bulk solution concentration, n accounts for the ionic state of the polymer (n=2 for ionic polymers and n=1 for non-ionic polymers), T is the absolute temperature and R is the gas constant.

The area occupied by SEKL at the interface (a) can then be calculated following (eq 2):

$$a = M_w/(\Gamma N_A) \qquad (2)$$

where M_w is the molecular weight of SEKL (10 kg/mol) and N_A is Avogadro's number.[13] The computed (Γ) and (a) for all systems are shown in Figures 1a and 1b.

The results display a continuous increase in the interfacial loading (Γ) when more SEKL is available in the bulk system (Figure 1a). The number of SEKL polymers at the interface reached the maximum amount of 7.3×10^{-4}, 9.2×10^{-4}, and 9.6×10^{-4} mol/m^2 for xylene, cyclohexane, and decane systems, respectively. The trend for interfacial loading of SEKL at the oil interface follows the trend in the surface pressure at these interfaces, (Table 2), which reveals the higher interfacial activity of SEKL at the decane interface. Moreover, as the adsorption of SEKL increased at the interface, the area of occupation of SEKL decreased accordingly. Results in Figure 1b depicted

the smallest surface occupation (a) for the SEKL at the interface of decane (17.2-23.6 nm^2) and the largest at the interface of xylene (22.7-32.3 nm^2). Therefore, it can be concluded that the oil type plays a vital role in the interfacial activity of SEKL at the interface.

Various surface-sensitive techniques, such as neutron reflectometry (NR),[57] vibrational sum-frequency generation spectroscopy (SFG),[58] ellipsometry[39] or interfacial Langmuir trough[36] were previously implemented to experimentally measure the surface loading or area of occupation of molecules at air-water or oil-water interfaces. These methods reported results that were aligned with the theoretical Gibbs adsorption equation for analyzing surface or interfacial tension for a wide range of surfactants and polymers.[59] Perkins et al.[60] reported the experimental surface loading (Γ) of polyethylene glycolated lignin polymers at air-water interface via ellipsometry and the results were correlated to the surface tension using the Gibbs adsorption equation. Also, variations between theoretical and experimental results would be possible, which depend on the accuracy of the theoretical models and the nature of surfactants (i.e., cationic or anionic).[61]

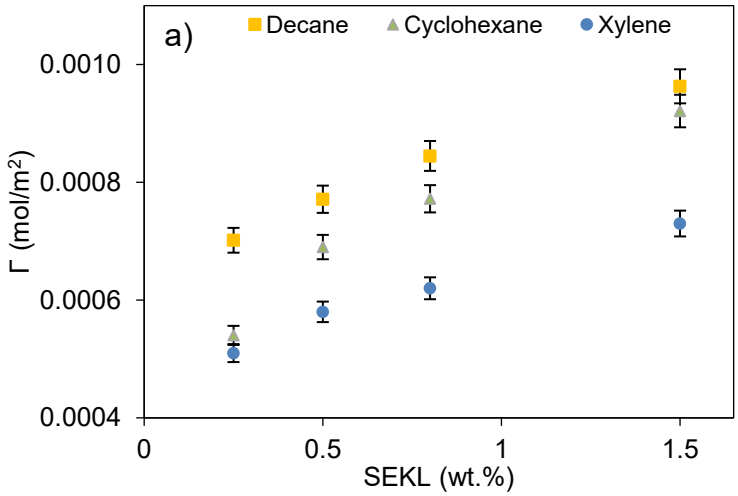

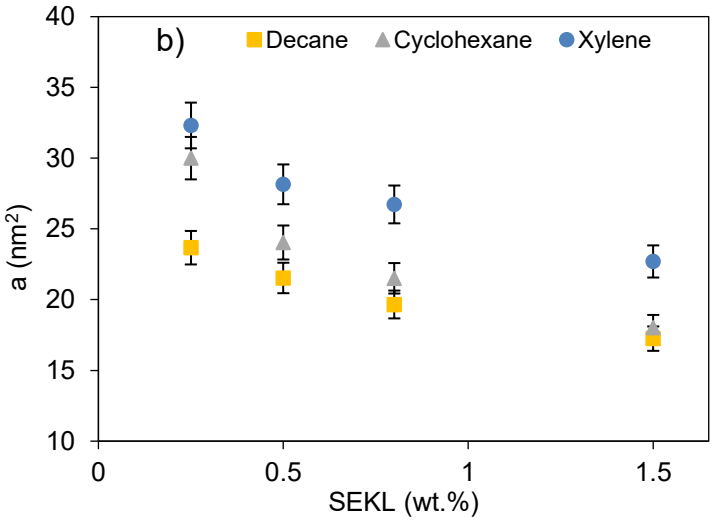

Figure 6.1: a) Computed (Γ) and b) computed (area, a) for SEKL as a function of bulk concentration (wt.%) at xylene, cyclohexane, and decane interfaces.

6.4.3.3 Diffusion into Oil Interface

The three main types of adsorption kinetics for polymers at interfaces have been reported to be diffusion-controlled, energy-barrier controlled, or a mixed barrier-diffusion.[62] It is generally accepted that the adsorption process at the pristine interface is diffusion-controlled when there is no energy barrier.[62] In this case, polymer molecules easily migrate from the bulk to the pristine interface and freely adsorb. For a better understanding of the adsorption process, the analysis of the effective diffusivity (D^*) of SEKL into the oil interface is important. Finding effective D^* to be much smaller than the estimated diffusion in the bulk phase indicates the existence of an adsorption barrier, while similar values show diffusion-controlled adsorption.[63] In the present work, the estimated diffusion coefficient of SEKL in bulk water was anticipated to be 2×10^{-12} m^2/s using the Stokes-Einstein equation (equation 3):[64]

$$D = \frac{KT}{6\Pi\mu R_h} \qquad (3)$$

where k is the Boltzman constant, T the absolute temperature, μ is the viscosity of the solution, and R_h is the hydrodynamic radius of SEKL.[64]

The modified Ward and Tordai diffusion model[31] was implemented to express the diffusion phenomenon of SEKL from the bulk system (i.e., water) to the interface. Assuming the adsorption barrier is not significant at the pristine interface, equation 3 can be applied as previously used for polymers and proteins.[64-66] In this case, the adsorption process is characterized by $D^*_{t\rightarrow 0}$, effective

diffusion coefficients in a short time ($t \rightarrow 0$), in which a single SEKL polymer is adsorbed onto a free interface:

$$\gamma = \gamma_0 - 2nRTC_0\sqrt{\frac{D^{*t\rightarrow 0}}{\pi}} \times \sqrt{t} \qquad (4)$$

Here, γ is the dynamic interfacial tensions at time t and, γ_0 at pristine interface, respectively, n is 1 for non-ionic polymers and 2 for ionic ones. Co is the SEKL concentration in the solution (i.e., water), T is the temperature and R is the universal gas constant (8.314 J /mol. K).

The changes in γ vs $\sqrt{t}$ in the initial time ($\sqrt{t} = 15\ \sqrt{s}$) is shown in Figure 2, where the sharpest decline in γ was observed (Figure A3.9). Remarkably, we detected two distinguishable straight lines of γ against $\sqrt{t}$ as shown in Figure 2 for the early stages of adsorption. While the changes of γ in the first stage are small ($t_{\rightarrow 0}$), a larger slope of γ vs $\sqrt{t}$ was observed for the second stage ($t_{\rightarrow t1}$). The transition between two stages happens sooner for SEKL at the decane interface than at cyclohexane and xylene interfaces. Accordingly, $D^{*}_{t\rightarrow 0}$ and $D^{*}_{t\rightarrow t1}$ is obtained from (eq 4) using the slope of a plot of γ vs $\sqrt{t}$ from Figure 2 for both stages (slopes are shown in Figure A3.11).[67]

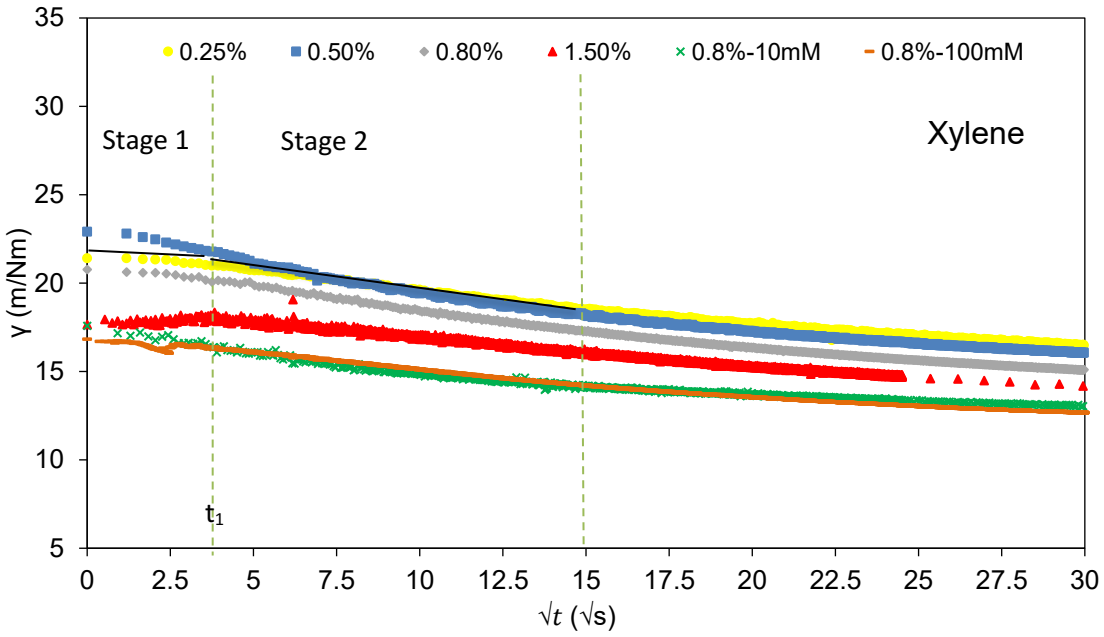

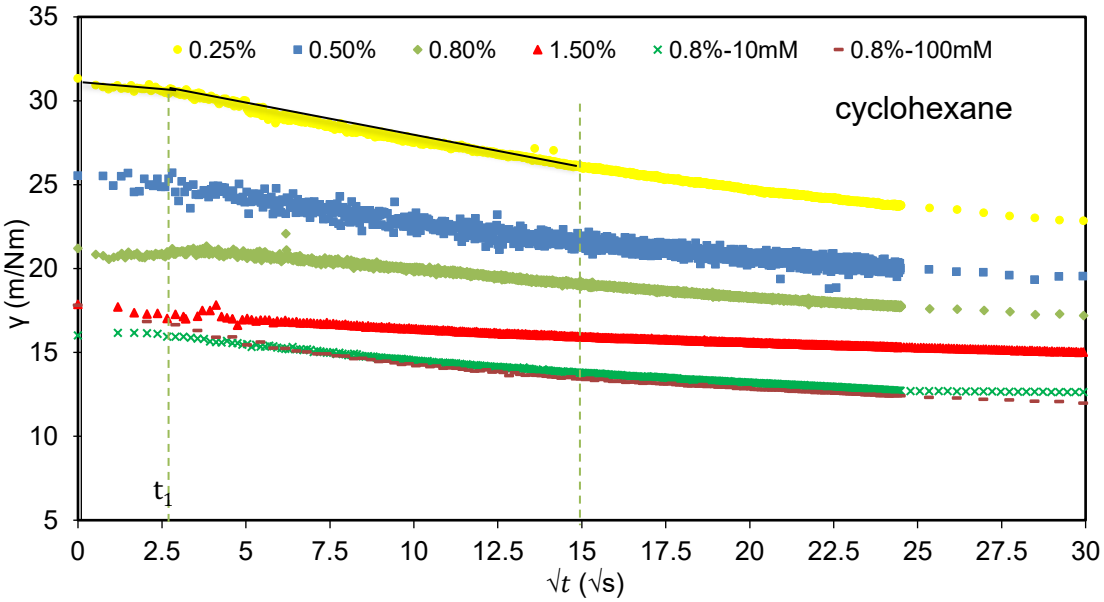

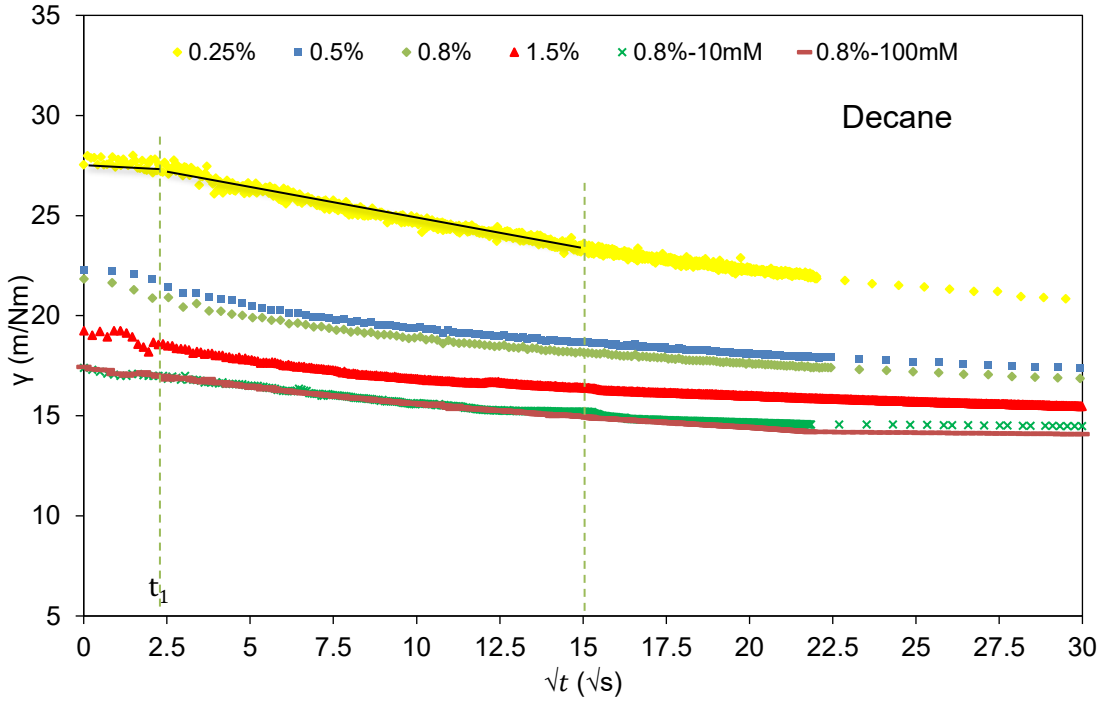

Figure 6.2: plots of γ vs $\sqrt{t}$ showing 2 different stages of interfacial depletion at different oil systems with increasing SEKL wt.% and ionic strengths.

The $D^*_{t \to 0}$ and $D^*_{t \to t1}$ of SEKL at different oil interfaces are depicted in Figure 3a-b and is compared with bulk diffusion D (2×10^{-12} m^2/s) to find out the adsorption mechanism, which is not similar in all situations and will be further discussed here.

Equation 5 was applied to quantify the differences between D and D^*,[68] where $\Delta Ep_{\rightarrow 0/t1}$ determines the extent to which adsorption is kinetically limited (not diffusion-controlled), or is the activation energy of attachment of SEKL at the interface.[64,69]

$$D^*_{t \rightarrow 0/\,t1} = D \exp\left(-\frac{\Delta Ep_{\rightarrow 0/t1}}{k_B T}\right) \qquad (5)$$

This equation can explain the situation in which the diffusion of a molecule and subsequently its adsorption at the interface is hampered for some reasons, e.g., steric or electrostatic repulsions as well as restructuring in the case of bulky macromolecules, such as polymers and proteins.[70,71] Considering the results of $D^*_{t \rightarrow 0}$ and D in Figure 3a, the apparent inconsistencies exist with bulk D depending on the oil type and polymer concentrations, and $\Delta Ep_{\rightarrow 0}$ calculations identify this difference as an energy barrier upon adsorption (Figure 3c).

In the case of the decane system, the $D^*_{t \rightarrow 0}$ was greater than the bulk D, which reveals the diffusion-controlled adsorption in the early stage of adsorption (stage 1), since the diffusion-controlled adsorption model of Ward and Tordai assumes that the step of transfer from the subsurface to the interface is faster compared to the transport from the bulk to the subsurface.[62] Therefore, we obtained $\Delta Ep_{\rightarrow 0} \approx 0$ k_BT (i.e., the order of thermal fluctuations) for all SEKL concentrations, indicating the validity of eq 4 and diffusion-controlled adsorption in stage 1 at the decane interface.[62,72]

However, in the case of cyclohexane interface, this validation is only approved in the concentration range of 0.25-0.5 wt.%; while at 0.8 and 1.5 wt.% SEKL concentrations, the $D^*_{t \rightarrow 0}$ decreased to 2.22×10^{-14} and 6.65×10^{-15} m^2/s, which is 2 to 3 orders of magnitude smaller than bulk D (22×10^{-12} m^2/s) (Figure 3a), resulting in the $\Delta Ep_{\rightarrow 0}$ of 4.5 and 5.7 k_BT, respectively. Therefore, the adsorption kinetics of SEKL at the water-cyclohexane interface is only diffusion-controlled below its CAC point (0.8 wt%), above which an energy barrier exists (due to $\Delta Ep_{\rightarrow 0} \geq 0$ k_BT). At the xylene interface, variations between $D^*_{t \rightarrow 0}$ and bulk D is applicable at all SEKL wt.% ranges, which resulted in $\Delta Ep_{\rightarrow 0}$=1.6-7 k_BT, suggesting that an energy barrier to the adsorption exists and adsorption is no longer diffusion-controlled.[72]

In the second stage, different behavior is observed, and the discrepancy is only visible at concentrations beyond CAC point (1.5wt.%) for all oil systems (Figure 3b). As a result, $\Delta Ep_{\rightarrow t1}$=0 for stage 2 (Figure 3d) is associated with diffusion-controlled adsorption for all oil interfaces.

SEKL consists of hydrophilic segments of sulfonate and hydroxyl groups and hydrophobic aromatic and aliphatic cores.[56] The first step of SEKL adsorption was found to be kinetically

limited at cyclohexane and xylene interfaces (Figure 3c) due to the existing energy barrier, while it was barrier free (ΔEp=0) at decane interface. Ionic molecules, e.g., SEKL, are unable to easily diffuse into the interface due to the strong hydrogen bonds formed with water molecules.[73] On the other hand, the net interactions between SEKL and the oil surface may include not only van der Waals and hydrophobic attraction but also electrostatic repulsion due to the ionic characteristics of SEKL (ζ of -45 mV).[30] Hence, it is suggested that the superior hydrophobic interactions of SEKL with decane should have resulted in a barrier free adsorption by exceeding the H-bonding and electrostatic repulsion, while the hydrophobic interactions at cyclohexane and xylene were less significant (OCA results in Figure A3.8). As is schematically illustrated in Figure 4, when SEKL arrives at the hydrophobic interface of oil, the hydrophobic segment of SEKL initially interacts with the oil interface and restructures by facing its hydrophilic moieties outward the water phase and the hydrophobic segments toward the oil phase, which is analogous to protein denaturation at an oil interface.[14,72] This can be ascribed to the "unfolding" of SEKL at the water-oil interface, as the interactions switch from SEKL-water in the bulk to SEKL-oil at the interface.[25,63] This step of restructuring of polymers at oil interfaces was shown to be diffusion-controlled (Figure 3d). The elimination (or reduction) of H-bonding and effective restructuring of SEKL at oil interfaces should have further associated with stronger hydrophobic interactions and less electrostatic repulsion between SEKL-oil interfaces, therefore the energy barrier no longer exists. In stage 2, two processes would occur simultaneously: (1) the diffusion process of new molecules from bulk solution, which makes the adsorbed layer denser that caused the continues depletion of the interfacial tension; and (2) the reorientation of SEKL segments within the adsorption layer leading to a diffusion control process as was reported in the past.[74,75]

The observable ΔEp beyond the CAC point (at 1.5 wt.%) could be associated with the changes in the conformation or nano-aggregation of active solutes, i.e., macromolecules.[63,76] CAC is stated to have a significant effect in diffusivity of macromolecules that caused an abrupt change in $D^*_{t \rightarrow t1}$ (Figure 3b), which further restricted restructuring at the interface.[63]

Ultimately, it could be summarized that SEKL showed a better interfacial activity at the decane interface in the initial stage of adsorption, however, this activity improved later at xylene and cyclohexane interfaces in the second stage, in which diffusion-controlled adsorption was developed at all oil interfaces.

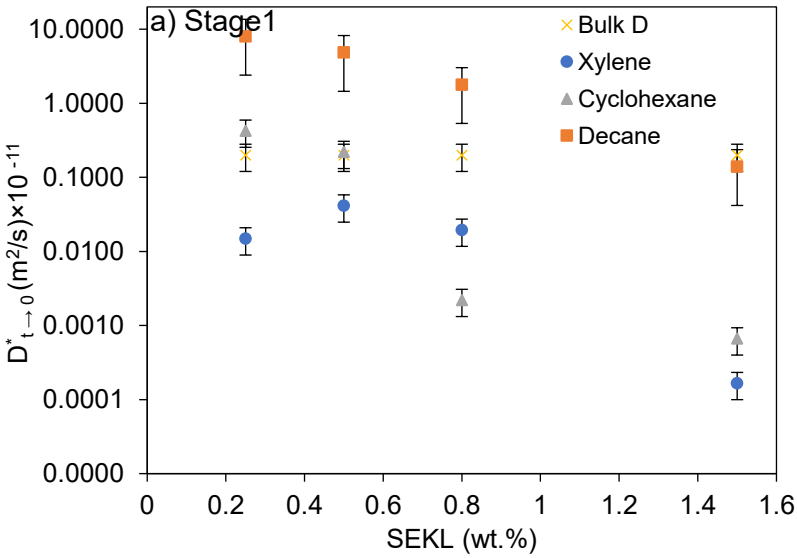
a) Stage1
Bulk D
Xylene
Cyclohexane
Decane
10.0000
1.0000
0.1000
0.0100
0.0010
0.0001
0.0000
$D^*_{t\to 0}$ (m²/s)×10⁻¹¹
0
0.2
0.4
0.6
0.8
1
1.2
1.4
1.6
SEKL (wt.%)

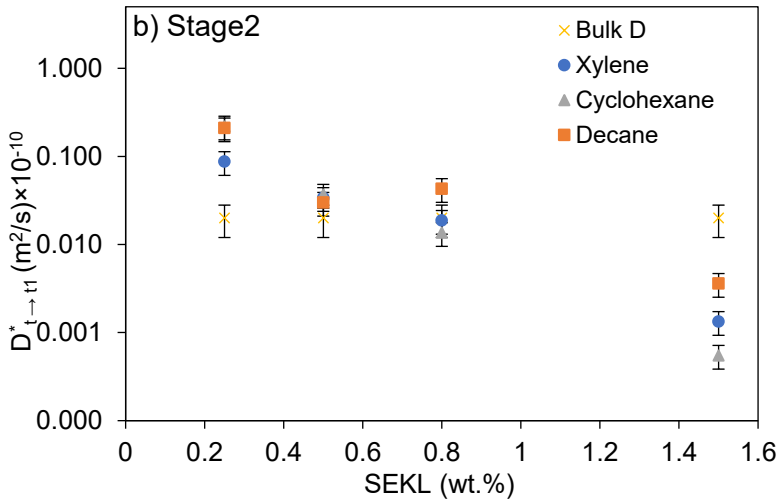
b) Stage2
Bulk D
Xylene
Cyclohexane
Decane
1.000
0.100
0.010
0.001
0.000
$D^*_{t\to t1}$ (m²/s)×10⁻¹⁰
0
0.2
0.4
0.6
0.8
1
1.2
1.4
1.6
SEKL (wt.%)

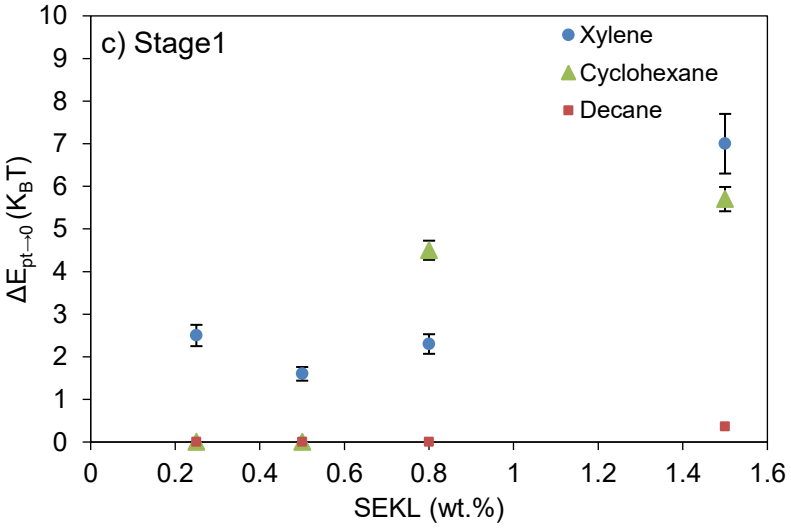
c) Stage1
Xylene
Cyclohexane
Decane
10
9
8
7
6
5
4
3
2
1
0
$\Delta E_{pt\to 0}$ ($K_B T$)
0
0.2
0.4
0.6
0.8
1
1.2
1.4
1.6
SEKL (wt.%)

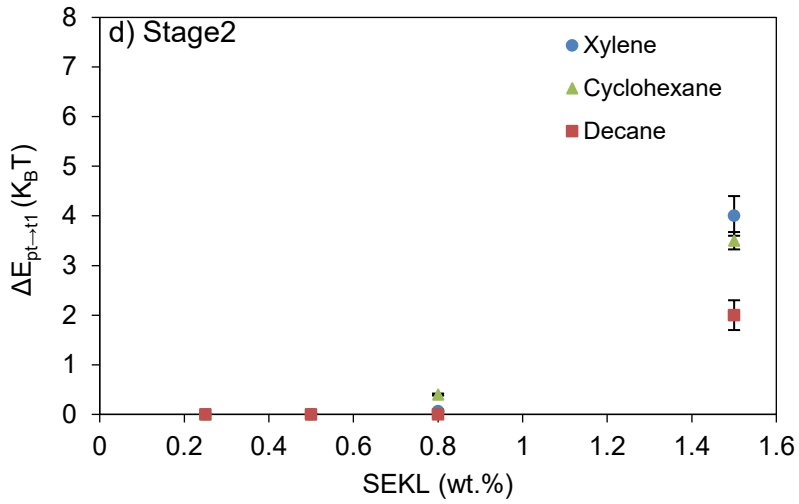

Figure 6.3: a) diffusion coefficients $D^*_{t\rightarrow 0}$ (eq 4) in stage 1, b) $D^*_{t\rightarrow t1}$ (eq 4) in stage 2, c) energy barrier $\Delta Ep_{t\rightarrow 0}$ (eq 5) in stage 1 and d) $\Delta Ep_{t\rightarrow t1}$ (eq 5) in stage 2 of the SEKL of different concentrations (0.25-1.5 wt. %) at different oil interfaces.

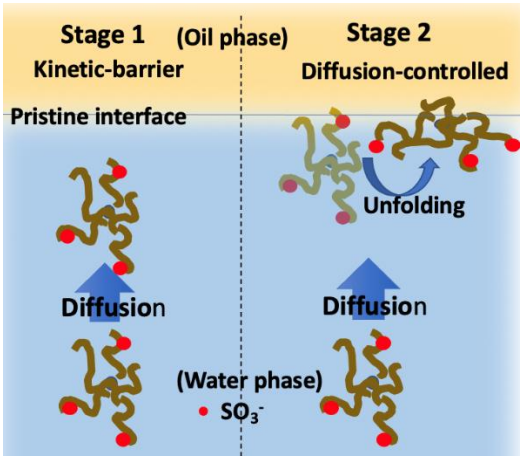

Figure 6.4: Schematic illustration of SEKL adsorption in stage 1 and stage 2 at cyclohexane and xylene interface in a salt free system.

6.4.3.4. Diffusion and Adsorption Mechanisms in Salty Systems

The changes in $D^*_{t\rightarrow 0}$ and $D^*_{t\rightarrow t1}$ (calculated according to equation 4 and the slopes in Figure A3.11) and corresponding $\Delta Ep_{\rightarrow 0}$ and $\Delta Ep_{\rightarrow t1}$ (equation 5) at the early stages of adsorption in accelerated salinity systems are also summarized in Table 3.

An interesting observation in stage 1 was the increment in $D^*_{t\rightarrow 0}$ by the orders of 1 to 2 magnitude at the elevated salinity compared to the salt-free system for cyclohexane and xylene interfaces, which made $\Delta Ep_{\rightarrow 0}$= 0 k_BT at 100 mM. It indicates that the salt concentration (100 mM) was

sufficient to eliminate the adsorption barrier since the diffusivities calculated from Ward and Tordai would recover the bulk values measured with DLS, and therefore, diffusion-controlled adsorption is valid.[63] The increment in $D^*_{t\to 0}$ and reduction in energy barrier at higher salinity was previously reported to associate with the reduced polymer-interface repulsion.[32] Similarly, electrostatic repulsion among SEKL polymers was shown to be weakened at elevated saline systems based on zeta potential (Table1) and stronger hydrophobic interactions were formed at oil interface (OCA results in Figure A3.8), which resulted in effective adsorption at xylene and cyclohexane interfaces in the presence of SEKL.

Interestingly, a reverse shift was observed at the decane interface compared to xylene and cyclohexane interfaces for SEKL adsorption in the first stage, and $D^*_{t\to 0}$ decreased at 100 mM salinity resulting in $\Delta Ep=1.1\ K_BT$. As hydrophobic interactions were already dominant in the case of SEKL adsorption at the decane interface with diffusion-controlled adsorption in the first stage of the salt-free system, charge elimination did not accelerate the diffusion (Table 3). On the other hand, the bulkier clusters of SEKL had slower diffusion into the interface due to SEKL's agglomeration (Table 1). Therefore, a barrier is determined against adsorption at 100 mM salt concentration.

In stage 2, $D^*_{t\to t1}$ is decreased in opposition to stage 1 and $\Delta Ep_{\to t1}$ increased to less than 1 k_BT. In the salty system, the already adsorbed clusters are bulkier and therefore more difficult to restructure at the interface. Therefore, a steric barrier existed for the restructuring of adsorbed SEKL as well as against the adsorption of new polymers from the bulk, which resulted in $\Delta Ep> 0\ K_BT$ in stage 2.

Table 6.3. Effect of KCl concentration on the kinetic parameters of SEKL adsorption at early stages of adsorption at different oil interfaces and 0.8 wt.% SEKL concentration.

Oil phase	KCl,	Stage 1		Stage 2	
	(mM)	$D^*_{t\to 0}$(eq4) (m^2/s)	$\Delta Ep_{\to 0}$(eq5) (k_BT)±0.5	$D^*_{t\to t1}$(eq4) (m^2/s)	$\Delta Ep_{\to t1}$(eq5) (k_BT)±0.5
Xylene	0	1.95×10^{-13}	2.3	1.87×10^{-12}	0.06
	10	1.01×10^{-12}	0.3	9.30×10^{-13}	0.40
	100	2.58×10^{-12}	0	2.58×10^{-13}	0.63

Cyclohexane	0	220×10^{-14}	4.5	1.36×10^{-12}	0.40
	10	7.83×10^{-13}	0.6	1.90×10^{-12}	0.20
	100	2.86×10^{-12}	0	5.80×10^{-13}	0.60
Decane	0	1.78×10^{-11}	0	4.30×10^{-12}	0.00
	10	2.10×10^{-12}	0	5.80×10^{-13}	0.80
	100	3.64×10^{-13}	1.1	5.25×10^{-13}	0.70

6.4.4 Emulsions Observation

Physical observation and stability of emulsion were analyzed through microscopic imaging and physical stability analysis under centrifugal forces. The emulsion phase rested atop the excess aqueous phase, suggesting that the system was an oil-in-water (O/W) emulsion,[50] which was anticipated from contact angle measurements ($\theta < 90°$) (Figure A3.8).

6.4.4.1 Confocal Images

The confocal images of emulsions formulated from different oils are presented in Figures 5. The oil phase is demonstrated by green color as was stained by the dye. The variations in the oil droplet size are observable by changing the oil type and bulk concentration. It is inferred that xylene, as the oil phase, contributed to the formation of the largest oil droplets (~15 μm), while decane showed the smallest droplet size (< 7 μm) at 0.25 wt.% SEKL concentration. The findings are in accordance with previous observations reported on the formulation of larger oil droplets for polar oils compared to non-polar oils.[77] Also, a possible explanation might be the higher interfacial loading at the decane interface, which facilitated the production of small droplets, as was reported previously.[78]

By further increasing the bulk concentration, the size of oil droplets dropped in all formulated emulsions (xylene ~7 μm, cyclohexane ~5 μm, and decane ≤ 2.5 μm at 1.5 wt.%). In a lower SEKL concentration, the number of polymers adsorbed at the interface is not sufficient, therefore coalescence or flocculation is probable, which resulted in larger oil droplets.[79] In addition, rising the salinity of the system dropped the oil droplet size to less than 2.5 μm for all systems without further coalescence or flocculation. Charge screening is evident to cause more packing of SEKL at the oil-water interface that formed a smaller oil droplet size.

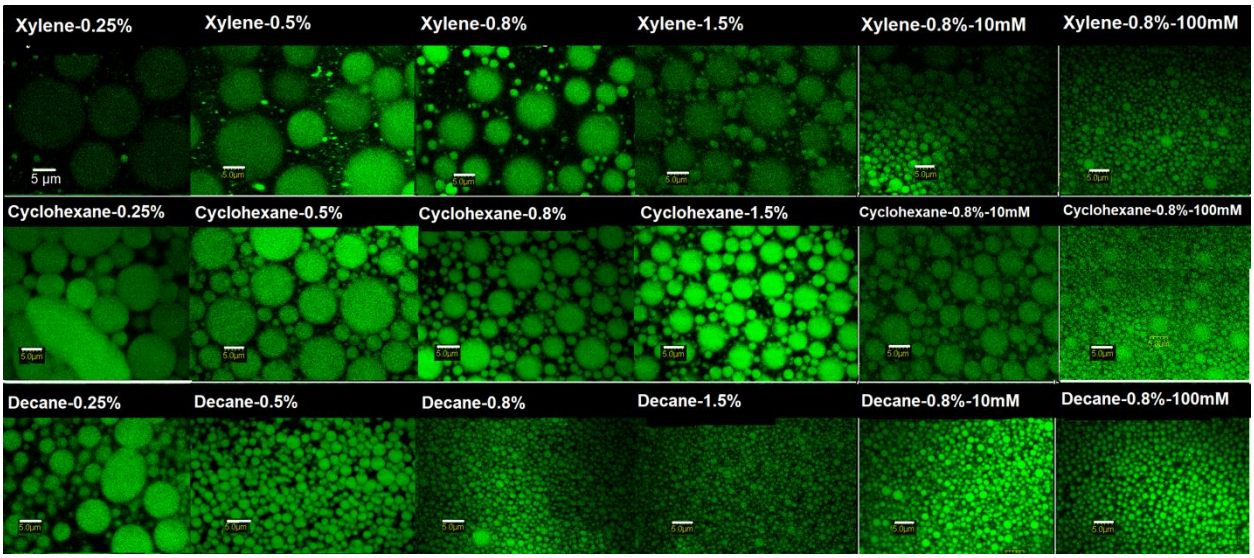

Figure 6.5: Confocal images of the emulsions prepared from xylene, cyclohexane, and decane as the oil phase and SEKL aqueous solutions at concentration ranges of (0.25-1.5 wt.%) and salinities (10 and 100 mM). Scale bar is 5 µm in all images.

6.4.4.2 Stability of Emulsions

The stability of the emulsions was compared considering the changes in accelerating physical instability index (Figure A3.12) and zeta potential (ζ) of emulsions. The comparison of instability indices (Figure A3.12) shows that formulated emulsion with decane as the oil phase is more stable compared to the other two oils, and the stability for all systems improved by concentrating the bulk solution (instability index decreased). Moreover, the instability index reduction was limited to 0.36 and 0.25 in the case of xylene and cyclohexane systems, respectively, while it reached 0.04 for the decane emulsion.

Instability index depletion with increasing bulk concentration is entirely consistent with the variations in droplet size (Figure 5), which follows Stoke's law stating the smaller the oil droplet size, the lower the creaming rate of emulsions would be.[80,81] The creaming rate of emulsions also decreased with increasing the bulk concentration, which would be evident from the smaller slopes of transmittance graphs with position and the integral transmission as a function of time[82] in Figure A3.13a and figure A3.13b, respectively (showed only for the decane system). All ζ values were negative at the lowest SEKL dosage (decane -36, cyclohexane -35 and xylene -36 ±2 mV) due to the presence of sulfonate anionic groups.[83] The magnitude of zeta potential of emulsions increased for all three oils by concentrating the SEKL bulk solution.[83] Moreover, decane

exhibited the highest absolute potential at a 1.5% SEKL dosage (-55 ±3 mV) compared to cyclohexane (-50 ±2 mV) and xylene (-47 ±2 mV), which agreed with the highest stability of emulsions with decane in a salt free system. These observations were coherent with the adsorption results shown in Figure 1a, reflecting that a higher Γ at decane interface led to higher stability that was associated with more packing and stronger barrier at decane interface. The fact that further reduction in the ζ of emulsions was correlated to the superior stability and smallest droplet size imparted that electrostatic repulsive forces among oil droplet is the main mechanism of droplet stabilization in salt free system.[84]

A substantial reduction in the instability indices for all emulsions at higher salinity was obtained as the oil droplet size was significantly reduced (Figure 5). The instability index reached 0.01, 0.01 and 0.04 for xylene, decane, and cyclohexane systems at 100 mM salt, respectively, suggesting the ultra-stable emulsion formulation in the saline systems (the images of the emulsions after centrifuging are presented in the supplementary material in Figure A3.14). In this case, the reduced electrostatic repulsion between SEKL and interface (due to the reduced charge of polymers in bulk solution, Table 1) and elevated hydrophobicity of SEKL formed a stronger intermolecular interaction between SEKL-oil interface in the saline system (WCA and OCA results as shown in Figure A3.8), which resulted in the concentrating SEKL at oil interfaces.[12] It is suggested that the main mechanism of droplet stabilization in salty systems is a steric barrier based on the bulkier polymers and the reduced ζ potential of solutions at higher ionic strengths (Table 1).[85]

Moreover, a strong correlation is observed between the magnitude of instability indices and the results of the OCA at different oil systems (Figure A3.8). For instance, the largest and smallest OCA at the decane and xylene interfaces were associated with the smallest (most stable) and largest oil droplets (least stable) (Figure 5 and A3.12) in a salt-free system, respectively. The intense increment in the OCA in the salty systems (Figure A3.8) is also associated with the highly stable emulsions with the smallest oil droplet (Figure 5). This made the emulsion stability independent of the oil choice, as the emulsions with xylene and cyclohexane are as stable as the one with decane.

6.5. Comparison

Comparing the physical properties of emulsions of different systems is challenging as the oil type, content, and emulsification conditions can greatly affect the macroscopic properties and, ultimately the stability of the system. The quantitative analysis from the previously used bio-based

polymers for stabilizing oil-water systems is summarized in Table 4. As seen, several studies have quantitatively characterized the kinetics of adsorption at the interface by calculating diffusivity.[66,83,86] For instance, the D_{eff} was calculated for citrus pectin with different degrees of esterification, and diffusion-controlled adsorption kinetics was reported at 1 wt.% bulk concentration for the Rapeseed oil-water system.[86] Compared with the results of the present study, the oil droplet size was much larger, and increasing salt concentration further enlarged the droplet size to 50 µm, which caused demulsification due to substantial droplet coalescence.[86] A fairly similar diffusivity rate ($1.22 \times^{-13}$ m^2/s) to the result of the present study was reported for lentil protein isolates (LPI) at the olive oil interface.[66]

The two-stage transition for SEKL adsorption at oil interface was also identified for amphiphilic derivatives of chitin or chitosan,[87] bovine serum albumin (BSA) protein,[68] and hydrophilic (poly (ethylene glycol) PEG NPs.[72] These results showed to be diffusion-controlled on the dynamic surface and interfacial analysis.

Another study using Acrysol TT-935, a polymeric surfactant, and soy lipophilic protein referred to the adsorption process of the polymer at the interface to follow the diffusion-controlled.[64] For this system, the surface loading based on Gibbs adsorption isotherms was reported to be 12.3 KT for Acrysol polymer.[64] In another study, the comparison between the emulsifying properties of lignin derivatives (kraft LA and calcium lignosulfonate LG) and whey protein WPI illustrated the better emulsifying properties of the more hydrophobic polymer (LA), which formed smaller oil droplets that were associated with a prominent decline in the interfacial tension.[88] Compared with those studies, better hydrophobic interaction in this study at the decane interface was associated with higher interfacial activity and better emulsifying properties (smaller oil droplet and instability index).

SEKL showed better emulsion properties compared to the previously reported lignin tannic acid (KL-TA) with higher charge density (-2.8 mmol/g) as a stabilizer, which formed a larger oil droplet size with greater instability.[11] It is known that the higher surface charges are associated with larger oil droplets that will cause instability over time.[89] Carboxymethylated lignin (CML) showed better emulsifying properties with a smaller oil droplet, however, one issue with CML is its limited affinity to lower the surface tension.[10] In another study, hydrophobically modified corn fiber gum (CFG) grafted by octenyl succinate anhydride (OSA) was reported to obtain stabilized emulsions under centrifugal forces in the dosage range of 1-1.5 wt.%,[19] which was comparable with SEKL's

performance. It should be stated that, compared with the oil fraction of the current study (50%), the oil fraction was much lower in the studies discussed above, which could greatly affect the emulsifying capacity of polymers.

Table 6.4. Comparison of SEKL as an emulsifier with previously used polymeric surfactants in terms of physical properties and interfacial analysis.

Emulsifier- dosage	Emulsion system/ oil content (wt.%)	Oil droplet size (μm)	Instability Index/instrument	Contact angle θ_{H2O}	Equilibrium interfacial tensions mN/m	D (m^2/s)	Ref.
SEKL, 0.25-1.5%	Xylene, Cyclohexane, Decane- 50%	15 to 2	0.8 to 0.04 (Lumisizer)	36˚	10.7, 12.2, 14.1	1.87×10^{-12}, 1.36×10^{-12}, 4.3×10^{-12}	This study
OSA-starches/ 0.125-1 wt.%	MCT- 5%	0.2-0.25	△T% =10-30% (Turbiscan)	-	38.1-24	6.9×10^{-7}- 4.7×10^{-6}	[83]
Pectin-1%	Rape seed oil- 30%	25-10	-	-	-	2×10^{-12}- 1.2×10^{-11}	[86]
LPI 0.1-30 mg/ml	Olive oil, 10%	12 to 0.4	ESI=24 to 386 h Gravitational settling		12	$1.22\times^{-13}$	[66]
LG-0.5wt.%	Sunflower oil- 10%	1.739	TSI, 9	30.50˚	5	-	[88]
LA		1.777	8	49.33˚			
WPI			15 (Turbiscan)	-			
KL-TA-1.5%	Cyclohexane- 50%	6-12	TSI 20 (Turbiscan)	20˚	21.7	-	[11]
CMLs-2%	Kerosene-30-70%	1.7-3	-		Surface tension 65-62	-	[10]

OSA-CFG- 0.5-1.5%	Soybean 5.0%	1.5-2.5	0.75 to 0.25 (Lumisizer)	33 to 25	Interfacial viscoelasticity studies	[19]

△T: Transmission difference

ESI: Emulsifying stability index

6.6. Conclusions

For the first time, a systematic analysis of the interfacial behavior of a polymeric lignin surfactant (SEKL) was provided to identify the adsorption performance of SEKL at the interface of different oil-water systems. Firstly, altering the polarity and chemical structure of the oil affected the surface pressure $\Delta\gamma$, surface loading Γ, and contact angle θ of SEKL at the oil interfaces, which revealed the highest adsorption performance at decane interface. These observations were associated with stronger hydrophobic interactions in the order of decane>cyclohexane>xylene at the interface. Secondly, the adsorption behavior of SEKL was noticed to happen in two distinguishable stages analogous to diffusion and denaturation of proteins at the oil interface. Thirdly, the implication of a modified Ward Toradai diffusion model for kinetic adsorption analysis revealed that although the diffusion was kinetically limited in the very first seconds of adsorption at interfaces of oils (except for decane), the restructuring in the second stage was diffusion-controlled for all systems. The changes in the interactions from SEKL-water (stage 1) to SEKL-oil (stage 2) eliminated (or reduced) the strong H-banding of water molecules with SEKL and associated with stronger hydrophobic interaction upon restructuring at the oil interfaces. Furthermore, charge screening at higher salinity eliminated the energy barrier for the SEKL adsorption in the first stage at xylene and cyclohexane interfaces. Nonetheless, a new steric hinderance was generated in the second stage, which hindered the diffusion-controlled reorientation of SEKL clusters at oil interfaces. The overall adsorption of SEKL at the interface was diffusion-controlled (considering stage 2 as the determining stage) at all oil interfaces in a salt-free system. In a saline system, the adsorption at the interface was strictly limited due to the formation of bulkier SEKL clusters. SEKL led to strong stability against a phase separation via increasing the bulk concentration and ionic strength, which were confirmed by a considerable decrease in the oil droplet size and instability indices under centrifugal forces. The decrease in the zeta potential of emulsions in salt free systems suggested that the mechanism behind the stabilization of droplets to be electrostatic repulsion. However, it is believed that the steric barrier is associated with droplet stabilization in salty systems due to the

adsorption of bulkier polymers at oil interfaces. In addition, a direct correlation was exhibited for the first time between oil contact angle, surface pressure and surface loading Γ of SEKL at the oil interface and the oil droplet size and instability of the systems. The results in this study, for the first time, helped to understand the mechanism of adsorption and interfacial behavior of sulfonated lignin surfactants at the interface of different oil systems. More studies are suggested to explore the impact of lignin polymer structure and charged groups on the stability of oil-water emulsions. Also, the rheological and strength of the deposition of lignin surfactants on oil droplet can be studied in future.

6.7. References

[1] L. Bai, L. G. Greca, W. Xiang, J. Lehtonen, S. Huan, R. W. N. Nugroho, B. L. Tardy, O. J. Rojas, *Langmuir* **2018**, *35*, 571-588.

[2] D. J. McClements, C. E. Gumus, *Adv. Colloid Interface Sci.* **2016**, *234*, 3-26.

[3] K. S. Mikkonen, *Green Chem.* **2020**, *22*, 1019-1037.

[4] S. Kalliola, E. Repo, V. Srivastava, F. Zhao, J. P. Heiskanen, J. A. Sirviö, H. Liimatainen, M. Sillanpää, *Langmuir* **2018**, *34*, 2800-2806.

[5] T. Tadros, *Adv. Colloid Interface Sci.* **2009**, *147*, 281-299.

[6] C. C. Chang, R. Letteri, R. C. Hayward, T. Emrick, *Macromolecules* **2015**, *48*, 7843-7850.

[7] D. J. Mcclements, *Crit. Rev. Food Sci. Nutr* **2007**, *47*, 611-649.

1) [8] D. J. McClements, *Food emulsions: principles, practices, and techniques*, CRC press, **2015,** 185-238.

[9] S. Li, D. Ogunkoya, T. Fang, J. Willoughby, O. J. Rojas, *J. Colloid Interface Sci.* **2016**, *482*, 27-38.

[10] S. Li, J. A. Willoughby, O. J. Rojas, *ChemSusChem* **2016**, *9*, 2460-2469.

[11] S. Gharehkhani, N. Ghavidel, P. Fatehi, *ACS Sustainable Chem. Eng.* **2018**, *7*, 2370-2379.

[12] N. Ghavidel, P. Fatehi, *ChemSusChem* **2020,** *13*(16) 4567-4578.

[13] K. S. Silmore, C. Gupta, N. R. Washburn, *J. Colloid Interface Sci.* **2016**, *466*, 91-100.

[14] C. Beverung, C. J. Radke, H. W. Blanch, *Biophys. Chem.* **1999**, *81*, 59-80.

[15] P. J. Beltramo, M. Gupta, A. Alicke, I. Liascukiene, D. Z. Gunes, C. N. Baroud, J. Vermant, *Proc. Natl. Acad. Sci.* **2017**, *114*, 10373-10378.

[16] L. Dokić, . Krstonošić, I. Nikolić, *Food Hydrocoll.* **2012**, *29*, 185-192.

[17] P. Bertsch, P. Fischer, *Adv. Colloid Interface Sci.* **2020**, *276*, 102089-102104.

[18] F. Liu, C.-H. Tang, *Food Hydrocoll.* **2016**, *60*, 606-619.

[19] Y. Wei, Y. Xie, Z. Cai, Y. Guo, M. Wu, P. Wang, R. Li, H. Zhang, *J. Colloid Interface Sci.* **2020**, *580*, 480-492.

[20] B. Doshi, S. Hietala, J. A. Sirviö, E. Repo, M. Sillanpää, *J. Mol. Liq.* **2019**, *291*, 111327-111340.

[21] X. Pei, K. Zhai, X. Liang, Y. Deng, Y. Tan, P. Wang, K. Xu, *Langmuir* **2017**, *33*, 3787-3793.

[22] C. Ybert, J.-M. Di Meglio, *Langmuir* **1998**, *14*, 471-475.

[23] Z. Wan, X. Yang, L. M. Sagis, *Langmuir* **2016**, *32*, 3679-3690.

[24] N. Bizmark, M. A. Ioannidis, *Langmuir* **2017**, *33*, 10568-10576.

[25] D. Wu, A. Honciuc, *Langmuir* **2018**, *34*, 6170-6182.

[26] S. N. Tan, D. Fornasiero, R. Sedev, J. Ralston, *Colloids Surf. A Physicochem. Eng. Asp.* **2004**, *250*, 307-315.

[27] P. Joos, A. Tomoaia-Cotisel, A. J. Sellers, M. Tomoaia-Cotisel, Colloids Surf. B: Biointerfaces **2004**, *37*, 83-91.

[28] Y. Matsushita, M. Imai, A. Iwatsuki, K. Fukushima, *Bioresour. Technol.* **2008**, *99*, 3024-3028.

[29] A. Ward, L. Tordai, *J. Chem. Phys* **1946**, *14*, 453-461.

[30] R. Miller, E. Aksenenko, V. Fainerman, *Adv. Colloid Interface Sci.* **2017**, *247*, 115-129.

[31] V. Fainerman, A. Makievski, R. Miller, *Colloids Surf. A Physicochem. Eng. Asp.* **1994**, *87*, 61-75.

[32] V. R. Dugyala, J. S. Muthukuru, E. Mani, M. G. Basavaraj, *Phys. Chem. Chem. Phys.* **2016**, *18*, 5499-5508.

[33] A. Teo, K. K. Goh, J. Wen, I. Oey, S. Ko, H. S. Kwak, S. J. Lee, *Food Chem.* **2016**, *197*, 297-306.

[34] A. Klaus, G. J. Tiddy, C. Solans, A. Harrar, D. Touraud, W. Kunz, *Langmuir* **2012**, *28*, 8318-8328.

[35] N. Ghavidel, P. Fatehi, *RSC adv* **2019**, *9*, 17639-17652.

[36] J. Bi, F. Yang, D. Harbottle, E. Pensini, P. Tchoukov, S. b. Simon, J. Sjöblom, T. Dabros, J. Czarnecki, Q. Liu, *Langmuir* **2015**, *31*, 10382-10391.

[37] F. Pan, Z. Li, T. Leyshon, D. Rouse, R. Li, C. Smith, M. Campana, J. R. Webster, S. M. Bishop, R. Narwal, *ACS Appl. Mater. Interf.* **2017**, *10*, 1306-1316.

[38] J. A. Riddick, W. B. Bunger, T. K. Sakano, **1986**.

[39] N. J. Alvarez, S. L. Anna, T. Saigal, R. D. Tilton, L. M. Walker, *Langmuir* **2012**, *28*, 8052-8063.

[40] S. Zeppieri, J. Rodríguez, A. López de Ramos, *J. Chem. Eng. Data* **2001**, *46*, 1086-1088.

[41] B. Duncan, R. F. Landis, H. A. Jerri, V. Normand, D. Benczédi, L. Ouali, V. M. Rotello, *small* **2015**, *11*, 1302-1309.

[42] Y. Zheng, Z. Li, C. Zhang, B. Zheng, Y. Tian, *Food Chem.* **2020**, *311*, 125932.

[43] W. Hoffmann, *Dairy Sci Technol* **2016**, *96*, 251-259.

[44] S. a. Contreras, A. R. Gaspar, A. Guerra, L. A. Lucia, D. S. Argyropoulos, *Biomacromolecules* **2008**, *9*, 3362-3369.

[45] J. Wang, Y. Qian, L. Li, X. Qiu, *ChemSusChem* **2020**, *13*(17) 4420-4427.

[46] H. K. Christenson, *J. Chem. Soc., Faraday Transactions 1: Physical Chemistry in Condensed Phases* **1984**, *80*, 1933-1946.

[47] E. J. W. Verwey, J. T. G. Overbeek, K. Van Nes, *Theory of the stability of lyophobic colloids: the interaction of sol particles having an electric double layer*, Elsevier Publishing Company, **1948,** 90-200.

[48] D. Langevin, *Adv. Colloid Interface Sci.* **2000**, *88*, 209-222.

[49] M. Norgren, H. Edlund, *Nord Pulp Pap Res J.* **2003**, *18*, 400-403.

[50] C. Fritz, C. Salas, H. Jameel, O. J. Rojas, *Nord Pulp Pap Res J.* **2017**, *32*, 572-585.

[51] S. Hill, *Appl Organomet Chem.* **2000**, *14*, 130-131.

[52] V. Garbin, J. C. Crocker, K. J. Stebe, *J. Colloid Interface Sci.* **2012**, *387*, 1-11.

[53] K. J. Huston, A. Kiemen, R. G. Larson, *Langmuir* **2018**, *35*(8), 2898-2908.

[54] H. N. Xu, Y. H. Li, L. Zhang, *Langmuir* **2018**, *34*, 10757-10763.

[55] J. Bergfreund, Q. Sun, P. Fischer, P. Bertsch, *Nanoscale Adv.* **2019**, *1*, 4308-4312.

[56] N. Alipoormazandarani, P. Fatehi, *Langmuir* **2018**, *34*, 15293-15303.

[57] P. X. Li, Z. X. Li, H. H. Shen, R. K. Thomas, J. Penfold, J. R. Lu, *Langmuir* **2013**, *29*(30), 9324-9334.

[58] A. A. Shahir, K. T. Nguyen, A. V. Nguyen, *Phys. Chem. Chem. Phys.* **2016**, *18*(13), 8794-8805.

[59] L. Martínez-Balbuena, A. Arteaga-Jiménez, E. Hernández-Zapata, C. Márquez-Beltrán, *Adv. Colloid Interface Sci.* **2017**, *247*, 178-184.

[60] K. M. Perkins, C. Gupta, E. N. Charleson, N. R. Washburn, *Colloid Surf. A Physicochem. Eng. Asp.* **2017**, *530*, 200-208.

[61] P. X. Li, R. K. Thomas, J. Penfold, *Langmuir* **2014**, *30*(23), 6739-6747.

[62] R. Miller, A. Makievski, V. Fainerman, *Studies in interface science, Vol. 13*, Elsevier, **2001**, 287-399.

[63] B. Sauerer, M. Stukan, J. Buiting, W. Abdallah, S. Andersen, *Langmuir* **2018**, *34*, 5558-5573.

[64] E. Hernández-Baltazar, G. Reyes-Sandoval, J. Gracia-Fadrique, *Colloids Surf. A Physicochem. Eng. Asp.* **2004**, *238*, 113-122.

[65] Z. M. Gao, J. M. Wang, N. N. Wu, Z. l. Wan, J. Guo, X. Q. Yang, S. W. Yin, *J. Agric. Food Chem.* **2013**, *61*, 7838-7847.

[66] M. Joshi, B. Adhikari, P. Aldred, J. Panozzo, S. Kasapis, C. Barrow, *Food Chem.* **2012**, *134*, 1343-1353.

[67] C. Tan, M. C. Lee, A. Abbaspourrad, *ACS Sustainable Chem. Eng.* **2018**, *6*, 16657-16664.

[68] L. Liggieri, F. Ravera, A. Passerone, *Colloids Surf. A Physicochem. Eng. Asp.* **1996**, *114*, 351-359.

[69] F. Ravera, L. Liggieri, A. Steinchen, *J. Colloid Interface Sci.* **1993**, *156*, 109-116.

[70] M. Mahato, P. Pal, T. Kamilya, R. Sarkar, G. Talapatra, *J. Phys. Chem. B* **2010**, *114*, 495-502.

[71] A. Giustiniani, W. Drenckhan, C. Poulard, *Adv. Colloid Interface Sci.* **2017**, *247*, 185-197.

[72] C. Tian, J. Feng, H. J. Cho, S. S. Datta, R. K. Prud'homme, *Nano letters* **2018**, *18*, 4854-4860.

[73] N. Feng, T. Zhao, Y. Zhao, P. Song, G. Li, G. Zhang, *Colloids Surf. A Physicochem. Eng. Asp.* **2020**, *586*, 124215-124227.

[74] T. D. Senra, S. P. Campana-Filho, J. Desbrières, *Eur. Polym. J.* **2018**, *104*, 128-135.

[75] S. Y. Lin, T. L. Lu, W. B. Hwang, *Langmuir* **1995**, *11*(2), 555-562.

[76] C. Wilke, P. Chang, *AIChE J.* **1955**, *1*, 264-270.

[77] L. Bai, S. Lv, W. Xiang, S. Huan, D. J. McClements, O. J. Rojas, *Food Hydrocoll.* **2019**, *96*, 699-708.

[78] J. Surh, E. A. Decker, D. J. McClements, *Food Hydrocoll.* **2006**, *20*, 607-618.

[79] N. Kasiri, M. Fathi, *Int. J. Biol. Macromol* **2018**, *106*, 1023-1031.

[80] G. Pi, Y. Li, M. Bao, L. Mao, H. Gong, Z. Wang, *ACS Sustainable Chem. Eng.* **2016**, *4*, 3095-3102.

[81] K. S. Mikkonen, D. Merger, P. Kilpeläinen, L. Murtomäki, U. S. Schmidt, M. Wilhelm, *Soft Matter* **2016**, *12*, 8690-8700.

[82] Q. Jin, X. Li, Z. Cai, F. Zhang, M. P. Yadav, H. Zhang, *Food Hydrocoll.* **2017**, *70*, 329-344.

[83] S. Zhao, G. Tian, C. Zhao, C. Lu, Y. Bao, X. Liu, J. Zheng, *Food Hydrocoll.* **2018**, *85*, 248-256.

[84] V. S. Kulkarni, *Handbook of Non-Invasive Drug Delivery Systems, CHAPTER 3 - Emulsions and Microemulsions for Topical and Transdermal Drug Delivery*, Elsevier Publishing Company, **2010**, 59-94.

[85] R. T. Shimada, M. S. Fonseca, D. F. Petri, *Colloids Surf. A Physicochem. Eng. Asp.* **2017**, *529*, 137-145.

[86] U. Schmidt, L. Schütz, H. Schuchmann, *Food Hydrocoll.* **2017**, *62*, 288-298.

[87] J. Desbrières, V. Babak, *Soft Matter* **2010**, *6*, 2358-2363.

[88] A. Czaikoski, A. Gomes, K. C. Kaufmann, R. B. Liszbinski, M. B. de Jesus, R. L. da Cunha, *Ind. Crops Prod.* **2020**, *154*, 112762-112773.

[89] C. C. Berton-Carabin, K. Schroën, *Annu Rev Food Sci Technol* **2015**, *6*, 263-297.

Chapter 7: Chemical reactivity and sulfo-functionalization response of hydrolysis lignin

7.1 Abstract

This study focuses on the physicochemical characterization of six different hydrolysis lignin (HL) samples obtained as the by-product of enzymatic hydrolysis of wood biomass. It was revealed that the samples with the least internal ether linkages associated with the highest cleavage of β-O-4 aryl ether and lignin-carbohydrate (LCC) bonds had superior phenolic hydroxyl and carboxylate groups, respectively. These correlations were revealed from a reverse relation observed between the content of identified internal ether linkages by x-ray photoelectron spectroscopy (XPS) and two-dimensional ^{1}H-^{13}C heteronuclear single quantum coherence NMR (2D HSQC NMR) with the hydroxyl group contents from ^{31}phosphorus NMR (^{31}P-NMR) analysis. Moreover, the least sugar content associated with smaller but more porous samples.

The chemical reactivity analysis of unmodified HL samples toward various sulfo-functionalization routes (sulfonation S, sulfomethylation SM and sulfoethylation SE) validated a direct correlation between the degree of substitution (DS) of the functionalized HL and phenolic guaiacyl (G) and condensed hydroxyl group content of unmodified HL. Also, the sugar content and particle size of unmodified HL were reversely related to the DS of sulfo-functionalization of lignin. The highest chemical functionalization was attained for the SM reaction. The HL derivatives of SM and S with adequate water solubility (9-10 g/L), CD (≥1.9 mmol/g) and small particle size (5 μm) were shown to be effective stabilizers for clay suspensions with noticeably reducing the instability index (TSI~10) and settling velocity (-4 %/h) of clay particles in the suspension.

Keywords: Hydrolysis lignin, Physicochemical properties, Sulfo-alkylation, Chemical reactivity.

7.2 Introduction

Biochemicals and biofuels from wood biomass are green replacements for synthetic chemicals from petrochemicals.[1] Enzymatic hydrolysis is a well-known process for fractionating lignocellulosic materials into cellulosic ingredients and lignin.[2,3] In this process, cellulosic materials are considered the main product for biochemical or biofuel productions and lignin is regarded as an undesired by-product.[2,3] On the other hand, the pulp and paper industry is generally known as a traditional source of lignin production, mostly in the form of kraft or lignosulfonate.[4] Despite their interesting properties, the sulfur content of kraft lignin and lignosulfonate may limit their potential applications.[5] Although hydrolysis lignin, HL, is not a 100% sulfur free by-product,

its sulfur content is much lower (≤1%) than KL or LS (1-8%), which may promote its potential use.[6]

Structurally, the mild conditions of enzymatic processes of biomass would impart less internal bonding deprivation in HL, and it was reported that HL might even exist in the form of lignin-carbohydrate complex (LCC).[7, 8] Moreover, the functional groups, such as phenolic hydroxyl and alcoholic hydroxyl, of HL are considered preserved compared to other lignin resources.[9] Owing to these interesting characteristics, the potential use of HL in many applications may need to be explored. However, obtaining precise knowledge of the physicochemical properties of HL is required for advancing its utilization. The most frequently technique to identify the ether bond including LCC bond is the two-dimensional ^{1}H-^{13}C heteronuclear single quantum coherence nuclear magnetic resonance spectroscopy (2D-HSQC NMR), because it avoids the issue of overlapping peaks in the single proton or carbon NMR.[10] However, this method is usually implemented for a comparative analysis between samples rather than yielding quantitative information, because the cross-peaks and the concentration of chemical groups in the sample are not exactly proportional.[11] Moreover, 1D ^{31}phosphorus NMR (^{31}P-NMR) analysis is an established method to quantify the hydroxyl functional groups of lignin samples.[12] As HL is a relatively unknown material with complicated structure, the main objective of this work was to assess the physicochemical properties of HL following various analytical techniques. The physicochemical characteristics of lignin could affect its reactivity toward varied modification reactions.[13] In this respect, lignin originating from different sources (e.g., hardwood, softwood and annual plants) and technical processes (e.g., organosolv, kraft, soda, and sulfite pulping) were previously studied with respect to their reactivity toward phenolation,[14] oxyalkylation,[15] esterification[16] and Mannich reaction.[17] However, HL did not receive the deserved attention for its valorization. Valorizing HL will not only help with the proper use of HL, but also could promote the enzymatic hydrolysis of biomass as a feasible technique to generate valuable products. To valorize HL, Zhang and Fatehi[9] reported on the production of a HL based coagulant by the periodate oxidation of HL. In another study, HL was activated using a NaOH/urea aqueous solution to enhance its sulfonation degree and dispersion property.[18] Despite these specific studies on one type of HL, to the best knowledge of the authors, there is no report for correlating the physicochemical properties and reactivity of various HL samples toward chemical sulfo-functionalization.

The sulfo-functionalization of lignin is among the facile approaches to alter the physicochemical properties of lignin to produce potential dispersants or emulsifiers.[19] The most received facile sulfo-functionalization pathways of lignin are sulfonation, sulfo-methylation and sulfo-ethylation.[20-21] Structurally, these chemical routes modify lignin in different ways. For example, the sulfur containing functionality may occur on aliphatic, aromatic hydroxyl or directly on the aromatic ring of lignin following these sulfo-functionalization pathways. Hence, the second objective of this work was to evaluate the chemical reactivity of HL with variable physicochemical properties towards sulfonation, sulfo-methylation and sulfo-ethylation to identify the most suitable and effective approach for valorizing HL.

Sulfo-functionalized kraft lignin products were previously used as dispersants for the stabilization of cement, dye or inorganic suspensions.[23-27] To study the performance of sulfo-functionalized HL as value-added products, the dispersion performance of these products in a clay suspension was comprehensively studied. The novelties of this work are to develop 1) a precise correlation between the physicochemical properties of HL samples 2) a correlation between the physicochemical properties and chemical reactivity of HL for sulfo-functionalization reactions and 3) the effectiveness of functionalized HL derivatives as dispersants for clay suspensions.

7.3 Experimental Sectıon

7.3.1 Materials

Six enzymatically hydrolyzed lignin (HL) samples were received from FPInnovations, Pointe Claire, QC, Canada and were named HL1-HL6. Initially they were produced based on the patented technology of a biomass fractionation process[2] and then were chemically or physically modified to a variable extent. The hydrolysis process using cellulolytic enzymes was reported to carry out at a pH between 3 to 9, temperature 10-80 °C, biomass consistency of 2-30% for up to 144 hours.[2] Clay was supplied from Old Hickory Clay Company, Hickory, KY, USA. The following chemicals were purchased from Sigma-Aldrich (Canada) and used without further purification: deuterated chloroform ($CDCl_3$), pyridine (C_5H_5N), cyclohexanol ($C_6H_{12}O$), chromium (III) acetylacetonate, 2-chloro-4,4,5,5-tetramethyl-1,3,2-dioxaphospholane, sulfuric acid (98 wt%), sodium hydroxide pellets, sodium sulfite (Na_2SO_3), formaldehyde (CH_2O 37 wt.%), 2-bromoethanesulfonate salt (NaBES 98%), polydimethyldiallyl ammonium chloride (PDADMAC 100,000–200,000 g/mol), para-hydroxybenzoic acid, silicon oil, and poly (ethylene oxide). Dialysis membrane (Cut off of 1,000 g/mol) was provided by Spectrum Labs. Deionized water

with a resistivity of less than 18 MΩ/cm was generated using a Millipore water purification system, and it was used for all the experiments conducted in this study.

7.3.2 ^{31}P NMR and ^{1}H-^{13}C HSQC Analysis of HL samples

The hydroxyl functional groups of HL samples were determined following the established ^{31}P-NMR analysis.[28] At first, phosphitylation reaction was conducted with (2-chloro,4455-tetramethyl-1,3,2 dioxaphospholane). In this experiment, 24 mg of HL samples was dissolved in a 1.6/1 v/v chloroform-d (CCl_3D) and pyridine (C_5H_5N) solvent mixture. Cyclohexanol (0.20 mmol/mL) and chromium (III) acetylacetonate (0.20 mmol/mL) solutions were added to the sample solution as the internal standard and relaxation agent, respectively. After stirring for 1 h and complete solubility of H-lignin samples, 100 µL of phosphitylation agent was added and reacted for another 1 h. A 90° pulse width and a 5 s relaxation delay with 128 acquisitions were followed to acquire ^{31}P-NMR spectra. The peak assignments were followed as previously described in the literature.[28]

For the ^{1}H-^{13}C HSQC experiment, 50 mg of HL samples was added to 0.7 mL of deuterated dimethyl sulfoxide, DMSO-d6, and stirred at 45 °C overnight. The following adjustments were implemented using a standard Bruker pulse sequence; 13 ppm spectra width in F2 (1H) dimension with 1024 data points (95.9 ms acquisition time), 210 ppm spectra width in F1 (13C) dimension with 256 data points (6.1 ms acquisition time), a 90° pulse, 0.11 s acquisition time, 1.5 s pulse delay, 1JC-H of 145 Hz and 48 scans.[12] NMR data were processed using the TopSpin 4.1.1 software (Bruker BioSpin).

7.3.3 Sugar analysis

For determining carbohydrate content of the HL samples, the samples were hydrolyzed with 4 wt% sulfuric acid at 120 °C for 1 h to convert all poly sugars to mono sugars following the procedure described by Liu.[29] The content of mono sugars was then determined using an ion chromatography (IC) unit (Dionex ICS-5000+ DP. Thermo Scientific) equipped with Dionex CarboPac SA10 column, Thermo Scientific, and pulsed amperometric detector (Thermo Scientific Electrochemical Detector). KOH was used as the eluent with the 1 mM concentration and 1 mL/min flow rate.

7.3.4. Surface area analysis (BET). The samples were initially dried in an oven at 105 °C overnight and before analysis, 0.05 g of sample was pretreated for 4 h at 250 °C. Branuer-Emmett-Teller (BET) method was followed via adsorption-desorption isotherms using nitrogen gas at the

pressure range of 0.01 and 0.99 Pa at -180 °C with a Quantachrome surface area analyzer, Nova2200e (USA) to determine the specific surface areas of HL samples.

7.3.5 X-ray Photoelectron Spectroscopy (XPS)

The surface chemical compositions of the different HL samples in the powder form were analyzed using X-ray photoelectron spectroscopy (XPS) measurements. Oven-dried HL powders were transferred onto a double-sided carbon tape and measurements were performed on a Kratos Axis Supra with a monochromatic Al Kα radiation (1486.7 eV) operating at 15 kV (90 W) in a FAT mode (fixed analyzer transmission) with a pass energy of 40 eV for the ROI region and 80 eV for the survey region. The high-resolution XPS spectra of the samples were analyzed using ESCApe software.

7.3.6 Sulfoalkyation of lignin

In our previous studies, varied sulfo-functionalization routes were investigated under different reaction parameters, such as time, temperature, molar ratio using kraft lignin.[20-21] Based on these systematic studies, appropriate reaction conditions were chosen for sulfo-functionalization of HL samples in the present work.

7.3.6.1 Sulfonation

In this set of reactions, [20] 0.5 g of HL samples were dispersed in water in a three-neck flask with a magnetic stirrer to make a 15 g/L lignin concentration, then Na_2SO_3 powder in the molar ratio of 1/1 was added to the mixture. The reaction medium was adjusted to pH≈11 with NaOH solution (1M) and was transferred to a water bath heating at 90 ℃ for 3 h. The solution was then cooled to room temperature, neutralized with 5% H_2SO_4(aq) and then kept in membrane dialysis for two days, while changing the water every 2 h for the first 6 h and then once a day for two days for purification. Then, the dried sulfonated H-lignin samples were obtained by evaporating the water of solutions at 60 ℃ in an oven and the samples were named S1- S6.

7.3.6.2 Sulfomethylation

The sulfomethylation of HL samples was conducted as previously described.[21] A 40 g/L lignin solutions were prepared in a three-neck flask, which was followed by the addition of formaldehyde (37 wt.%) at the formaldehyde to lignin molar ratio of 1.4/1. The solutions were adjusted to pH≈11 with NaOH solution (2.5 mol/L) and were heated in a water bath at 75 ℃ for 2 h. Then, Na_2SO_3 powder was added to the mixture at the Na_2SO_3 to lignin molar ratio of 1/1 and allowed for reaction

for another 3 h at 90 ℃. After completion of the reaction, the purification and drying steps were followed as explained in the previous section. The samples were named SM1-SM6.

7.3.6.3 Sulfoethylation

Sulfoethylated HL samples were produced following our previous work.[22] Shortly, grounded HL powder (0.5 gr) was dispersed in deionized water in a three-neck flask to make a 20 g/L suspension. The pH of the suspension was adjusted to 11 by adding 1M NaOH solution. Then, 2-bromoethanesulfonate salt (NaBES) was fed to the reaction medium at the NaBES to HL molar ratios of 2/1. The reaction was heated in a water bath at 80 ºC for 4 h. After completion of the reaction, the purification and drying steps were followed as explained in the previous section. The samples were named SE1-SE6.

7.3.7 Charge density and solubility analysis

The solubility and charge density of HL derivatives were obtained according to the process described previously[30] using a Particle Charge Detector (BTG Mutek, PCD 03, Germany).

7.3.8 Elemental analysis

The elemental analysis of unmodified and HL derivatives was performed using an Elementar Vario EL Cube elemental analyzer by a combustion analysis method. The samples were first dried in a 105 °C oven overnight in order to remove any moisture. Approximately, 2 mg samples were weighed and loaded in the integrated carousel of the elemental analyzer. Furthermore, the samples were automatically transferred into a combustion tube and burned at 1200 °C. The reduced combustion gases were further analyzed for carbon, hydrogen, nitrogen, and sulfur contents of the samples. The oxygen content was determined by a mass balance.

The degree of substitution (DS, mol/mol) for the sulfoalkylation reactions was calculated based on the sulfur content of the samples according to equation 2.[31]

$$DS = \frac{180\times(S_{SL}-S_{HL})/32}{M_w-32\times(S_{HL})} \qquad (2)$$

Where 180 (g/mol) was considered as the molecular weight of lignin, 32 (g/mol) was the atomic mass of sulfur element, S_{SL} was the sulfur content of S, SM or SE and S_{KL} was the sulfur content of KL. M_w was the molecular weight of grafted groups onto lignin (M_w = 80 g/mol for S, M_w = 94 g/mol for SM and M_w = 108 g/mol for SE).

7.3.9 Particle size

The average particle size of unmodified HLs and their derivatives in an aqueous system was determined using a laser diffraction particle size analyzer (Malvern Mastersizer 3000,

Worcestershire, UK) at the room temperature. In this set of experiments, the aqueous suspensions of all samples (3 wt.%) were stirred overnight prior to the test at room temperature. Then, 1 mL of each suspension was introduced to a chamber containing 700 mL of water under stirring (1000 rpm). The particle size distribution based on D [3,2] was measured using the instrument software (Malvern 3000).

7.3.10 Dispersion analysis

The dispersibility of clay suspension was investigated in the presence of unmodified HLs and their derivatives using a Turbiscan Lab Expert, Formulaction, France. In this set of experiments, clay suspensions (100 g/L) were prepared in the presence of HL and its derivatives at the fixed dosage of 16 mg/g clay in a water bath shaker at 150 rpm and 30 °C for 1 h. The changes in the stability of the suspensions were analyzed for 2 h by scanning the cell vertically every 2 min at 30 °C. Based on the obtained data, the destabilization index was determined using Turbisoft 2.1 software. The velocity of particle settlement (%) based on the slope of backscattered light changes vs time was obtained using the Turbisoft 2.1 software.

7.3.11 Zeta potential

The zeta potential of the dispersed clay suspensions in the presence or absence of HL derivatives was measured using a ZetaPALS analyzer (Brookhaven Instruments Corp, USA). In this experiment, 0.4 mL of clay suspensions from the dispersed portion of clay suspensions were separated by a pipette and diluted with 20 mL of filtered KCl solution (0.1 mM), and 3 mL of the solutions were transferred to glass cells for the zeta pontifical analysis.

7.4 Results and discussion

7.4.1 Physicochemical characterization of HL

The HL samples were characterized for their chemical composition, sugar content, functional groups and specific surface area and the results are summarized in Table 1.

Table 7.1. Physicochemical properties of different H-lignin samples.

Sample	Elemental compositions, wt.%*				Total sugar% **	Hydroxyl groups, mmol/g***					Surface area, m^2	D [3,2], µm (±3)
	C	H	S	O		OH Aliphatic	Ph-OH (Cond.)	Ph-OH (S)	Ph-OH (G)	CO OH		
HL1	53.6	6.3	0.1	40.0	30.0	3.58	0.17	0.30	0.18	0.03	17.0	38
HL2	54.0	6.5	0.1	39.5	29.5	3.00	0.22	0.24	0.17	0.10	17.6	35
HL3	55.0	6.3	0.8	36.0	22.5	8.37	0.47	2.00	0.76	0.01	40.3	26

HL4	59.7	6.3	1.5	32.2	19.5	4.38	3.42	0.68	1.15	0.52	48.4	22
HL5	57.0	6.3	1.2	34.0	16.0	8.51	3.9	0.65	1.36	0.37	37.9	21
HL6	58.0	6.4	1.2	33.9	24.5	3.43	1.65	0.36	0.56	0.21	33.9	30

[a] Elemental analyzer

[b] IC

[c] ^{31}P-NMR

The HL samples had 0.1 to 1.5 wt% sulfur, which may originate from wood or sulfuric acid used in the HL samples treatment.[32] It is observed that HL1 to HL3 had a lower carbon composition, but higher oxygen compared to HL4 to HL6. The HL samples had substantial sugar content associated with the existence of lignin-carbohydrate complexes (LCC) in the samples.[7,8,33] Also, samples with a higher oxygen content had a higher sugar content (Table 1). The type of HL samples was identified to be G/S based on the identified syringyl and guaiacyl structures in 2D-HSQC correlations (will be discussed later). With that consideration, the detectable -OH groups for the samples based on their ^{31}P NMR spectra were aliphatic OH (145-150 ppm), phenolic OH including C5 substituted condensed phenolic OH, 5-5 (140.1-141.6 ppm), and β-5 (143.6-144.5 ppm), syringyl phenolic OH (S) (142-143.6 ppm), guaiacyl phenolic OH (138.8-140.1 ppm), and carboxylic acid OH (133.6-136.6 ppm).[12]

Correlations were made between the chemical and physical properties of HL and the results are shown in Figure 1a-c. Generally, the reduction in the sugar content of the samples led to an increase in the Ph-OH content of the samples. As accessibility to reaction sites/groups and thus surface area is a critical parameter in the sulfoalkylation of lignin, the properties of the HL were reported in regard to their surface area by dividing the mass-based properties of the samples by their surface area (Table 1). With this change, it can be assumed that all groups are accessible and, for example, located on the surface of the samples. A linear correlation (R^2= 0.76) between Ph-OH and sugar content of samples was seen in Figure 1a, suggesting that the reduction in sugar would moderately lead to a predictable Ph-OH increase in the HL. However, such a correlation was not observed with aliphatic OH content (R^2=0.23, Figure A4.1 in appendix material). The correlation of physical and chemical properties of the samples are depicted in Figures 1b and 1c. Interestingly, the sugar content of the samples was inversely related to its pore volume and particle size, while its Ph-OH was directly correlated with its pore volume and particle size. These results suggest that by reducing sugars, the samples became smaller but more porous, and more Ph-OH of the samples would be exposed/available (Figures 1b and 1c).

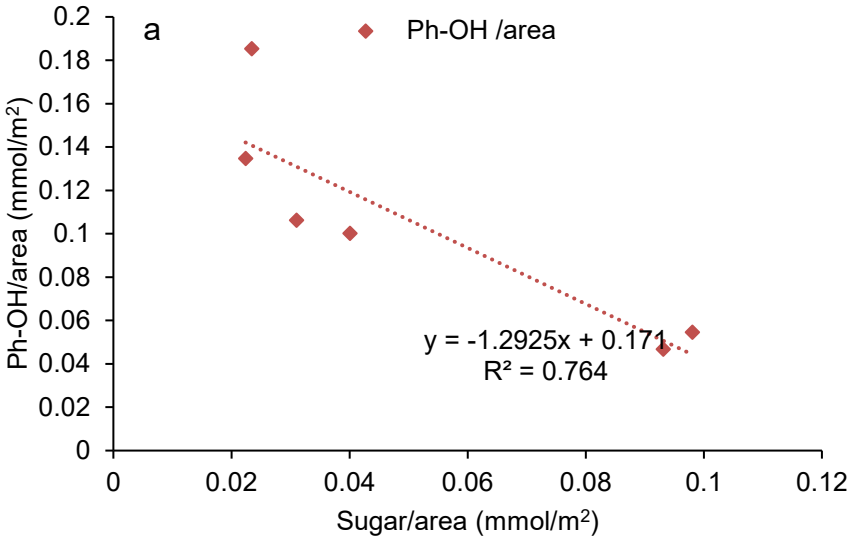
a
Ph-OH /area
Ph-OH/area (mmol/m²)
Sugar/area (mmol/m²)
y = -1.2925x + 0.171
R² = 0.764
0.2
0.18
0.16
0.14
0.12
0.1
0.08
0.06
0.04
0.02
0
0
0.02
0.04
0.06
0.08
0.1
0.12

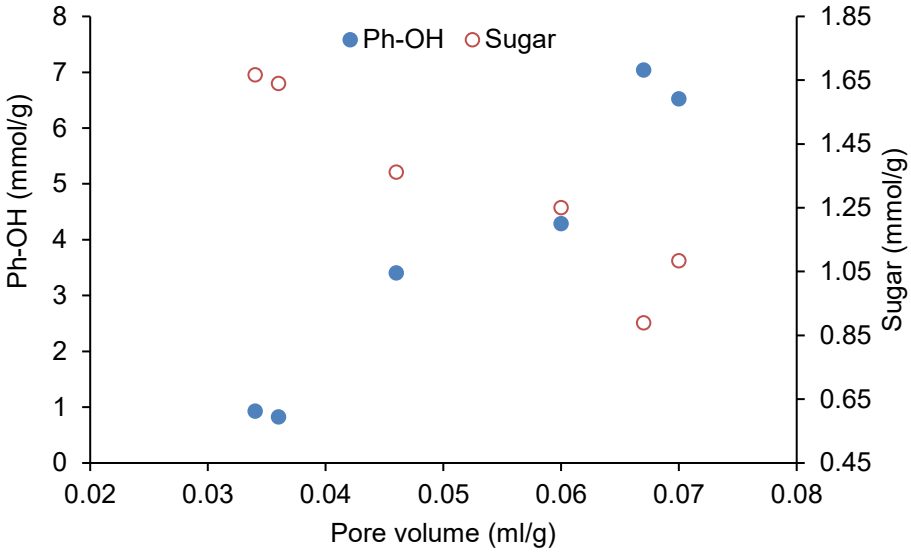
Ph-OH
Sugar
Ph-OH (mmol/g)
Sugar (mmol/g)
Pore volume (ml/g)
8
7
6
5
4
3
2
1
0
1.85
1.65
1.45
1.25
1.05
0.85
0.65
0.45
0.02
0.03
0.04
0.05
0.06
0.07
0.08

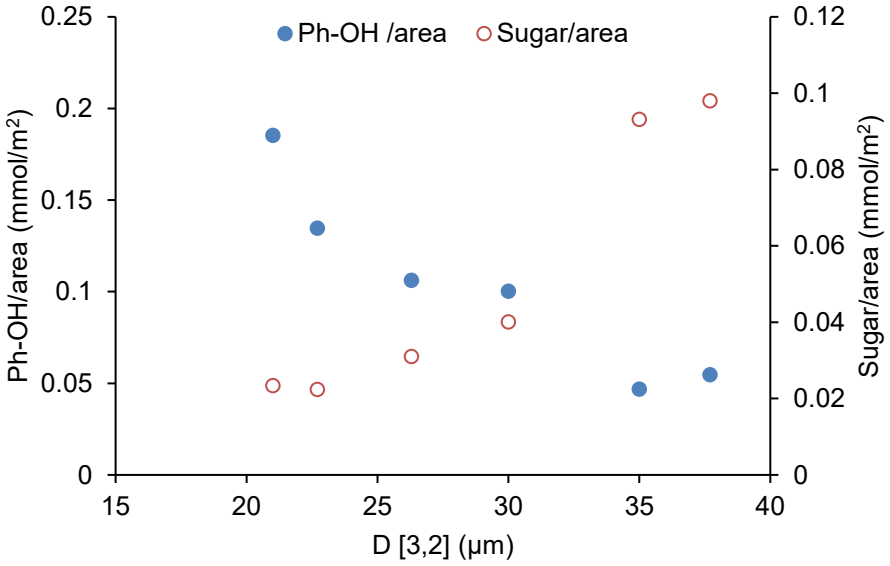
Ph-OH /area
Sugar/area
Ph-OH/area (mmol/m²)
Sugar/area (mmol/m²)
D [3,2] (μm)
0.25
0.2
0.15
0.1
0.05
0
0.12
0.1
0.08
0.06
0.04
0.02
0
15
20
25
30
35
40

Figure 7.1: Correlations between chemical and physical properties of HL samples. The sugar content is deducted from the reported Ph-OH data in all figures.

To further explore the correlation between the chemical characteristics of the samples, the internal chemical bonds of HL samples were quantitatively examined by the XPS analysis and verified by 2D-HSQC NMR. The modeling for the mentioned bonds from C1s peak of XPS for different HL samples are shown in Figure 2 and quantitative results are summarized in Table 2. In general, the C 1s peak from XPS spectra derived from individual peaks corresponding to C-C linkages (≈285 eV), C-O linkages in ethers and alcohols (≈286 eV), C=O linkages in acetals (≈288 eV) and O-C=O linkages in esters (≈289 eV).[34]

It is noticeable that the composition of internal bonds varies depending on the HL, while the distinctive variation is evident for C-C and C-O composition bonds. Two type of variations are notable among samples, C-O > C-C (for HL1 and HL2) or C-C > C-O for the rest of the samples. The higher sugar content in HL samples (Table1) might have contributed to the elevated ether bond in HL samples that will be further discussed from HSQC analysis.[35,36] The C3 (C=O) bond associated with internal linkages among propyl alcohol units of lignin slightly varied among various samples. A variation is more noticeable in C4 (O-C=O) bond that is linked with carboxylate group and is predominant for HL4 and HL5, which supports the results of the P-NMR analysis in Table 1.

Linear or cyclic C-O-C bonds are considered to be the most important bonding in lignin, where the nonphenolic β-O-4 is the most abundant ether linkage in lignin.[37-39] The cleavage of β-O-4 bond is known to generate phenolic units.[40] Moreover, the presence of carbohydrate would associate with elevated ether linkages known as LCC bonds.[37-39] The cross-peaks analysis of HSQC was considered to qualitatively compare these ether bonds in HL samples as depicted in Figure 3. The cross-peaks of carbohydrates are visible in δ_C/δ_H 70-75/3-3.5 ppm in all samples.[41] In addition, β-O-4 and LCC bonds were identified and HL1-HL3 are associated with the highest distribution of β-O-4 (δ_C/δ_H 60.0/3.2-3.9, 72.6/4.8 and 83.8/4.2 (G) ppm) and two distinguishable LCC bonds namely, phenylglycoside PG (δ_C /δ_H 99.5-100/4.28-5.17 ppm) and γ-ester GE (δ_C /δ_H 62.0-65.0/4-4.5 ppm).[41] However, only β-O-4 at δ_C/δ_H 60.0/3.2-3.9 ppm and PG as the LCC bonds were identified for HL4 and HL5. The content of β-O-4 and LCC bonds is comparatively higher for HL6 compared to HL4 and HL5. Therefore, the analysis of HSQC data confirmed that the

higher C-O linkage in HL1-HL3 samples is indeed related to the β-aryl ether and LCCs bonds,[37] while this linkage had comparatively fewer distribution in HL4 and HL5 samples. In addition to the information from the internal linkages, the comparison of HSQC cross-peaks with hydroxyl groups content from P-NMR, reveals the direct relation of higher cleavage of β-O-4 in HL4 and HL5 samples with their highest phenolic hydroxyl content as was similarly reported elsewhere.[12] The lack of β-O-4 at cross-peaks of δ_C /δ_H 83.8/4.2 ppm (G) and 72.6/4.8 ppm in these two samples, are associated with the highest content of G and condensed phenolic hydroxyl in them. Another interesting correlation is associated with the fewer LCC bonds in HL4 and HL5 (lacks GE), which is correlated with the higher carboxylate groups in these two samples (Table 1 and 2). This direct correlation between LCC bond and carboxylate group content was reported to connect with the cleavage of the ester bonds from lignin-carbohydrate linkages.[12,42] Moreover, the higher contribution of condensed Ph-OH of HL4-HL6 are visualized from the cross-peaks associated with these structures namely, phenylcoumaran (β-5) (C) and Dibenzodioxcin (5-5) (DBD)[41] as labeled in Figure 3, which are not observed in HL1-HL3 due to the very low content.

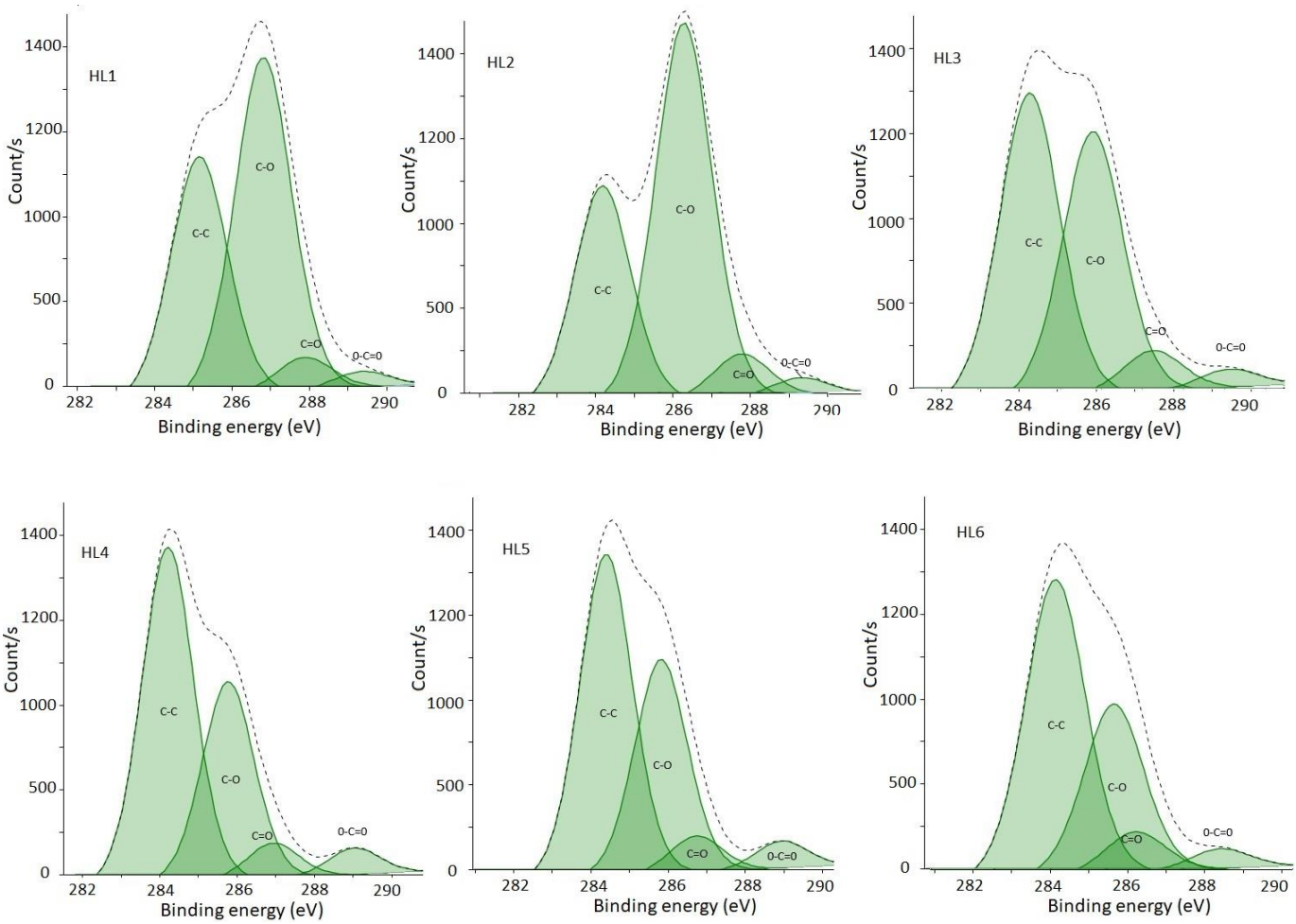

Figure 7.2: XPS spectra of C 1s for HL1-HL6 samples.

Table 7.2. Quantitative chemical bonds at the surface of HL samples as determined by XPS analysis.

Sample	C 1s mass conc. %			
	C1 (C-C)	C2 (C-O, C-O-C)	C3 (C=O)	C4 (O-C=O)
HL1	38.31±2.21	53.49±2.43	6.60±2.01	2.72±1.16
HL2	33.19±1.16	57.41±1.29	6.68±0.96	2.72±0.63
HL3	48.52±2.44	41.83±2.40	6.62±1.39	3.02±1.30
HL4	56.27±1.76	33.26±1.65	5.90±0.94	4.53±0.95
HL5	53.62±2.0	35.67±1.74	6.10±1.70	4.59±0.98
HL6	56.13±1.87	32.11±1.79	7.83±2.09	3.93±0.94

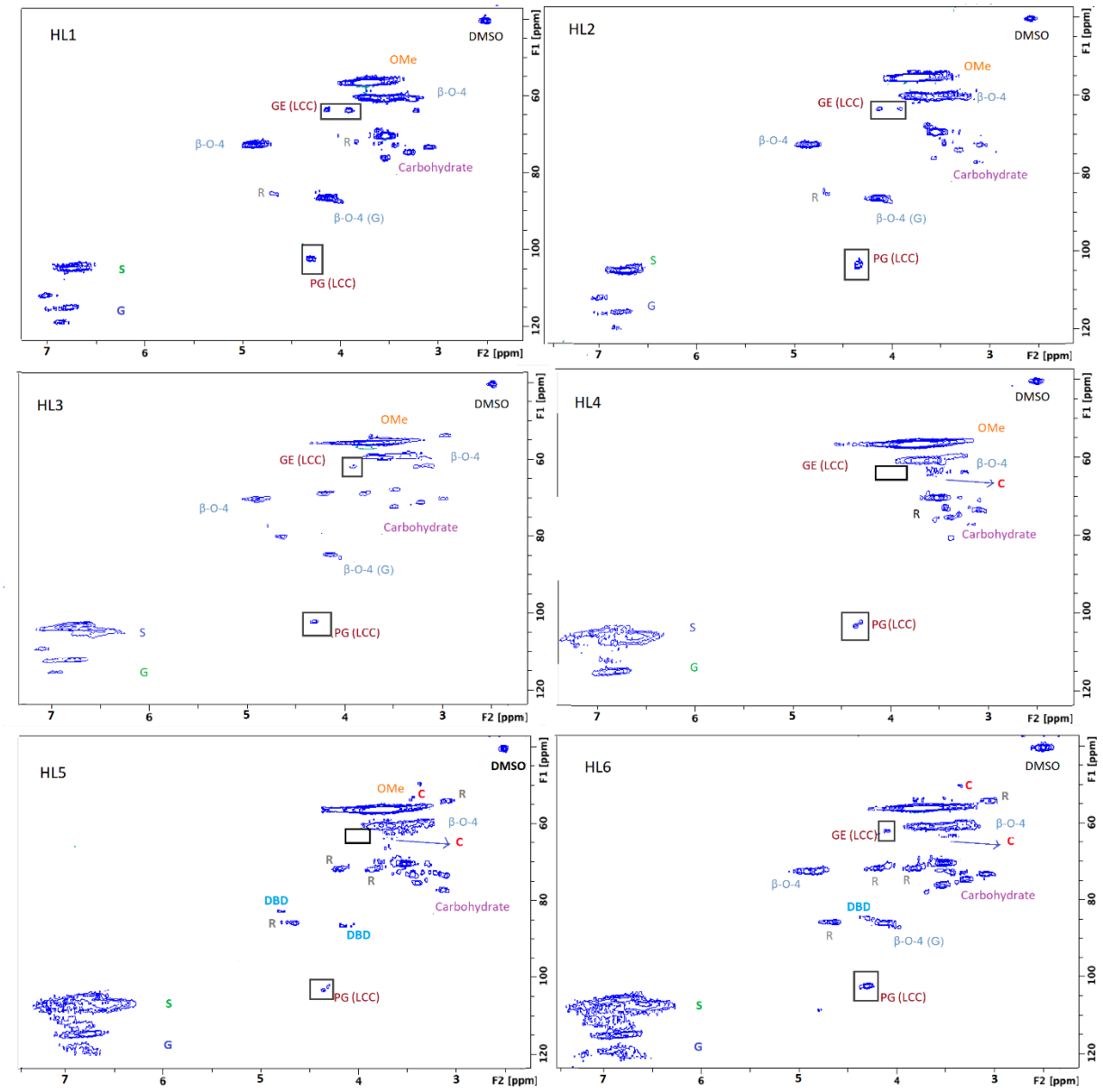

Figure 7.3: 2-D HSQC spectra of HL1-HL6 samples. The identified cross peaks are: β-O-4, β-O-4 Aryl ether; β-O-4 (G), β-O-4 aryl ether in Guaiacyl; GE (LCC), γ-ester; PG (LCC), Glycoside; OMe, Methoxy group; S, Syringyl; G, Guaiacyl; C, Phenylcoumaran (β-5); DBD, Dibenzodioxcin (5-5); R, Resinol.

7.4.2 HL chemical reactivity towards sulfo-alkylation reactions

To find out the chemical reactivity of different HL samples, three different routes of sulfo-alkylation reactions with known substitution mechanisms were evaluated. To distinguish the

reactivity differences, first various mechanisms of chemical reactions are briefly explained in here, while detailed explanations with schemes are provided in the appendix data (Figure A4.2).

Sulfonation (S) tends to occur at the α-position of aliphatic chain of lignin in an alkaline environment due to the formation of a quinone methide intermediate with phenolic substrates as the first step. Next, sulfite addition happens at the α position and further at the β position, resulting in the cleavage of the β-aryl ether bond.[20,43] Sulfomethylation (SM) reaction starts with an electrophilic addition of formaldehyde on the ortho position of Ph-OH after the dissociation of OH groups in an alkaline medium.[21] Then, the substitution of new methyl hydroxyl group occurs in the presence of sulfite ions. Lastly, sulfoethylation (SE) reaction follows a nucleophilic substitution on the bromine atom of SEB substrate with dissociated hydroxyl nucleophiles of HL in an alkaline medium.[22]

The reactivity of different HL samples toward described chemical reactions were compared based on the water solubility, charge density (CD), degree of substitution DS (based on elemental analysis), and particle size of the products, and the results are summarized in Table 3. Overall, the observation of the results shows the higher CD and DS in the order of SM>S>SE modifications for most of the samples. Among all samples, HL1 and HL2 had the lowest reactivity with DS ≤0.009 mol/mol for all the reactions. HL3 and HL6 showed higher reactivity compared to HL1 and HL2 and obtained the DS between 0.04-0.08 mol/mol with a CD of 0.7-1.8 mmol/g. The most reactive samples were HL4 and HL5 with a CD between 1.9 and 2.2 mmol/g for the S and SM reactions. Interestingly, the particle size of HL derivatives reduced greatly for most of the HL samples after modification compared to the unmodified HL (Table 1) except for HL1 and HL2.

Table 7.3. Characterization of sulfo-functionalized HL derivatives.

Derivative	Modification route	Solubility (g/L) (±1)	Charge density (mmol/g) (±0.1)	DS (mol/mol) (±0.001)	D [3,2], μm (±3)
S1		2.0	0.4	0.001	25
S2		2.0	0.4	0.004	26
S3		5.0	1.5	0.07	9
S4	S	8.5	1.9	0.11	7
S5		9.0	2.0	0.14	6
S6		6.3	1.2	0.06	15.8
SM1		2.1	0.4	0.006	30
SM2	SM	2.1	0.4	0.006	28

SM3		5.2	1.8	0.08	15
SM4		9.5	2.2	0.14	4
SM5		9.5	2.0	0.12	5
SM6		6.5	1.4	0.07	14
SE1		1.5	0.2	0.003	32
SE2		1.5	0.2	0.006	33
SE3		4.5	1.0	0.02	17
SE4	SE	6.8	1.2	0.03	14
SE5		6.5	1.1	0.05	13
SE6		6.0	0.8	0.01	16

To find out the influential reactivity factors of the samples toward the chemical modifications, different properties of the unmodified HL samples were correlated with the DS of modified ones and the graphs are shown in Figure 4 a-d.

The content of G type and condensed phenolic hydroxyl groups of samples showed almost a linear correlation with the DS of all reactions (Figure 4 a-b), implying that by increasing the phenolic G and condensed phenolic content the DS for all three reactions were improved. This correlation was stronger with G ($R^2 \geq 0.7$) than condensed phenolic ($R^2 \approx 0.7$). However, such correlation was not observed for the aliphatic OH content of HL (appendix material, Figure A4.3).

Moreover, from the correlations in Figure 4c, it is evident that the higher sugar content of samples with higher LCC bonds (Figure 3) tied to less reactivity and thus DS of HL samples. This should associate with less accessibility of functional groups to chemicals for progressing with reactions when attached to higher carbohydrate content.[12]

As depicted in Figure 4d, the particle size of HL samples was also reversely correlated to the DS of reactions. Apparently, the functional groups of smaller but more porous HL (Table 1) promote accessibility to chemicals for the reaction.

It is notable that despite the observed correlations between physicochemical properties of samples and the DS of reactions, S and SM modifications were more effective than SE reactions in all graphs. This fact speaks of the important role of various mechanisms of sulfo-alkylation reactions on chemical reactivity.

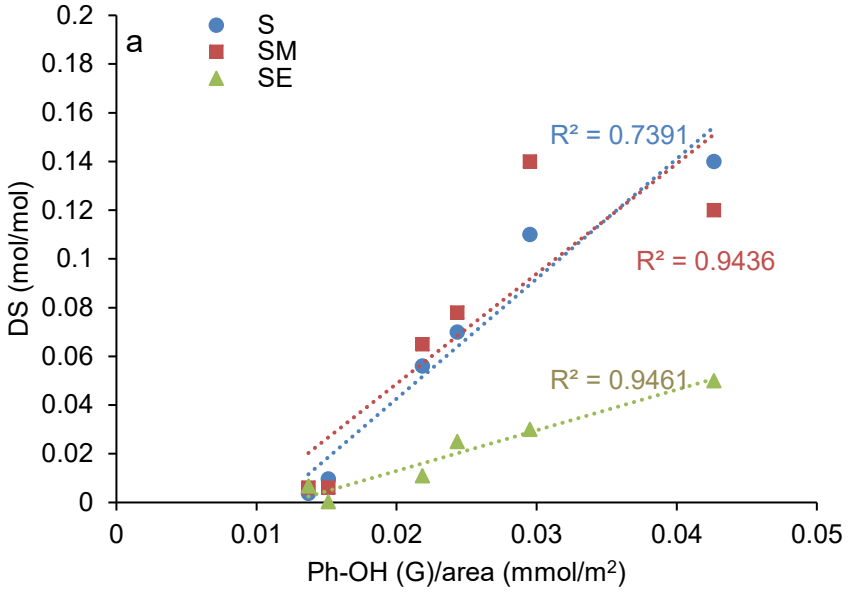
a
S
SM
SE
R² = 0.7391
R² = 0.9436
R² = 0.9461
DS (mol/mol)
Ph-OH (G)/area (mmol/m²)
0.2
0.18
0.16
0.14
0.12
0.1
0.08
0.06
0.04
0.02
0
0
0.01
0.02
0.03
0.04
0.05

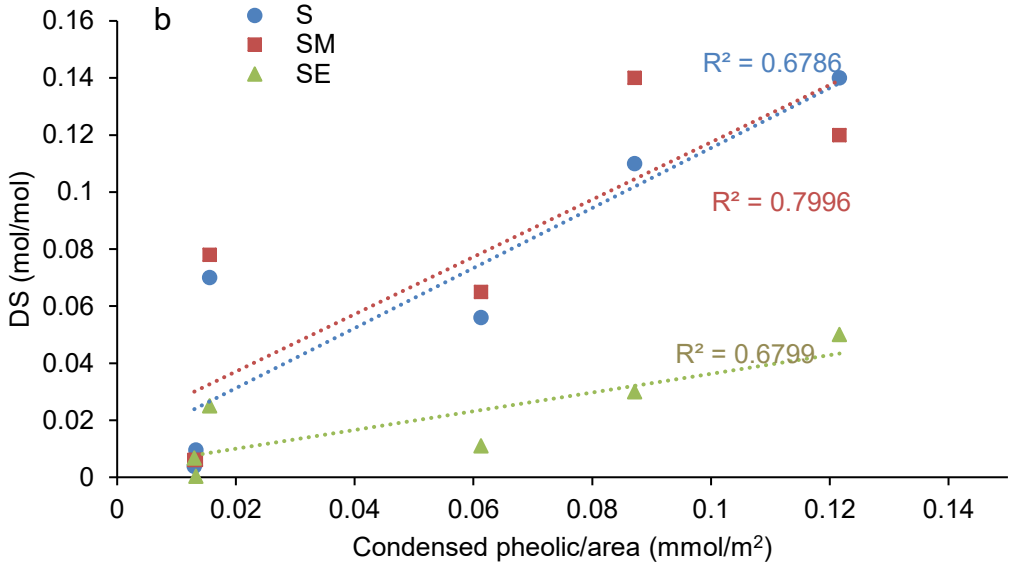
b
S
SM
SE
R² = 0.6786
R² = 0.7996
R² = 0.6799
DS (mol/mol)
Condensed pheolic/area (mmol/m²)
0.16
0.14
0.12
0.1
0.08
0.06
0.04
0.02
0
0
0.02
0.04
0.06
0.08
0.1
0.12
0.14

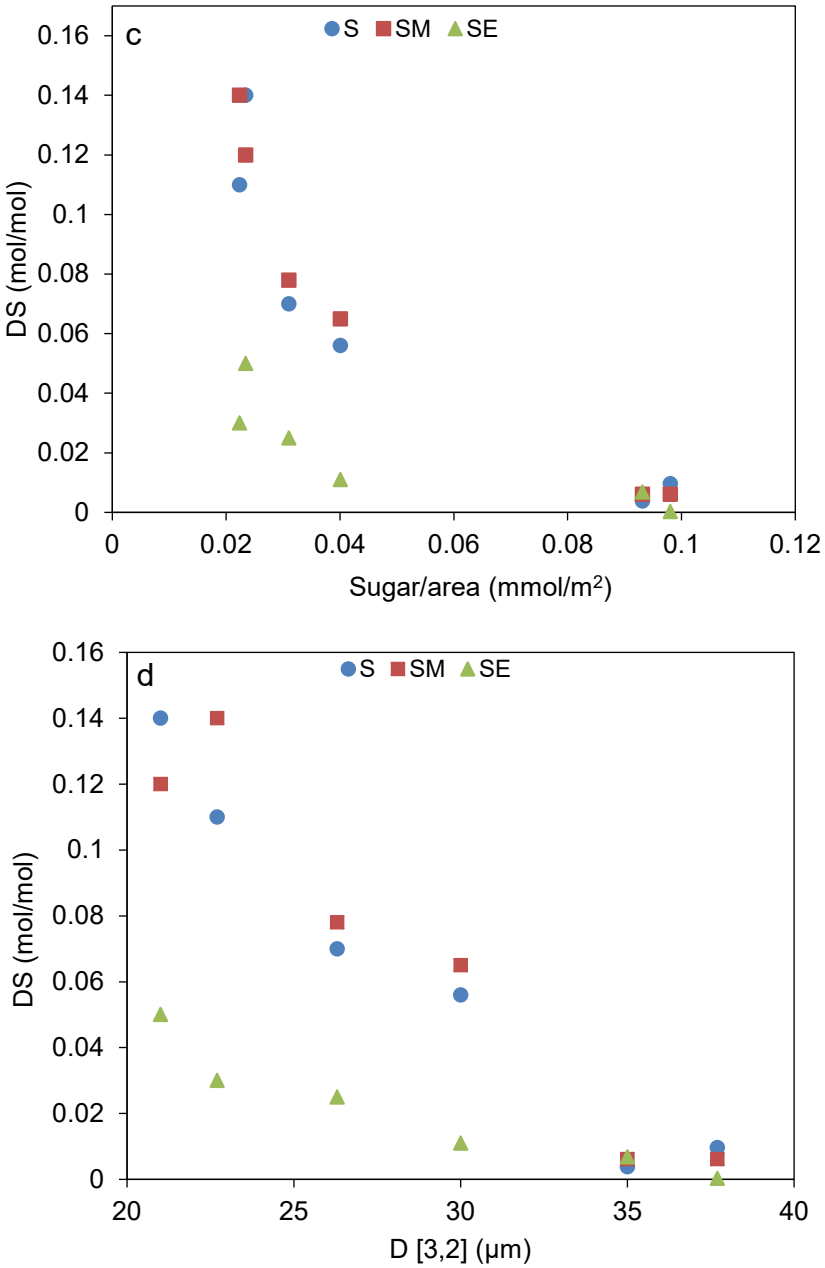

Figure 7.4: Correlation between DS (mol/mol) of the substitution reactions (S, SM and SE) with a) Ph-OH (G) b) condensed Ph-OH (the sugar content is deducted) c) sugar content of samples, and d) particle size D [3,2] of unmodified HL samples.

7.4.3 Dispersion evaluation

The effectiveness of different sulfo-functionalized HL derivatives was evaluated as dispersants for stabilizing mineral clay suspensions to identify the most effective route of modification. The clay particles tend to agglomerate and settle over time due to the lack of electrostatic or steric repulsion

among particles.[44] The basal faces of clay particles carry a permanent negative charge, which is balanced by exchangeable cations (e.g., Na^+, Ca^{2+}) adsorbed at the surfaces of particles.[45] Adding a charged dispersant to the aqueous suspensions changes the overall surface charge density of particles by adequate adsorption on the particles,[46] which will lead to the stability of particles in the suspension. As an analytical method of evaluation, the static stability of clay particles in the suspension were obtained over 2 h, and the changes in TSI% (destabilization index) vs time are available in Figure A4.4 in appendix information.

The higher TSI value depicts the least stability of suspensions[30] as the blank clay suspension indicated TSI of 90% showing a fast settlement over time. First, it was shown that the unmodified HL samples marginally affected the stability of clay particles (TSI ≥60% in Figure A4.4). A brief overview of the graphs reveals that all samples were not equally effective. For better interpretation, the trend of TSI changes via polymer solubility and charge density for different modification routes were graphed (Figure 5a-b). A linear relationship is observed for these correlations; implying that the higher solubility and CD are associated with enhanced stability of clay suspensions. In addition, the graphs revealed that S and SM samples were highly effective in dispersing clay suspensions with the adequate solubility range and CD by decreasing TSI to ~10-20%, while SE derivatives were not efficient and in the best situation TSI reached 30%.

The CD of polymers is reported to be an important variable when investigating the dispersibility of kaolin suspensions.[47] In this study, HL polymers with the lower charge of CD <0.8 mmol/g marginally changed the stability of clay particles while the TSI improved using HL polymers with the CD range of 0.8-1.8 mmol/g and the highest stability was obtained with CD >1.9 mmol/g. This shows the vital contribution of the properties of the HL derivatives rather than the modification routes.

Moreover, the improvement in the zeta potential of the suspension with a higher CD in Figure 5c agrees with the previous studies showing that the highest stability of clay suspensions at the most negative zeta potential of -40 to -45 mv would be achieved,[48] which was obtained with polymers with CD >1.9 mmol/g.

The settlement velocity of clay particles was obtained from the slope of TSI vs time graphs (from Figure A4.4) and further correlated to the particle size of HL polymers in Figure 5d. It indicates that the smaller the particles are, the slower the rate of clay suspension settlement would be. Wherein, the settlement happened faster using SE derivatives with the largest particle size while

smaller S and SM derivatives further hindered the fast settlement of clay suspension. Ultimately, SM derivatives of HL4 and HL5 with the highest solubility, CD and lowest particle size, were the most sufficient dispersants for the stability of clay particles followed by S derivatives of the same HL. However, SE derivatives, due to the limited chemical reactivity, were not efficient stabilizers for the clay suspension. The results emphasize the underlying role of raw material with the appropriate physicochemical properties for further chemical reactions to meet the required final properties, which were high CD, solubility and low particle size.

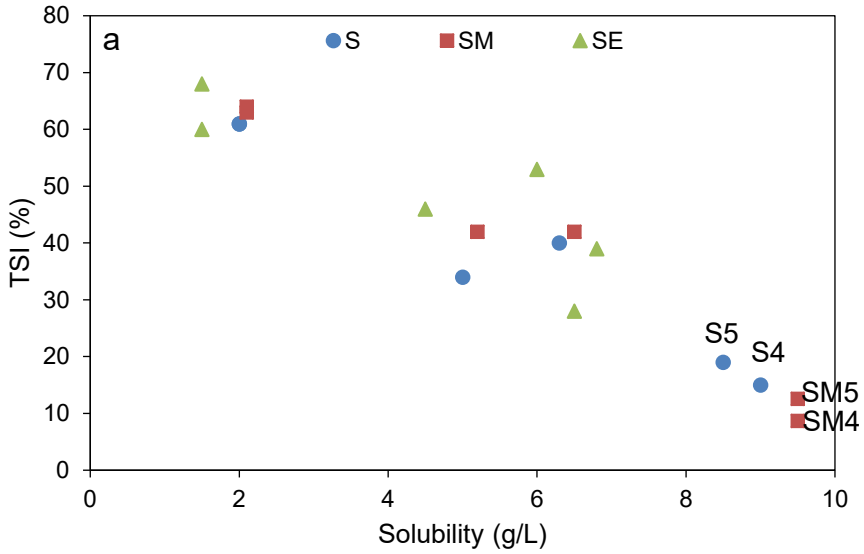

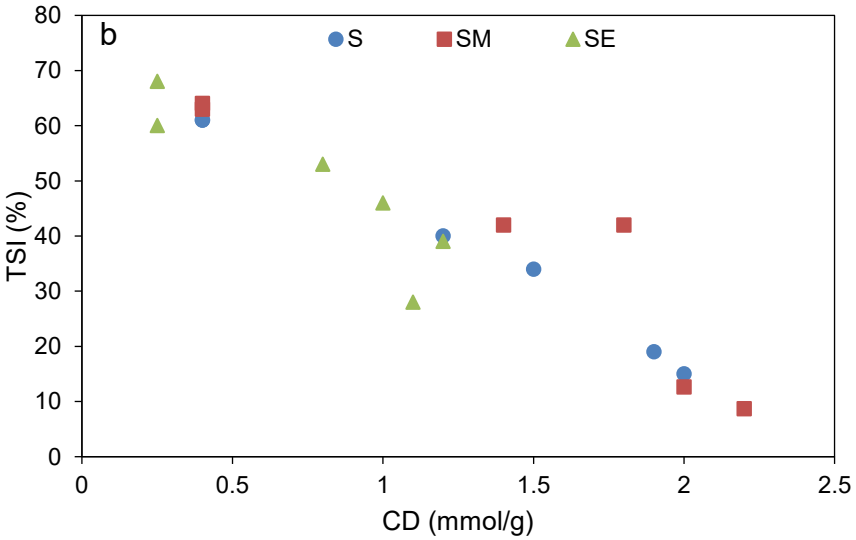

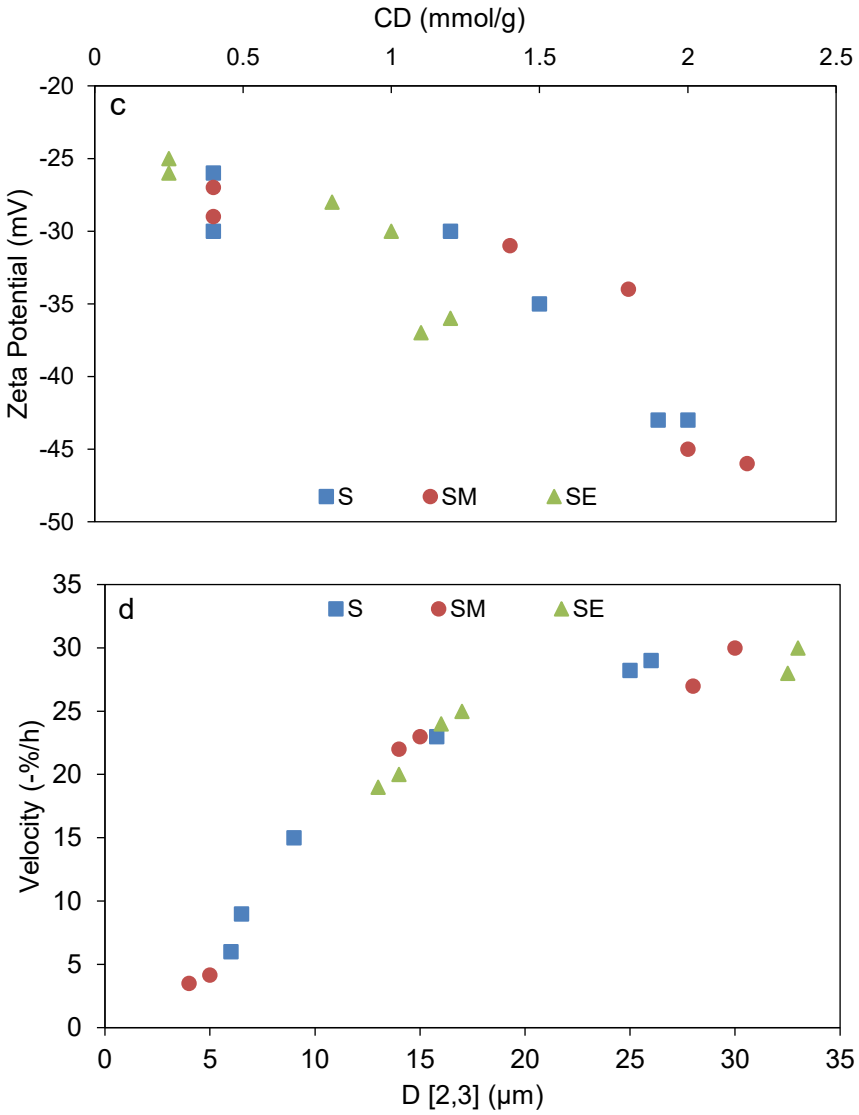

Figure 7.5: Instability index (TSI) of clay suspension at 16 mg/g dosage of S, SM and SE derivatives of HL samples vs a) polymer solubility, b) CD and c) zeta potential changes of clay particles vs CD of polymers and d) the settlement velocity of clay particles vs particle size of HL derivatives D [2,3].

7.4.4 The optimal physicochemical properties

Among all samples examined in this study, HL4 and HL5 depicted not only the highest chemical reactivity towards S and SM modifications but were also highly effective in clay dispersibility. More precisely, the physicochemical properties of these two samples with the lowest percentage of C-O-C internal linkages (Table 2), fewer identified β-O-4 and LCC cross peaks (Figure 3), least sugar content (Tables 1), the smallest particle size and highest pore volume, and phenolic content (Table 1) provided them the advantages compared to other HL samples. Most importantly, the

lowest content of β-aryl ether bonds identified in HL4 and HL5 samples were related to the highest content of phenolic hydroxyl contents in these samples, which showed to directly correlate with the highest DS of reactions (Figure 4). The correlation results in Figures 1 and 4 emphasized the underlying role of residual sugar on the accessibility and activity of hydroxyl groups. The fewer LCC bonds identified in HL4 and HL5 associated with the highest carboxylate groups and smallest particle size, which resulted in effective chemical reactions. The identified condensed phenol groups (β-5 and 5-5) in these two samples also effectively correlated with higher chemical reactivity.

The mechanism of modification reaction also played an important role in the final DS of reactions since SE modification was not as effective as S and SM reactions for HL4 and HL5. Therefore, in addition to the right choice of HL, finding the right reagent for the chemical reaction is crucial for generating sulfo-alkylated lignin with adequate properties as a dispersant.

7.5 Conclusions

In this study, the comparison between six different enzymatic hydrolysis lignin (HL) revealed the fundamental role of β-aryl ether and residual carbohydrate on the physicochemical properties and chemical reactivity of the samples to generate dispersants for the clay suspension.

Based on the observed correlations among properties of HL samples, the HL samples with a fewer distribution of β-O-4 and LCC bonds from HSQC cross peaks had the highest Ph-OH and carboxylate group content, respectively. Based on the XPS and HSQC analysis, the higher ratio of C-O, C-O-C/ C-C bonds was associated with the superior contribution to the β-aryl ether and LCC bonds among samples. The samples with the lowest sugar content were the smallest and most porous one that should have facilitated the chemical reactivity by providing higher accessibility for functional groups. The optimal physicochemical properties (e.g., highest Ph-OH and lowest aryl-ether and sugar content, smallest particle size, and highest surface area) were identified based on a direct correlation developed between HL properties to the highest degree of substitution (DS) toward chemical reactions. Whereas sulfomethylation (SM) and sulfonation (S) reactions were more effective modification routes compared to sulfoethylation (SE) on modifying HL.

Consequently, the samples with the optimal physicochemical properties were associated with the highest solubility, CD (≥1.9 mmol/g) and smallest particle size of HL derivatives of S and SM that were highly effective in stabilizing clay suspensions. The optimal derivatives of S and SM

modifications reduced the zeta potential of clay suspension to ~-40 mv and TSI to 10-20% compared to unstable clay suspension (TSI=90%) without the HL dispersant.

7.6 Reference

[1] D. Y. Kim, S. C. Yim, P. C. Lee, W. G. Lee, S. Y. Lee, H. N. Chang, *Enzyme Microb. Technol.* **2004,** *35*(6-7), 648-653.

[2] Z. Yuan, T. C. Browne, X. Zhang, U. S. Patent 0143411 A1, **2011**.

[3] R. P. Chandra, R. Bura, W. Mabee, D. A. Berlin, X. Pan, J. Saddler, Substrate pretreatment: the key to effective enzymatic hydrolysis of lignocellulosics?, Biofuels, Springer **2007**, 67-93.

[4] F. Liang, Y. Song, C. Huang, J. Zhang, B. Chen, *Catal. Commun.* **2013,** *40*, 93-97.

[5] L. Matsakas, V. Raghavendran, O. Yakimenko, G. Persson, E. Olsson, U. Rova, L. Olsson, P. Christakopoulos, *Bioresour. Technol.* **2019,** *273*, 521-528.

[6] J. Cho, S. Chu, P. J. Dauenhauer, G. W. Huber, *Green Chem.* **2012,** *14*(2), 428-439.

[7] C. G. Yoo, M. Li, X. Meng, Y. Pu, A. J. Ragauskas, *Green Chem.* **2017,** *19*(8), 2006-2016.

[8] M. N. Alam, T. G. Van De Ven, *J-FOR* **2014,** *4*(3), 22-26.

[9] Y. Zhang, P. Fatehi, *Ind. Crops Prod.* **2019,** *130*, 81-95.

[10] C. Heitner, D. Dimmel, J. Schmidt, D. Dimmel, J. Schmidt. *Lignin and Lignans: Advances in Chemistry*, CRC Press, **2016,** 333-341.

[11] M. T. Amiri, S. Bertella, Y. M. Questell-Santiago, J. S. Luterbacher. *Chem. Sci.* **2019**, *10*(35), 8135-8142.

[12] Q. Sun, Y. Pu, X. Meng, T. Wells, A. J. Ragauskas, *ACS Sustainable Chem. Eng*. **2015,** *3*(9), 2203-2210.

[13] I. Kühnel, B. Saake, R. Lehnen, *React. Funct. Polym* **2017,** *120,* 83-91.

[14] J. Podschun, A. Stücker, B. Saake, R. Lehnen, *ACS Sustainable Chem. Eng.* **2015,** *3*(10), 2526-2532.

[15] C. A. Cateto, M. F. Barreiro, A. E. Rodrigues, M. N. Belgacem, *Ind. Eng. Chem. Res.* **2009,** *48*(5), 2583-2589.

[16] A. Gandini, M. N. Belgacem, Z. X. Guo, S. Montanari, Lignins as macromonomers for polyesters and polyurethanes, Chemical Modification, Properties, and Usage of Lignin, Springer **2002**, 57-80.

[17] N. E. El Mansouri, J. Salvadó, *Ind. Crops Prod.* **2006,** *24*(1), 8-16.

[18] B. Zhang, D. Yang, H. Wang, Y. Qian, J. Huang, L. Yu, X. Qiu, *ACS Sustainable Chem. Eng.* **2018,** *7*(1), 1120-1128.

[19] D. S. Bajwa, G. Pourhashem, A. H. Ullah, S. G. Bajwa. *Ind. Crops Prod.* **2019**, *139*, 111526-111537.

[20] W. Gao, J. P. Inwood, P. Fatehi, J. *Wood Chem. Technol.* **2019,** *39*(4), 225-241.

[21] M. K. Konduri, P. Fatehi, *ACS Sustainable Chem. Eng.* **2015,** *3*(6), 1172-1182.

[22] N. Ghavidel, P. Fatehi, *ChemSusChem* **2020,** *13*(16), 4567-4578.

[23] X. Ouyang, L. Ke, X. Qiu, Y. Guo, Y. Pang, *J Dispers. Sci. Technol.* **2009,** *30*(1), 1-6.

[24] Y. Qin, D. Yang, X. Qiu, *ACS Sustainable Chem. Eng.* **2015,** *3*(12), 3239-3244.

[25] D. Zhang, S. Qiu, W. Huang, D. Yang, H. Wang, Z. Fang, *J. Colloid Interface Sci.* **2019,** *556*, 47-53.

[26] Y. Qin, M. Yuan, Y. Hu, Y. Lu, W. Lin, Y. Ma, X. Lin, T. Wang, *Int. J. Biol. Macromol* **2020,** *152*, 280-287.

[27] U. Kim, W. M. Carty, *J. Ceram. Soc. JAPAN* **2016,** *124*(4), 484-488.

[28] Y. Pu, S. Cao, A. J. Ragauskas, *Energy Environ. Sci.* **2011,** 4(9), 3154-3166.

[29] S. Liu, *J. Biobased Mater. Bioenergy* **2008,** *2*(2), 135-147.

[30] S. Gharehkhani, N. Ghavidel, P. Fatehi, *ACS Sustainable Chem. Eng.* **2018,** *7*(2), 2370-2379.

[31] Y. Guo, W. Gao, P. Fatehi, *Ind. Crops Prod.* **2018,** *124*, 273-283.

[32] F. Monteil-Rivera, M. Phuong, M. Ye, A. Halasz, J. Hawari, *Ind. Crops Prod.* **2013,** *41*, 356-364.

[33] P. Zheng, L. Fang, Y. Xu, J. J. Dong, Y. Ni, Z. H. Sun, *Bioresour. Technol.* **2010,** *101*(20), 7889-7894.

[34] A. Fatona, R. M. Berry, M. A. Brook, J. M. Moran-Mirabal, *Chem. Mater.* **2018,** *30*(7), 2424-2435.

[35] L. Yao, C. Chen, X. Zheng, Z. Peng, H. Yang, Y. Xie, *BioResources*, **2016**, *11*(3), 6692-6707.

[36] T. T. You, L. M. Zhang, S. K. Zhou, F. Xu, *Ind. Crops Prod.* **2015**, *71*, 65-74.

[37] C. Zhang, J. Lu, X. Zhang, K. MacArthur, M. Heggen, H. Li, F. Wang, *Green Chem*. **2016,** *18*(24), 6545-6555.

[38] M. E. Jazi, G. Narayanan, F. Aghabozorgi, B. Farajidizaji, A. Aghaei, M. A. Kamyabi, C. M. Navarathna, T. E. Mlsna, *SN Appl. Sci.* **2019,** *1*(9), 1094-1205.

[39] T. Li, Y. Yin, S. Wu, H. Ma, F. Zhang, *Bioresour. Technol*. **2020**, *317*, 124034-124041.

[40] C. Zhao, J. Huang, L. Yang, F. Yue, F. Lu, *Ind. Eng. Chem. Res*. **2019**, *58*(14), 5707-5714.

[41] D. M. D. Carvalho, M. H. Lahtinen, M. Lawoko, K. S. Mikkonen. *ACS Sustainable Chem. Eng*. **2020**, *8*(31), 11795-11804.

[42] S. Nakagame, R. P. Chandra, J. F. Kadla, J. N. Saddler. *Biotechnol. Bioeng*. **2011**, *108*(3), 538-548.

[43] T. Aro, P. Fatehi, *ChemSusChem* **2017,** *10*(9), 1861-1877.

[44] X. Kang, Z. Xia, R. Chen, H. Sun, W. Yang, *Appl. Clay Sci.* **2019**, *181*, 105220-105232.

[45] A. McFarlane, K. Bremmell, J. Addai-Mensah, *J. Colloid Interface Sci.* **2006,** *293*(1), 116-127.

[46] P. Marco, J. Llorens, *Colloids Surf. A Physicochem. Eng. Asp.* **2005,** *270*, 291-295.

[47] D. Yang, X. Qiu, M. Zhou, H. Lou, *Energy Convers. Manag.* **2007,** *48*(9), 2433-2438.

[48] X. Kang, Z. Xia, R. Chen, P. Liu, W. Yang, *Appl. Clay Sci.* **2019**, *176*, 38-48.

Chapter 8: Conclusion and Future Work

Various lignin derivatives, such as lignin-grafted-polystyrene (KL-PS), functionalized sulfoethylated (SEKL), sulfonated (SHL), sulfomethylated (SMHL) lignins, and particles of N-SEKL with tunable physicochemical properties were produced in this thesis. A comprehensive physicochemical characterization of unmodified and derivatives of lignin were followed. Based on the results in this thesis, the post-modification of lignin materials should be carefully selected to tailor the properties depending on the final application, and it is only possible with the right choice of raw material with known physicochemical properties and the right choice of the modification process. For the first time, a comprehensive understanding of surface and interfacial properties of lignin derivatives were revealed. Valid direct correlations were established between the functional group contents and internal ether linkages to the chemical reactivity of HL samples toward sulfo-functionalization reactions. Moreover, the application of lignin derivatives in various technologies as an adsorbent, emulsifier, and dispersant was evaluated. KL-PS was successfully implemented to adsorb copper ions (45 mg/g) from an aqueous medium. SEKL formed a stabilized conventional emulsion for 5 h with 50% oil separation, while phase separation was reduced to only 15% after 24 h, using N-SEKL with a Pickering stabilization. Finally, SHL and SMHL efficiently stabilized the clay suspension by reducing the instability index (TSI) to 10-20% compared to the unstable clay suspension (TSI=90%).

For future studies, the analysis of ^{13}C- and HSQC NMR for KL-PS polymer is suggested to precisely identify its chemical structure to prove the H-NMR assignments. The comparison between the surface properties of the polymerized KL-PS and the mixture of KL and PS could also be considered to find out the role of the polymerization reaction. It is suggested that the functionalization of KL-PS adsorbent for more efficient ion adsorption be considered. This could happen via amination or sulfonation substitution reactions of the phenolic ring of PS or the remained hydroxyl groups of lignin.

The functionalized N-SEKL particles are suggested to be precipitated in a more controlled process of self-assembly (e.g., solvent exchange) to form spherical particles rather than irregular shape particles observed with TEM imaging in this study. The comparison of N-SEKL performance as an emulsifier based on their shape (i.e., irregular vs spherical) and with commercial products such as lignosulfonate (LS) could be the subject of further fundamental analysis of adsorption at the oil-water interface.

Chapter 9: Appendix

9.1 Synergistic effect of lignin incorporation into polystyrene for producing sustainable superabsorbent

9.1.1 Polymer characterization

Table A.1.1 lists the properties of KL, KL-PS and PS. The increase in the C/H ratio via polymerization depicts the increment in the proportion of aromatic double bonds, i.e., benzyne group, in kg mol-1 than KL-PS (M_W of 296 kg/mol), inferring that the homo-polymerization of styrene was more favored than its polymerization with lignin in the reaction.

Table A1.1. Properties of KL, KL-PS and PS.

Sample	M_W (kg/mol)	Surface area (m^2/g)	Pore volume (cm^3/g)
KL	29±4	24	0.035
KL-PS	296±15	44	0.053
PS	880±20	15	0.021

[a] based on mass balance

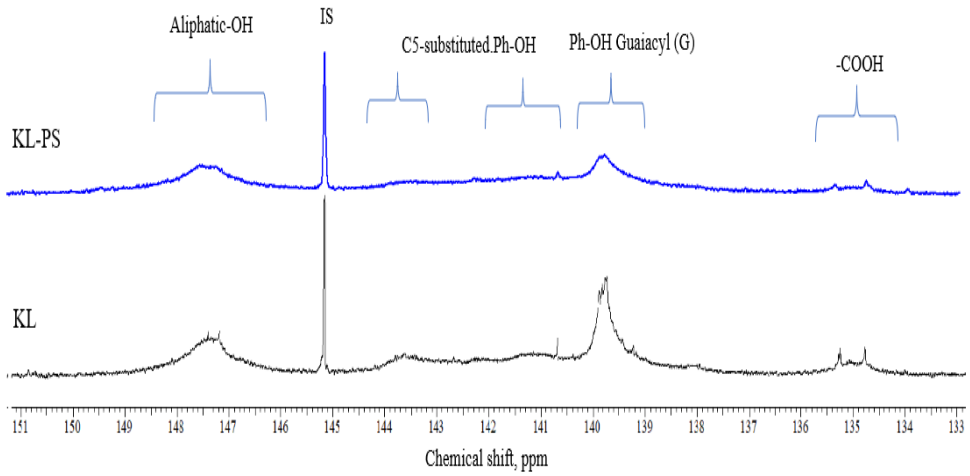

Figure A1.1: P-NMR spectra of KL and KL-PS

Table A1.2 Surface tension of the test liquids and polar, dispersive, acidic and basic components.[1]

σ (Mn/m)	water	diiodomethane	glycerol
Total	72.8	50.8	63.4
Dispersive	26.4	50.8	37.0
Polar	46.4	-	30.0
Acidic (+)	23.2	-	3.92
Basic (-)	23.2	-	57.4

9.1.2 Surface properties of PS, KL and KL-PS substrates

Contact angle of water, diiodomethane and glycerol on the PS, KL and KL-PS coated substrates are summarized in Table A1.3, and also images of the water droplets' contact angle on the substrates using sessile drop measurements are available in Fig. 3. Film generated via coating KL on the glass slide had a contact angle of 50.2˚ for water droplets. Contact angles of water droplet in the range of 46˚ and 60˚ were reported for lignin film on glass slides,[2,3] and differences in results are originated from the difference in the type of lignin used.[3] The water droplet's contact angle on PS coated surface was 85.5˚. The incorporation of lignin into PS reduced contact angle of KL-PS to 63˚ compared to PS. This reduction originated from the introduction of functional groups in the final KL-PS product.

Table A1.3. Contact angles (°) of the test liquids on the coated KL, KL-PS and PS Films

Surface	water	diiodomethane	glycerol
KL	50.2±1	22.53±0.5	49.6±1
KL-PS	63.1±0.4	22.6±0.5	52.2±0.1
PS	85.5±2	35.2±1	86.3±2

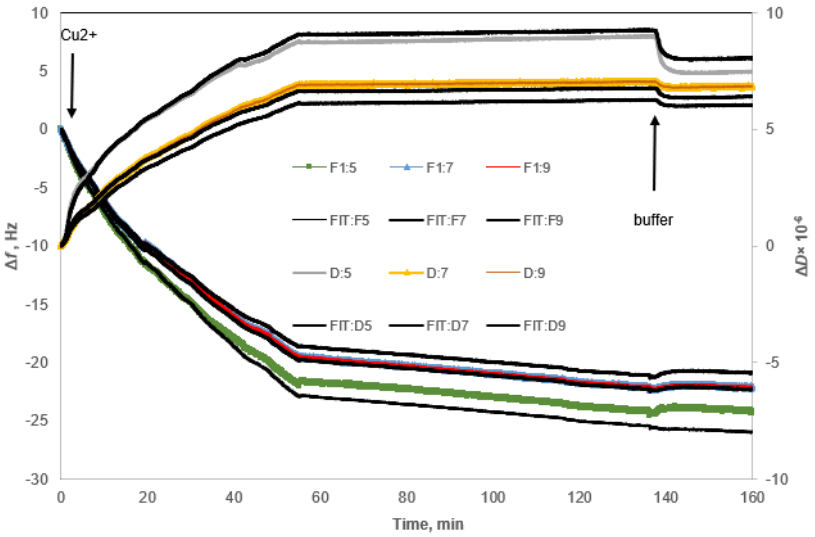

Figure A1.2: representative *Δf* and Δ*D* vs time curves for Cu^{2+} adsorption on KL-PS surface. Black lines show the fitted Voigt model for the adsorption of Cu^{2+} on the KL-PS coated sensors.

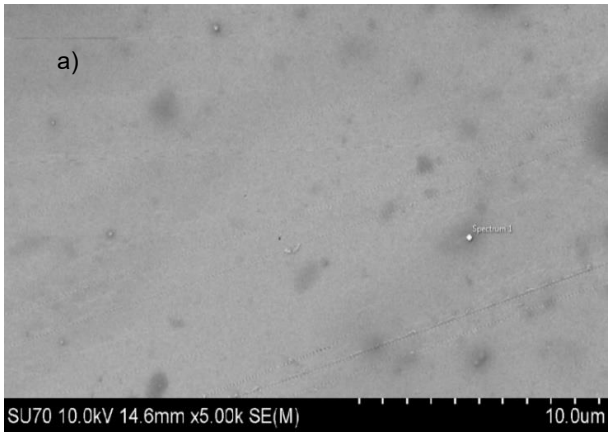

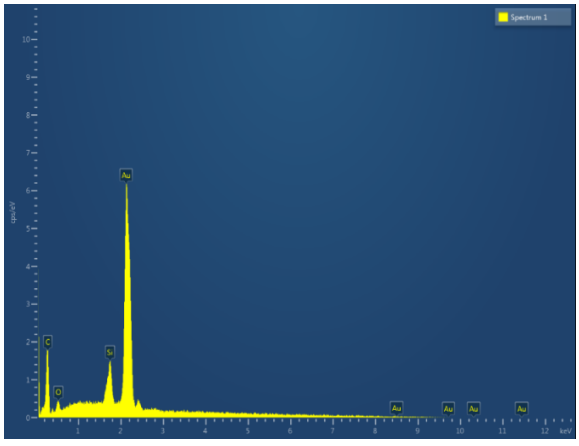

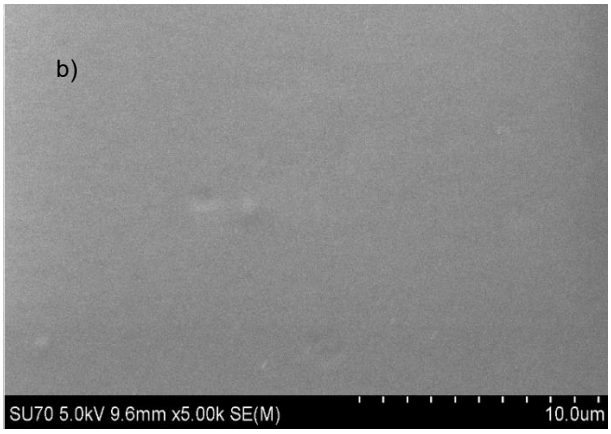
b)
SU70 5.0kV 9.6mm x5.00k SE(M)
10.0um

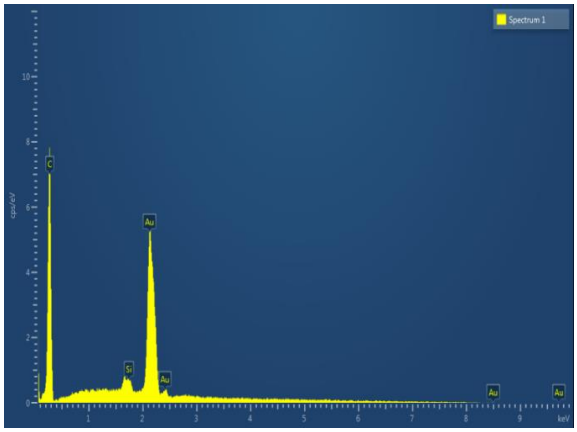
Spectrum 1
C
Au
Si
Au
Au
Au

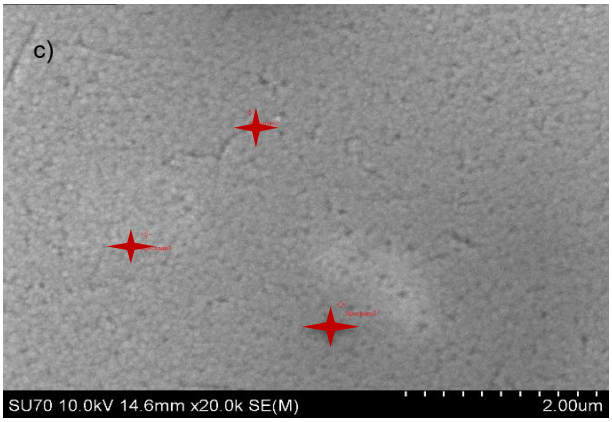
c)
SU70 10.0kV 14.6mm x20.0k SE(M)
2.00um

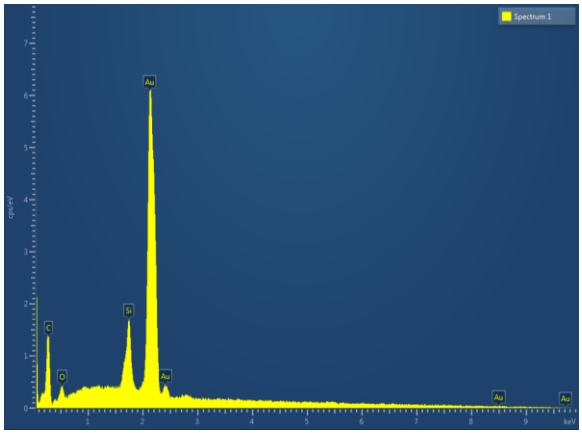
Spectrum 1
Au
Si
C
O
Au
Au
Au

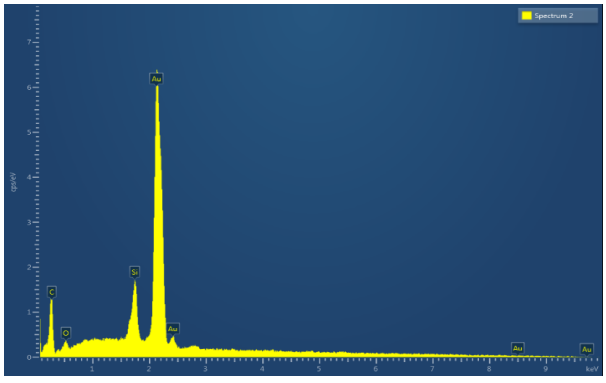
Spectrum 2
Au
Si
C
O
Au
Au
Au

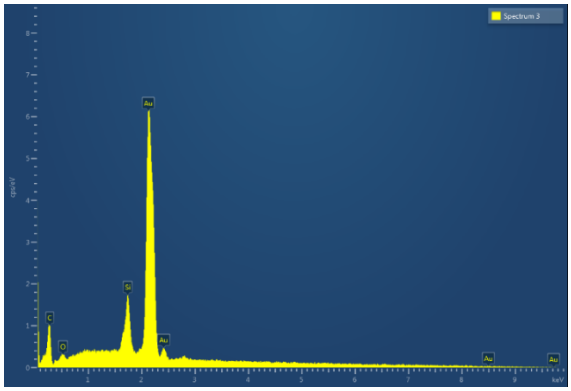
Spectrum 3
Au
Si
C
O
Au
Au
Au

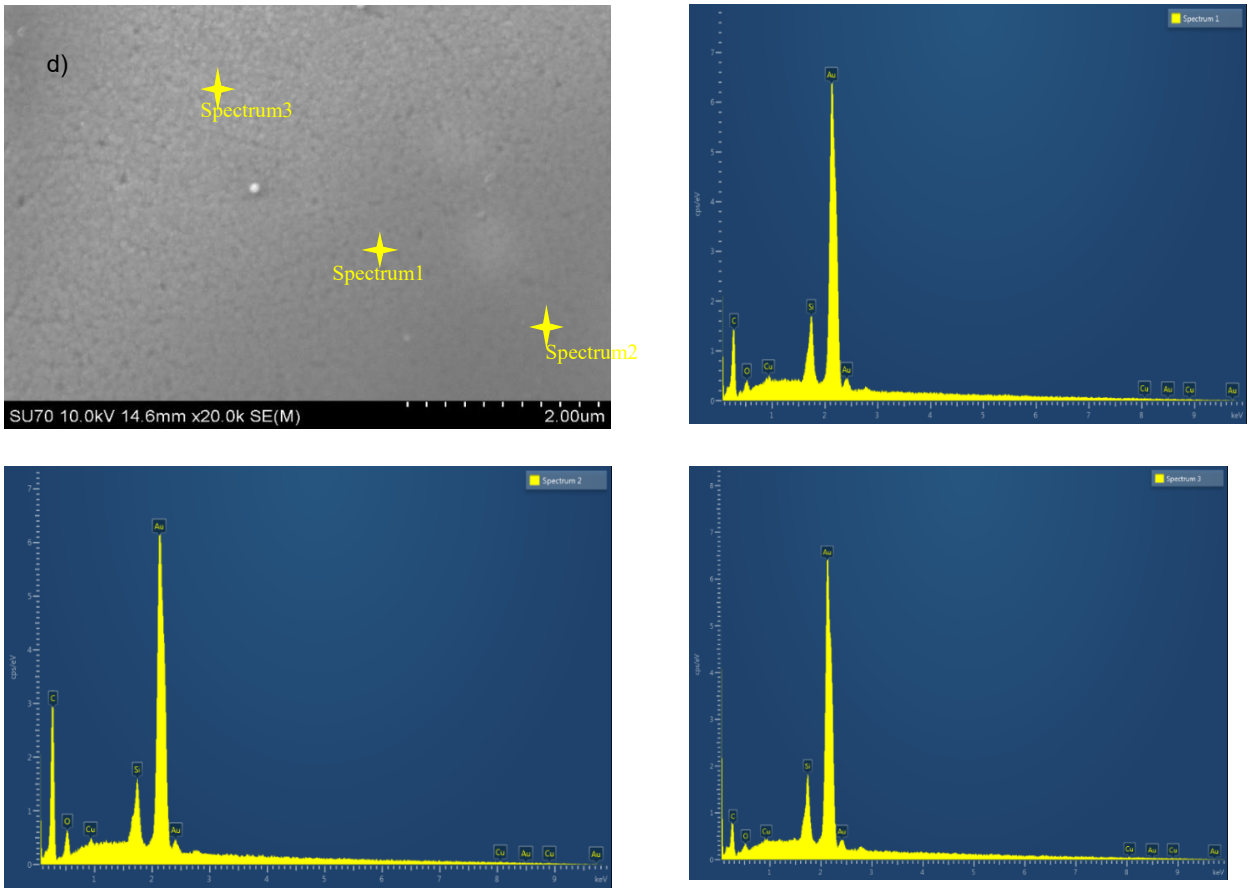

Figure A1.3: SEM/EDX images of coated gold sensors a) KL b) PS and KL-PS c) before and d) after Cu^{2+} adsorption in different areas.

9.1.3 References

[1] E. M. Harnett, J. Alderman and T. Wood, *Colloids Surf. B*, **2007**, *55*(1), 90-97.

[2] S. M. Notley and M. Norgren, *Langmuir*, **2010**, *26*, 5484-5490.

[3] M. Norgren, S. M. Notley, A. Majtnerova and G. Gellerstedt, *Langmuir*, **2006**, *22,* 1209-1214.

9.2 Pickering/non-Pickering emulsions of nano structured sulfonated lignin derivative

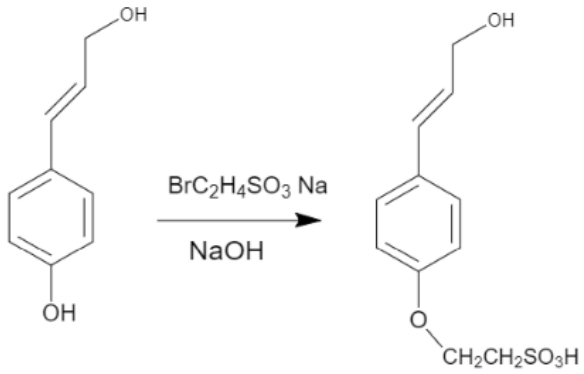

Figure A2.1: Scheme of substitution reaction on lignin hydroxyl group.

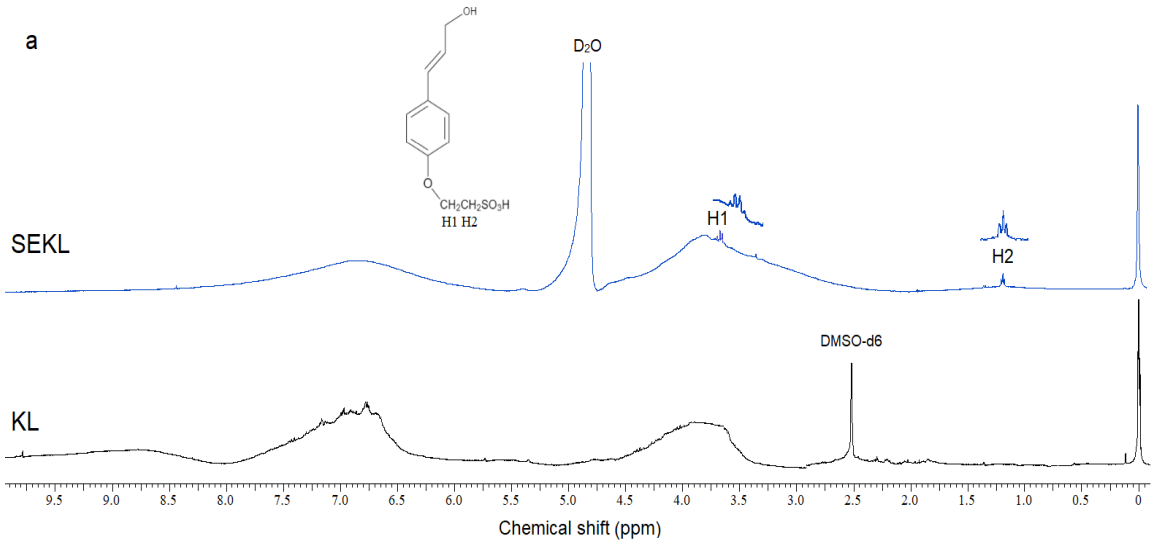

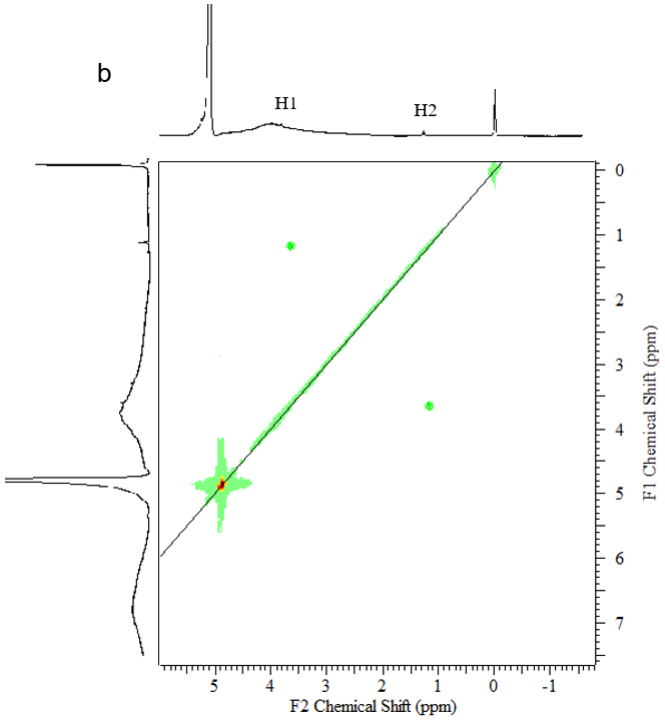

Figure A2.2: a) ^{1}H and b) ^{2}H-H-NMR spectra of KL and SEKL polymer.

Table A2.1. KL and SEKL chemical properties

Material	M_w (kg/mol)	M_w/ Mn	Sulfonate content (mmol/g)
KL	6.5±0.5	2.1	-
SEKL	10±1	1.8	1.2±0.1

Figure A2.3: Stable SEKL solution at pH 7 after 1 month.

9.2.1 Quantitative determination of acid groups

Potentiometric titration with NaOH was performed to quantify the acid group of SEKL. The titration curves obtained using a conventional titrator are shown in Figure A.2.4a and 4b for water as blank and SEKL solution. The base consumption (NaOH) for various functional groups

were determined from the first derivatives (dpH/dv) of the titration curves (Figure A2.4b) representing the titration endpoints (Ep) obtained automatically from the software of titrator (blue lines).

Using this approach, three types of functional groups of SEKL with corresponding acid dissociation constant (pKa) were quantified: sulfonate (pKa_1= 2.8±0.1), carboxylate (pKa_2= 5.1±0.1) and phenolate (pKa_3= 9±0.3). The corresponding contents of these groups were 1.2, 0.2 and 0.2 mmol/g as explained previously.[1] pKa of sulfonate group (pKa_1) is equal to the pH at the half-way point to the first equivalence point (EP1) as is illustrated by red line in Figure A.2.4 The second pKa_2 (carboxyl group) is equal to the pH mid-way between EP1 and EP2 and etc..[2]

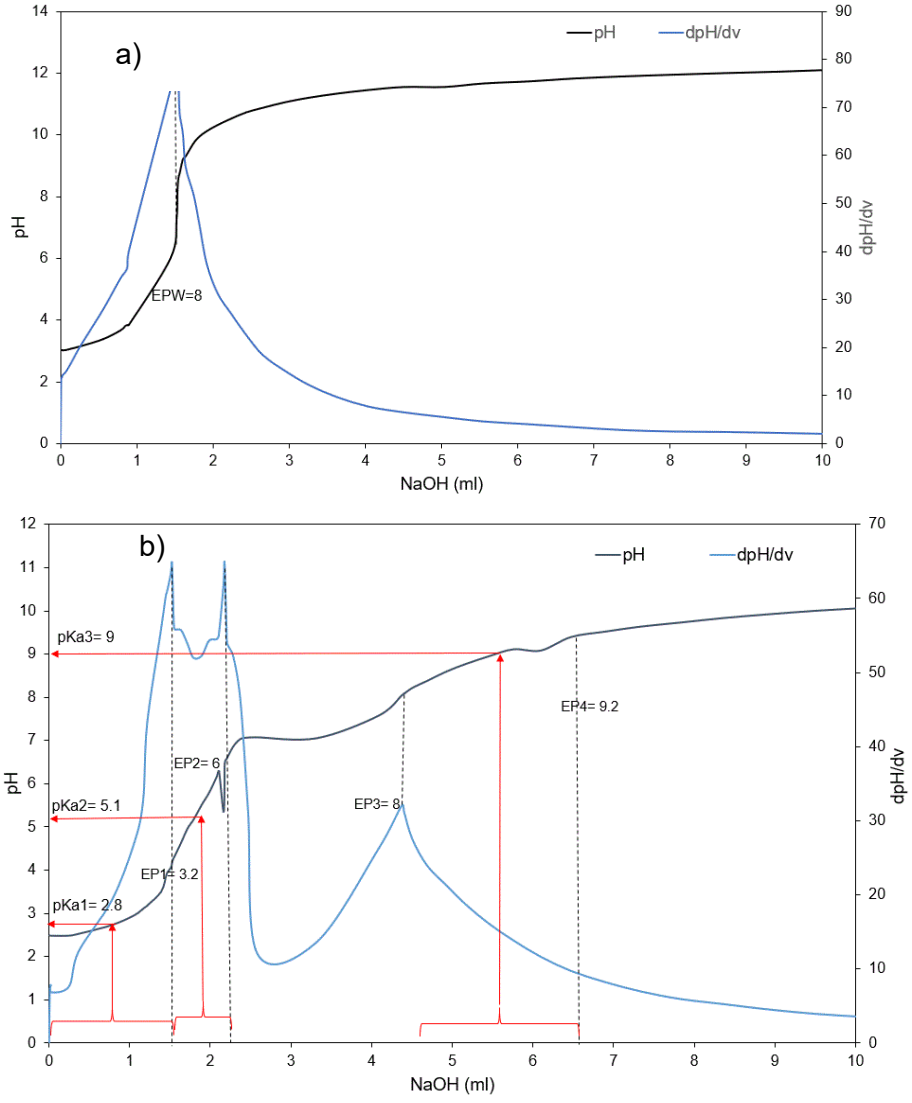

Figure A2.4: Titration curves obtained using a titrating device for a) water (blank) b) SEKL solution. Blue lines indicate the first derivative.

9.2.2 Phosphorus NMR

For quantitative analysis of lignin functional groups, the phosphitylation of KL with 2-chloro-4,4,5,5-tetramethyl-1,3,2- dioxaphospholane was followed as is explained previously.[3] To acquire a spectrum, a 90° pulse with 5 s relaxation delay and 128 acquisitions with an inverse gated decoupling pulse were employed. Peak assignments and calculations were followed as reported previously in literature, the results are summarized in Figure A2.5 and Table A2.2.[4]

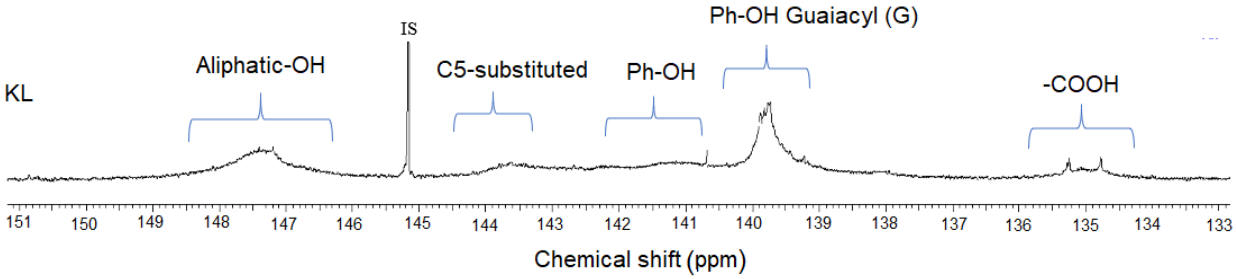

Figure A2.5: ^{31}P-NMR spectra for unmodified kraft lignin

Table A2.2. Functional groups (mmol/g) of KL studied by means of ^{31}P-NMR

Sample	Aliphatic -OH	C5-substituted	Ph-OH guaiacyl (G)	Total cond. phenolate	Carboxylate	Sulfonate content (mmol/g)
KL	1.62±0.1	0.80±0.06	1.40±0.06	2.2±0.08	0.14±0.01	N/A

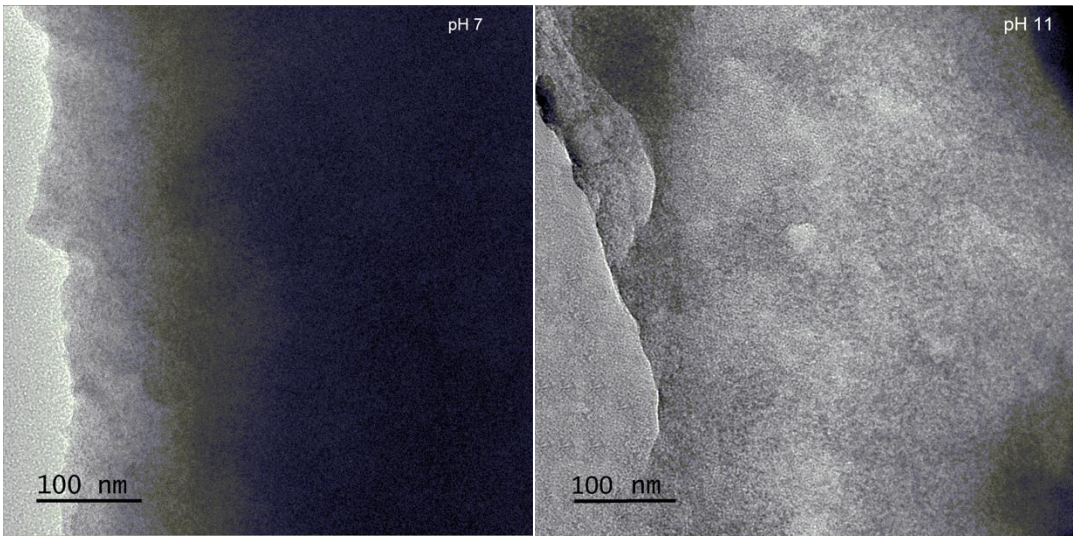

Figure A2.6: TEM image of SEKL film at pH 7 and 11 in a dried state (×100 nm).

Figure A2.7 indicates the SiO_2-coated QCM gold sensor before and after xylene film formation through spin-coating experiment. The darker color and appearance of black spots are the confirmation of xylene presence at the surface. The results of energy dispersive X-ray (EDX) proves the formation of the xylene film via an increase in the carbon intensity from 20 to 90 eV compared to a clean SiO_2-coated sensor (Figure A2.7). In addition, the WCA of the sensor shows the transformation of a hydrophilic SiO_2 surface (35˚) to a hydrophobic film of xylene (75˚).

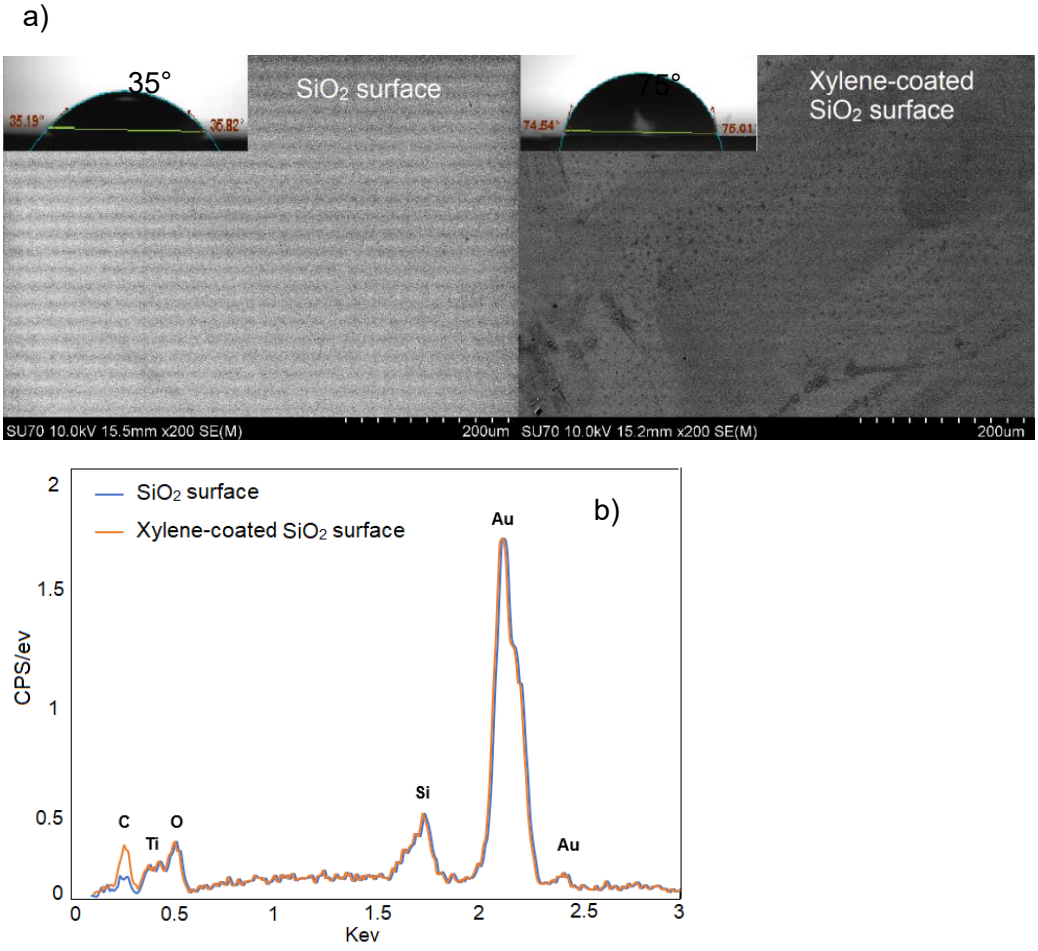

Figure A2.7: a) SEM and water contact angle images of clean and xylene-coated SiO_2 gold sensors b) energy dispersive X-ray (EDX) elemental analysis of the surface of a clean and xylene-coated SiO_2 gold sensor.

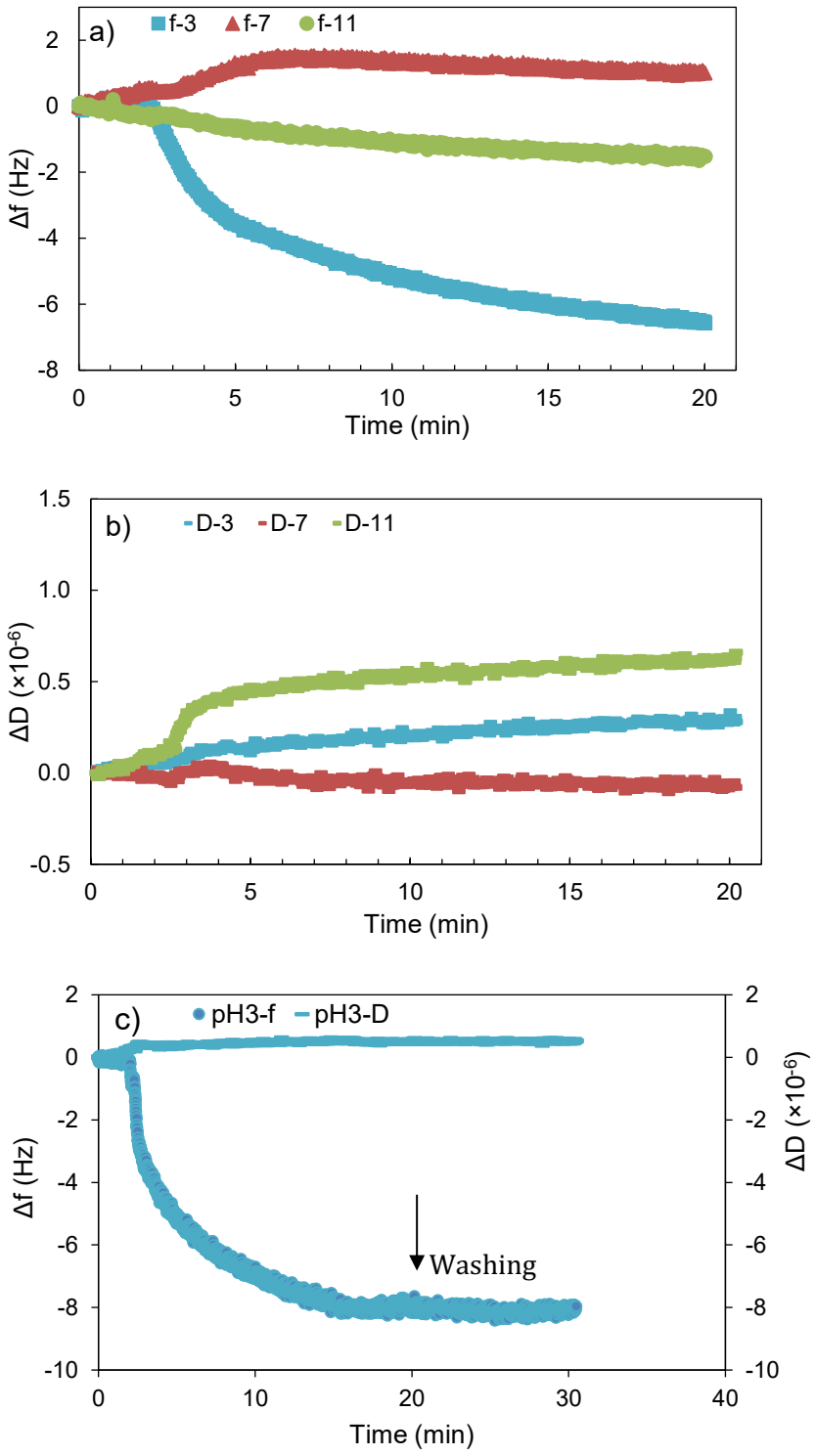

Figure A2.8: Changes in a) F and b) D at 7th overtone vs time for 20 min for the adsorption of SEKL/N-SEKL at pH 3, 7 and 11 and c) adsorption at pH3 followed by a washing step with buffer at the same pH on xylene-coated SiO_2 sensor.

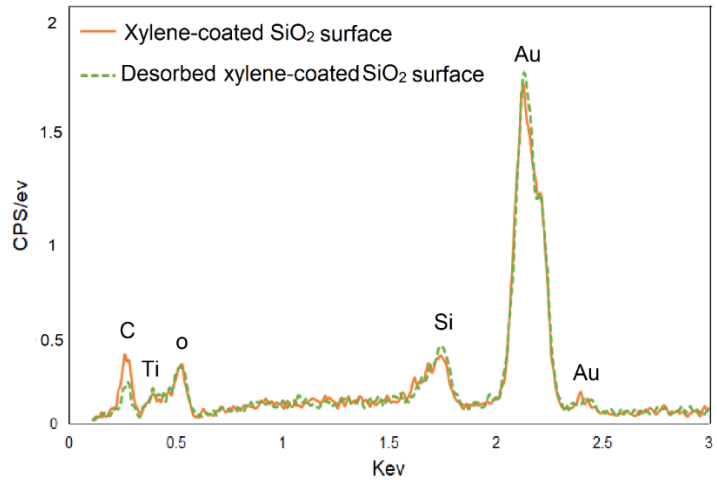

Figure A2.9: Elemental analysis via energy dispersive X-ray (EDX) analysis of the surface of xylene film coated on SiO_2 coated sensor after SEKL adsorption at pH 7 (QCM-D), which shows the desorption of xylene and reduced carbon content.

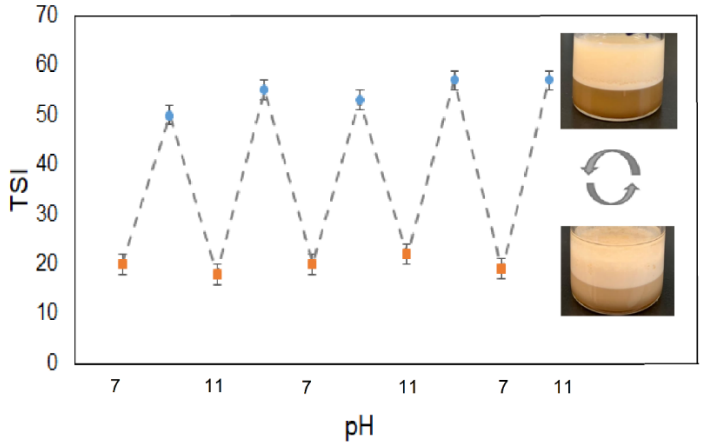

Figure A2.10: pH-responsive cycling for 5 cycles between emulsification-demulsification between pH 7 and 11.

9.2.3 References

[1] M. K. Konduri, P. Fatehi, *ACS Sustain. Chem. Eng.*, **2015,** *3*(6), 1172-1182.

[2] S. S. Zumdahl, S. A. Zumdahl, *Chemistry*, (**2007**).

[3] N. Ghavidel, P. Fatehi, *RSC Adv.* **2019,** *9* (31), 17639-17652.

[4] Y. Pu, S. Cao, A. J. Ragauskas, *Energy Environ. Sci*. **2011**, 4, 3154-3166.

9.3 Dynamic interfacial and emulsion evaluation of polymeric lignin surfactant at different oil/water systems

9.3.1 Nuclear Magnetic Resonance

One-dimensional ^{1}H-NMR and two-dimensional ^{1}H-^{1}H homonuclear correlation spectroscopies were carried out on KL and SEKL to confirm the success of sulfoethylation reaction on KL. The samples were prepared by dissolving 25 mg of KL and SEKL in 500 µL of DMSO-d_6 and D_2O, respectively. INOVA-500 MHz instrument (Varian, USA) was used to record the ^{1}H-NMR spectra of samples in the following adjustments: 64 number of scans, a 45° pulse width and a relaxation delay of 1.0 s for 1 dimensional NMR analysis; and the relaxation time of 4.0 s, 16 number of scans in 128 increments in a 45° pulse width for the two dimensional NMR analysis.[1]

9.3.2 Sulfonate Group Analysis

An automatic potentiometer, Metrohm, 905 Titrado, (Switzerland) was used to quantitatively measure the sulfonate group content of SEKL following the procedure explained earlier.[2] In this experiment, a 0.1 g sample of KL or SEKL was dissolved in 100 mL of distilled water and the pH of the solution was adjusted to 3.0 using 0.1 M HCl. The titration was then followed by adding 0.1 M NaOH to the solution to determine the number of sulfonate groups on the lignin samples.

9.3.3 Molecular Weight and Hydrodynamic Size Analysis

The molecular weight of SEKL was evaluated using a gel permeation chromatography (GPC), Malvern Viscotek GPCmax, (Malvern, UK) with a UV detector. In this set of experiments, 4 mg/mL sample solutions were prepared by dissolving dried powders of SEKL in 10 mL of 0.1 mol/L $NaNO_3$ solutions. After filtration with a 0.2 µm nylon filter (13 mm diameter), the samples were passed through PolyAnalytic, PAA206, and PAA203 columns, at 35 °C at the flow rate of 0.70 mL/min, while polyethylene oxides were used as standard polymers for calibration.

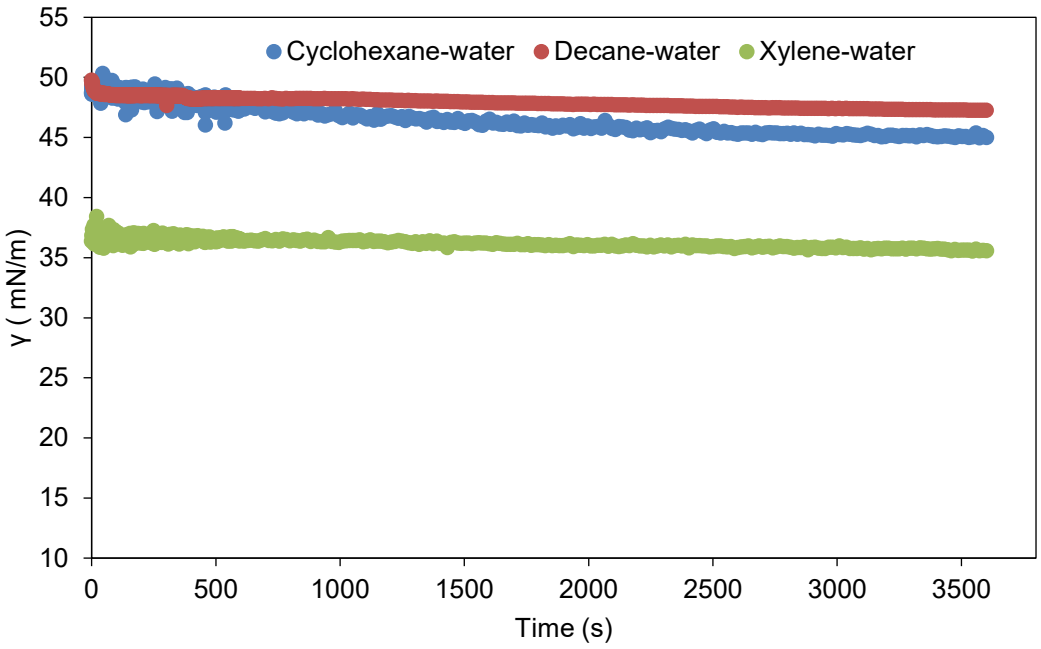

Figure A3.1: The reference baseline for the γ of the oil-water systems in the absence of SEKL.

9.3.4 Critical aggregation concentration (CAC) determination

A tensiometer equipped with a Du Nouy ring (Sigma 701, Biolin Scientific) and OneAttension software was used to determine the changes in surface tension of water at an elevated concentration of SEKL to determine the CAC point of SEKL in an aqueous system. The petri dish and the ring were washed with water and acetone before the analysis. The samples with a predetermined concentration (0.2-2 wt.%) were then prepared to monitor the surface tension variations.

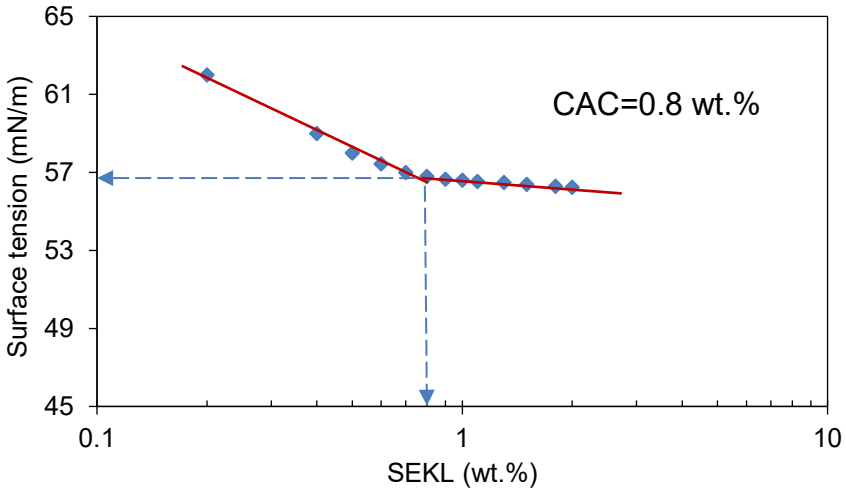

Figure A3.2: Surface tension of SEKL solution as a function of concentration and determined CAC point.

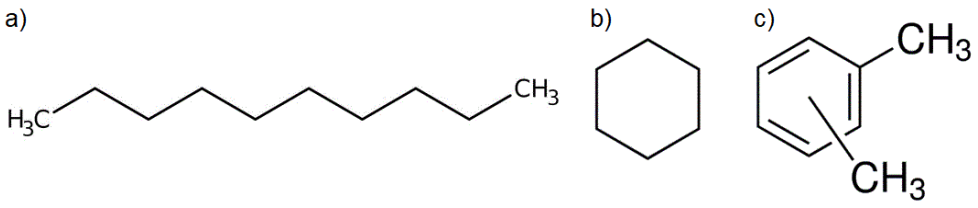

Figure A3.3: Chemical structure of a) decane, b) cyclohexane and c) xylene (a mixture of isomers).

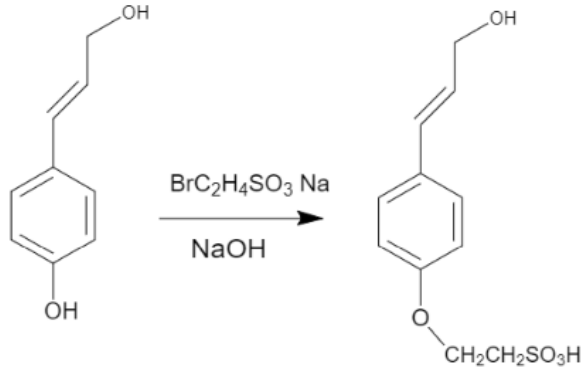

Figure A3.4: Scheme of substitution reaction on the lignin hydroxyl group.

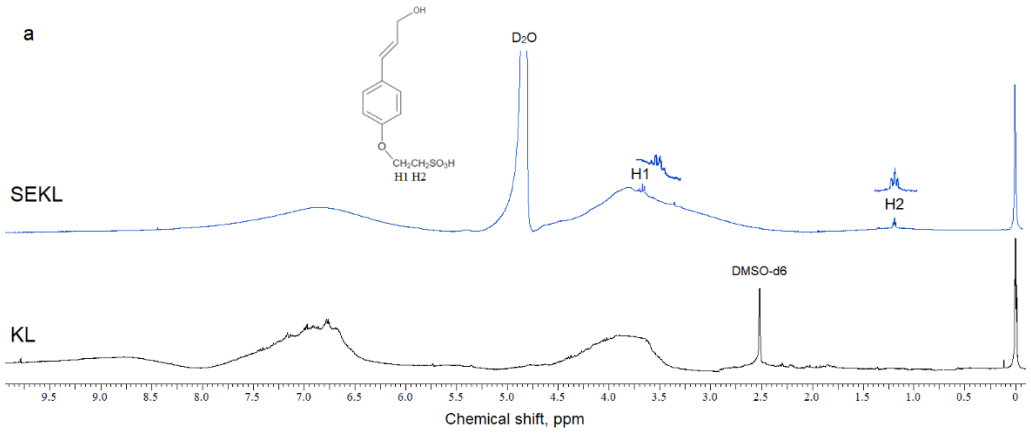

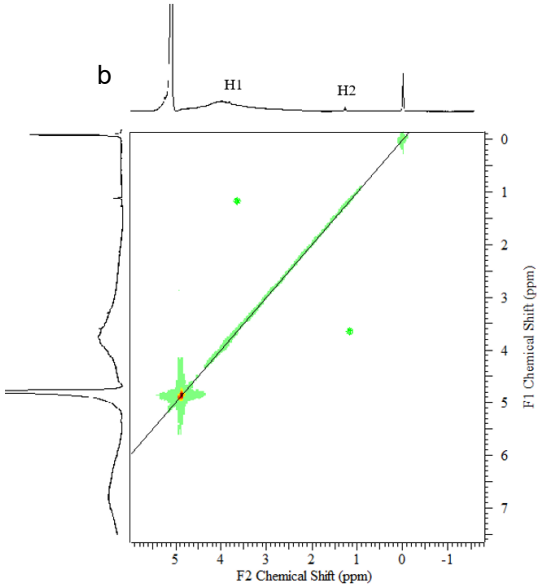

Figure A3.5: a) ^{1}H and b) ^{2}H-H-NMR spectra of KL and SEKL polymer.

Table A3.1. KL and SEKL chemical properties

Material	M_w, kg/mol	M_w/ Mn	Charge density, mmol/g	Sulfonate content, mmol/g
KL	6.5±0.5	2.1	0.10±0.05	-
SEKL	10±1	1.8	1.3±0.1	1.2±0.1

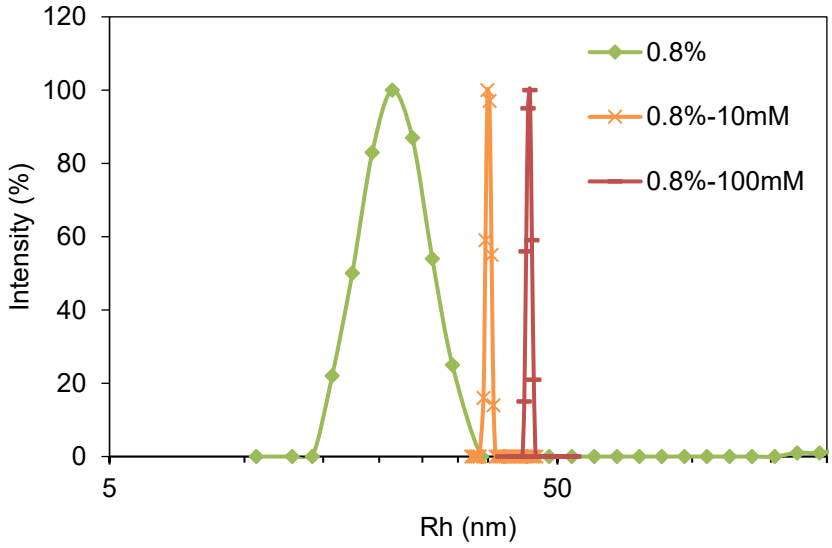

Figure A3.6: Hydrodynamic size (R_h) distribution of SEKL at 0.8 wt.% at 0 mM KCl and ionic strength ranges of 10 and 100 mM KCl.

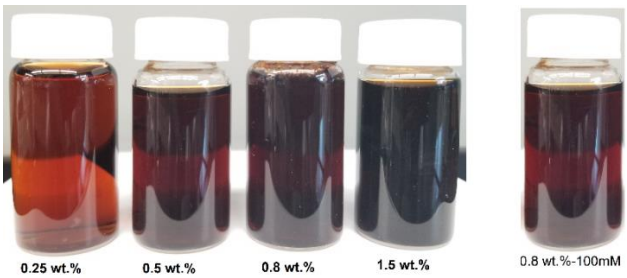

Figure A3.7: Stable SEKL solution in different concentrations and 100 mM KCl.

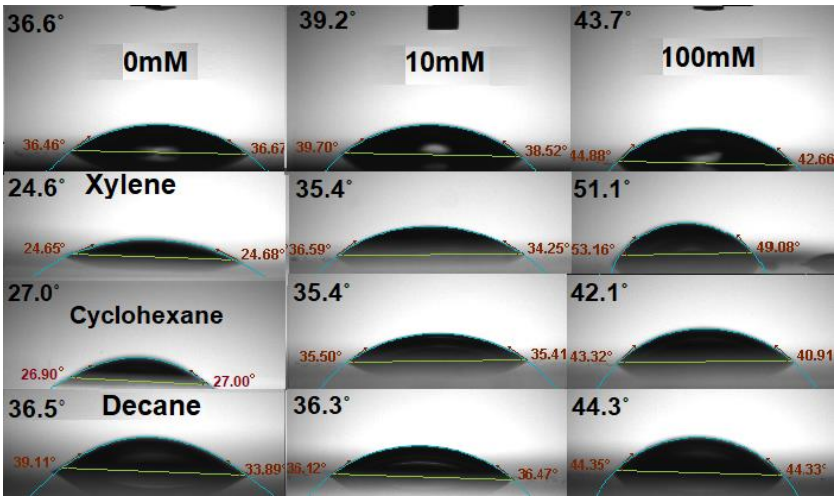

Figure A3.8: WCA and OCA of SEKL at various ionic strengths 0, 10, and 100 mM KCl.

Table A3.2. Physical properties of oils.[3]

Oil	Polarity Index	Dielectric constant
Decane	0.1	1.95
Cyclohexane	0.2	2.02
Xylene (mixture)	2.5	2.56

9.3.5 Solubility of the SEKL in organic solvents

The maximum solubility of the SEKL at saturation was determined as follows: 70 mg of the solid SEKL polymer was weighted in 5 mL vials, then 2 mL organic fluids (xylene, cyclohexane, or decane) was added to the vial. In total, three vials were prepared for each solvent tested. After 3 h, 200 µL of the polymer solution was collected from the supernatant in each vial, the solvent was evaporated in the oven at 110 ºC and the final solid residue was weighed.[4]

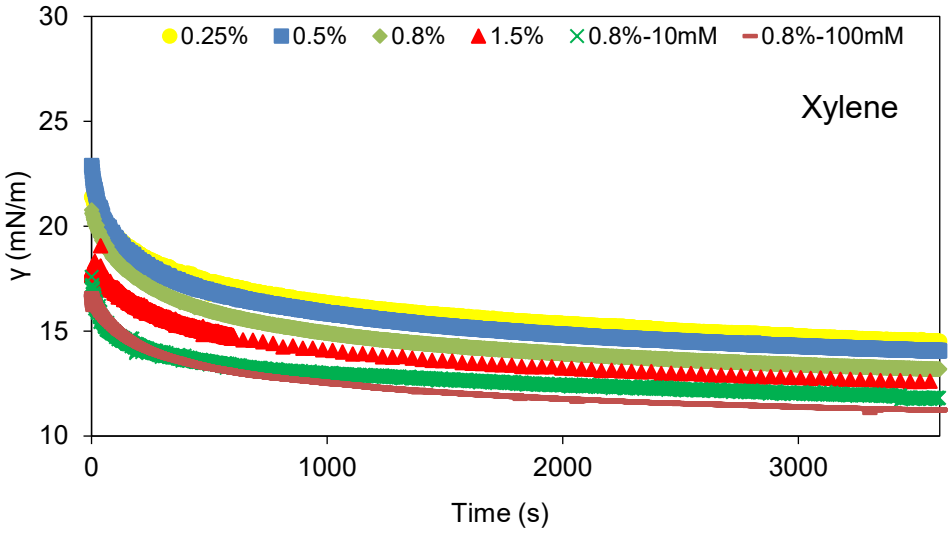
0.25%
0.5%
0.8%
1.5%
0.8%-10mM
0.8%-100mM
Xylene
γ (mN/m)
Time (s)
30
25
20
15
10
0
1000
2000
3000

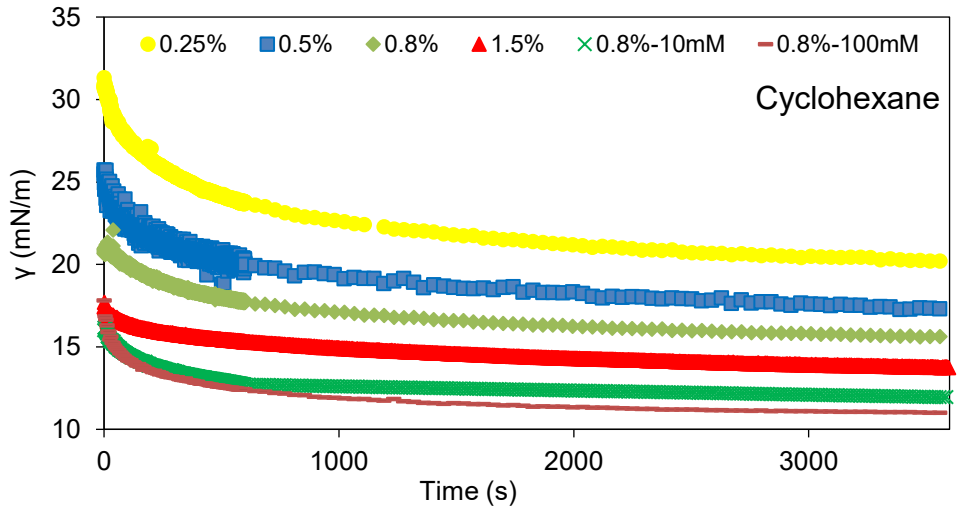
0.25%
0.5%
0.8%
1.5%
0.8%-10mM
0.8%-100mM
Cyclohexane
γ (mN/m)
Time (s)
35
30
25
20
15
10
0
1000
2000
3000

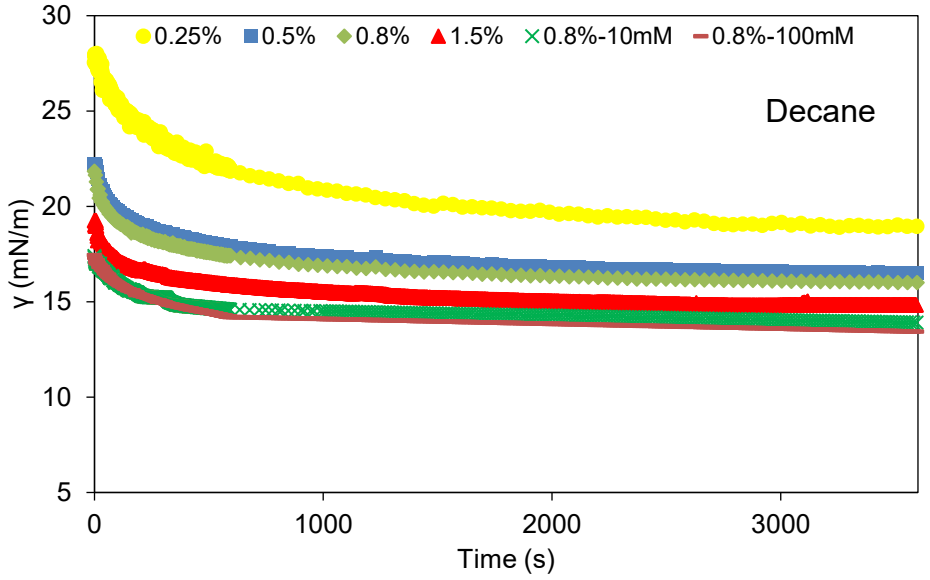

Figure A3.9: Interfacial tension (γ) of the xylene, cyclohexane, and decane in aqueous solutions of SEKL at various polymer concentrations (wt.%) in a salt-free, 10 and 100 mM KCl systems over 3600 s.

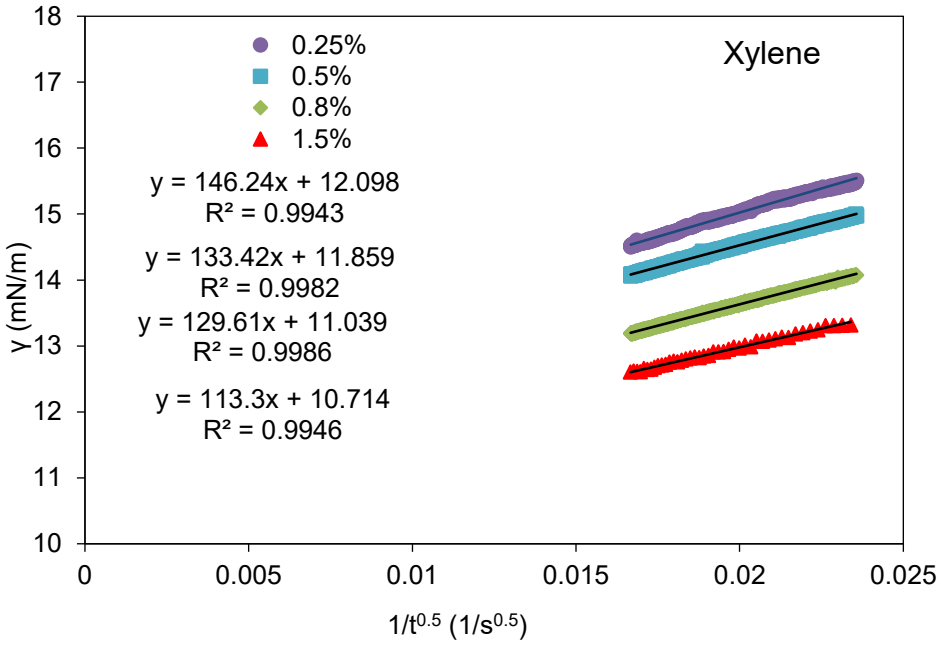

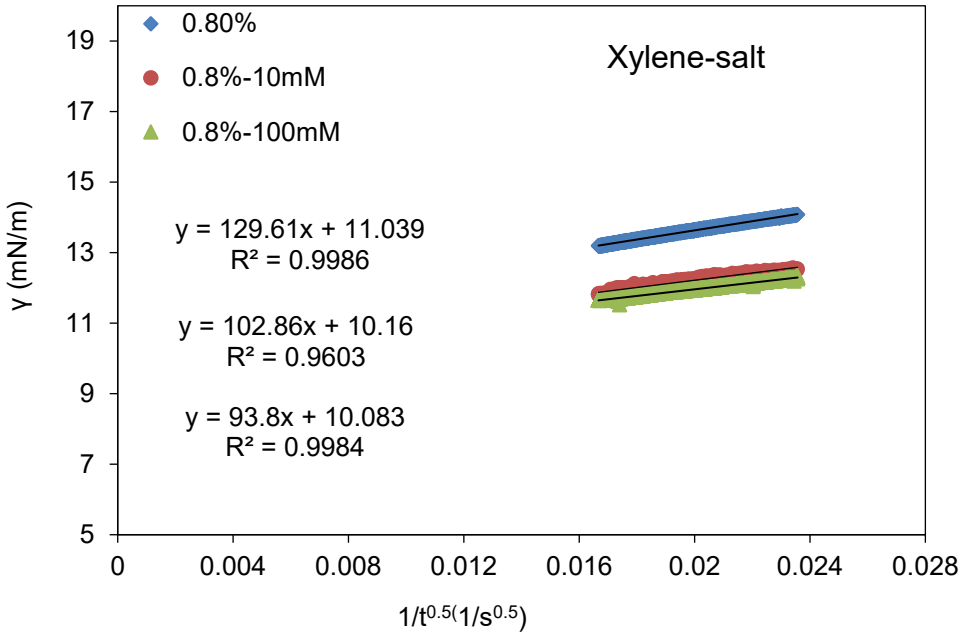
0.80%
0.8%-10mM
0.8%-100mM
Xylene-salt
y = 129.61x + 11.039
R² = 0.9986
y = 102.86x + 10.16
R² = 0.9603
y = 93.8x + 10.083
R² = 0.9984
y (mN/m)
19
17
15
13
11
9
7
5
0
0.004
0.008
0.012
0.016
0.02
0.024
0.028
1/t^0.5(1/s^0.5)

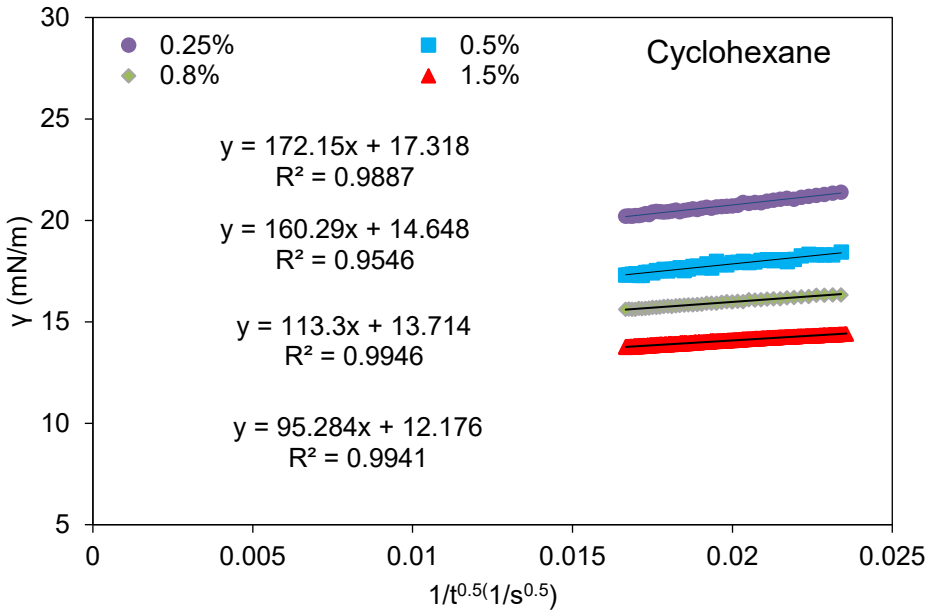
0.25%
0.8%
0.5%
1.5%
Cyclohexane
y = 172.15x + 17.318
R² = 0.9887
y = 160.29x + 14.648
R² = 0.9546
y = 113.3x + 13.714
R² = 0.9946
y = 95.284x + 12.176
R² = 0.9941
y (mN/m)
30
25
20
15
10
5
0
0.005
0.01
0.015
0.02
0.025
1/t^0.5(1/s^0.5)

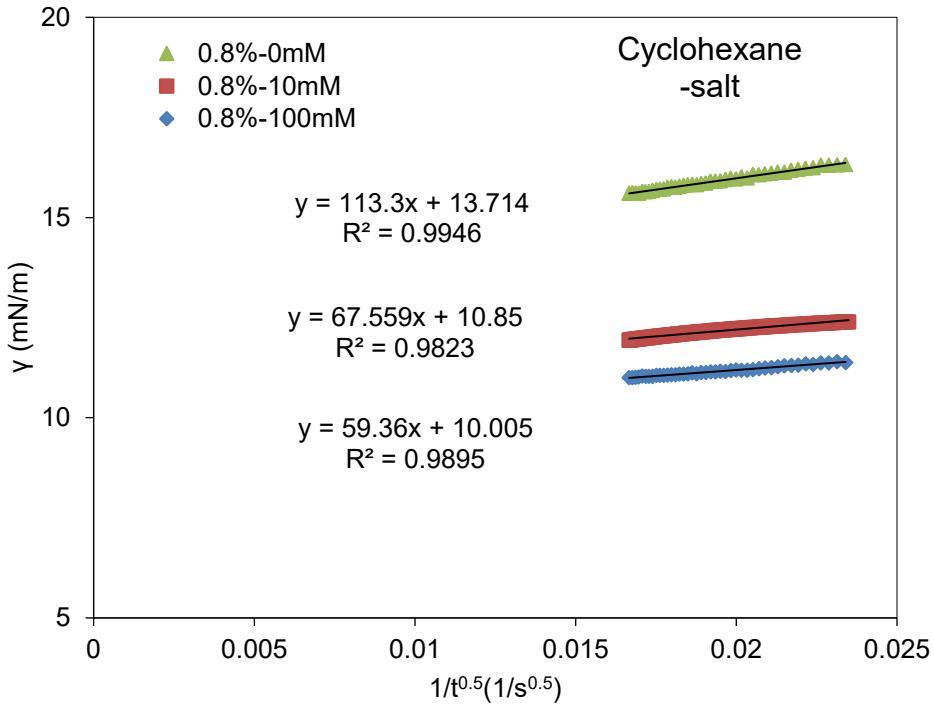
Cyclohexane
-salt
0.8%-0mM
0.8%-10mM
0.8%-100mM
y = 113.3x + 13.714
R² = 0.9946
y = 67.559x + 10.85
R² = 0.9823
y = 59.36x + 10.005
R² = 0.9895
y (mN/m)
1/t^0.5(1/s^0.5)
20
15
10
5
0
0.005
0.01
0.015
0.02
0.025

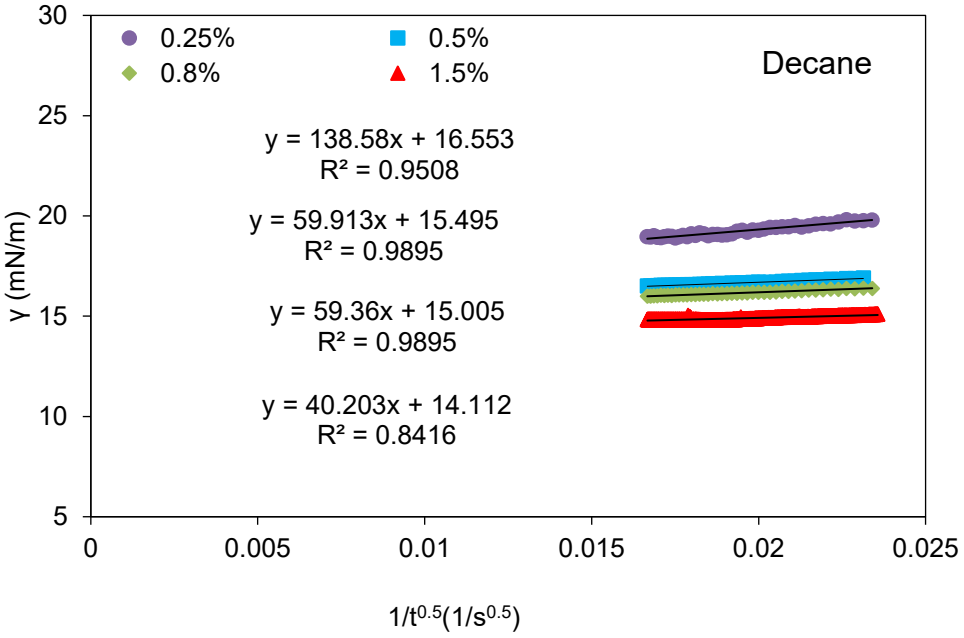
Decane
0.25%
0.5%
0.8%
1.5%
y = 138.58x + 16.553
R² = 0.9508
y = 59.913x + 15.495
R² = 0.9895
y = 59.36x + 15.005
R² = 0.9895
y = 40.203x + 14.112
R² = 0.8416
y (mN/m)
1/t^0.5(1/s^0.5)
30
25
20
15
10
5
0
0.005
0.01
0.015
0.02
0.025

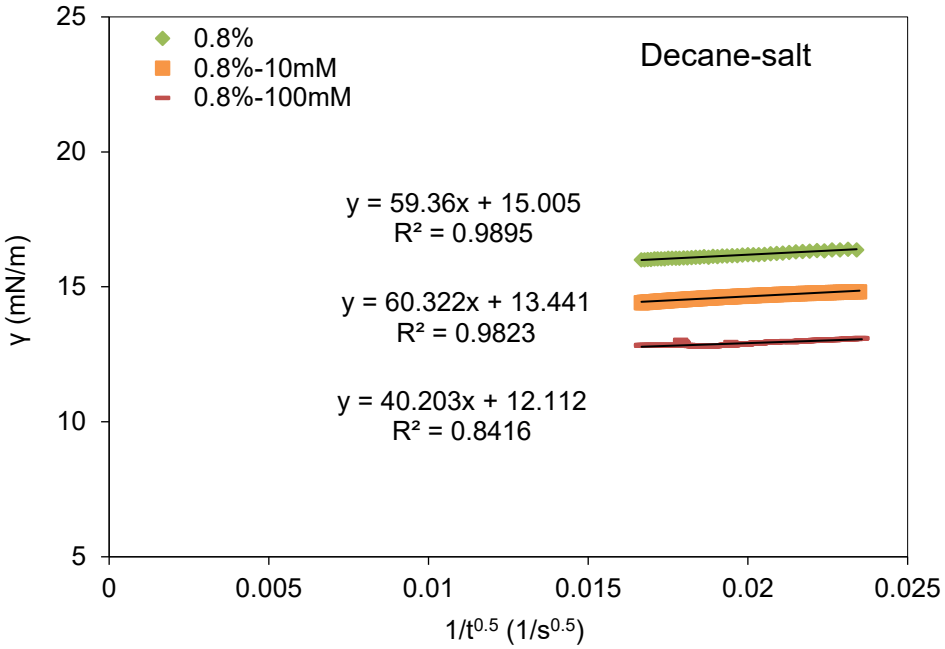

Figure A3.10: The steady-state interfacial tensions (γ_∞) determination for SEKL aqueous solutions in the concentration range of (0.25-1.5 wt.%) at xylene, cyclohexane, and decane interfaces at 0 mM ionic strength or constant 0.8wt.% SEKL with 10- and 100-mM ionic strength. (data of t >1900 s from Figure A3.8)

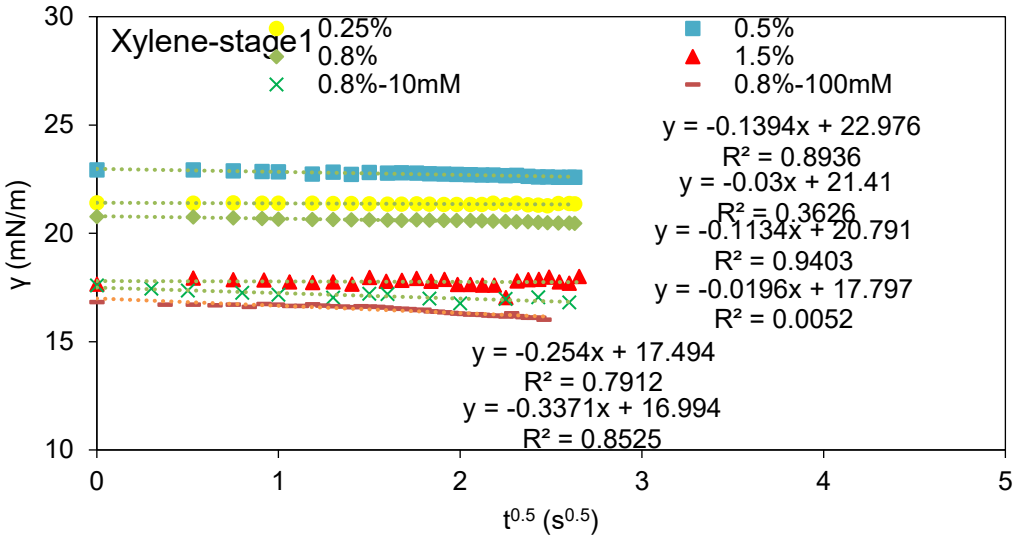
Xylene-stage1
0.25%
0.8%
0.8%-10mM
0.5%
1.5%
0.8%-100mM
y = -0.1394x + 22.976
R² = 0.8936
y = -0.03x + 21.41
R² = 0.3626
y = -0.1134x + 20.791
R² = 0.9403
y = -0.0196x + 17.797
R² = 0.0052
y = -0.254x + 17.494
R² = 0.7912
y = -0.3371x + 16.994
R² = 0.8525
γ (mN/m)
t0.5 (s0.5)

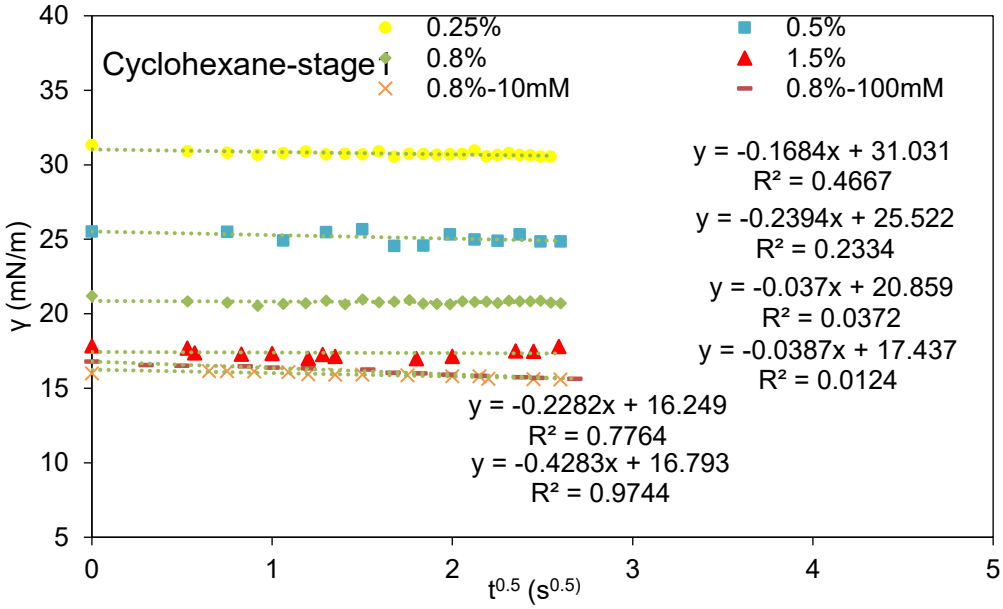
Cyclohexane-stage1
0.25%
0.8%
0.8%-10mM
0.5%
1.5%
0.8%-100mM
y = -0.1684x + 31.031
R² = 0.4667
y = -0.2394x + 25.522
R² = 0.2334
y = -0.037x + 20.859
R² = 0.0372
y = -0.0387x + 17.437
R² = 0.0124
y = -0.2282x + 16.249
R² = 0.7764
y = -0.4283x + 16.793
R² = 0.9744
γ (mN/m)
t0.5 (s0.5)

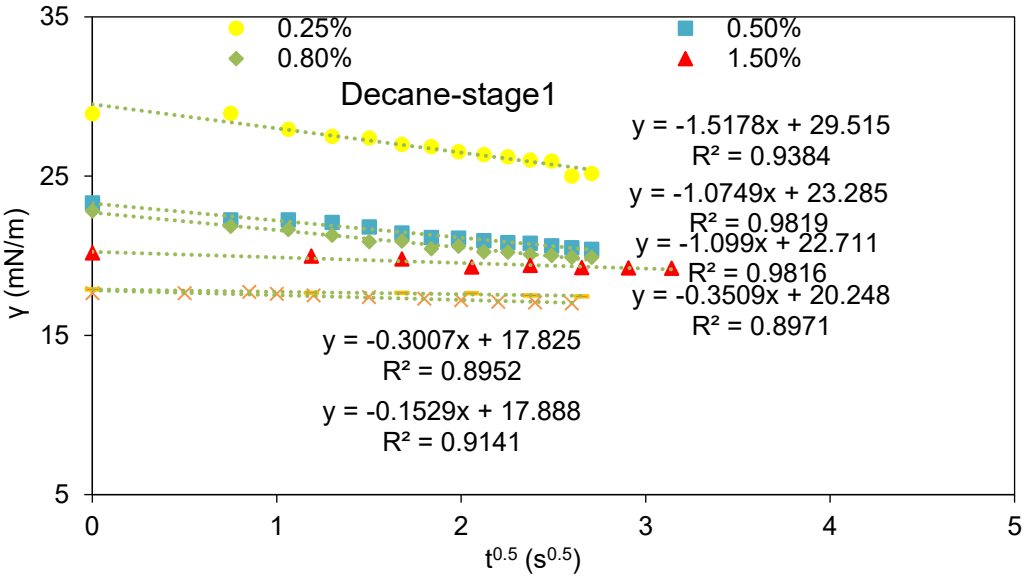
0.25%
0.80%
0.50%
1.50%
Decane-stage1
y = -1.5178x + 29.515
R² = 0.9384
y = -1.0749x + 23.285
R² = 0.9819
y = -1.099x + 22.711
R² = 0.9816
y = -0.3509x + 20.248
R² = 0.8971
y = -0.3007x + 17.825
R² = 0.8952
y = -0.1529x + 17.888
R² = 0.9141
γ (mN/m)
t^0.5 (s^0.5)

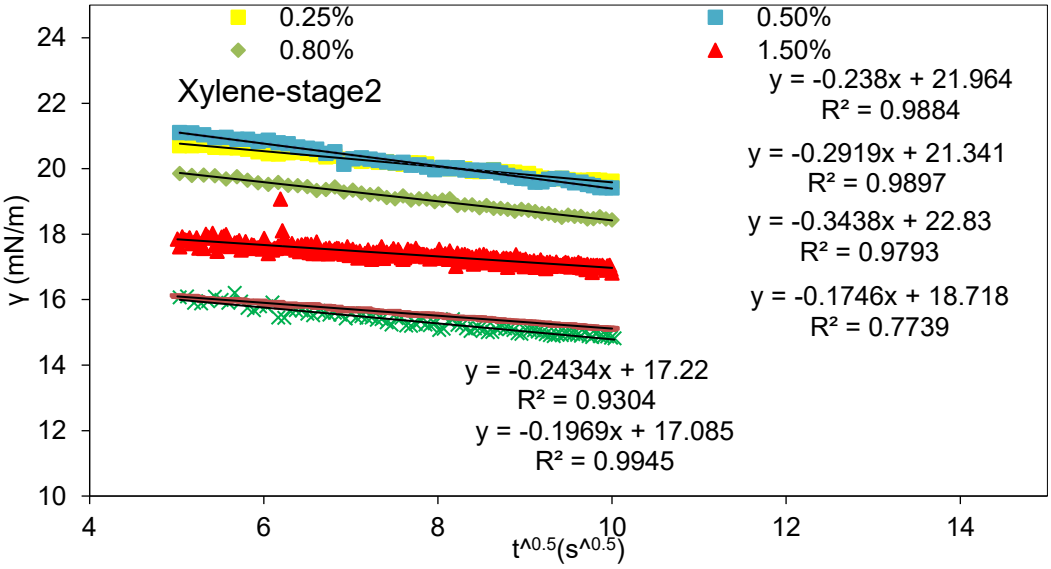
0.25%
0.80%
0.50%
1.50%
Xylene-stage2
y = -0.238x + 21.964
R² = 0.9884
y = -0.2919x + 21.341
R² = 0.9897
y = -0.3438x + 22.83
R² = 0.9793
y = -0.1746x + 18.718
R² = 0.7739
y = -0.2434x + 17.22
R² = 0.9304
y = -0.1969x + 17.085
R² = 0.9945
γ (mN/m)
t^0.5(s^0.5)

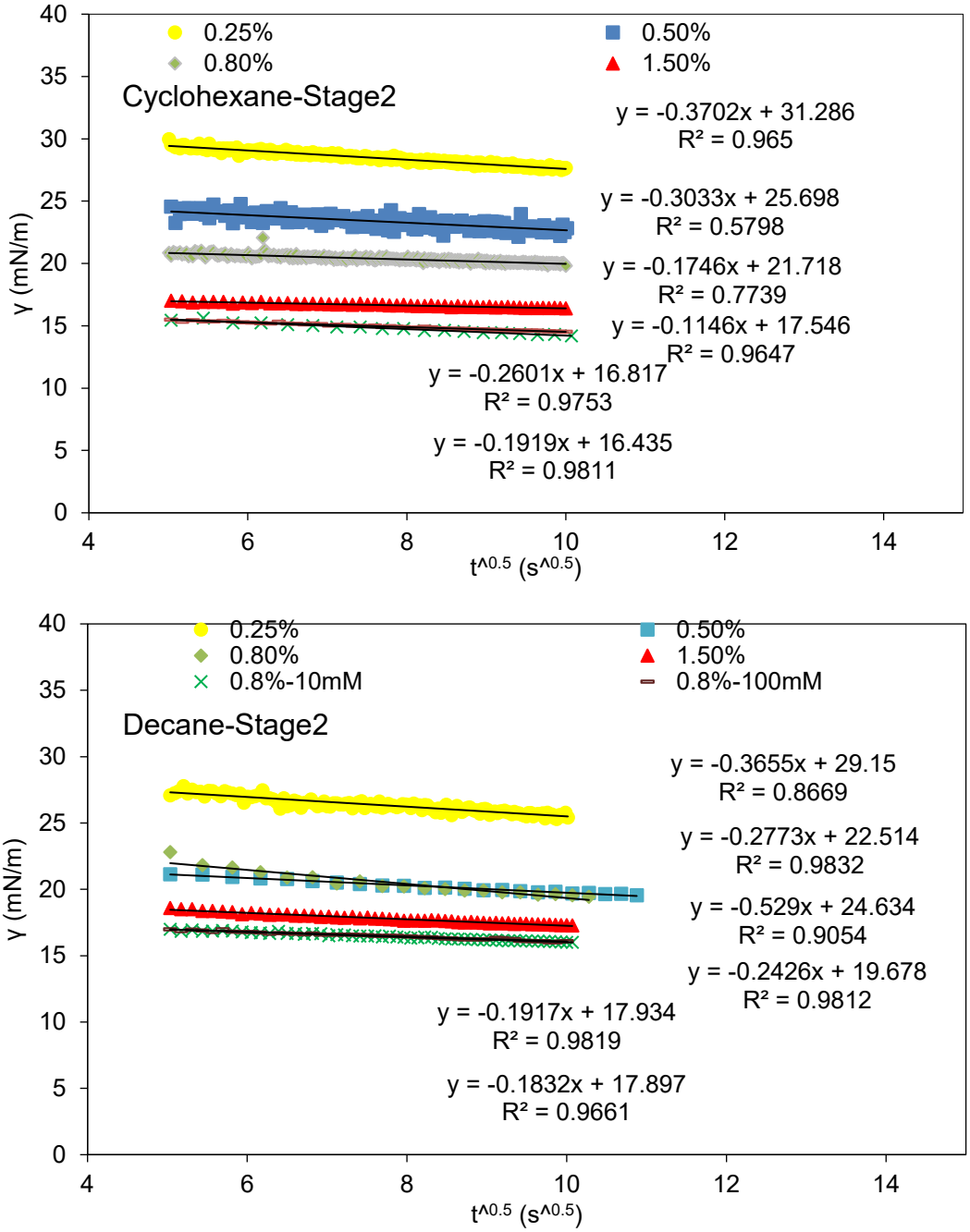

Figure A3.11: Fits short-time interfacial tension (γ) data for xylene, decane, and cyclohexane with water interface for stage 1 and stage 2 at 0.25-1.5 wt.% SEKL at 0 mM ionic strength and 0.8 wt.% at 10 and 100 mM KCl solution. (data of t < 6.5 s for stage 1 and 20 <t< 100 for stage 2 from Figure 2).

9.3.6 Emulsion stability

Upon the centrifugation, the heavier and lighter phases started to separate, and migration happened through the cell, which caused light transmission through the cells of emulsions. The higher

concentration of SEKL reduced the phase separation and subsequently light transmission during the centrifuging process. As is observed, the light transmittance is maximum at 0.25% and minimum at 1.5 wt% of SEKL in Figure A3.13a.

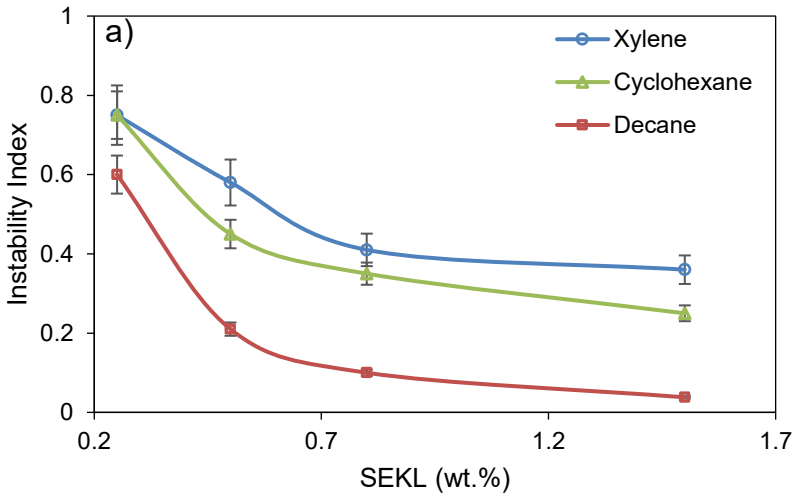

Figure A3.12: The accelerating physical instability index of emulsions formed by different mixtures; as a function of SEKL wt.% concentration.

a)

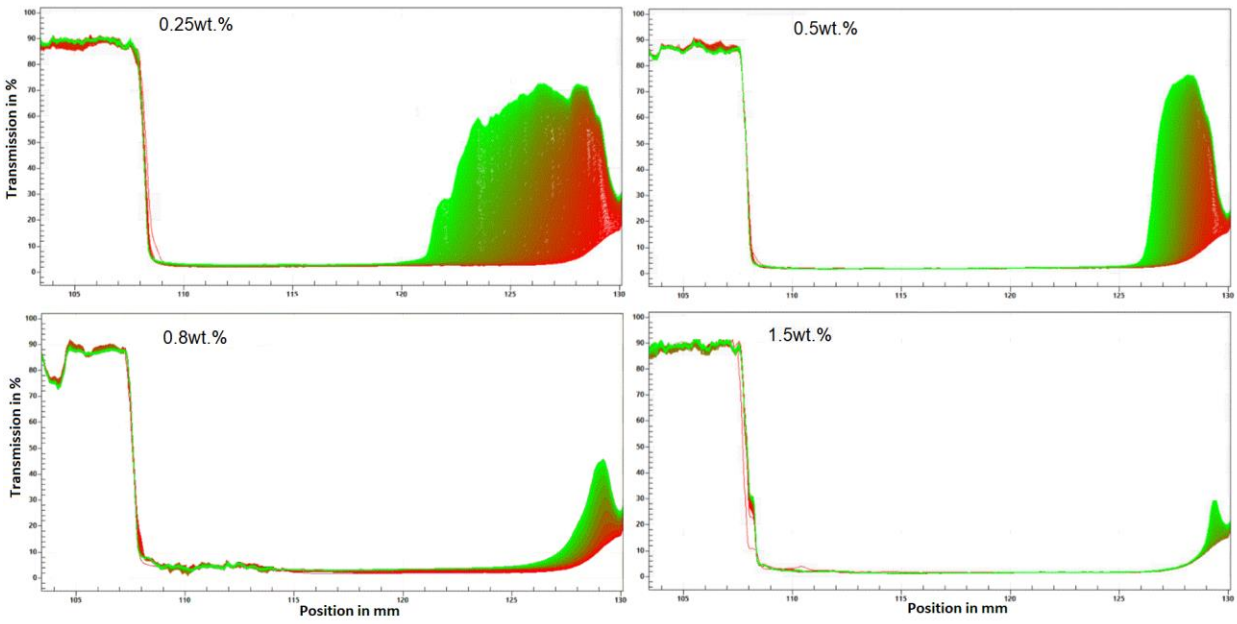

b)

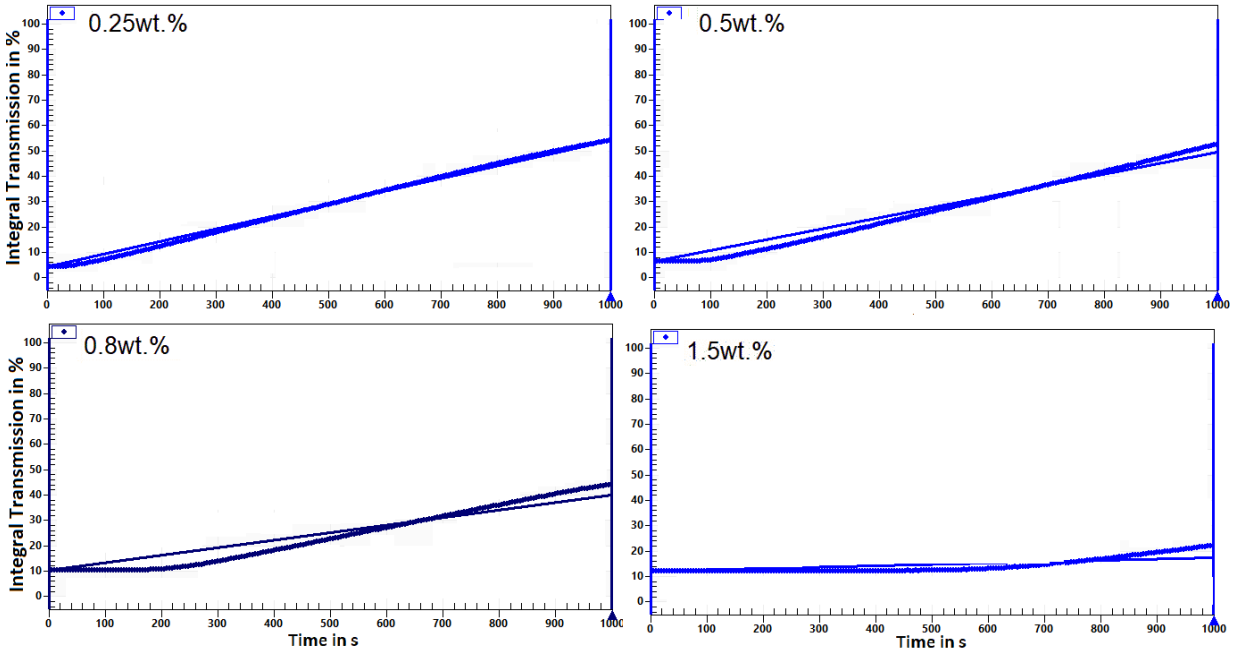

Figure A3.13: Evolution of (a) transmission profiles, % and (b) the integrated transmission-time plots for emulsions presented with the slopes of changes as a straight line, prepared from the volumetric ratio of 1/1 decane: SEKL solution at 0.25-1.5wt.% concentrations.

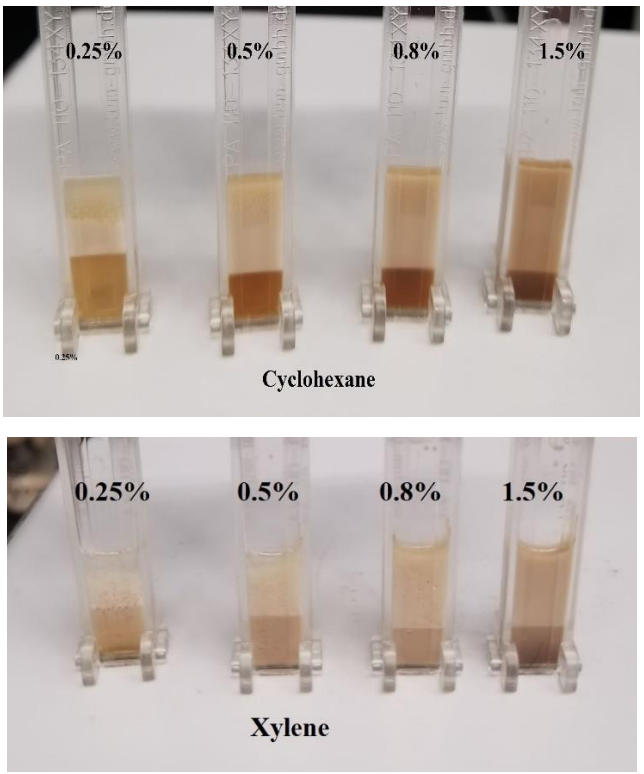

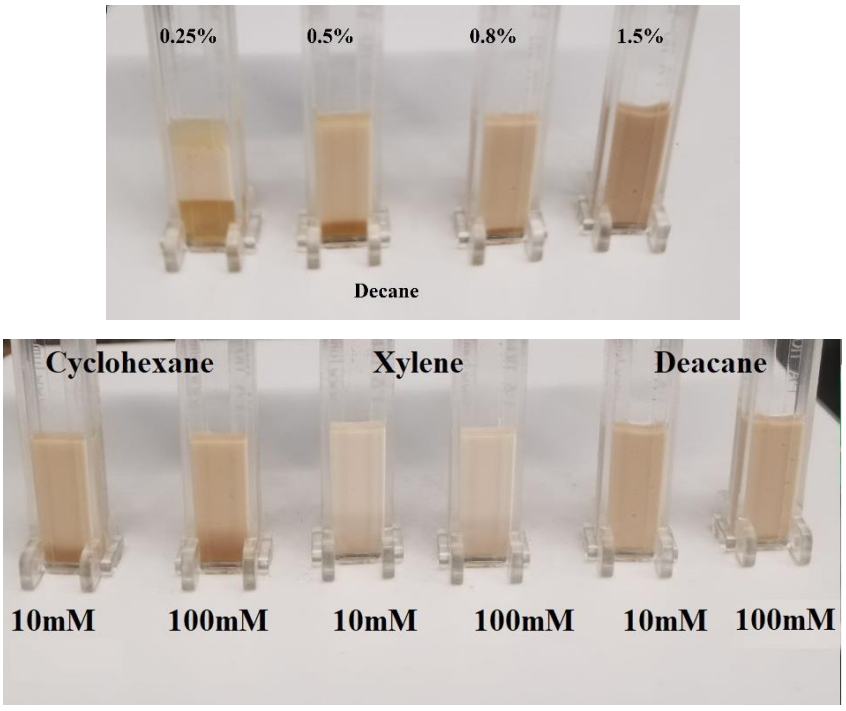

Figure A3.14: Image of emulsions after centrifugal in different SEKL dosages and ionic strength.

9.3.7 References

[1] N. Ghavidel Darestani, A. Tikka, P. Fatehi, *Polymers* **2018,** *10*(8), 928-940.

[2] M. K. Konduri, P. Fatehi, *ACS Sustainable Chem. Eng.* **2015,** *3*(6), 1172-1182.

[3] J. A. Riddick, W. B. Bunger, T. K. Sakano, Organic solvents: physical properties and methods of purification, (**1986**).

[4] D. Wu, A. Honciuc, *Langmuir* **2018,** *34*(21), 6170-6182.

9.4 Effect of physicochemical properties of raw hydrolysis lignins on chemical reactivity toward various sulfo-functionalization routes and its effect on dispersion performance

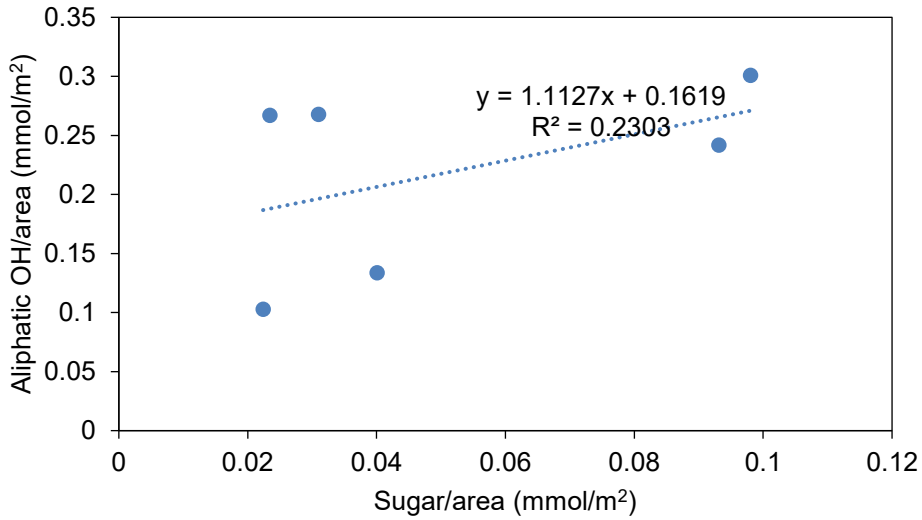

Figure A4.1: Correlations between Aliphatic OH of HL samples and sugar content per area of samples.

9.4.1 Reaction schemes

Sulfonation tends to occur at the α-position of the aliphatic chain of lignin in an alkaline environment due to the formation of a quinone methide intermediate with phenolic substrates as the first step. Next, sulfite ions would be added to this intermediate structure at the α position. Further electron-withdrawing effect of the first sulfonic group on the α position facilitates the addition of another sulfonic acid group at the β position, resulting in the cleavage of the β-aryl ether bond.[1, 2]

Sulfomethylation reaction first starts with an electrophilic addition reaction with formaldehyde on the carbon atom with a rich electron cloud on the ortho position of Ph-OH after the dissociation of OH groups in alkaline medium.[3] Then, the substitution reaction on the new methyl hydroxyl group occurs in the presence of sulfonate group. Sulfonate substitution is also probable to occur on the aliphatic hydroxyl group or α position as well.

Sulfoethylation reaction follows a nucleophilic substitution mechanism that starts with the formation of hydroxyl nucleophiles which attacks the Br-CH_2- linkage in SEB substrate for the substitution with Br.[4] Since SEB is a primary alkyl halide, the steric hindrance and nucleophile strength are important parameters in the success of the SN_2 mechanism.

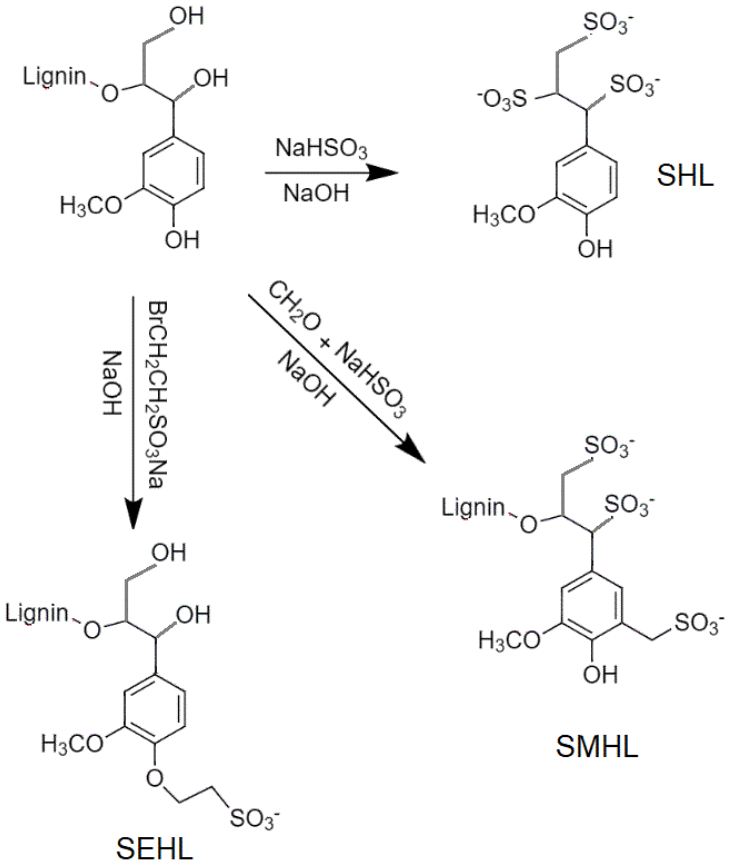

Figure A4.2: Substitution routes for chemical reactions of sulfonation, sulfomethylation and sulfoethylation of H-lignin samples.

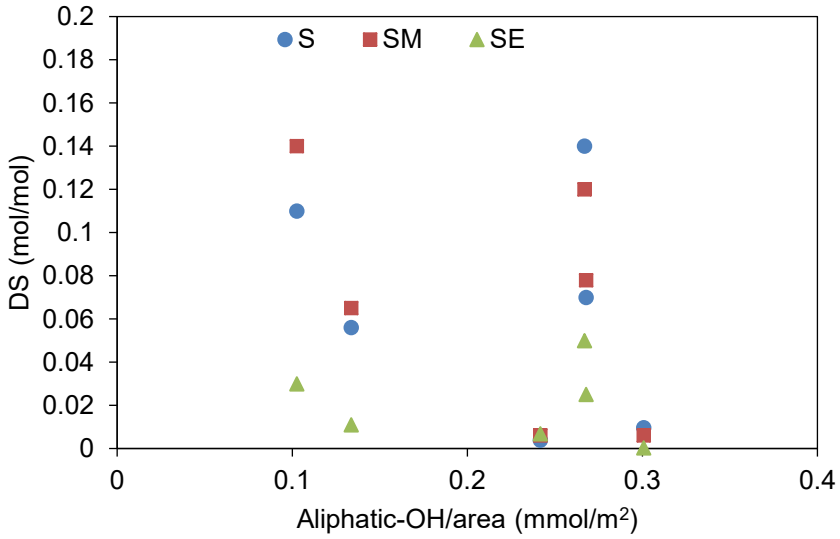

Figure A4.3: Correlation between DS (mol/mol) of the substitution reactions (S, SM and SE) with aliphatic-OH content. (The sugar content is deducted).

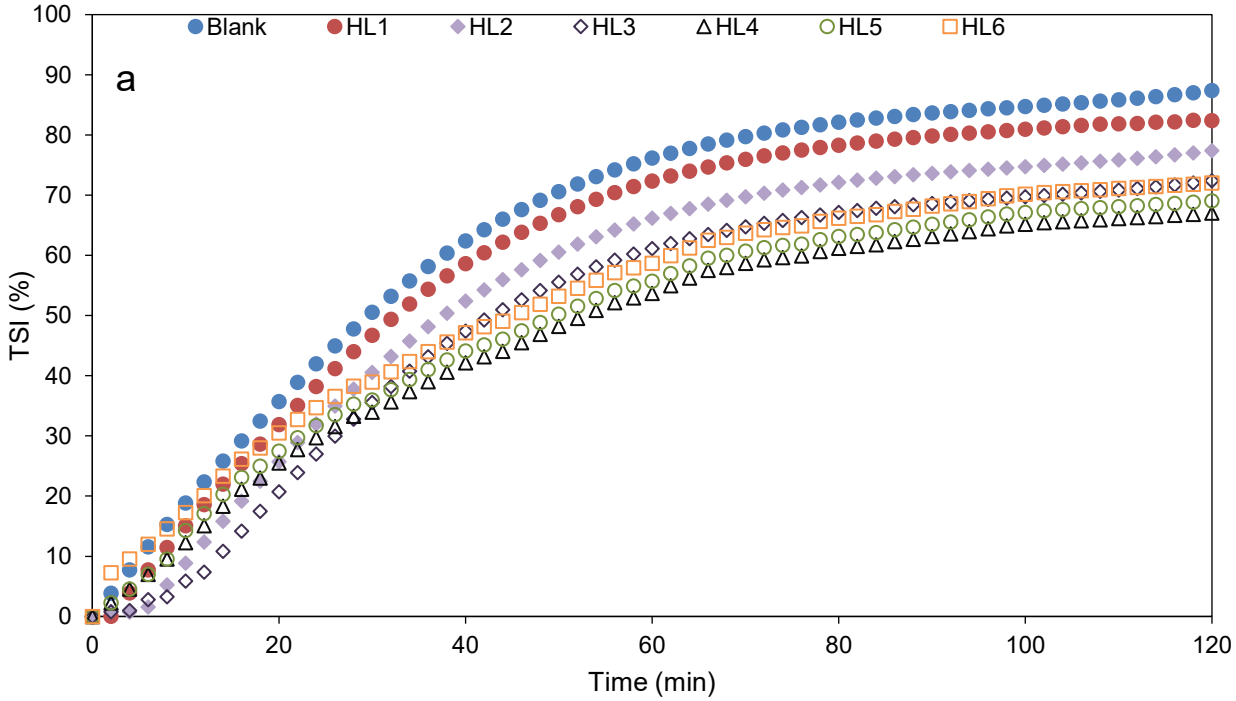

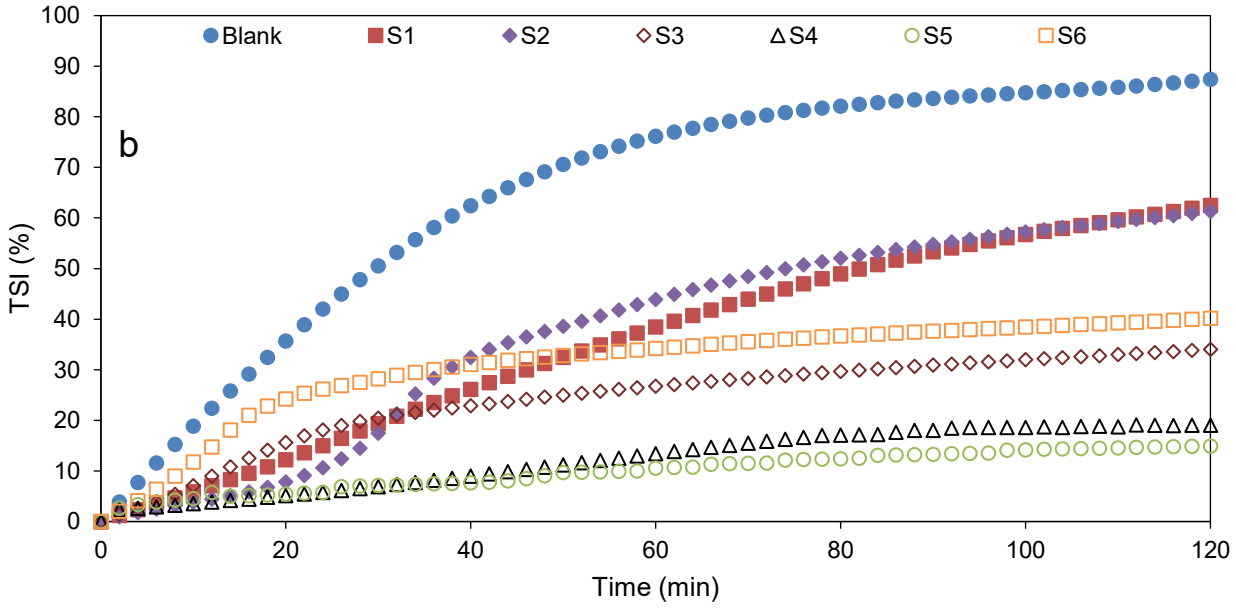

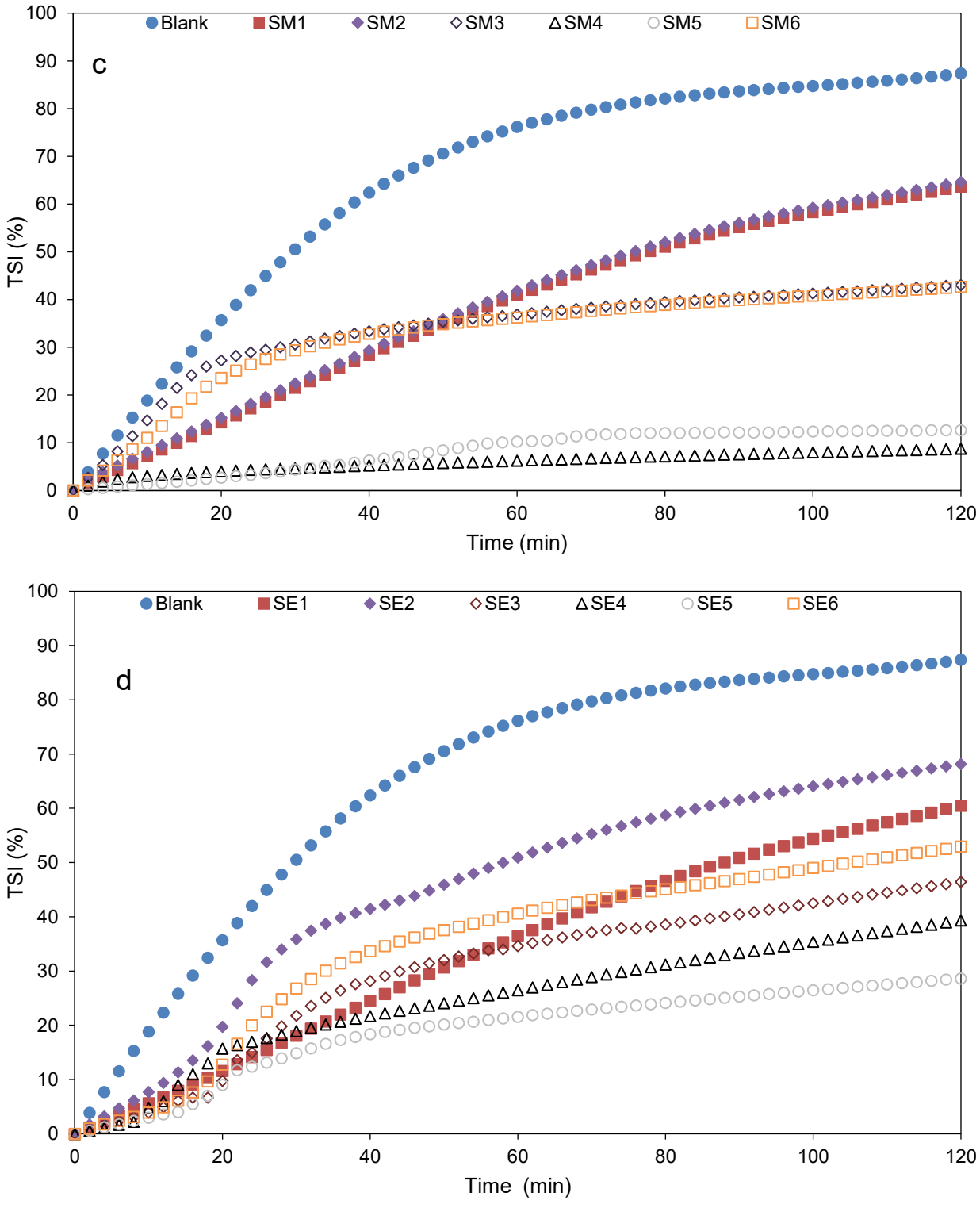

Figure A4.4: Static stability of clay particles evaluated as changes in TSI vs time for a) unmodified HL, b) S c) SM and d) SE modified HL derivatives.

9.4.2 References

[1] W. Gao, J. P. Inwood, P. Fatehi, *J. Wood Chem. Technol*. **2019,** *39*(4), 225-241.

[2] T. Aro, P. Fatehi, *Chemsuschem* **2017,** *10*(9), 1861-1877.

[3] M. K. Konduri, P. Fatehi, *ACS Sustainable Chem. Eng*. **2015,** *3*(6), 1172-1182.

[4] N. Ghavidel, P. Fatehi, *Chemsuschem* **2020,** *13*(16), 4567-4578.